AMPK regulates the release of exosomal miRNAs to facilitate neuron-germ line communication during the dauer stage

Christopher Wong

Department of Biology, McGill University, Montreal

August 2024

A thesis submitted to McGill University in partial fulfilment of the requirements of the degree of Ph.D. in Biology

Table of Contents

List of figures and tables

Chapter 1

Chapter 2

Figure S2.1. Mutants partially suppress the dauer germline hyperplasia and post-dauer sterility associated with loss of AMPK.

Figure S2.2. The abnormal abundance and distribution of chromatin marks typical of dauer larvae that lack AMPK is corrected in *rr166* mutants.

Figure S2.3. The *rr166* mutation restores appropriate chromatin remodeling in post-dauer AMPK mutants.

Figure S2.4. *tbc-7(rr166)* is a hypomorphic allele.

Figure S2.5. TBC-7 does not work in the body wall muscle or excretory system to regulate germ cell integrity.

Figure S2.6. *rab-7* functions in the neurons while *rab-10* functions in the germ line.

Figure S2.7. *mir-1; mir-44; daf-2* double mutants display the same post-dauer germline defects.

Figure S2.8. Tissue-specific TBC-7::GFP used as a sensor for RNAi efficiency and specificity in the neurons and the germ line.

Table S2.1. Mutants isolated from an EMS suppressor screen partially suppress the post-dauer somatic defects of AMPK mutants.

Table S2.2. *daf-2; aak(0); rde-1* mutants with tissue-specific expression of *rde-1* exhibit tissue-specific RNAi phenotypes.

Table S2.3. Post-dauer fertility after RNAi treatment against *rab* genes.

Table S2.4. *daf-2; aak(0); rde-1; tbc-7* mutants with tissue-specific expression of *rde-1* exhibit tissue-specific RNAi phenotypes.

Table S2.5. Predicted *mir-1* and *mir-44* seed sequences in the 3’ UTR of *tbc-7*.

Chapter 3

Acknowledgements

I would like to express my heartfelt gratitude to Professor Richard “Rick” Roy. Our journey together started in 2018 when I joined his lab as an undergraduate student, devoid of any laboratory experience. Throughout these years, Rick has gone above and beyond not only as a mentor in science but also as a lifelong friend and occasional fashion advisor. Thank you for allowing me to work in his lab, providing the freedom to explore and learn from my errors, and coaching me become a better scientist. In addition to his scientific tutelage, Rick has also taught me to be a better writer and public speaker. I want to thank him for providing the opportunity to present our work at multiple international scientific conferences, reigniting my passion for skiing, guiding me around multiple European cities, and serving as a pillar of stability for the lab and myself during the COVID-19 pandemic. Thank you Rick for your unwavering availability to discuss science, life/career choices, and every topic in between. Thank you for all the time that you have invested into me, as this work would not be possible without your guidance and inspiration.

I would like to thank Shaolin Li for always being available to answer any of my questions, whether it is regarding experimental designs, scientific hypotheses, health, sports, or current events. Thank you for acting as my life coach, scientific advisor, and best friend throughout my time in the lab. I will always remember the fun times we went skiing together and meeting at Jolicoeur metro station in the early mornings.

I would like to thank Elena Jurczak, my co-author and friend. Thank you for all the scientific discussions and the countless times you have helped me with tasks over the weekends. Your feedback on my experimental designs are priceless. In addition, thank

you for your friendship and always being my conference partner. I will always remember the great time we had in Paris. Lastly, thank you for translating my abstract in French.

I would like to thank Dr. Pratik Kadekar for introducing me to *C. elegans* in 2017. Without that lifechanging conversation during the BIOL 200 “FRezCa” on the 5th floor of the Schulich library, I most likely would not have gone into research. Thank you for welcoming me into the lab and teaching me all the laboratory techniques. Thank you for your friendship and mentorship.

I would like to thank all present and past members of the Roy lab, particularly Dr. Pratik Kadekar and Dr. Patrick Narbonne for paving the way for all of the projects in this thesis. Thank you to Dr. Arindam Das, Dr. Bing Sun, Sabih Rashid, and McLean Sherrin. Thank you to all of the undergraduate students, Sarah Gaudreau, Maddy Perry, Olivia Costanzo, and Maxime Verreault, who have assisted me in my projects.

Thank you to all Zetka Lab members for being amazing neighbours. Thank you to Professor Monique Zetka for providing valuable feedback during my lab meeting presentations and always extending a helping hand. Huge thank you to Ryan Dawson for his expertise in dissections, troubleshooting with microscopy, and providing valuable strains. Thank you to Alexandar Vujin for helping me with statistical analyses and correctly predicting that siRNAs could be bad for the dauer larvae. Thank you to Alyssa Centonza-Brenie, Silma Subah, and Amir Hossein Pournamdar Sarcheshmeh for their friendship and encouragement.

Thank you to my thesis committee members, Professor Abigail Gerhold, Professor Christian Rocheleau, and Professor Thomas Duchaine for their critical comments, continual support, and reagents throughout the course of my PhD. Thank you to Professor

Mike Strauss, the Facility for Electron Microscopy Research (FEMR), and the Centre for Applied Nanomedicine (CAN) for their assistance and expertise.

Thank you to all the professors and graduate students that I have worked with during my teaching assistant experience. Special thank you to Professor Ken Hastings for all these years of collaboration.

Thank you to those who continually encourage me and check in on me. Thank you to Justin Li, Alexis Marion, Saim (Lisa) Shin, Megan Zhou, Esther Nam, Leo Shen, Cynthia Feng, and Anita Raja. Thank you to my badminton boys: Zhen Li, Sai Kiran, and Jordan Scott-Talbi. Thank you to Sai Kiran for providing lab reagents and primer runs.

Last but not least, I would like to thank my parents, Carmen and Colin; sister, Carissa; and grandparents for their many years of support and encouragement throughout my life. Without them, this journey would not have been possible.

Abstract

Communication between tissues is essential for coordinating adaptive changes in response to environmental fluctuations. Cells share information using mechanisms that depend both on proximity and tissue/cell type. In *Caenorhabditis elegans*, the germ cells enter a state of quiescence in response to reduced nutrient availability, which is dependent on signals of neuronal origin. This signal is propagated by AMPK signalling at the onset of the dauer stage. While AMPK mutants are superficial wild type in replete conditions, they suffer from severe germline and somatic defects when they enter the dauer stage. These mutants exhibit germline hyperplasia, misregulated epigenetic marks, and premature death as dauer larvae. Should they recover from this stage, they will exhibit a highly penetrant sterility as post-dauer adults.

Through a genetic screen, we identified a subset of genes, when disabled, suppress the AMPK germline defects. One of these genes is a RabGAP protein TBC-7. AMPK directly phosphorylates TBC-7 in the neurons, allowing for the production of exosomes through the activity of a Rab GTPase RAB-7. This communication is independent of classical neurotransmission and synaptic vesicles, but instead relies on neuronal exosomes derived from the endosomal trafficking network. Although vesicle-mediated signalling has been previously proposed to mediate tissue/tissue signalling, no such role for exosomes in a regulated physiological context has so far been demonstrated. I show here that environmental change associated with energy stress results in AMPK-regulated miRNA loading and subsequent release of neuronal exosomes. These exosomes carry a pro-quiescent miRNA cargo to the germ line to modify germline gene expression. The exosomes contain the *C. elegans* miRNA

Argonautes, which also accumulate in the germ cells. Using a germline miRNA sensor, we show that neuronally-expressed miRNAs can extinguish the expression of germline-mRNA targets. Our findings demonstrate how a neuronal response can change gene expression in distant tissues, akin to a classical neuroendocrine mechanism, but instead by re-directing RNA trafficking to load neuronal exosomes with specific miRNA cargo.

Résumé

La communication entre différents tissus est essentielle afin de coordonner l'exécution de changements adaptatifs en réponse aux fluctuations environnementales. Les cellules partagent les informations dont elles disposent en utilisant des mécanismes dépendant à la fois du type de tissu ou de cellule les recevant et de leur proximité. Chez les *Caenorhabditis elegans*, les cellules germinales entrent dans un état de quiescence en réponse à une faible disponibilité de nutriments, et cet acte dépend de signaux provenant des neurones. Ce signal est propagé à travers la voie de signalisation par l'AMPK lors de l'entrée dans l'état dauer. Bien que la mutation d'AMPK ne soit pas visible superficiellement, les animaux la portant souffrent de sévères défauts somatiques et germinaux lorsqu'ils entrent dans l'état dauer. Ces mutants présentent une hyperplasie de la lignée germinale, des marques épigénétiques déréglées et une mort prématurée en tant que larves dauer. Si les larves survivent au passage à travers cet état, elles seront stériles en tant qu'adultes post-dauer.

Un dépistage génétique nous a permis d'identifier un groupe de gènes qui, lorsqu'ils sont désactivés, suppriment les défaut germinaux des mutants AMPK. Un de ces gènes code pour la protéine RabGAP TBC-7. L'AMPK phosphoryle directement TBC-7 dans les neurones, permettant la production d'exosomes à travers l'activité d'une Rab GTPase, RAB-7. Cette communication est indépendante d'un type de neurotransmission classique et de vésicules synaptiques, se reposant au contraire sur des exosomes d'origine neuronale dérivant du réseau de transport endosomal. Bien que d'autres aient déjà proposé que la signalisation par vésicules puisse établir un système de signalisation entre différents tissus, il reste encore à établir un rôle pour les exosomes en tant

qu'éléments de communication majeurs au sein d'un contexte physiologique réglementé. Je démontre que des changements environnementaux associés à une forme de stress énergétique entraînent le chargement de miARN dans des exosomes neuronaux et leur relâchement ultérieur, et que ce mécanisme est règlementé par l'AMPK. Ces exosomes transportent des miARN encodant un signal de quiescence jusqu'à la lignée germinale, afin de modifier l'expression de gènes germinaux. Ces exosomes contiennent également les Argonautes spécifiques aux miARN chez *C. elegans*, et ces protéines sont elles-mêmes transportées jusqu'à la lignée germinale. Nous démontrons, en utilisant un détecteur de miARN germinal, que des miARN exprimés dans les neurones peuvent supprimer l'expression d'ARNm germinaux. Nos conclusions démontrent qu'une réponse neuronale peut altérer l'expression de gènes dans différents tissus, de façon analogue à un mécanisme neuroendocrinien classique, en redirigeant le trafic ARN afin d'associer des exosomes neuronaux avec une charge de miARN spécifique au contexte physiologique de l'organisme.

Preface

The thesis is organized in accordance with the manuscript-based thesis guidelines. It consists of 5 chapters:

- Chapter 1 is a literature review and introduction that is divided in to 4 sub-chapters. It will provide a comprehensive review of the relevant literature, as well as provide a rationale and the key objectives of the study undertaken.
- Chapter 2 is a research manuscript that has been published in PLOS Genetics.
- Chapter 3 is a research manuscript that is currently in review.
- Chapter 4 is a research manuscript with unpublished results.
- Chapter 5 is a general discussion and a final statement.

This thesis has been entirely written by the candidate in collaboration with the supervisor of the candidate. This thesis has been written according to the “Guidelines for thesis preparation” from the Graduate and Postdoctoral Studies.

Contribution to original knowledge

Chapter 2 is an original research article published in PLOS Genetics. The article characterizes the role of a RabGAP protein TBC-7 in suppressing the AMPK germline defects that occur during the dauer stage and the post-dauer sterility associated with a loss of AMPK signalling.

Chapter 3 is a manuscript that is in review. The article describes a novel pathway where AMPK stimulates the production of miRISC-containing exosomes in the neurons that are taken up at the germ line. These exosomes release the miRISC to regulate chromatin marks and germline gene expression during the dauer stage. The delivery of

this miRNA cargo is essential for essential for maintaining germline stem cell quiescence during the dauer stage and protecting post-dauer reproductive capacity.

Chapter 4 is a manuscript that is currently in preparation. The study describes the regulation of the expression of histone writers by exosomal miRNAs. Suppressing the expression of these writers corrects the aberrant gene expression typical of AMPK mutants to maintain germ cell integrity throughout the dauer stage.

Contribution of authors

Chapter 2 has been published in PLOS Genetics as follows,

> Wong C, Kadekar P, Jurczak E, Roy R (2023) Germline stem cell integrity and quiescence are controlled by an AMPK-dependent neuronal trafficking pathway. PLOS Genetics 19(4): e1010716. https://doi.org/10.1371/journal.pgen.1010716

Experiments were designed by C.W. and R.R. *tbc-7* was identified by P.K. *tbc-7* was characterized by C.W. and E.J. The analysis, validation, and revision experiments were done by C.W. The manuscript was written by C.W. and edited by R.R.

Chapter 3 is currently in review.

> Wong, C., Jurczak, E., Roy, R. (In review) Neuronal exosomes transport miRNA/RISC cargo to preserve germ cell integrity.

Experiments were designed by C.W. and R.R. E.J. performed some RNAi experiments, suggested experiments, and identified miRNAs containing EXOmotifs. All other experiments were performed by C.W. The manuscript was written by C.W. and edited by R.R.

Chapter 4 is an unpublished manuscript.

Wong C, Verreault M, Jurczak EM, Rashid S, Roy, R (2024) Neuronal miRNAs regulate the expression of histone writers to maintain quiescence and germ cell integrity.

Experiments were designed by C.W., M.V., E.J., and R.R. M.V. and C.W. performed the experiments and the bioinformatic analyses. S.R. performed the mRNA sequencing and analysis. The manuscript was written by C.W. and edited by C.W., M.V., E.J., and R.R.

Chapter 1: Introduction & literature review

Chapter 1.1 General introduction

The development of an organism is determined by its genetic material and how this material is expressed in response to a defined developmental program in addition to cues obtained from its environment (Cardoso-Moreira et al., 2019). In a closed system, such as during embryonic development, the organism will develop with little regard to the environmental circumstances, as they are using maternal resources. However, this situation dramatically shifts when the animals emerge from the embryo and are exposed to the external environment (Chason et al., 2011). In the juvenile stages, these environmental fluxes can be detrimental to development, therefore the animal must adapt their developmental course in order to survive.

Animals have adapted various strategies to survive harsh environments. For example, animals can choose to enter a dormant state, such as hibernation or sporulation, until growth conditions improve (Geiser, 2013; Rittershaus et al., 2013). To accomplish this, the animal must alter their physiology and behaviour to decrease energy expenditure and to ensure that their energy reserves last for the duration of the dormancy (Ahmadi and Roy, 2016; Duwat et al., 2001).

Stem cells are regulated largely by external influence (Morrison et al., 1997). Stem cells are undifferentiated or partially differentiated cells that are totipotent or pluripotent, meaning that they can differentiate into any cell type or proliferate to give rise to more stem cells (Mahla, 2016). Stem cells can undergo at least two different types of division; they can undergo symmetric division, where a stem cell grows and divides into two

daughter stem cells (Knoblich, 2008). Alternatively, they can undergo asymmetric cell division where a stem cell divides to produce one stem cell and another daughter cell, which is differentiated.

In response to unfavorable environments, stem cells can enter a quiescence stage, where all cell divisions are paused (Cheung and Rando, 2013; Urbán and Cheung, 2021). It is theorized that the stem cells become dormant to conserve energy as cell divisions are energy intensive and to maintain the integrity of the stem cells for when growth conditions improve. When stem cells lose the ability to maintain this quiescence, they can undergo unscheduled divisions and negatively affect the wellbeing or the fitness of the organism (Chen et al., 2016). In addition, the stem cells can lose their integrity and some functionality after the process of differentiation. Using this quiescent property of stem cells, we can decipher what pathways may be involved in regulating the cell cycle of a stem cell population and how individual stem cells maintain their integrity during periods of stress.

Caenorhabditis elegans as a model organism

Caenorhabditis elegans (*C. elegans*) is a free-living nematode that is about one millimeter in length as a full-grown adult (Kenyon, 1988). This multicellular eukaryotic organism has been used as a model organism in a laboratory setting since 1963. *C. elegans* are hermaphrodites that are capable of self-fertilization or sexual reproduction. They have a short generation time of about three days for wild-type animals. Wild-type animals have large brood sizes, making it an ideal model organism for large-scale genetic analysis and experiments that require an abundance of starting material. In addition, *C.*

elegans in a laboratory setting are grown on agar plates and are fed a mutant strain of *E. coli* “OP50”, which do not require any major laboratory safety measures. *C. elegans* can be frozen and stored long-term in liquid nitrogen, and when thawed, wild-type animals, most genetic mutants, and even mutants carrying extrachromosomal transgenes can recover to propagate a new isogenic population. Lastly, *C. elegans* possesses a transparent cuticle, which facilitates *in vivo* imaging of structures and artificially introduced fluorescent proteins through light or electron microscopy.

The entire connectome, the interactions between the 302 neurons in the hermaphrodite animal, and the lineages of every somatic cell of *C. elegans* have been determined, providing an advantage for studying development, neural circuitry, and/or how the neurons contribute to the regulation of germ line decisions (Cook et al., 2019). Furthermore, the RNA interference pathway has been well characterized in this organism and can be robustly used in the laboratory setting to knockdown the expression of genes complementary to the dsRNA in select tissues (Grishok, 2005; Kamath et al., 2000; Lee et al., 1993). The ease of use and affordability of RNAi experiments allows for an efficient means of conducting genome-wide surveys of gene functions (Kamath and Ahringer, 2003). In the past decade, the CRISPR/Cas9 genome-editing system has been developed in *C. elegans*, allowing for experiments that involve tagging endogenous protein with fluorescent molecules, making precise changes in the DNA sequence that introduce single amino acid mutations in polypeptides, or adding functional tags like degron used in the auxin-inducible degradation (AID) system onto endogenous proteins (Friedland et al., 2013; Zhang et al., 2015). Thus, *C. elegans* have been used efficiently as a model to study the RNAi/miRNA pathways, behaviour, neurobiology, metabolism,

cell biology/trafficking, cell cycle, cell polarity, apoptosis, ageing, spaceflight research, and much more (Arena et al., 1995; Grishok, 2005; Sato et al., 2014; Scott et al., 2023; Sengupta and Samuel, 2009; Soni et al., 2022; van den Heuvel and Kipreos, 2012; Watts and Ristow, 2017; Yuan and Horvitz, 1992; Zhang et al., 2020a; Zonies et al., 2010). Lastly, *C. elegans* is advantageous for this study because mutants that carry deletions of both catalytic subunits of AMPK develop like wild-type animals in replete conditions and only exhibit somatic and germline defects when allowed to enter the dauer stage, thus providing us with a model to study the regulators of germ cell quiescence (Kadekar and Roy, 2019). Most other commonly used model organisms are nonviable when one or both catalytic subunits of AMPK are deleted (Hardie, 2011).

The *C. elegans* dauer larvae

During the embryonic stage, *C. elegans* rely on maternal resources until they hatch and enter the first of the four larval stages. In replete conditions, *C. elegans* will develop through the four larval stages and molt into a reproductive adult (Figure 1.1). However, if the animal encounters an environment wherein growth conditions are unfavorable during the larval stages or as an adult animal, it can choose to execute alternative developmental pathways to preserve its internal energy stores and increase the chances of survival for itself or for its progeny (Rashid et al., 2021). At the end of the L1 stage, the early larvae are competent to make a developmental decision to enter an alternative pathway called the “dauer” state that is characterized by physiological and behaviour changes to the animal and is programmed for long term survival (Dalley and Golomb, 1992; Fielenbach and Antebi, 2008; Riddle et al., 1981).

In order to the enter the dauer stage, the animal undergoes an extended second larval stage to feed and store fat and carbohydrates. Then, it will undergo a pre-dauer L2D stage and finally enter the dauer stage. Several molecular pathways govern entry into the dauer stage (Gerisch et al., 2001; Gottlieb and Ruvkun, 1994; Jia et al., 2002; Riddle et al., 1981; Thomas et al., 1993; Vowels and Thomas, 1992). While in the dauer stage, these animals are stress-resistant. They are thin due to a radial constriction, and their mouths and buccal cavities are sealed off from the external environment, preventing feeding activity and desiccation. During this stage, they also convert their fat into glucose through the glyoxylate cycle, a variant of the tricarboxylic acid cycle, while suppressing aerobic respiration in favour of glycolysis and fermentative metabolism (Wadsworth and Riddle, 1989). They often remain immobile, but can disperse quickly when touched. They will also nictate, where they rear their bodies to increase their chances of dispersal. During this period of energy conservation, the global levels of transcription are reduced, however thousands of genes associated with stress-resistance and molecular chaperones are transcribed to ensure long-term survival (Dalley and Golomb, 1992; Klass and Hirsh, 1976). Upon entering this stage, the germline stem cells arrest at the G2 cell cycle stage (Fukuyama et al., 2006; Narbonne and Roy, 2006; Wong et al., 2023).

Wild-type animals can survive in the dauer stage for months with no consequences on their reproductive capacity. When conditions improve, the animal can exit the dauer stage and recover to post-dauer L3/4 animals and eventually into reproductive adults. They exhibit a normal brood size and life span. Mechanism(s) governing dauer exit are not well characterized yet, however recent research has shown that the depletion of sterol-binding proteins SCL-12 and SCL-13 and the production of dafachronic acid is

required to switch the animal from a quiescent state to a reproductive program (Schmeisser et al., 2024).

Chapter 1.2: *C. elegans* germ line

The *C. elegans* germ line is a great model for studying stem cell biology and cellular quiescence. Similar to other stem cell systems, the *C. elegans* germ line continuously generates new stem cells in the niche throughout the life span of the organism (Joshi et al., 2010). These stem cells continuously undergo spermatogenesis and oogenesis to ensure the continuity of the species. They are maintained by external signals secreted by neighbouring somatic cells, called the distal tip cells, as well as by other cell-cell communications (Kimble and Crittenden, 2007). The development of the germ line is highly plastic and is responsive to the physiological conditions of the animal.

Germline specification

In the *C. elegans* hermaphrodite, the larval gonadal primordium consists of four cells (Figure 1.2) (Kimble and Hirsh, 1979). The Z1 and Z4 progenitor cells will undergo several rounds of mitotic division to give rise to the somatic gonad. The Z2 and Z3 progenitor cells are referred to as the primordial germ cells and will generate the germline stem cells. In replete conditions, the germ line will develop uninterrupted from the first larval stage (L1) until the animal becomes a reproductive adult. As an adult, the stem cells in proximity to the niche will continually undergo cell division to maintain a steady population of stem cells that will differentiate into sperm and oocytes as they move away

from the signalling centre for the entire duration of the animal's lifespan. Wild-type animals in replete conditions usually give rise to about 200-300 progeny.

During early embryogenesis, maternally contributed germ granules in the 1-cell zygote (P0) are progressively segregated to the germ line blastomeres or the P cells (P1, P2, P3, and P4) through 4 asymmetric cell divisions (Hird et al., 1996; Kawasaki et al., 1998; Updike and Strome, 2010). The P4 cell then undergoes one more cell division to generate the progenitor germ cell (PGC) daughter cells Z2 and Z3. These two cells adopt the germline fate and will produce all of the germ cells in the animal. The Z2 and Z3 will not contribute to the development of the soma. Because these germ granules are only segregated to the P cell lineage through asymmetric divisions, they are termed P granules (Kawasaki et al., 2004). Interestingly, these P granules are not essential for specifying the germ cell fate of the P cells, although mutants that lack P granules have impaired germline development (Cassani and Seydoux, 2022).

P granules are RNA-rich, non-membrane-bound ribonucleoprotein organelles specific to the germ line (Updike and Strome, 2010; Wang and Seydoux, 2014). Some notable gene families and proteins that are essential for the development of the germ line include the PGL/RGG motif family, VASA-related GLH/DEAD box helicase motif family, RNA helicase CGH-1, cap-binding translation initiation factor IFE-1, PIE-1, and other CCCH finger proteins (Gruidl et al., 1996; Kawasaki et al., 2004; Kawasaki et al., 1998; Kuznicki et al., 2000).

The PIE-1 protein is required to specify germ cell fate (Mello et al., 1992; Mello et al., 1996). This protein was first discovered when screening for maternal-effect mutant embryos that produce too many pharyngeal and intestinal cells at the expense of

specifying the germline blastomere P4. This phenotype arises when germline-destined cells mistakenly acquire a somatic cell fate; for example, the transformation of the P2 germline blastomere into a somatic blastomere like its neighbouring cell EMS (Mello et al., 1992). Thus, PIE-1 is maternally provided and required for the P2 cell to follow a germ cell fate rather than a somatic fate.

PIE-1 accumulates in the nucleus and functions as a transcriptional repressor (Seydoux et al., 1996). This conclusion is supported by three observations (Seydoux et al., 1996). First, in early embryos, newly transcribed RNA is detected in somatic blastomeres but not in the germline blastomeres. Second, in *pie-1* mutants, RNA is detected in somatic and germline blastomeres. Lastly, driving the ectopic expression of PIE-1 in somatic cells represses embryonic transcription. Further examination of the PIE-1 primary sequence supports the role of PIE-1 as a transcriptional inhibitor at the step of elongation. In wild-type scenario, TFIIH phosphorylates Ser5 of the heptapeptide repeats of the CTD of RNA polymerase II to initiate transcription (Chapman et al., 2005; Corden et al., 1985; Rimel and Taatjes, 2018). To transition from initiation to elongation, CDK9 must phosphorylate Ser2 of the CTD of RNA polymerase II (Kim et al., 2002; Zhou et al., 2000). PIE-1 also contains heptapeptide sequence repeats that are very similar to the repeats of the RNA polymerase II CTD, therefore PIE-1 competes for CDK9 binding and prevents CDK9 from phosphorylating RNA polymerase II to stimulate elongation (Batchelder et al., 1999; Seydoux and Dunn, 1997; Zhang et al., 2003). Thus, PIE-1 maintains a germ cell fate by blocking transcriptional elongation of genes that would specify for a somatic fate.

The mes (maternal effect sterile) family genes are also required for the specification of the germ cell fate (Capowski et al., 1991). In *C. elegans*, there are four *mes* genes that form two distinct complexes (Xu et al., 2001). MES-2, MES-3, and MES-6 form one complex (Bender et al., 2004). MES-2 has a SET domain, which functions in depositing methylation marks on lysine residues of histone tails (Holdeman et al., 1998). Specifically, MES-2 methylates lys27 of histone H3, which is associated with heterochromatin and transcriptional repression (Cao and Zhang, 2004; Holdeman et al., 1998). MES-4 is part of its own complex and also possesses a SET domain (Bender et al., 2004; Fong et al., 2002). MES-4 associates with chromatin, while the MES-2/3/6 complex is concentrated mainly in the nucleoplasm rather than at the chromatin (Holdeman et al., 1998; Korf et al., 1998; Xu et al., 2001). Once the transcriptional repression by PIE-1 is lifted, the MES complex functions to mark certain segments of chromatin or individual genes to regulate the gene expression of Z2 and Z3 to specify germ cell fate.

While the P cells are protected from a somatic fate through the activity of PIE-1 and the MES-2/3/6 complex, recent studies suggest that there are mechanisms in place that protect somatic cells from acquiring a germline fate. In mog interacting, ectopic p granules (*mep-1*) mutants, somatic cells have germline characteristics, like the expression of PGL-1 and other P-granule genes that should only be active in germ cells (Barstead et al., 2002; Unhavaithaya et al., 2002). Consequently, these mutants arrest as young larvae (Unhavaithaya et al., 2002). MEP-1 interacts with two components of the nucleosome remodeling and deacetylase (NuRD) complex LET-418 and HDA-1. Intriguingly, the ectopic expression of PIE-1 phenocopies the *mep-1* mutant phenotype,

suggesting that PIE-1 directly interacts with MEP-1 to inhibit the activity of the MEP-1/LET-418/HDA-1 complex (Shin and Mello, 2003; Unhavaithaya et al., 2002). The MEP-1/LET-418/HDA-1 complex in turn inhibits the activity of the MES-domain and SET-domain containing proteins, which silences genes to ensure a germline gene expression pattern in the early embryo. Thus, the P granules and PIE-1 are not partitioned in the somatic cells and therefore, the MEP-1/LET-418/HDA-1 complex is active to promote a somatic cell fate. Meanwhile, in germline cells, PIE-1 inhibits the MEP-1/LET-418/HDA-1 complex to promote a germ cell fate.

Development of the somatic gonad

The somatic gonad consists of five structures that develop alongside the primordial germ cells (Hall et al., 1999; Kimble and White, 1981; McCarter et al., 1997). These structures are distal tip cells, gonadal sheath, spermatheca, spermatheca-uterine valve, and uterus. Unlike the nonreproducible divisions of the Z2 and Z3 cells, the Z1 and Z4 somatic precursor cells follow an invariant pattern of cell divisions, migrations, and differentiations (Kimble and Hirsh, 1979). There are two major mitotic events that occur in the first and third larval stages.

The Z1 and Z4 cells start dividing in the mid L1 larval stage to give rise to 12 cells by the L1-L2 molt (Kimble and Hirsh, 1979). These cells do not divide again until the late L2 or early L3 stage. The somatic cells are increasingly separated from each other by the expanding pool of germline stem cells with Z1.aa at the anterior tip and Z4.pp at the posterior tip. These two cells will become the distal tip cells, which serve a critical role in the development of the germ line. They serve as leader functions, preceding the

extension of the two gonadal arms. The other 10 cells will give rise to nine blast cells and one anchor cell. The nine blast cells serve as the somatic gonad primordium, eventually becoming the somatic gonadal sheath cells, the spermatheca, and the uterus, while the anchor cell is a transient cell that functions to pattern the cells of the vulva (Kimble and Hirsh, 1979; McCarter et al., 1997).

The hermaphrodite DTC has a major function as a migratory/morphogenetic leader (Kimble and Hirsh, 1979). One DTC lies at the distal end of each gonad primordium and migration commences at the L2 larval stage. First, the DTCs migrate away from the midbody on the ventral basement membrane. During the L3 stage, the DTC make two turns; they first turn away from the basement membrane, then again to migrate back towards the midbody. Finally, at the L4 larval stage, the DTCs migrate on the basement membrane that overlies the dorsal muscles. The migration process stops at the onset of the adult stage. This process creates the two U-shaped gonadal arms in the hermaphrodite animal.

The gonadal sheath cells are formed from the SS blast cells after the first mitotic event of the Z1 and Z4 progenitor cells (Hubbard and Greenstein, 2000; Killian and Hubbard, 2004; McCarter et al., 1997). To form the gonadal sheath, five pairs of cells form a single layer covering the germline component of each gonadal arm (Killian and Hubbard, 2004). These cells have a stereotyped position along the gonad proximal-distal axis. The first pair overlies the distal germ line, covering the germ cells in the transition zone and the pachytene region. The second pair overlies the loop of each U-shaped gonad, covering the germ cells in diplotene. Sheath cell pairs 3-5 cover the proximal germ line and the developing oocytes. The borders of each sheath cell partially overlap,

creating occasional gap junctions and adherens junctions between cells (Hall et al., 1999). In addition to its structural function, the sheath cells and its precursors promote germline proliferation and gametogenesis during the process of germline sex specification (McCarter et al., 1997; Miller et al., 2001a; Miller et al., 2003). They are also necessary for oocyte maturation and ovulation and allow for the passive uptake of yolk protein by oocytes (Grant and Hirsh, 1999; Hall et al., 1999).

The entire gonad, including the DTCs and germ cells are surrounded by the germline basement membrane (Blelloch et al., 1999; Broday et al., 2004). Basement membranes are thin, specialized extracellular matrices that surround most tissues (Huang et al., 2003; Hutter et al., 2000). During their migration, the DTCs secrete many basement membrane components, including laminin, collagen, nidogen, argin, papilin, and hemicentin (Clay and Sherwood, 2015). This newly remodeled basement membrane allows for gonadal expansion and acts as a structure for germline components to promote or orient migration.

Germline proliferation and differentiation

Upon hatching, the gonad consists of four cells; the primordial germ cells (PGCs), Z2 and Z3, are flanked by the somatic gonad precursor cells, Z1 and Z4, in their surrounding basement membrane (Kimble and White, 1981). These primordial germ cells will remain mitotically quiescent until the mid-L1 larval stage (Sulston et al., 1983). In replete conditions, Z2 and Z3 will begin to divide. These divisions are nonreproducible and the placement of the daughter cells are varied. The germ cells will continually divide throughout the first two larval stages. At this point, the PGCs at the L1 stage are cellular,

but at the second L2 larval stage, the germ line becomes syncytial, meaning each germ cell is connected through a common pool of cytoplasm, termed the rachis (Hirsh et al., 1976). At the L3 larval stage, the most proximal germ cells lose notch signalling and are displaced from the stem cell niche, inducing them to begin meiosis (Austin and Kimble, 1987). This process establishes polarity in the germ line, where the distal germ cells remain in the mitotic stage, while the more proximal germ cells are in the various stages of meiotic prophase (Crittenden et al., 2002; Crittenden et al., 2003). The germ line will continue to develop and form two U-shaped gonads filled with germ cells in the adult stage during replete conditions. However, should the animal enter the dauer stage at the end of the L2 larval stage, the germ line will again become mitotically quiescent (Narbonne and Roy, 2006).

At the L4 larval stage and young adult stages, there is a four-fold increase in the total number of germ cells (Pazdernik and Schedl, 2013). This increase in the number of germ cells is governed by the Notch signalling pathway (Kimble and White, 1981). In the distal germline region, the germ cells receive delta-like ligand signalling from the DTCs, which activates the GLP-1 Notch receptors and therefore these germ cells remain in a mitotic state (Crittenden et al., 2003; Henderson et al., 1997; Henderson et al., 1994; Kimble and Simpson, 1997; Seydoux and Schedl, 2001). GLP-1 signalling at the distal germ line prevents the germ cells from entering meiosis, therefore specifying for the stem cell fate. This region is termed the stem cell niche, as the germline stem cells are maintained in a proliferative state by external factors. When activated, the GLP-1 receptor is cleaved releasing the intracellular domain (ICD) of GLP-1 (Hubbard and Schedl, 2019). The GLP-1(ICD) translocates to the nucleus and associates with the DNA binding protein

LAG-1 to activate gene transcription. LAG-1 is a DNA binding co-factor for both GLP-1(ICD) and LIN-12(ICD). The loss of *lag-1* results in L1 larval lethality, while a hypomorphic *lag-1* mutant results in a partial loss of germline stem cells due to premature entry into the meiotic prophase (Chen et al., 2020b). The loss of *glp-1* in the larval or adult stages results in the loss of all germline stem cells, as the relief of Notch signalling allows all germ cells to enter the meiotic stage. On the other hand, the gain of function mutation of *glp-1* results in a tumourous germ line, with an excess of germline stem cells and little or no cells found in the meiotic prophase state (Berry et al., 1997).

The active GLP-1(ICD)/LAG-1 and LIN-12(ICD)/LAG-1 complex activates the transcription of various targets, including *lst-1* and *sygl-1* (Brenner and Schedl, 2016; Crittenden et al., 2002; Kershner and Kimble, 2010; Shin et al., 2017). These two genes are redundantly required to promote the stem cell fate. The double mutant of these genes has the same phenotype as a loss of *glp-1*, a premature entry of all cells into the meiotic prophase (Shin et al., 2017). Conversely, the ubiquitous overexpression of these two genes results in the same *glp-1* gain-of-function tumourous germline phenotype. LST-1 and SYGL-1 are mainly expressed in the distal germ line and bind with Pumilio family RNA binding proteins FBF-1 and FBF-2. This complex triggers the degradation and the translational repression of the *gld-1*, *gld-2*, and SCF^{PROM-1} mRNA transcripts to inhibit the expression of meiotic entry pathway genes.

As the number of germ cells increase, they are further pushed towards the proximal end of the germ line, exiting the mitotic zone, and entering the transition zone. At the transition zone, the germ cells lose GLP-1 signalling and they enter the meiotic pathway (Austin and Kimble, 1987; Chen et al., 2020b; Crittenden et al., 2003; Seydoux

and Schedl, 2001). Gametogenesis begins at the late L4 larval stage and occurs continuously throughout the adult stages (Seydoux and Schedl, 2001). Spermatogenesis begins during the L4 stage, while oogenesis begins during the adult stage (L'Hernault, 2009). To prepare for fertilization, the cell transitions from diakinesis and metaphase of meiosis I to nuclear envelope breakdown, rearrangement of the cortical cytoskeleton, and meiotic spindle assembly (Fan and Sun, 2019; He et al., 2021). As with most animal species, the oocytes arrest during meiotic prophase I and complete meiosis in response to fertilization, in which major sperm protein acts as a hormone to trigger meiotic maturation (Mehlmann, 2005; Miller et al., 2001b). In *C. elegans*, the process of meiotic maturation and fertilization happen concurrently. The contraction of the oviduct forces the oocyte into the spermatheca, exposing the oocyte to sperm (Hubbard and Greenstein, 2000). (Chase et al., 2000; McNally and McNally, 2005). Simultaneously, an impermeable eggshell forms around the embryo.

The dauer stage and the dauer germ line

Most organisms delay their germline development when they encounter energetic stress. In *C. elegans*, there are four larval stages followed by a transition into a reproductive adult stage. Upon hatching, if nutrients are absent, the primordial germ cells will remain mitotically quiescent at the L1 stage (Baugh and Sternberg, 2006; Hong et al., 1998). In the adult stage, upon encountering starvation, the animal can enter the adult reproductive diapause (ARD), where the germ line, except for a small population of germline stem cells, undergoes apoptosis (Angelo and Van Gilst, 2009). In both

scenarios, when nutritional conditions improve, the primordial germ cells or germline stem cells will proliferate to populate the germ line.

At the end of the L2 larval stage, if the animal encounters unfavourable growth conditions, such as crowding/presence of dauer-inducing pheromone, high temperatures, or lack of nutrients, it can enter the dauer stage (Fielenbach and Antebi, 2008; Riddle et al., 1981). The dauer stage is an alternative developmental stage where the animal shifts away from reproductive development and instead enters a stress-resistant stage. This stage is preceded by a pre-dauer/L2d stage and is characterized by delayed development and darker intestines from increased fat storages. Animals in the dauer stage can survive for up to four months. Importantly, this stage is not permanent; it is a transient stage that animals can exit from when they encounter more favourable growth environments. Animals that exit the dauer stage enter the L4 larval stage and resume reproductive development.

There are several signalling pathways that act downstream of environmental cues to induce dauer entry. Genetic screens for animals displaying abnormal dauer formation classified these genes into two categories: genes that when mutated result in the formation of the dauer stage, termed Daf-c (abnormal dauer formation-constitutive) and genes that when mutated prevent entry into the dauer stage despite poor growth conditions, termed Daf-d (abnormal dauer formation-defective) (Gottlieb and Ruvkun, 1994). Further analysis of these genes revealed three independent parallel pathways that regulate dauer entry: insulin-like signalling IGF-1/*daf-2*/*daf-23*, TGF-β/*daf-7*, and cGMP/*daf-11* (Kimura et al., 1997; Ren et al., 1996; Schackwitz et al., 1996; Vowels and Thomas, 1994). All three pathways converge on a steroid hormone, dafachronic acid, and

its cognate nuclear receptor (Antebi et al., 2000; Motola et al., 2006). In favourable environments, cytochrome p450/DAF-9 produces a steroid hormone, dafachronic acid to activate DAF-12. Active DAF-12 will initiate downstream gene expression. In unfavourable growth environments, like starvation or reduced insulin-like signalling, DAF-12 will form a complex with co-repressor DIN-1 to allow for the initiation of the dauer program, enabling the animal to survive during poor growth conditions (Ludewig et al., 2004).

Cell division is an energy intensive process. Thus, as *C. elegans* larvae enter the dauer stage, they exhibit global cell cycle quiescence (Narbonne and Roy, 2006). Germline stem cells and somatic tissue cells steadily decrease the number of mitotic divisions until they completely arrest. Germ cells arrest at the G2 cell cycle stage. Therefore, the dauer germ line is completely quiescent. In mammalian systems, insulin signalling regulates Akt/PKB (AKT-1 and AKT-2 in *C. elegans*) activity to progress through the G1/S and G2/M checkpoints (Paradis and Ruvkun, 1998). Progression through the G1/S checkpoint relies on the activity of two CDK inhibitors p21 and p27 (Sherr and Roberts, 1999). p21 and p27 are kinase inhibitors and block the kinase activities of the cyclin-E-CDK and cyclin-A-CDK complexes (Abukhdeir and Park, 2008). Overexpression of p27, and presumably p21, prevents CDK activation and therefore entry into the S phase of the cell cycle. Similarly in *C. elegans*, RNAi mediated knockdown of *cki-1*, the *C. elegans* homolog of p21 and p27, results in abnormal divisions in the germ line (Hong et al., 1998; Kostić et al., 2003; Kostić and Roy, 2002). Thus, this data suggests that the germline stem cell quiescence during the *C. elegans* dauer stage uses similar cellular machinery to regulate the germ cell cycle. Interestingly, the germline stem cells do not

arrest at the G1 cell cycle stage and instead exhibit G2/M phase arrest in dauer larvae. These germ cells also contain twice the amount of DNA compared to somatic cells in G1 cell cycle arrest (Fukuyama et al., 2006). Altogether, these data suggest that the germ cells arrest in the G2/M cell cycle stage by using some components of the G1/S checkpoint inhibitors to maintain germline quiescence during the dauer stage.

Since there are no divisions in the germ lines of wild-type dauer larvae, we would also expect no Notch signalling. However, the germ cells do not execute meiosis, which would normally occur when GLP-1 is no longer activated. Interestingly, the LAG-2 Notch ligand in the DTCs and the GLP-1 Notch receptor in the germ line is still expressed, suggesting that Notch signalling could be active, although the germ cells are arrested in G2/M cell cycle stage (Kadekar, unpublished). This finding calls into question the possibility that there are other mechanisms are in place downstream of Notch signalling to ensure that the germ line remains quiescent during the dauer stage. However, further studies that examine the localization of the GLP-1(ICD) are needed to examine if LAG-2 is complexing with GLP-1 and is activating Notch signalling in the germ cells (Shaffer and Greenwald, 2022).

LKB1/AMPK signalling in maintaining germline quiescence

Genetic analysis implicated the LKB1-AMPK signalling axis in the regulation of germline stem cell quiescence during the dauer stage in *C. elegans* (Kadekar et al., 2018; Narbonne et al., 2010; Narbonne and Roy, 2006, 2009). Further tests showed that the upstream kinase of AMPK, LKB1/PAR-4, and PTEN/DAF-18 are all required to maintain quiescence during the dauer stage (Narbonne and Roy, 2006). LKB1 or serine/threonine

kinase 11 (STK11) is a protein kinase that regulates cell polarity and functions as a tumour suppressor (Shackelford and Shaw, 2009). It acts as an upstream inhibitor of AMPK, which acts as a master metabolic regulator to maintain energy homeostasis (Woods et al., 2003). LKB1 is allosterically activated by the binding of the Ste20-like adaptor protein STRAD/*strd-1* and the adaptor protein MO25/*mop-25.2* (Chien et al., 2013; Hawley et al., 2003; Narbonne et al., 2010). This heterotrimeric complex is capable of phosphorylating and activating AMPK, 12 other AMPK-related kinases, and a class of microtubule affinity related kinases (MARK) (Hawley et al., 2005; Hurley et al., 2005; Lizcano et al., 2004; Manning et al., 2002; Woods et al., 2003). Activation of AMPK and AMPK-related kinases by LKB1 suppresses growth and proliferation when energy levels are low (Figure 1.3) (Nakano and Takashima, 2012). By maintaining cell polarity, LKB1 also inhibits the expansion of tumour cells (Baas et al., 2004). Consequently, the loss of LKB1 in *C. elegans* during the dauer stage leads to disrupted cell polarity and germline hyperplasia (Narbonne and Roy, 2006).

In *C. elegans*, LKB1/PAR-4 was first identified as a mutation that was defective in the partitioning of cellular components during the first zygotic division (Kemphues et al., 1988; Mehenni et al., 1998). In the first cell cycle of development, the Par genes are responsible for establishing cellular asymmetries. The *par-2* gene is responsible for the unequal first cleavage and asymmetries in cell cycle length and spindle orientation in the first two daughter cells (Boyd et al., 1996). In the germline P lineage, PAR-2 and PAR-1, a MARK kinase, exhibit similar asymmetric cortical localization (Wu and Griffin, 2017). In LKB1/*par-4* mutants, the posterior localization of PAR-1 and PAR-2, and the anterior localization of PAR-6 is lost, resulting in a symmetrical division (Morton et al., 2002; Watts

et al., 2000). The loss of one of the downstream targets of LKB1/PAR-4, AMPK, results in germline hyperplasia, suggesting that LKB1 impinges on AMPK signalling to maintain quiescence during the dauer stage (Kadekar and Roy, 2019; Narbonne and Roy, 2006). Interestingly, in *par-4; aak(0)* triple mutants, there is an increased severity of germline hyperplasia, suggesting that AMPK is not the only downstream target of LKB1/PAR-4 and that LKB1/PAR-4 phosphorylates additional targets to maintain germline stem cell quiescence (Kadekar et al., 2018). These findings are consistent with reports of LKB1 regulating cell cycle dynamics in hematopoietic stem cells in both AMPK-dependent and AMPK-independent manners (Nakano and Takashima, 2012).

PTEN/DAF-18 (Phosphatase and Tensin homolog deleted from chromosome ten) is a tumour suppressor that is one of the most commonly mutated tumour suppressors in human disease (Abdulkareem and Blair, 2013). PTEN acts as a protein and lipid phosphatase. Its primary target is the lipid messenger phosphatidylinositol-3,4,5-triphosphate (PIP3) and removes the phosphate from the D3 position producing phosphatidylinositol-4,5-bisphosphate (PIP2) (Ogg and Ruvkun, 1998). PI3K/AGE-1 counteracts PTEN activity by phosphorylated PIP2 into PIP3. Resting cells have low levels of PIP3, but in response to growth signals, the levels of PIP3 increase, thus acting as a secondary messenger for cell cycle progression and mimics growth factor stimulation (Chen et al., 2018; Keniry and Parsons, 2008). Thus, PTEN activity works to halt the cell cycle, while PI3K activity works to activate cell proliferation. Consequently, in *C. elegans*, the loss of PTEN/DAF-18 results in a loss of germline quiescence during the dauer stage, while AGE-1 works redundantly with DAF-2 to extend lifespan (Narbonne and Roy, 2006) (Ogg and Ruvkun, 1998).

The structure of AMPK

A forward genetic screen identified a dominant negative allele of the *C. elegans* orthologue of the catalytic subunit of AMP-activated protein kinase (AMPK) in the regulation of germline quiescence during the dauer stage (Narbonne and Roy, 2006). It was first identified as an AMP-dependent regulator of 3-hydroxy-3-methylglutaryl coenzyme A (HMG-CoA) reductase and acetyl coenzyme A (Acetyl Co-A) carboxylase, hence this enzyme was termed AMP-dependent protein kinase (Smythe et al., 1998). AMPK is a heterotrimeric $\alpha\beta\gamma$ complex that functions as a regulator of energy homeostasis (Ross et al., 2016; Yan et al., 2018). In mammals, each subunit has alternative isoforms: two α subunits (α1 and α2), two β subunits (β1 and β2), and three γ subunits (γ1, γ2, and γ3). Together, they can form up to 12 different $\alpha\beta\gamma$ isoform complexes. The α subunits contain a canonical Ser/Thr kinase domain, an autoinhibitory domain (AID), an adenine nucleotide sensor segment called an α-linker, and a β subunit-interacting C-terminal domain (termed the α-CTD). The β subunit-interacting domain contains the ST loop, which contains the phosphorylation sites for AKT, PKA, and GSK (Hawley et al., 2014; Hurley et al., 2006; Suzuki et al., 2013).

The β subunits contain a myristoylated, unstructured N-terminus, a glycogen-binding carbohydrate-binding module (CBM), a scaffolding C-terminal domain (β-CTD) that interactions with both γ subunit and the α-CTD of the α subunit, and an extended β-linker loop motif that connects the CBM with the β-CTD (Chen et al., 2018; Xiao et al., 2011; Yan et al., 2021; Yan et al., 2018). The three γ subunits have N-termini of different lengths and unknown functions. It also contains a conserved adenine nucleotide-binding domain that contains four cystathione β-synthetase (CBS) AMP/ADP/ATP binding sites

(Day et al., 2007; Scott et al., 2004). The four CBS domains are in two tandem repeats known as a Bateman domain with CBS1 and CBS2 in the first Bateman domain and CBS3 and CBS4 in the second Bateman domain. CBS1 binds ATP and CBS4 binds AMP, while CBS3 can bind to all AMP/ADP/ATP. The ribose binding Asp residue of CBS2 is replaced by an Arg and has never been observed to bind any nucleotide in the heterotrimeric structure.

The catalytic core of AMPK is formed from one γ subunit with the α-CTD and β-CTD (Xiao et al., 2011; Yan et al., 2021). The β-CTD is sandwiched between the γ subunit and the α-CTD. While the catalytic core of AMPK is stable, the remaining domains are highly dynamic, and their positions are determined by the binding of ligands and post-translational modifications. For this reason, AMPK was initially crystalized in isolated domains and the holo-enzyme can only be crystallized in the presence of multiple stabilizing ligands or through protein engineering (Chen et al., 2009; Handa et al., 2011; Yan et al., 2018).

As the levels of AMP/ADP increase relative to the abundance of ATP, AMPK is activated and will phosphorylate ATP-generating catabolic pathways and downregulate anabolic pathways to preserve precious nutrients (Yan et al., 2018). Thus, AMPK is activated by AMP and ADP and the addition of AMP to recombinant AMPK *in vitro* increases its phosphorylation activity by ten-fold (Davies et al., 1995; Gowans et al., 2013; Xiao et al., 2011). AMP and ADP act as allosteric regulators of AMPK at the Bateman domains, causing a conformation change in the γ subunit to expose the activation loop (Xiao et al., 2011). In its inactive state, the α-linker that connects AID and α-CTD is directly bound by the γ subunit. A segment of the linker, termed the regulatory subunit-

interacting motif 2 (αRIM2) interacts with AMP at CBS3, suggesting that αRIM2 functions as an adenine nucleotide sensor and that it mediates the transduction of the adenine-binding signal to the kinase domain. As the levels of AMP increases and ATP decreases, the interaction between the isolated α-linker and core AMPK decreases.

Kinase domains have a highly conserved structure (Taylor and Kornev, 2011). It is made of a smaller N-terminal lobe that consists of a β-sheet, two α-helices, and a large α-helical C-terminal lobe. The cleft between the N-terminal and C-terminal lobe is the binding site for substrates and Mg^{2+}-ATP (Yan et al., 2018). The two lobes are separated by a flexible hinge that can open or close to cycle through the substrate-accessible open and the catalytically-competent closed conformations. The kinase domain is composed of three important elements: 1. The activation loop at the entrance of the catalytic cleft; 2. The α-helix in the N-lobe which positions the ATP-binding lysine (K47 in human α1) and the Mg^{2+}-binding Asp-Phe-Gly loop; 3. The substrate-binding catalytic loop in the C-terminal lobe (Kornev et al., 2006; Kornev and Taylor, 2015; Meharena et al., 2013). AMPK is a type of Arg-Asp kinase, where the phosphorylation of this kinase stabilizes the interaction between the negatively charged phosphate on the activation loop and the positively charged residue with the αC helix (K62 in α1), the activation loop (N164), and the catalytic loop (R140) (Yan et al., 2018). This conformation stabilizes the αC helix and positions the Arg and Asp of the catalytic loop for substrate binding.

The regulation of AMPK activity

AMPK activity is regulated by three major events that affect the phosphorylation state of Thr172 on the α1-subunit of AMPK (Yan et al., 2018): 1. The level of

phosphorylation at the activation loop by upstream kinases, including the LKB1/STRAD/MO25 complex, calcium/calmodulin-dependent protein kinase kinase II (CAMKK2), and TGF-β-activated kinase 1 (TAK1); 2. The activity of upstream phosphatases, including protein phosphatase 2A (PP2A), protein phosphatase 2C (PP2C), and Mg^{2+}-/Mn^{2+}-dependent protein phosphatase 1E (PPM1E); 3. Phosphorylation-independent regulation by allosteric regulators AMP/ADP/ATP. Increased levels of phosphorylation on Thr172 of AMPK α1-subunit (or Thr174 of the α2-subunit) by upstream kinases increases the activity of AMPK by 100-fold. Increased levels of AMP binding to AMPK increases phosphorylation activity by up to 10-fold, while binding of ATP inhibits AMPK activity (Gowans et al., 2013; Sanders et al., 2007; Xiao et al., 2011; Yan et al., 2021). Binding of ADP weakly protects the activation loop of AMPK from being dephosphorylated, but does not allosterically activate AMPK kinase activity (Gowans et al., 2013; Oakhill et al., 2011; Xiao et al., 2011). Binding of AMP to AMPK blocks phosphatases from the Thr172 residue on the AMPK α1-subunit, preventing the dephosphorylation and inactivation of AMPK. Binding of ATP causes a large conformation shift in AMPK. The kinase domain of the α subunit dissociates from its active-state conformation and instead associates with the γ subunit, then rotates approximately 180° in the conformational change (Li et al., 2015; Xiao et al., 2011). Upon dissociation of the kinase domain, Thr174 is now exposed to upstream phosphatases, which will dephosphorylate Thr174, rendering AMPK inactive. Thus, the structural conformation and activity of AMPK are highly dependent on the abundance of adenine nucleotides in the cell.

Additionally, AMPK is also regulated by CAMKK2 (Hawley et al., 2003; Hawley et al., 2005; Woods et al., 2005). CAMKK2 part of the serine/threonine-specific protein kinase family, specifically the Ca^{++}/calmodulin-dependent protein kinase subfamily. CAMKK2 has several phosphorylation targets, one of which is AMPK. In the presence of increased levels of intracellular Ca^{2+}, CAMKK2 is activated. It has been shown that CAMKK2 then phosphorylates and activates AMPK at Thr174 in the hypothalamus (Anderson et al., 2008). This mechanism of AMPK activation is only dependent on the levels of intracellular Ca^{2+} and independent of the abundance of adenine nucleotides.

In addition to binding adenine nucleotides, other important energy metabolites, such as glucose, glycogen, and nicotinamide adenine dinucleotides, also regulate AMPK allosterically. (Gu et al., 2017; Polekhina et al., 2005; Zhang et al., 2017; Zhang et al., 2014). Glucose does not directly bind to AMPK, but glycogen, NADPH, and NADH can directly bind to AMPK. (Polekhina et al., 2005; Zhang et al., 2017; Zhang et al., 2014). The physiological relevance of glycogen, NADPH, and NADH binding to AMPK is unknown (Gu et al., 2017). Lastly, AMPK is also subjected to regulation by ubiquitination and proteasomal degradation in various tissues in response to high levels of glucose (Lee et al., 2013b).

The function of AMPK

When AMPK is activated, it increases the ATP-generating catabolic processes while decreasing energy-consuming anabolic processes (Zhang et al., 2014). AMPK phosphorylates CoA carboxylase 1 and sterol regulatory element-binding protein 1c (SREBP1c) to modify lipid metabolism to increase the supply of energy (Smythe et al., 1998). AMPK also stimulates glucose uptake in skeletal muscles by phosphorylating a RabGAP protein TBC1D1 (Kjøbsted et al., 2019). TBC-containing proteins function by enhancing the inherent GTP hydrolysis ability of Rab proteins, converting it from its active GTP-bound form into its inactive GDP-bound form. The inactivation of TBC1D1 by AMPK phosphorylation allows RAB2A, RAB8A, RAB10, and RAB14 to remain in its active GTP-bound form, allowing for the translocation of the GLUT4 glucose transporter to the plasma membrane (Mafakheri et al., 2018). Additionally, AMPK phosphorylates 6-phosphofructo-2-kinase (PFK2), fructose-2,6-bisphosphatase 2/3 (FBPase-2), glycogen phosphorylase, and glycogen synthesis to indirectly regulate the rates of glycolysis and gluconeogenesis (Marsin et al., 2000). Lastly, AMPK inhibits gluconeogenesis by inhibiting transcription factors hepatocyte nuclear factor 4 (HNF4) and CREB regulated transcription coactivator 2 (CRTC2) (Lee et al., 2010a).

AMPK also directly phosphorylates a catabolic enzyme adipose triglyceride lipase in *C. elegans*. In *C. elegans*, AMPK mutants die prematurely during the dauer stage due to the depletion of their energy stores (Narbonne and Roy, 2009). Upon encountering energy stress, AMPK directly phosphorylates and inhibits adipose triglyceride lipase ATGL (ATGL-1 in *C. elegans*), an enzyme responsible for the initial step in triglyceride hydrolysis, therefore, preventing the premature depletion of the triglyceride stores.

Further experiments showed that AMPK phosphorylates ATGL-1 at Ser303 to block lipolysis. The phosphorylation at Ser303 generates a 14-3-3 binding site for PAR-5, which sequester ATGL-1 away from lipid droplets and instead targets it for proteasome-mediated degradation. These data suggest that AMPK regulates the levels of triglycerides by modulating the activity of ATGL-1 in order to preserve lipid reserves during the dauer stage.

In times of energy stress, the LKB1/AMPK signalling pathway conserves energy resources by impinging on the mammalian target of rapamycin complex 1 (mTORC1) and shutting down its activity (González et al., 2020). AMPK switches off the mTORC1 complex through two parallel mechanisms. 1. AMPK phosphorylates a negative regulator of mTOR signalling, tuberous sclerosis complex protein 2 (TSC2) at Thr1271 and Ser1387 (Corradetti et al., 2004). These phosphorylation events are assumed to promote the GTPase-activating protein (GAP) activity of TSC2 which in turn hydrolyzes GTP-bound Rheb GTPase into inactive GDP-bound Rheb GTPase. Active Rheb GTPase is an activator of the mTOR pathway, thus contributing to the protein synthesis and cellular growth. 2. AMPK directly phosphorylates and inhibits the activity of the RAPTOR/DAF-15 component of mTORC1 at two sites: Ser722 and Ser792 (Gwinn et al., 2008). RAPTOR is a scaffold protein that is required to assemble the mTOR complex. In *C. elegans*, no TSC1 or TSC2 homologues have been identified yet, thus is it unclear if AMPK maintains germline quiescence by inactivating the activity of the TOR/LET-363 complex or if there are alternative pathways in which AMPK maintains germline quiescence independent of TOR activity.

AMPK also regulates autophagy in *C. elegans* (Alers et al., 2012; Lee et al., 2010b). Autophagy is a conserved degradation system that removes unnecessary or dysfunctional components through a lysosome-dependent engulfment to degrade or recycle proteins. Initiation of autophagy is dependent on the activity of a serine/threonine kinase ULK1 and its regulatory proteins Atg13 and Atg17 (Alers et al., 2012). AMPK activates autophagy using two methods simultaneously. It can directly phosphorylate and activate ULK1 and also inactivate mTORC1, where the activity of mTORC1 will inactivate autophagy. Therefore, AMPK activity promotes autophagy to increase the supply of energy.

Regulation of the germ line by AMPK signalling

LKB1 is required for the establishment of polarity in the early *C. elegans* embryo, *Drosophila melanogaster* oocytes, and cultured cells to create asymmetric cell divisions (Baas et al., 2004; Nakano and Takashima, 2012; Shackelford and Shaw, 2009). This polarity is established with the activity of the MARK kinases. AMPK is also implicated in the establishment of cell polarization. In mammalian systems, AMPK activity is required for the polarization of proteins involved in the formation of tight and adherens junctions (Zhang et al., 2006). Further evidence also shows that AMPK phosphorylates CLIP-170 to control the speed of microtubule polymerization and directional cell migration (Nakano et al., 2010). Loss of either AMPK or non-phosphorylated CLIP-170 results in disrupted microtubule organization or perturbed directional cell migration. All these defects can be rescued through an introduction of a phosphomimetic CLIP-170 mutant, suggesting that AMPK directly phosphorylates CLIP-170 to regulate microtubule dynamics.

Three genome-wide RNAi screens in *C. elegans* identified downstream targets of the protein kinases LKB1/PAR-4 and AMPK (Kadekar et al., 2018). In *C. elegans,* the loss of either PAR-4 or AMPK signalling results in germline hyperplasia in the dauer larvae, where the number of germ cells increase four- to six-fold (Kadekar et al., 2018; Kadekar and Roy, 2019; Narbonne and Roy, 2006). Through these RNAi screens, a subset of genes were identified to either phenocopy the *par-4*-dependent germline hyperplasia or suppress the germline hyperplasia in *par-4* or *aak(0)* mutants (Kadekar et al., 2018). A subset of gene candidates that suppressed the defects are also involved in the regulation of cell polarity and cytoskeletal function downstream of *par-4* and in an AMPK-independent manner. These data suggest that PAR-4 must interact with these AMPK-independent targets to regulate cell polarity and cytoskeletal dynamics during the dauer stage to ensure germline quiescence. Consistent with these findings, the loss of *par-4* during the dauer stage results in disorganized actin structure. In wild-type dauer larvae, the actin filaments are localized at the rachis membrane, however, in *par-4* mutants, the filaments are not localized to the rachis and are completely disorganized. However, these defects are later resolved, suggesting an additional regulator of cytoskeletal dynamics can compensate for the loss of *par-4*.

AMPK has also been shown to indirectly regulate gene expression through the phosphorylation of key epigenetic regulators in mammalian systems (Marin et al., 2017). To increase the expression of nuclear genes involved in mitochondrial biogenesis, AMPK phosphorylates DNA methyltransferase I (DNMT1) and histone acetyltransferase 1 (HAT1). DNMT1 is responsible for the deposition of methylation marks that condense the chromatin, limiting the access of general transcription factors to promoters. On the

contrary, HAT1 acetylates the CTD of histones to promote the formation of euchromatin to promote transcription. Both histone writers can be bound by another AMPK target, retinoblastoma binding protein 7 (RBBP7). The phosphorylation of RBBP7 enhances the interaction between DNMT1 and RBBP7 and between HAT1 and RBBP7, overall enhancing the transcription of genes related to mitochondrial biogenesis.

Additionally, AMPK has been shown to directly regulate gene expression. In mammals, AMPK can directly phosphorylate histone H2B to active stress-related gene transcription (Bungard et al., 2010). In *C. elegans*, animals must arrest their primordial germ cells in the L1 stage in response to starvation to ensure proper developmental timing (Demoinet et al., 2017). AMPK plays a role in blocking the deposition of chromatin marks during L1 starvation to ensure that the gene expression is in accordance with the levels of energy supplies. In AMPK mutants, these chromatin marks are inappropriately established in starved L1 larvae, which is correlated with a premature division of the primordial germ cells, overall leading to a loss of germline integrity due to misregulated gene expression. These inappropriate histone marks accumulate throughout several generations despite these latter generations never encountering any starvation events, eventually resulting in a mortal germline phenotype. The mortal germline phenotype is characterized by progressive sterility over the course of a few to several dozen generations. To prevent these marks, AMPK directly inhibits the COMPASS (complex proteins associated with Set1) histone modifying complex to ensure that no epigenetic marks are deposited until nutrient contingencies are met during the L1 stage. Altogether, AMPK relays the metabolic status of the organism to the cell cycle through chromatin

modifications to ensure that the correct gene expression program is expressed during periods of energetic stress.

Recently, AMPK has been shown to directly regulate the biogenesis and transport of small RNAs to affect changes in the germ lines of *C. elegans* during the dauer stage (Kadekar and Roy, 2019). AMPK cell non-autonomously establishes germline quiescence to preserve the reproductive capacity of the germline stem cells until growth conditions improve. In the absence of AMPK signalling, the germline stem cells undergo hyperplasia and lose their integrity, rendering the post-dauer animal sterile. These defects are accompanied with an increased abundance and altered distribution of histone marks in the germ line, which leads to abnormal germline gene expression. Interestingly, when the components of small RNA biogenesis, *dcr-1* and *rde-1*, and siRNA Argonautes, *ergo-1*, *csr-1*, and *hrde-1*, are compromised using RNAi, the AMPK germline defects are suppressed, suggesting that the production and activity of siRNAs is somehow maladaptive for the reproductive capacity of the animals. To further support this finding, compromising the expression of one of the dsRNA-gated channels, *sid-1*, can also partially restore the post-dauer fertility. Together, these data suggest that blocking siRNAs produced in the soma from entering the germ line during the dauer stage is somehow critical for the proper regulation of germ cell integrity and for maintaining quiescence during the dauer stage.

A recent study has further shown that the production and the activity of siRNAs may not be maladaptive for the animals, but rather the harmful effects of siRNA production come from the sequestration of the resources necessary for miRNA biogenesis (Jurczak et al., 2023). This discovery stemmed from a study to uncover the mechanism of the

insensitivity towards exogenous RNAi in AMPK mutants. Compared to wild-type animals, AMPK mutants do not display robust RNAi phenotypes, regardless of the method of introducing dsRNA. AMPK mutants expressing extra copies of *dcr-1* in the somatic cells display robust RNAi phenotypes, suggesting that a lack of resources necessary for the processing of dsRNAs could be the culprit. Surprisingly, the introduction of extra copies of *dcr-1* also suppresses the AMPK germline defects, suggesting that the production of small RNAs must be critical during the dauer stage. Analysis of the amino acid sequence of DCR-1 and its binding partner, RBPL-1, revealed strong AMPK phosphorylation motifs. Dicer has been shown to associate with two RNA-binding proteins – PACT/*rbpl-1* and TRBP/*rde-4*. PACT, or RBBP6 (retinoblastoma binding protein 6 or P2-R) is a multidomain protein that regulates cell proliferation, differentiation, and apoptosis (Lee et al., 2013a; Wilson et al., 2015). It is also an activator of protein kinase R, a protein involved in innate immune response and response to stress. TRBP (TAR RNA binding protein) also regulates many cellular processes. It performs the opposing function as PACT and inhibits the activity of PKR. Interestingly, TRBP can also bind to PACT to regulate its function. While both contribute to RNA interference, how these two proteins contribute to small RNA production with Dicer/*dcr-1* was poorly understood. In an *in vitro* reconstituted system, PACT and TRBP binding changes the conformation of Dicer to produce different small RNA substrates (Lee et al., 2013a). TRBP-Dicer complex favours the processing of pre-siRNA substrates, while PACT-Dicer complex inhibits the processing of pre-siRNA substrates and instead favours pre-miRNAs as its substrate. These results indicate that the activity of Dicer is modified according to its binding partner and in turn can alter the target-binding specificities of its substrates.

In *C. elegans*, the introduction of extra copies of either DCR-1 or RBPL-1 in the somatic cells can suppress the AMPK germline defects during the dauer stage (Jurczak et al., 2023). Coimmunoprecipitation experiments in *daf-2* animals show that DCR-1 preferentially binds to RBPL-1, while in AMPK mutants, DCR-1 is bound to RDE-4, suggesting that there must be an AMPK-dependent switch from siRNA to miRNA production at the onset of the dauer stage. Phosphomimetic mutations on either one of these two proteins suppresses the AMPK germline defects, suggesting that AMPK directly phosphorylates components of the miRNA biosynthesis complex to ensure miRNA production at the onset of the dauer stage.

Curiously, adding extra copies of a single miRNA through a transgene is sufficient to suppress the AMPK germline defects. Altogether, these data suggest that locking DCR-1 and RBPL-1 in a complex, whether through phosphomimetic mutations or introducing exogenous miRNAs, ensure miRNA production. These miRNAs can then be transported from the somatic cells into the germ line to halt the germline cell cycle, preserving the reproductive capacity of the stem cells throughout the dauer stage.

Chapter 1.3: Exosomal miRNA in *C. elegans*

miRNA biogenesis and miRISC

Noncoding RNAs are approximately 22 nucleotides in length and play an important role in the post-transcriptional regulation of gene expression in all organisms. The first noncoding RNA identified was the *lin-4* RNA in 1993 when studying the developmental timing of *C. elegans* (Lee et al., 1993). The loss of function mutation of *lin-4* resembled a

gain-of-function mutation of *lin-14*, both resulting in developmental delays and heterochronic developmental patterns such as a loss of vulval and cuticle structures. Upon closer examination, the sequence of the *lin-4* RNA contained complementary sequences to the 3'UTR of the *lin-14* mRNA with 7 distinct binding sites each with 9 base pairing nucleotides. When base-paired, the *lin-4*:*lin-14* complex has a kink structure due to base stacking of the mismatched base pairs. It was later revealed that *lin-4* acted as a negative regulator of *lin-14* mRNA expression by preventing the translation of *lin-14* and the transition to the next developmental larval stage. Another small noncoding RNA, *let-7* also functions in a similar manner (Reinhart et al., 2000). Expressed later in development, it acts to repress the expression of heterochronic genes *lin-14*, *lin-28*, *lin-4*1, *lin-4*2, and *daf-12* to trigger the transition from the late-larval stage to the adult stage. The *let-7* and *lin-4* RNAs are now recognized as miRNAs, a class of small, single-stranded noncoding RNA that are 21-23 nucleotides in length and are involved in RNA silencing and post-transcriptional regulation of gene expression.

The understanding of the functions and biogenesis of miRNAs is best explained through the lens of another class of small noncoding RNAs known as small interfering RNAs (siRNAs) and the role of both in RNA interference. During RNAi, double-stranded RNA, either in a bimolecular duplex or in an extended hairpin, is processed into short, single-stranded RNA molecules (Figure 1.4) (Okamura et al., 2004). This single-stranded RNA serves as a guide RNA to repress the translation of a transcript and target the mRNA for degradation, all through complementary base-pairing (Conte et al., 2015). While siRNAs perfectly base pair with their target mRNA, miRNAs exhibit imperfect binding and therefore form a loop where there are mismatched base pairs. After binding, siRNAs

induce the destruction of the mRNA through mRNA cleavage and degradation. On the other hand, the binding of the miRNA does not lead to the direct degradation of the mRNA but instead results in the translational suppression of the target.

miRNA biogenesis starts with the processing of a primary transcript transcribed by RNA polymerase II or III (Ha and Kim, 2014). In humans and mice, about half of all identified miRNAs are intragenic and found within introns, with a small number found within exons (De Rie et al., 2017; Kim and Kim, 2007). Others are intergenic and are transcribed independently from the promoter of the host gene. Instead, they are transcribed from their own promoter. Sometimes, miRNA families that have similar or identical seed sequences are transcribed as one long transcript known as a cluster (Tanzer and Stadler, 2004). miRNA biogenesis is classified into one canonical and two non-canonical pathways.

In the canonical pathway, pri-miRNAs are transcribed and processed into pre-miRNAs in the nucleus by RNA binding protein DiGeorge syndrome critical region 8 (DGCR8/*pash-1*) and a ribonuclease III enzyme Drosha/*drsh-1*, which form the microprocessor complex (Denli et al., 2004). This event requires the recognition of the junction between the stem loop and the flanking single-stranded RNA of the pri-miRNA hairpin by DGCR8/*pash-1*. *In vitro* cleavage reactions show that the pri-miRNA must have N(6)-methyladenosine (m(6)A) marks deposited on the GGAC and other motifs by methyltransferase-like 3 (METTL3) to facilitate proper processing (Alarcón et al., 2015). Although the *C. elegans* genome does not contain an ortholog of the METTL3 methylase or its binding partner METTL14, RNAi screens of RNA methyltransferases suggest that F33A8.5, an ortholog of the human ZCCHC4 gene, and C38D4.9, an ortholog of the

human METTL5 gene are generally responsible for the methylation of ribosomal RNAs, while METTL4/C18A3.1 and METTL16/*mett-10* are responsible for the methylation of U2 and U6 snRNA (Ju et al., 2023; Sendinc et al., 2020). After binding of the miRNA by DGCR8/*pash-1*, Drosha/*drsh-1* cleaves the pri-miRNA duplex at the base of the hairpin structure of the pri-miRNA (Han et al., 2004). This cleavage forms 2 nucleotide 3' overhangs on the newly synthesized pre-miRNA. The pre-miRNA is then exported to the cytoplasm by an exportin 5 (XPO5)/RanGTPase complex for further processing (Okada et al., 2009). *C. elegans* do not have an ortholog of XPO5, but instead uses the transporter XPO-1 to transport pre-miRNAs in a cap-binding complex (CBP20/*cbp-20* or *ncbp-2* and CBP80/*cbp-80* or *ncbp-1*)-dependent manner (Büssing et al., 2010). The loss of *xpo-1* phenocopies the loss of core components of the *C. elegans* miRNA pathway, such as *alg-1*, one of the two miRNA Argonautes, resulting in vulval bursting and "alae gap" phenotypes.

In the cytoplasm, the RNase III endoribonuclease Dicer/*dcr-1* removes the terminal loop, resulting in an approximately 22 nucleotide long, mature miRNA duplex (Denli et al., 2004; Zhang et al., 2004). The mature miRNA is named after the directionality of the miRNA strand; the 5p strand arises from the 5' end of the pre-miRNA hairpin, while the 3p strand arises from the 3' end of the hairpin (Khvorova et al., 2003; Yoda et al., 2010). One of the two strands can be then loaded into the Argonaute protein (AGO1-4 in humans and ALG-1/2 in *C. elegans*), however, both strands can form the active miRNA-induced silencing complex (miRISC). The selection of the strand for loading is largely dependent on the cell type or cellular environment and can result in equal-loading proportions or one strand being predominant over the other. The selection for the strand is dependent on the

thermodynamics of the stability of the 5’ end of the miRNA duplex and on the presence of a 5’ uracil on position 1. The strand with lower 5’ stability or 5’ uracil is preferentially loaded into the Argonaute and is termed the guide strand. The unloaded strand is termed the passenger strand and will be either cleaved by AGO2/*alg-2* if it contains no mismatches with the guide strand or passively unwound and degraded if it contains mismatches (Ha and Kim, 2014).

There are multiple non-canonical miRNA biogenesis pathways. Mainly, they can be grouped into either DGCR8/*drsh-1*-independent or Dicer/*dcr-1*-independent pathways (O'Brien et al., 2018). Pre-miRNAs produced in the DGCR8/*drsh-1*-independent closely resemble Dicer/*dcr-1* substrates in terms of structure. For example, mirtrons are produced from the introns of mRNAs during splicing and 5-methylguanosine (m^7G)-capped pre-miRNAs that are exported to the cytoplasm by exportin 1/*xpo-1* fall into the DGCR8/*drsh-1*-independent pathway (Xie et al., 2013). In the Dicer/*dcr-1*-independent pathway, miRNAs are processed by Drosha from an endogenous short hairpin RNA transcript and require further processing and trimming by AGO2/*alg-2* to fully mature (Yang et al., 2010).

The miRISC consists of the guide strand and an Argonaute protein (Kawamata and Tomari, 2010). After formation of the miRISC, the Argonaute with the guide strand binds to specific sequences at the 3’UTR of their mRNA targets to induce translational repression, mRNA deadenylation, and decapping. There are reports of miRNAs binding to 5’UTR and coding regions of mRNAs, and also to promoter regions. However, the effects of miRNA binding are variable, and more studies are required to understand their functional significance. The specificity of the miRISC comes from the interaction between the miRNA guide strand and the complementary sequences on the target mRNA, also

known as the miRNA response elements (MREs) (Jo et al., 2015). The degree of complementarity in the MRE determines whether there is an AGO2-dependent slicing of target mRNA or miRISC-mediated translation inhibition and target mRNA decay.

In most animal cells, the miRNA and MRE interaction is not fully complementary (Jonas and Izaurralde, 2015). There are mismatches between the miRNA and the target mRNA that prevent AGO2 endonuclease activity (Ellwanger et al., 2011). The 5' seed region of the miRNA (nucleotides 2-8) mediates most of the interaction. Additional binding between the 3' end of miRNA and the mRNA aids in the stability and specificity of the miRNA:mRNA interaction. In *C. elegans*, the base pairing of the seed region (nucleotides 2-8) is essential for miRNA target, while the functions of these 3' non-seed regions are less understood (Duan et al., 2022). Using the miRNA *let-7a*, where the nucleotides 9-22 are conserved across all bilaterians, a study showed that 3' non-seed sequence functionally distinguishes *let-7a* from its family paralogs. The perfect pairing between nucleotides 11-16 are essential for the targeting of key targets, such as *lin-4*1, *daf-12*, and *hbl-1*. The nucleotides 17-22 are less critical but can compensate for mismatches in the nucleotides 11-16. These data show that the 3' non-seed regions, in addition to the 5' seed sequences, of miRNAs are essential for their function.

Once the miRNA has based paired with its mRNA target, the formation of the miRISC begins. The GW182/*ain-1/2* protein family is first required (Behm-Ansmant et al., 2006). These proteins provide the scaffolding necessary for the recruitment for other effector proteins. The target mRNA is then poly(A)-deadenylated partially redundantly by the activity of the catalytic subunit PAN2 and the adaptor protein PAN3 and CCR4-NOT deadenlyase complex (Behm-Ansmant et al., 2006; Christie et al., 2013). The

deadenylated mRNAs are then decapped by the decapping protein 2 (DCP2/*dcap-2*) (Braun et al., 2012). DCP2 require the binding of cofactors for proper function, such as DCP1/*dcap-1*, enhancer of decapping 3 (EDC3/*edc-3*), EDC4/*edc-4*, PATL1/*patr-1*, and DEAD box protein 6 (DDX6/*cgh-1*). Afterwards, the decapped and deadenylated mRNA is degraded by major cytoplasmic nuclease 5'-to-3' exoribonuclease 1 (XRN1), preventing the mRNA from being expressed and translated.

Overview of the endosomal network

The endosomal network plays a critical role in the organization and trafficking of cellular components in eukaryotic cells. It is involved in many essential processes, such as nutrient uptake, receptor-mediated signalling, membrane turnover, and development (Platta and Stenmark, 2011; Samaj et al., 2004). Generally, endocytosed macromolecules from several trafficking pathways at the plasma membrane are funneled towards the common early endosome, which acts as the sorting hub of the cell (Scott et al., 2014). Housekeeping receptors and other proteins are recycled back to the plasma membrane at the stage of the early endosome or later in the network at the recycling endosomes. Cellular components that are not recycled and remain at the early endosome are either destined towards the trans-Golgi network, secreted in exosomes, or degraded in the lysosomes. The maturation from early to late endosome is marked by changes in protein and lipid composition, as well as the acidification of the endosomal lumen (Scott and Gruenberg, 2011). The vacuolar-type ATPase (V-ATPase) is a multi-subunit proton pump that acidifies the lumens of early endosomes and late endosomes/lysosomes to a pH value of approximately 6.2 and 5.5/5.0, respectively (Lafourcade et al., 2008). This

acidification of the late endosome/lysosome is critical for its proper functioning in receptor-ligand uncoupling, lysosome enzyme activity, and transport.

Prior to fusion with the lysosome, proteins can be sorted into the late endosome or into intralumenal vesicles, which are formed through the invagination and pinching off of the late endosomal membrane (Scott et al., 2014). These intralumenal vesicles are cargo-containing vesicles within the late endosome. This entire entity is now known as a multivesicular body (MVB) or endosomal carrier vesicle (ECV). These MVBs can fuse with lysosomes to degrade their cargo or with the plasma membrane to release the intralumenal vesicles as exosomes. The late endosome can also fuse with the autophagosome to degrade its contents. The autophagosome is a double membrane structure that engulfs materials destined for degradation.

The structure and function of Rab GTPases

To understand how the endosome system functions, we must discuss the role of various Rab proteins and their regulators. Rab proteins are part of the Ras superfamily (Wandinger-Ness and Zerial, 2014). Rab GTPases are monomeric proteins that regulate multiple aspects of vesicle transport at specific sites within the cell. In humans, there are approximately 70 Rab GTPases, while there are 31 in the *C. elegans* genome (Gallegos et al., 2012; Wandinger-Ness and Zerial, 2014). Common to all members of the Ras superfamily, Rab GTPases have a GTPase domain, which is composed of six-stranded β-sheet flanked by five α-helices (Pereira-Leal and Seabra, 2001; Pfeffer, 2005). The C-terminus of the GTPase fold is the hypervariable region where two cysteine residues are prenylated (Andres et al., 1993; Desnoyers et al., 1996). As with all members of the RAS

superfamily, Rab proteins alternate between the GTP-bound active and the GDP-bound inactive forms (Hutagalung and Novick, 2011; Lee et al., 2009). In its active form, the Rab protein can bind to its effectors until the GTP is hydrolyzed. The regulation of Rab proteins is highly dependent on their binding partners. In isolation, Rab GTPases remain in their GTP-bound conformation for relatively long, as they exhibit poor GTP hydrolysis activity. Once hydrolyzed, GDP remains tightly bound, thus remaining in its inactive form (Nielsen et al., 2008). Thus, two major groups of regulatory proteins are required to change the conformation of Rab GTPases. GTPase-activating proteins (GAPs) act as a Rab inactivator by enhancing the inherent hydrolysis ability of Rab GTPases. In its inactive form, guanine nucleotide dissociation inhibitor (GDI) removes the Rab protein from the membrane (Collins, 2003; Pfeffer, 2001). Guanine exchange factors (GEFs) perform the contrary function by promoting the release of the bound GDP, which is then quickly replaced by GTP from the cytoplasm. This exchange activates the Rab protein allowing it to interact with effector proteins to help facilitate trafficking in its respective pathway. In its active form, the Rab protein is inserted into the appropriate membrane with the help of GDP dissociation inhibitor (GDI) dissociation factor (GDF). This alternation between active and inactive states is known as the Rab cycle.

Ras, Rho, and Rab family members are prenylated at the C-terminal cysteines (Andres et al., 1993; Desnoyers et al., 1996). The addition of this prenyl group allows for membrane targeting and the proper functioning of Rab proteins. Ras and Rho family proteins are prenylated by farnesyl transferase (FTase) or geranyl geranyl transfer I (GGTase I). Rab proteins are targeted by Rab geranyl geranyl transferase II (Rab GGTase II), which prenylates a five amino acid motif that consists of two adjacent

cysteines in any orientation, for example XXXCC, XXCCX, CCXXX, XCCXX, and in rare occasions CXXX, where X is any amino acid (Casey and Seabra, 1996; Gallegos et al., 2012). These motifs are not directly recognized by GGTase II, but instead by Rab escort proteins (REP) (Rak et al., 2004). REPs form a complex with Rab proteins through their Rab-binding platform and C-terminal binding region, which allows the binding of Rab GGTase II to become prenylated on one or both C-terminal cysteines present on the Rab protein. All Rab proteins rely on Rab-REP interactions to undergo prenylation.

Role of Rab7/RAB-7 in regulating endosomal trafficking

One member of the Rab GTPase family is Rab7 (RAB-7 in *C. elegans*). Rab7 is primarily found on the late endosomal member and on MVBs (Hyttinen et al., 2013). It is involved in the maturation of the endosomes from early to late endocytic compartments of the cell. Early endosomes are generally marked by the presence of Rab5, another member of the Rab family (Wilson et al., 2000). As the endosome matures, Rab5 is replaced by Rab7 (Kinchen and Ravichandran, 2010). Removal of Rab7 through RNAi affects the trafficking between the early and late endosomal stages (Vanlandingham and Ceresa, 2009). Interestingly, the loss of Rab7 also blocks the fusion of the late endosome and MVBs from fusing with other membranes, resulting in the accumulation of enlarged, densely packed late endosomes and MVBs. The removal of Rab7 also decreases the size and number of lysosomes. In addition, Rab7 has also been implicated in other roles. For example, Rab7 has been shown to function in the maturation of autophagosomes, as well as biogenesis and maintenance of lysosomes.

Rab7 is regulated by the general upstream effectors typical of Rab GTPases. The homotypic fusion and vacuole protein sorting complex (HOPS), consisting of vacuolar protein sorting 11 (Vps11), Vps16, Vps18, Vps33, Vps39, and Vps41 were initially considered to be GEFs for Rab7 (Pawelec et al., 2010; Wurmser et al., 2000a). However, recent studies suggest that Mon1/Ccz1 are the GEFs of Rab7, while HOPS is just an effector (Borchers et al, 2023). TBC1D15 is one of the known GAPs for Rab7 (Zhang et al., 2005). Rab7 interacts with REP-1 to assist in prenylation (Rak et al., 2004). There are multiple downstream effectors for Rab7. RILP (Rab7-interacting lysosomal protein) and FYCO1 (FYVE (Fab1-YotB-Vac1p-EEA1) and coiled-coil domain containing 1) proteins act in trafficking (Cantalupo et al., 2001). The Mon1/Ccz1 complex functions in the conversion of Rab5 to Rab7 (Kucharczyk et al., 2009; Wang et al., 2002). The heterohexameric HOPS-tethering complex acts as a Rab7 effector and functions in the fusion of the late endosome, autophagosomes, and AP-3 vesicles with lysosomes (Pawelec et al., 2010; Rink et al., 2005). The retromer trafficking complex, composed of sorting nexin subunits and the VPS26/29/35 trimer, regulates retrograde transport from the endosomal system to the trans-Golgi network, while also playing a role in the late stages of endosomal maturation (Liu et al., 2012; McGough and Cullen, 2011). The Rab7-interacting ring-finger protein (Rabring 7) and Rubicon protein control trafficking and fusion with other membranes by interacting with and affecting Rab7 function (Mizuno et al., 2003). In addition to these examples, there are many more interacting protein complexes and effectors of Rab7, highlighting the important role that Rab7 has in the regulation of endo-lysosomal and autophagosomal membrane trafficking in the cell (Hyttinen et al., 2013).

The regulation of RAB-7 GTPase by RabGAP proteins

All the characterized RabGAP proteins to date contain a conserved TBC (Tre2/Bub2/Cdc16) domain (Richardson and Zon, 1995). There are 44 and 17 predicted RabGAP proteins in the TBC domain-containing RAB-specific GAPs families in humans and *C. elegans*, respectively (Hutagalung and Novick, 2011). The TBC domain is the catalytic domain of RabGAP proteins that confer GAP activity. Analysis of the crystal structure of RabGAP proteins revealed that the GAP activity relies on a conserved arginine finger that interfaces with the Rab nucleotide binding pocket to stimulate GTP hydrolysis (Du and Novick, 2001; Rak et al., 2000). Other studies on RabGAP proteins with different Rab substrates also indicate that a glutamine residue can also stimulate GTP hydrolysis (Pan et al., 2006). The Arg- and Glu-finger containing proteins are known as classical RabGAPs. However, in the human genome, 15 unconventional RabGAPs that lack Arg- or Glu-fingers have been identified. These unconventional RabGAPs are further categorized into 5 subcategories, but no substrate has yet been identified for these proteins, suggesting that they use a different mode of action.

There are several identified GAP proteins for Rab7/RAB-7 that use the conserved TBC domain to activate GTP hydrolysis. The GAP Armus/TBC1D2A was the first GAP that was identified to regulate Rab7 (Frasa et al., 2010). Homology models of Armus/TBC1D2A and Rab7 showed that the conserved glutamine from the GAP activates a water molecule that will be used for the hydrolysis of GTP (Pan et al., 2006; Waterhouse et al., 2018). Simultaneously, a conserved arginine from the GAP stabilizes the newly formed GDP leaving group. The positive side chain from the arginine helps stabilize the planar transition-state form of the γ phosphate. Because RabGAPs use this “dual finger”

mechanism as compared to GAPs for Ras GTPases, which rely on a single arginine finger, RabGAPs can still stimulate GTP hydrolysis in catalytically-dead mutant Rab GTPases (De Antoni et al., 2002; Gu et al., 2017).

RabGAP proteins can contain various other domains in addition to the TBC domain. It can contain lipid-binding domains, coiled-coil motifs, LC3-interacting regions, domains that can interact with other small GTPases, and other domains with GAP and GEF activity (Fukuda, 2011). The combination of these domains will determine where the RabGAP will localize to in the cell. Thus, the cellular localization in addition to complementary protein interaction surfaces dictate which RabGAP proteins act on which Rab proteins (Li and Marlin, 2015).

To date, there are four known RabGAPs for Rab7. The first described Rab7-specific GAP was Armus/TBC1D2A (Frasa et al., 2010). It was first identified in a yeast two-hybrid screen for effectors of the Rac1 GTPase. TBC1D2A was found to regulate cell-cell adhesion and E-cadherin degradation. It contains two LC3-interacting domains and one PH domain in addition to its TBC domain. Thus, it has been shown to bind with LC3A and GABARAP-L1, two of the six LC3 proteins that positively regulate autophagy. Overexpression of TBC1D2A blocks endocytosis and degradation of E-cadherin, presumably due to the reduction in the levels of active Rab7 and therefore impaired endosomal maturation and lysosome fusion. Interestingly, RNAi of TBC1D2A stabilizes cell-cell adhesion. This effect is likely due to increased levels of active Rab7 and increased levels of endosomal maturation.

The *C. elegans* ortholog of Armus/TBC1D2A is TBC-2 (Chotard et al., 2010). *In vitro*, TBC-2 has been shown to have GAP activity towards RAB-5 and RAB-7. While it

might be tempting to conclude that TBC-2 in *C. elegans* regulates both RABs, this study only expressed the TBC domain of TBC-2, thus this recombinant protein may not contain all the necessary components for Rab target specificity. Regardless, even if TBC-2 has GAP activity towards RAB-5 and RAB-7, it could be an evolutionarily conserved method to inactive both early and late endosomal markers to allow for the endosome to fuse with other vesicles. Essentially, TBC-2 would be a safety net that inactivates RAB-5 if RAB-5-specific GAPs are absent. There is another protein, TBC1D2B, that has 63% protein sequence similarity and identical domain structures as Armus/TBC1D2A (Letunic et al., 2015; Sievers and Higgins, 2018). It can also bind with various LC3 proteins, similar to TBC1D2A (Behrends et al., 2010). However, no Rab specificity has been shown for TBC1D2B (Stroupe, 2018).

The second Rab7-specific GAP is TBC1D5 (Seaman et al., 2009). It was first identified as a retromer-binding protein. Retromer proteins are involved in protein sorting in the endocytic pathway, recycling to the plasma membrane, and trafficking between the endosome and trans Golgi network (Arighi et al., 2004; Yin et al., 2013). The retromer is an effector of Rab7/Ypt7p. It consists of a five-subunit complex that is made of two subcomplexes: a cargo-binding trimer of Vps26, Vps29, and Vps35, and a membrane-binding dimer of sorting nexins (Liu, 2016). TBC1D5 interacts with the retromer via Vps29 and this interaction could promote retromer function (Jia et al., 2016). When TBC1D5 function is compromised either through RNAi or CRISPR-mediated deletion, retromer function is decreased, suggesting that the function of the retromer may be negatively regulated by GTP-bound Rab7 activity (Jimenez-Orgaz et al., 2018; Popovic et al., 2012). However, it is important to note that the exact function of TBC1D15 on retromer activity

is hotly debated and is an active field of research. Lastly, similar to Armus/TBC1D2A and TBC1D2A, TBC1D5 co-localizes with LC3 machinery and plays a role in autophagy by interacting with an integral membrane protein Atg9 and a kinase Ulk1 that initiate autophagosome biogenesis (Popovic et al., 2012; Young et al., 2006; Zavodszky et al., 2013). Thus, the knockdown of TBC1D5 expression prevents the formation of LC3-positive structures such as autophagosomes, presumably because of overactive Rab7 activity (Popovic et al., 2012).

TBC1D15 is another Rab7 GAP that localizes to the mitochondria to regulate mitochondrial physiology (Yamano et al., 2014). TBC1D15 binds to the mitochondrial fission regulator Fis1/*fis-1* and is dependent on Fis1/*fis-1* for localization to the mitochondria (Onoue et al., 2013; Yamano et al., 2014). As such, a loss of either TBC1D15 or Fis1/*fis-1* results in the accumulation of autophagosomes and reduced mitophagy (Yamano et al., 2014). TBC1D15 also interacts with LC3 complex components through its LC3-interacting domain. When TBC1D15 is absent, the autophagosomes grow unusually large, presumably due to an excess of active Rab7. RNAi of Rab7 in TBC1D15$^{-/-}$ cells suppresses this defect, suggesting that the cause of the large autophagosomes is indeed due to Rab7 activity.

TBC1D15 also regulates mitochondrion-lysosome contacts (Wong et al., 2018). These contact sites are mediated through active Rab7 activity and are critical for mitochondrial fission. Expression of a GTPase-deficient Rab7 mutant or a GAP-deficient TBC1D15 mutant reduces the number of mitochondrion-lysosome contacts and therefore causes elongated mitochondrion. Consistent with the role of Fis1 in proper TBC1D15 localization, a Fis1 mutant that cannot bind to TBC1D15 also results in the loss of

mitochondrion-lysosome contacts. On another note, TBC1D15 has been shown to interact with Vac14, a scaffolding protein that stimulates PIKfyve, a kinase that phosphorylates PI(3)P to generate $PI(3,5)P_2$, however the significance of this interaction is unknown (Schulze et al., 2014). TBC1D15 also interacts with Rab5 GTPase and is speculated to prevent premature Rab7 activation at the early endosomes, thereby allowing more cargo to accumulate (Itoh et al., 2006). TBC1D15 also interacts with TBC1D17, but neither the Rab target of TBC1D17 nor the significance of the TBC1D15:TBC1D17 interaction have been described (Yamano et al., 2014).

The last identified GAP protein of Rab7 is Gyp7p. Gyp7p is a GAP for Ypt7p, the yeast ortholog of the Rab7-like protein (Brett et al., 2008; Vollmer et al., 1999). There are no other known domains of Gyp7p, asides from the presence of a TBC domain (Yamano et al., 2014). The deletion of Gyp7p has almost no phenotype, except for a small increase in vacuole size, probably due to increase homotypic vacuole-vacuole fusion mediated by Ypt7p/Rab7 (Brett et al., 2008). Conversely, Gyp7p overexpression causes vacuole fragmentation and blocks vacuole fusion. Interestingly, Gyp7p deletion does not affect autophagy, despite its target Rab Ypt7p being essential for autophagy (Wurmser et al., 2000b).

Biogenesis of multivesicular bodies

In this study, we will focus on the role of Rab7 in the formation of late endosomes and eventually exosomes through the fusion of MVBs with the plasma membrane. The early endosome is marked by the presence of Rab5/*rab-5* (Kinchen and Ravichandran, 2010). Rabex5 is the GEF of Rab5 and activates Rab5 activity (Zhu et al., 2007).

Rab5/*rab-5* promotes the maturation of endosomes by recruiting effectors such as VPS34/*vps-34*, which increases the abundance of phosphatidylinositol 3-phosphate (PI(3)P) on the endosomal structures. The PI(3)P further recruits more Rab5, therefore creating a strong positive feedback loop in endosomal maturation (Shin et al., 2005).

The critical step in endosomal maturation is the transition from Rab5 to Rab7. The Mon1-Ccz1 protein complex displaces Rabex5 and activates a VPS39 from the HOPS complex (Wang et al., 2002). This action simultaneously decreases Rab5 function and activates Rab7 activity. Mon1/*sand-1* inhibits the activation of Rab5 to prepare for the exchange of Rab5 for Rab7 on the endosomes. Studies show that Mon1-Ccz1 must bind cooperatively to sequester Rab5 from the endosomal membrane and precedes the localization of Rab7 to the endosome (Kinchen and Ravichandran, 2010; Poteryaev et al., 2010). Once sufficient levels of Rab7 have been embedded in the membrane, it is ready for fusion with lysosome.

Other studies have shown that VPS39 from the HOPS complex is not the GEF for Rab7, rather it is Mon1-Ccz1 itself, as shown in yeast (Poteryaev et al., 2010; Vieira et al., 2003). This finding was further supported by a study of the *C. elegans* orthologue of Mon1, *sand-1*, where the loss of either *sand-1* or *rab-7* results in a similar phenotype, the accumulation of giant early and late endosomes due to blocked early endosomal maturation (Poteryaev et al., 2007). A knockdown of *rab-5* did not show the same phenotype, suggesting that SAND-1 is acting as a GEF for RAB-7 in *C. elegans*. Interestingly, the knockdown of *sand-1* does not affect Rab7 function at the lysosomes.

The association of Mon1-Ccz1 to the early endosome must be carefully timed, as the endosome must accumulate enough cargo for degradation before maturation and

eventual fusion with the lysosome. There are two hypotheses for the regulation of the timing of Mon1-Ccz1 recruitment. Mon1/*sand-1* has been suggested to be able to detect levels of PI(3)P (Vieira et al., 2003). The accumulation of PI(3)P is critical for the recruitment of Mon1-Ccz1 complex, as this complex binds to endosomes enriched with PI(3)P. Another hypothesis is that change of pH and the acidification of the endosomal lumen could be a critical factor in the inactivation of Rab5 and recruitment of Rab7 (Binder and Holzhütter, 2012).

At this stage, the late endosome can undergo further maturation to become a multivesicular body. The endosomal membrane undergoes membrane invaginations to form intraluminal vesicles to eventually form a multivesicular body (Hurley et al., 2010). In the process of undergoing invaginations, cargoes, such as proteins, lipids, or nucleic acids, are specifically sorted into these intralumenal vesicles. There are many mechanisms governing the formation of the multivesicular body. Generally, these mechanisms are sorted into either endosomal sorting complex required for transport (ESCRT)-dependent and ESCRT-independent pathways (Han et al., 2022).

The ESCRT complex consists of a series of subcomplexes, ESCRT-0, ESCRT-I, ESCRT-II, and ESCRT-III, and the ATPase VPS4, that act in a stepwise manner (Vietri et al., 2020). The ESCRT-0 subcomplex is composed of Hrs and STM proteins. Using their ubiquitin binding domains, they recognize mono- or poly-ubiquitinated cargo proteins and tether this cargo to clathrin-coated microdomains on the limiting membrane of the endosome using their FYVE zinc finger domain that binds to PI(3)P. Then ESCRT-I and ESCRT-II are recruited to form a saddle-shaped protein complex, creating an ESCRT-III binding site (Schöneberg et al., 2017). Using the energy generated from ATP hydrolysis

events by VPS4, ESCRT-III subcomplexes undergo sequential polymerization and drive membrane deformation and fission to produce an intralumenal vesicle (Pfitzner et al., 2020). The formation of the ESCRT complex leads to the recruitment of deubiquitination enzymes to remove ubiquitin from cargo proteins before incorporation into the vesicles, however, this step is not mandatory for all cargoes. Two other auxiliary pathways, the Alix- and HD-PTP-dependent pathways, use different mechanisms to capture its cargo, however they both eventually impinge on the activity of ESCRT-III and VPS4 to complete membrane invagination (Baietti et al., 2012). The ALG-2 interacting protein X (Alix)-dependent pathway relies on the activity of the Syndecan-Syntenin-Alix pathway, where both Syndecan and Syntenin recognize cargo in a ubiquitin-independent manner (Baietti et al., 2012; Dores et al., 2016). In the HD-PTP-dependent pathway, HD-PTP binds to ESCRT-0 or ESCRT-I and recruit ESCRT-III and VPS4 to complete the formation of the intralumenal vesicle (Kazan et al., 2021).

Multivesicular bodies are also formed through ESCRT-independent pathways. Exosomes are rich in cholesterol, sphingolipids, phosphatidylserine, and ceramide, a composition that resembles membrane lipid rafts (Dawson, 2021; Skotland et al., 2019). Thus, it has been proposed that components of lipid rafts have key functions in ESCRT-independent intralumenal vesicle formation. The nSMase2-ceramide-dependent pathway is the most characterized ESCRT-independent mechanism (Trajkovic et al., 2008). nSMase2 is an enzyme that converts sphingomyelin into ceramide. Blocking the activity of nSMase2 prevents the sorting of specific cargo, such as proteolipid protein, prions, and several RNAs, into intralumenal vesicles, suggesting that the production of ceramide is critical to the invagination of the endosomal membrane (Guo et al., 2015; Trajkovic et al.,

2008). The exact mechanism in which ceramide promotes endosomal membrane invaginations is unknown. However, studies speculate that because ceramide can self-oligomerize through hydrogen bonding, it can form large macrodomains to trap other molecules such as CD95 and CD40 to traffic specific cargo into vesicles (Gulbins and Kolesnick, 2003; Savio et al., 2020). The cone-shaped structure of ceramide induces spontaneous negative curvature of the membrane, promoting the invagination of the membrane. More research is needed to identify whether ceramide requires the activity of other proteins to promote the deformation and fission of the endosomal membrane. In addition, other components of lipid rafts, such cholesterol, cholesterol-binding protein caveolin-1 and flotillins, are implicated in the capturing of cargo and the formation of intralumenal vesicles (Albacete-Albacete et al., 2020; Eden et al., 2016; Phuyal et al., 2014). Tetraspanins, which are a family of membrane scaffold proteins that incorporate proteins into tetraspanin-rich microdomains and coupled with apolipoproteins (eg. CD63 with Apo-E), promote intralumenal vesicle formation (Kummer et al., 2020; van Niel et al., 2011).

Function of multivesicular bodies

The mature MVBs can fuse with other mature MVBs or with other vesicles within the cell. Under certain conditions, autophagosomes can fuse with MVBs to form amphisomes, which are categorized as a special type of mature MVB (Zhao et al., 2021). These amphisomes can then fuse with the lysosome to degrade the contents of the MVB or fuse with the plasma membrane to secrete the exosomes. There is another special type of MVB known as the recycling endosomal MVB found in some cancer cell lines and

is marked by Rab11/*rab-11* and is distinct from CD63+ MVBs/late endosomes (Savina et al., 2005). Glutamine depletion or mTORC1 inhibition promotes the generation of these recycling endosomal MVBs and the secretion of Rab11+ exosomes that are supposed to be recycled instead (Fan et al., 2020). In neutrophils, MVBs can be derived from the nuclear envelope (Arya et al., 2022). Similar to the recycling endosomal MVBs, these nuclear envelope-derived MVBs are distinct from CD63+ MVBs in size and composition, and instead are rich in 5-lipoxygenase (5-LO)/5-LO activating protein (FLAP). These examples show that MVBs are highly heterogeneous, and their composition and size are dependent on their origin and maturation route. Given the heterogeneity of MVBs, the exosomes are also categorized according to their composition, size, and their origin.

The multivesicular body now has two fates (Han et al., 2022). It can undergo fusion with lysosomes to degrade their content. These MVBs are known as degradative MVBs (dMVBs). Alternatively, it can be transported to the plasma membrane by intracellular molecular motors where the MVB fuses with the plasma membrane to secrete the intralumenal vesicles into the extracellular space as exosomes. These MVBs are known as secretory MVBs (sMVBs). This decision between degradation and secretion is controlled by the activity of Rab7. However, depending on the context and the organism, the activation of Rab7 can lead to different MVB fates.

There are examples where the inactivation of Rab7 promotes the secretion of exosomes. In HEK293T and HeLa cells, the Arl8b/SKIP/HOPS cascade recruits a Rab7 RabGAP TBC1D15 to trigger Rab7 GTP hydrolysis to remove Rab7 from the late endosome/MVB membrane (Jongsma et al., 2020). After the removal of Rab7, the kinesin motors move the MVBs/late endosomes towards the plus-end, poising the entity for fusion

with the plasma membrane. Alternatively, RILP, a Rab7 effector, initiates dynein-dependent retrograde transport of the MVBs/late endosomes towards the minus-end. Another group also showed that Rab31 recruits the Rab7 RabGAP TBC1D2B to inactivate Rab7, thereby blocking the fusion of the MVB with the lysosome and instead promoting the fusion of the MVB with the plasma membrane for exosome secretion in HeLa and HEK293T cells (Wei et al., 2021). Supporting these findings, the activation of the Rab7 GEFs, Mon1a/b and neddylated Coro1a, activate Rab7 and inhibit exosome biogenesis (Fei et al., 2021).

Alternatively, there are some examples in which the activation of Rab7 is required for the formation and secretion of these exosomes. The knockdown of Rab7 in MDA-MB-231 breast cancer cells reduces the biogenesis, and subsequent secretion, of MVBs from the Syntenin-Syndecan-Alix-dependent and ESCRT-dependent pathways (Baietti et al., 2012). Additionally, removal of Rab7 function in HCT116 colorectal cancer cells inhibits exosome release and instead promotes the release of Rab11+ recycling MVB-derived exosomes (Fan et al., 2020). Compromise of Rab7 or the RAB7-binding kinesin-1 adaptor FYCO1 also inhibits the secretion of exosomes containing the matrix metalloproteinase MT1-MMP from small actin-rich membrane protrusions called invadopodia (Beghein et al., 2018; Pedersen et al., 2020). In summary, these examples show that Rab7 plays different yet critical roles in the regulation of MVB/exosome biogenesis and exosome secretion in different models.

The transport, tethering/docking, and fusion with the plasma membrane of the secretory MVBs are highly dependent on the activity of Rab GTPases. Through RNAi analyses in HeLa cells, many Rab proteins have been identified to be involved in the

regulation of exosome function, including Rab2b, Rab9a, Rab5a, Rab27a and Rab27b (Ostrowski et al., 2010). Rab27a and its effectors, Slp4 and Munc13-4, play critical roles in the docking of MVBs to the plasma membrane, while Rab27b and its effector Slac2b regulates the transport of the MVBs from the minus to the plus end of the cell. Focusing on Slp4, it interacts with Rab27a through its N-terminal Slp homology domain and binds to SNARE complex via a central linker region, and the disruption of this interaction reduces exosome secretion in breast cancer cell lines (Alnaas et al., 2021). Munc13-4 interacts with several Syntaxins, including Syntaxin-1/2/4/7/11, which are components of SNARE complexes, to regulate membrane fusion and exocytosis (Boswell et al., 2012; He et al., 2016; Woo et al., 2017). The DENN domain-containing protein Rab3GEP/MADD and FAM45A are GEFs of Rab27a, while TBC1D10A/EPI64 is a GAP of Rab27a (Imai et al., 2013; Itoh and Fukuda, 2006). Other proteins are also involved in the regulation of Rab27a activity. KIBRA, a scaffolding protein involved in cell polarity, cell migration, and membrane trafficking primarily expressed in the kidney and brain, stabilizes Rab27a, preventing the proteasomal-mediated degradation of Rab27a and increasing the levels of exosome secretion (Song et al., 2019). Additionally, other Rab proteins and their effectors, such as Rab35, Rab11a, Rab17, Rab20, Rab37, and Rab39, are involved in exosome biogenesis or secretion in different experimental models (Han et al., 2022).

The soluble N-ethylmaleimide-sensitive fusion attachment protein receptor (SNARE) complex is involved in the fusion of the MVB with the plasma membrane (Yoon and Munson, 2018). Briefly, SNARE proteins constitute a large protein family that is primarily involved in the fusion of vesicles with a target membrane. These proteins are

usually post-translationally inserted into membranes through their C-terminal transmembrane domain or through post-translational lipid modifications such as palmitoylation (Han et al., 2017). All SNAREs share a SNARE motif in their cytosolic domain, which is composed of 60-70 amino acids and contains heptad repeats that can form coiled-coil structures. Vesicle-SNAREs (v-SNAREs) and target-SNAREs (t-SNAREs) can reversibly assembly into tight, four α-helix bundles called “trans”-SNARE complexes or a SNAREpin. In synaptic vesicles carrying neurotransmitters, a typical trans-SNARE complex is composed of syntaxin and SNAP-25 (t-SNAREs) on the target cell membrane, and synaptobrevin and synaptotagmin (v-SNAREs) on the vesicular membrane (Zhou et al., 2015). After fusion of the two membranes, the SNARE complex is disassembled by the adaptor protein, α-SNAP and the hexameric ATPase, NSF to unfold the SNARE proteins in an ATP-dependent process (Littleton et al., 2001; Marz et al., 2003). The SNARE proteins are then released and recycled to the appropriate membranes. Different SNARE complexes are proposed to mediate the fusion of the MVB with the plasma membrane in different model systems: SNAP25 and VAMP5 in bone marrow mesenchymal stem cells; SNAP23 and VAMP3 in hepatocellular carcinoma; VAMP7, Syntaxin-4, and SNAP23 in MDA-MB-231 human breast cancer cells; syntaxin-6 in prostate cancer; VAMP3 in neurons (Han et al., 2022).

In *C. elegans*, a small GTPase RAL-1 is involved in MVB biogenesis and its fusion with the plasma membrane (Hyenne et al., 2015). This protein was first identified in an RNAi-based screen designed to identify regulators of exosome secretion by epidermal Hyp cells and contribution to the formation of the alae. Electron microscopy analysis indicates that RAL-1 localizes to the membranes of secretory MVBs. In *ral-1* mutants,

sMVB were dramatically affected; the number of MVBs at the epidermal cell surface and the diameter of the MVBs were increased, while the number of intralumenal vesicles per MVB decreased. Overall, these data suggest that RAL-1 could be responsible for MVB formation or diverting MVBs destined for degradation towards secretion instead. The analyses of two null mutants of two exocyst subunits, an octameric protein complex that catches and tethers exocytic vesicles to the plasma membrane during exocytosis, *sec-5* and *sec-3*, reveals that the regulation of MVB formation and secretion do not require the exocyst complex, a common RAL GTPase effector. From the same RNAi screen, *syx-5*, a t-SNARE gene from the syntaxin family involved in anterograde ER-Golgi trafficking, was identified to be critical for the formation of alae in the L1 stage. Using classic genetics, they found that SYX-5 colocalizes with a constitutively active RAL-1 variant, but not with a dominant negative version of RAL-1, suggesting that RAL-1 may recruit SYX-5 to mediate the fusion of the MVB with the plasma membrane. When SYX-5 is absent, the MVBs cannot fuse with the plasma membrane, resulting in the accumulation of MVBs at the cell periphery. From the same study, the authors showed that in mammary tumour cells, RalA and RalB are required for the fusion of the MVB with the plasma membrane to secret exosomes into the culture media. Therefore, in addition to the activity of Rab GTPases, the Ral GTPases serve as another set of regulators of MVB biogenesis and fusion.

Characterization of exosomes

When exosomes were first described in 1983 while studying the maturation process of reticulocytes into erythrocytes, exosomes were thought to serve as a form of garbage disposal, filled with cellular junk to be excreted from cell (Harding and Stahl, 1983; M et al., 2017; Pan and Johnstone, 1983). These vesicles were shed from the cultured monolayer cells, but retained the transferrin receptor and other membrane-associated proteins. Consistent with the known role of degradative MVBs, the MVBs were thought to fuse with lysosomes to degrade the contents of the intralumenal vesicles and exosomes were thought to function as another method for the cell to remove unwanted material without degradation.

13 years later in 1996 when studying antigen presentation in B lymphoblastoid cells, it was demonstrated through electron microscopy that “characteristic internal membrane vesicles” with MHC class II molecules can fuse with the plasma membrane, releasing the exosomes into the cell culture media (Raposo et al., 1996). They isolated these exosomes from human and murine B lymphocytes using differential centrifugation and found that the protein composition of these exosomes was different compared to the plasma membranes of the donor cells. Next, they incubated these exosomes with a peptide, 418-427, that was known to stimulate an immune response in T cells, presumably, to allow it to bind to the MHC class II receptor on the exosome. These exosomes were then washed to remove unbound peptide, then incubated with T cell clones. Compared to exosomes that were not incubated with peptide, the exosomes bound with 418-427 were able to stimulate T cell responses, demonstrating for the first time that exosomes were not simply garbage trucks but could convey physiological effects

and could perhaps be a novel means of cell-cell communication. Since then, there has been a plethora of studies demonstrating the role of exosomes in intercellular communication in both normal physiology, such as lactation, inflammation, cell proliferation, immune response, and neuronal function, and in disease contexts, such as cancer, metabolic diseases, developmental delays, and neurodegenerative diseases (Harding et al., 2013; M et al., 2017).

Exosomes are highly heterogeneous. The characteristics of the exosomes differ in size, content, cellular origin, and can even have pleiotropic effects on recipient cells (Kalluri and LeBleu, 2020). Depending on the microenvironment and the physiological status of the cell, cells may incorporate different cargoes and biological markers into their exosomes. This difference in exosomal content may then influence the size of the exosome and the resulting pleiotropic effects on the recipient cell. Proteomic analysis and exosomal miRNA-sequencing reveal that not all exosomes have the same set of cargo nor the same abundance of each cargo type (Chevillet et al., 2014; Kowal et al., 2016). The heterogeneity of the exosomes is also determined by the donor tissue or cell type. Distinct proteins and nucleic acids are enriched in exosomes depending on their origin, suggesting that different cell types use specific protein and nucleic acid sorting machinery to load exosomal/intralumenal vesicle (Kalluri and LeBleu, 2020). Interestingly, the same batch of isolated exosomes can have varying effects on different receiving cell types. For example, the same exosomes can induce opposite cellular effects, such as cell survival and apoptosis. These observations could be explained by the difference in expression of SNARE proteins expressed on the receipt cells with different cell types taking up a different portion of a heterogenous mixture of exosomes, resulting in different phenotypes

(Wen et al., 2019). Thus, a combination of all these factors that influence the biogenesis and cargo-sorting of exosomes and the difference in machinery involved in the uptake of these exosomes lead to a higher order of complexity and heterogeneity in the physiological effects of exosomes.

Many different types of extracellular vesicles (EVs) have been characterized (Théry et al., 2018). The classical EVs are exosomes, microvesicles, and apoptotic bodies, while recent discoveries have described autophagic EVs, stressed EVs, and matrix vesicles (Sheta et al., 2023). While they carry different biomarkers and content to influence the fate of their receipt cells, they share common properties as cell-derived, lipid bilayer-surrounded vesicles. EVs are classified based on their biogenesis mechanism, content, and size. Briefly, exosomes are derived from MVBs that fuse with the plasma membrane and belong in the small EV class that range from 40-150 nm in diameter. Classical exosomes have CD63, CD9, and CD81 markers, while non-classical exosomes do not have any known markers. Microvesicles are derived from shedding of vesicles from the plasma membrane and are further categorized into three subcategories of classical microvesicles, large oncosomes, and ARMMs, which belong to the large (~150-1000 nm), large (1-10 μm), and small EV (~40-100 nm) classes, respectively. The classical microvesicles and large oncosomes are marked with annexin A1 and ARF6, while ARMMs are marked with ARRDC1 and TSG101. Apoptotic EVs are generated from vesicles that arise during the process of apoptosis and are subcategorized as apoptotic bodies and apoptotic vesicles, which belong to the large EV (1-5 μm) and small-to-large EV (~100-1000 nm) classes, respectively. Both are marked with annexin V and phosphatidylserine (PS).

Due to the large increase in the recent number of studies on exosomes involving different contexts and model systems, the International Society for Extracellular Vesicles (ISEV) published a set of standards for the proper characterization of EVs (Lötvall et al., 2014; Théry et al., 2018). Most eukaryotic cells can secrete EVs, including exosomes, microvesicles, microparticles, ectosomes, oncosomes, apoptotic bodies, and many others. These guidelines require meticulous information on the preparation methods and characterization results before ascribing specific functions to isolated EVs in all studies. For example, many bulk preparatory methods such as differential centrifugation followed by sucrose density gradient centrifugation can lead to a potentially contaminated and heterogeneous mixture of exosomes. Thus, the guidelines, the Minimal Information for Studies of Extracellular Vesicles in 2014 (MISEV2014) and MISEV2018, provide researchers with suggested protocols to ensure that the isolated EVs are homogeneous and properly categorized by their tissue and trafficking pathway of origin.

Sorting of cargo and miRNAs to exosomes

The primary function of exosomes is to facilitate intercellular communication. Until now, many different types of cargo have been observed in purified exosomes, including lipids, proteins, and various types of nucleic acids like mRNA, miRNAs, long non-coding RNAs (lncRNAs), circular RNAs (circRNAs), PIWI-interacting RNAs (piRNAs), and DNA (Kalluri and LeBleu, 2020). The loading of various types of cargo is dependent on the physiological status of the cell. Thus, the sorting of cargo into exosomes is a tightly controlled process.

Proteins can be sorted into exosomes through different pathways, mainly categorized into ESCRT-dependent and -independent pathways (Han et al., 2022). In the ESCRT-dependent pathways, proteins that are destined for sorting into intralumenal vesicles interact with the ESCRT-0 and VPS34. Other proteins can interact with HSP90α through interactions with a Rab coupling protein.

In a mouse cancer model, mutant p53 enhances the trafficking of HSP90α to exosomes for secretion (Zhang et al., 2020b). Through co-immunoprecipitation assays in three p53-null cell lines, they identified Rab11FIP1C, which is also known as Rab interacting protein (RCP)) as the upstream regulator of HSP90α sorting into exosomes. RCP contains a Rab11-binding motif in its C-terminus, which allows the sorting of cargo into Rab11a+ endosomes using RCP as an adaptor protein. Interestingly, the osteosarcoma Rab22a-NeoF1 fusion protein and their binding partner PYK2 are sorted by HSP90α through interactions with four putative KFERQ-like motif on the fusion protein (Zhong et al., 2021). The Rab22a-NeoF1 fusion protein/PYK2/HSP90 complex is then incorporated into intralumenal vesicles in an ESCRT-dependent pathway. Additionally, many other sorting pathways that impinge on the ESCRT pathway cytosolic have been shown, such as the sorting of AGO2 by Alix and cytosolic proteins by Hsc70 (Géminard et al., 2004; Iavello et al., 2016). There are also examples of ESCRT-independent sorting pathways, such as the sorting of KFERQ motif-containing proteins by LAMP2A and Hsc70, which requires Alix, Syntenin-1, Rab31, and ceramides (Ferreira et al., 2022). Overall, these examples highlight the selectivity and the complex protein-protein interactions necessary for the targeting of particular cargo into intralumenal vesicles that are destined for secretion as exosomes.

The sorting and secretion of DNA by exosomes is shrouded with contradictions, with different groups reporting different conclusions. This problem is compounded by the fact that many studies that show the secretion of DNA by exosomes were conducted in disease models or models involving cellular stress. One group showed that the secretion of DNA and histones were mediated by an exosome-independent process, while others showed that genomic DNA and nuclear proteins were selectively sorted into exosomes (Jeppesen et al., 2019; Takahashi et al., 2017). In ovarian cancer cells, genomic DNA and nuclear proteins interact with tetraspanin proteins, such as CD63 to be sorted into exosomes (Yokoi et al., 2019). In the cancer microenvironment, the cystine-glutamate antiporter, xCT is upregulated to help the cancer cells produce the antioxidant glutathione (Rabas et al., 2021). The upregulation of xCT in turn activates the metabotropic glutamate receptor 3 (mGluR3), which stimulates the Rab27-dependent release of exosomes. These exosomes are rich in mitochondrial DNA, which is loaded through a PINK1-dependent manner. The mitochondrial DNA in the exosomes activates Toll-like receptor 9, further promoting invasive cancer behaviours in the recipient cells. However, how the mitochondrial DNA is transferred out of the mitochondrial matrix and into the intralumenal vesicles is unknown. Further studies are needed to assess if nuclear DNA and proteins are also loaded into intralumenal vesicles using similar mechanisms as the mitochondrial DNA.

The sorting of RNA, particularly miRNAs has been a subject of interest in the recent years. Generally, RNA is sorted into exosomes by interacting with sequence-specific RNA-binding domains of RNA-binding proteins (RBPs) (Fabbiano et al., 2020; Han et al., 2022). Theses RBPs are then sorted into exosomes through protein-protein interactions.

Many RBPs have been implicated in the sorting of RNA into exosomes, including hnRNPA2B1, hnRNPK, YBX1, major vault protein (MVP), MEX3C, synaptotagmin-binding cytoplasmic RNA-interaction protein (SYNCRIP), Ago2, and FMR1, in different cell models and model systems (Han et al., 2022). It has been shown that hnRNPA2B1 and hnRNPA1 are involved in the loading of lncRNAs into exosomes (Chen et al., 2020a). SNF, a subunit of ESCRT-II, and hnRNPA2B1 load circRNAs into exosomes in glioma and colorectal cancer models (Chen et al., 2022; Pan et al., 2022). The exact mechanisms involved in the sorting of all these various types of RBPs into exosomes have not been precisely described, but the use of caveolin-1 and LC3-conjugation machinery have been described (Leidal et al., 2020; Robinson et al., 2021). In prostate and colorectal cancer cell lines, the heterogeneous nuclear ribonucleoprotein K (hnRNPK) binds miRNAs with AsUGnA motifs and interacts with the structural membrane protein caveolin-1 to be sorted into intralumenal vesicles (Chen et al., 2022). Components of the autophagy system also specify the secretion of cellular material within EVs. Two RBPs, hnRNPK and scaffold-attachment factor B (SAFB), interact with the MAP1LC3B (LC3)/ATG8 conjugation machinery to be secreted in EVs enriched with lipidated LC3 (Leidal et al., 2020). However, it is unknown how these RBPs such as hnRNPA2B1 and hnRNPK, which normally reside in the nucleus, are translocated into the cytoplasm for loading into the intralumenal vesicles.

Many of the aforementioned proteins are commonly found in liquid-liquid condensates (Han et al., 2022). These condensates, such as RNA granules, stress granules, and P-bodies, are ubiquitous membraneless compartments that are enriched with RBPs and RNAs (Alberti et al., 2019). Many target cargoes like hnRNPK and SABF

that are loaded in exosomes by the LC3-conjugated machinery are components of RNA granules (Leidal et al., 2020). The cargoes, as well as LC3 itself, colocalize with Rab5, a marker of early endosomes. hnRNPA2B1, which is well-studied for its ability to bind to the sequence motifs on miRNAs and target miRNAs for exosome-mediated secretion, is also found in liquid-liquid condensates and is a component of RNA granules (Ryan et al., 2018). Put together, these data suggest that condensates may be an important regulatory step of the loading of exosomes, where the condensate acts as a “pre-sorting” station before the cargo is either funneled towards secretory MVBs or targeted by other pathways towards degradative MVBs. There is some evidence that liquid-liquid condensates play a direct role in targeting miRNAs into intralumenal vesicles. The Y-box binding protein 1 (YBX1) has been previously found to be enriched in EVs and is required for the sorting of miR-223 into exosomes (Liu et al., 2021). Closer analysis of the YBX1 protein sequence reveals that it contains an intrinsically disordered region (IDR) that indicates that this protein may undergo phase separation. Introduction of point mutations in this IDR prevents YBX1 from undergoing phase separation and impairs miR-223 from being sorted into exosomes. These findings provide a possible mechanism in which components of liquid-liquid condensates can target specific miRNAs for incorporation into intralumenal vesicles. Interestingly, lncRNAs have also been shown to play a key role in the formation of liquid-liquid condensates (Roden and Gladfelter, 2021; Wang et al., 2021). Thus, one active field of study now is to determine whether lncRNA coordinates with RBPs to form condensates to facilitate the targeting of the miRNA-RBP complex for exosome incorporation.

Proteins are not the only determining factor of whether RNAs are sorted into exosomes. When assessing whether certain RNAs were specifically sorted into exosomes, the levels of miRNAs were drastically different in exosomes and in whole-cells, suggesting that there must be some level of regulation that actively sorts RNAs into exosomes (Villarroya-Beltri et al., 2013). Multiple alignment analysis of these exosome- and cell-enriched miRNAs showed an overrepresentation of two exosome motifs (EXOmotifs) and a cellular retention motif (CLmotif or CELLmotif), respectively. These motifs are short sequences, four to six nucleotides long, that can be found anywhere on the mature miRNA. Mutagenesis of these motifs affects the localization of the corresponding miRNAs. For example, converting the CELLmotif of miR-17 into an EXOmotif targets miR-17 into exosomes, whereas converting the EXOmotif of miR-601 into a CELLmotif retains miR-601 from secretion (Garcia-Martin et al., 2022). These data suggest that specific short motifs present on miRNAs determine whether the miRNA is sorted into exosomes or retained in the donor cell. Through pull-down assays targeting the EXOmotif of miR-198 or the CELLmotif of miR-17, hnRNPA2B1 and hnRNPA1 were identified to bind to only EXOmotifs and not CELLmotifs. Further experiments show that hnRNPA2B1 were found in exosomes and confocal analysis showed that hnRNPA2B1 colocalizes with MVB markers. Moreover, hnRNPA2B1 requires sumoylation to be preferentially sorted into exosomes. Inhibiting the sumoylation of hnRNPA2B1 decreases the levels of miR-198 bound to hnRNPA2B1 and in exosomes. Another study demonstrated that different tissue types preferentially use different EXOmotifs or CELLmotifs to sort miRNAs (Garcia-Martin et al., 2022). Another set of RBPs, Alyref, Rbmx, Sdpr, Fus, and Syncrip, was identified to be involved in the binding of the

EXOmotifs and sorting of miRNAs into exosomes. Altogether, these studies show that the sorting of RNA into exosomes is not only dependent on RBPs but also on the short nucleotide motifs on the mature RNA sequences itself, adding another layer of complexity in the targeting of cargo into MVBS for secretion in exosomes.

Physiological effects of exosomal miRNAs in cancer and therapeutics

Once the cargo is sorted into intralumenal vesicles, the MVB can fuse with the plasma membrane to secrete the exosomes into the extracellular space (Han et al., 2022). These exosomes can then be taken up by neighboring or distant recipient cells. Upon fusion of the exosome with the plasma membrane of the recipient cell, the contents of the exosomes are released into the cytosol, where miRISC assembled in the donor cells can now complementary base pair with its target mRNA. This process has been well described in the context of disease like cancer. For example, exosomal miR-105 released from breast cancer cell lines MCF-10A and MDA-MB-231 reduces the expression of the ZO-1 gene in endothelial cells to promote metastasis to the lung and brain tissues (Zhou et al., 2014). The human microvascular endothelial cell line, HMEC-1, secretes exosomal miR-214 to stimulate migration and angiogenesis in neighbouring HMEC-1 cells (van Balkom et al., 2013). Leukemia K562 cell lines secrete exosomal miR-92a to reduce the expression of integrin α5 in the human umbilical vein endothelial cells to enhance cell migration and tube formation (Umezu et al., 2013). Furthermore, because exosomal miRNAs have remarkable stability in blood, urine, and other bodily fluids, the identification and quantification of exosomal miRNAs have been used as a noninvasive biomarker to diagnose disease progression (Mathivanan et al., 2010). For example, the abundance of

let-7a, miR-1229, miR-1246, miR-150, miR-21, miR-223, and miR-23a in exosomes have been used as a diagnostic biomarker for colorectal cancer (Ogata-Kawata et al., 2014).

Exosomal miRNAs also have positive roles in the context of disease. Myocardial ischemia reperfusion injury (MIRI) is a phenomenon when interrupted myocardial blood supply is restored after a certain period of time (Tibaut et al., 2017). The interruption of blood flow is usually caused by an ischemic myocardium that damages the myocardial tissue. The pathogenesis of MIRI is associated with oxygen free-radical injury, intracellular calcium overload, and inflammatory injury. In a MIRI disease model, neonatal rat cardiomyocytes show improved cell survival rate and cardiac function when the expression of ERRFI was reduced by exosomal miR-126 treatment (Wang et al., 2019). Another study also showed that exosomal miR-423-3p secreted by cardiac fibroblasts increases cell viability and reduces apoptosis by downregulating the expression of RAP2C (Luo et al., 2019). Since the first description of the positive effects of exosomal miRNAs in reducing the severity and symptoms of MIRI, many more exosomal miRNAs have been identified to improve the prognosis of not only cardiac diseases but also multiple sclerosis and other central nervous system diseases (Zheng et al., 2021). Intriguingly, exosomal miR-21 and miR-29a, in addition to their canonical role in regulating the expression of target mRNAs, have also been shown to act as ligands that bind to toll-like receptors, TLR7 and TLR8 to activate immune cells (Fabbri et al., 2012). Thus, given the expansive role of exosomal miRNAs in disease diagnosis and treatment, exosomal miRNAs are a promising new stream of RNA-based therapeutics that can target specific genes.

The therapeutic potential for exosomal miRNAs is demonstrated in the evolutionary arms race between plants and fungi pathogens (Hilbi and Haas, 2012; Weiberg et al., 2013). *Botrytis cinerea* is the causative agent in gray mold disease, an aggressive fungal pathogen that infects more than 200 plant species. This fungus causes losses of 10 to 100 billion US dollars annually worldwide, thus there is interest in investing in methods to extinguish this grey fluffy mycelium. When this fungal pathogen infects plant cells, *B. cinerea* sends small RNAs to hijack the host's RNAi machinery to interfere with the expression of plant immunity genes (Weiberg et al., 2013). Thus, decreasing the expression of the host's RNAi machinery therefore increases the severity of the fungal infection. Conversely, the plant host also transfers small RNAs into the pathogen cells to inhibit genes involved with virulence (Cai et al., 2018). This trafficking of small RNAs between host and pathogen is a naturally occurring example of cross-kingdom RNAi, where small RNAs are used as an attack and defense mechanism.

In response to *B. cinerea* infection, *Arabidopsis* cells secrete exosome-like extracellular vesicles to deliver small RNAs into the fungal pathogen cell (Cai et al., 2018). While animal EVs are well categorized, plant EVs do not have specific guidelines. However, analysis of these host EVs shows that they are positive in two tetraspanin genes, TET8 and TET9, where both are structurally similar to CD63 and TSP-7 in mammals and *C. elegans*, respectively. Overall, these findings suggest that the plant EVs are close derivatives of exosomes or could be the plant version of exosomes. Tagging TET8 and TET9 with fluorescent markers showed that the fungal cells absorbed these exosomes within 2 hours of exposure and remained throughout the course of the infection, suggesting that host exosomes are taken up by the fungal cells. Analysis of the

exosomal small RNAs showed that it targets fungal vesicle-trafficking genes to prevent the trafficking of pathogen small RNAs into the host cell. Consistently, the levels of the pathogen mRNAs are downregulated when infected with wild-type *Arabidopsis* plants compared to mutant plants with impaired siRNA biogenesis. Similarly, *B. cinerea* with deletion mutants of these same vesicle-trafficking genes showed reduced virulence on *Arabidopsis*, showing that the host exosomal small RNAs target pathogen trafficking genes to boost host immunity.

Taking advantage of this cross-kingdom RNAi through exosomes, a spray that contains RNA encapsulated by artificial nanovesicles has been developed to combat *B. cinerea* (Qiao et al., 2021). Previous studies have shown that fungal Dicer-like proteins are essential for the production of pathogen small RNAs, and could therefore be a good mRNA target. Indeed, experiments of this RNA-encapsulated nanovesicle spray targeting Dicer-like pathogen genes on commercially-important crops, such as tomatoes, fruits, lettuce, roses, and tobacco plants, showed that these nanoparticles decreased fungal virulence. This spray can extend the shelf-life of products for a few weeks in a cost-efficient manner that is safe for human consumption. Overall, the development of this spray shows that RNA can be efficiently delivered through exosomes/lipid-based nanoparticles, underscoring the importance of exosomes (Qiao et al., 2021).

Exosomes and *C. elegans*

There is a growing body of evidence that exosomes/EVs play an important role in the metabolism, immunity, and aging/life span in *C. elegans* and parasitism in nematodes in general (Duguet et al., 2020; Ma et al., 2023; Nikonorova et al., 2022; Russell et al.,

2020). Most studies in *C. elegans* focus on EVs secreted from the animal, rather than between tissues. Russell et al conducted the first large-scale study of EV composition and RNA content of EVs in *C. elegans* (Russell et al., 2020). Analysis of these EVs secreted from the animal shows that the protein composition of these EVs is quite similar to the proteins found in EVs produced from mammalian models, which is consistent with the conserved nature of the endosomal system. RNA sequencing of these EVs showed that about two-thirds of the RNA content was rRNAs and about 10% accounted for small RNAs. While this study was the first large-scale study of EVs from *C. elegans*, it lacked experiments that confirmed the identity of these particles as true EVs, rather than other small particle sources or EV contamination from bacteria. Duguet et al also conducted RNA sequencing on the RNA isolated from exosomes to compare the miRNA profiles of *C. elegans* in culture to adult parasitic nematodes (Duguet et al., 2020). Consistent with the previous study, mass spectrometry of the isolated EVs revealed that most of the proteins secreted by *C. elegans* were similar to EVs isolated from mammalian systems. miRNA sequencing revealed that about 20% of the conserved, mature miRNAs in *C. elegans* were secreted in exosomes. Some of the most enriched miRNAs include *mir-58*/Bantam, *mir-36*, *let-7*, *mir-10*, *mir-36*, *mir-96*, and the *mir-51* family. Compared to the study by Russell et al, this study took the appropriate measures to ensure the purity of their EVs/exosomes. They conducted transmission electron microscopy to show that their EV population was homogeneous and nanoparticle tracking analysis to show that their median particle size was 107.3 nm. However, this study still lacks the appropriate Western analyses and immunogold labeling experiments to show that their EVs were indeed exosomes. As these studies were focused on creating and comparing datasets,

the authors did not show any functional relevance to the miRNAs or RNA populations identified in these EVs. Regardless, these two studies combined are some of the first published RNA datasets of EVs in *C. elegans*.

There are a few studies in which the physiological relevance of EVs secreted in the culture media or between animals is explored. Recently, Ma et al published a study on the effects of EVs on life span of *C. elegans* (Ma et al., 2023). They found that EVs isolated from dauer larvae extend the life span of adult hermaphrodite animals. By assessing various parameters such as body bending, body length, reproductive capacity, and reactive oxygen species levels of the animals treated with EVs, they concluded that these animals benefited from a "healthier" lifespan. While this study presents some interesting findings on the potential benefits of EVs derived from dauer larvae, it does not identify the components necessary for these effects. The authors did not perform vehicle controls to show that the lifespan extension is due to EVs rather than from the media or other contaminants introduced in the EV isolation process. In addition, the dauer stage is an alternative life stage that is marked for dispersal, sealing of the buccal cavity, and conservation of energy. Thus, this study begs the question of why adult animals whose primary function is to feed and undergo the energy-intensive process of reproduction would benefit from EVs isolated from dauer animals. Further research should be conducted before making sweeping claims about the benefits of EVs.

Another study by Nikonorova et al conducted a large-scale identification of EV cargo shed by *C. elegans* (Nikonorova et al., 2022). Male-specific ciliated sensory neurons secrete PKD-2+ EVs that are transferred to the vulvae of their mating partner. In addition to these male-specific neurons, males and hermaphrodites also possess a set of

six inner labial type 2 ciliated neurons whose cilia are exposed and can release EVs into the environment. Isolation and profiling of these EVs showed an enrichment for proteins involved in nucleotide binding, vesicular dynamics, trafficking, glycoproteins, glycoprotein binding proteins, nucleic acid binding, post-translational modifiers, chaperones, redox proteins, proteases, and scaffolding proteins. They also identified the various RNA- and nucleotide-binding proteins, such as the dsRNA transporter required for the import of environmental RNAi, SID-2, the ortholog of the human ectonucleotide pyrophosphatase/phophodiesterases (ENPPs), ENPP-1, and a DNA helicase minichromosome maintenance protein complex (MCM) component 3, MCM-3. By tagging ENPP-1 in male animals and tracking the movement of this protein in mated hermaphrodites, they were able to observe ENPP-1 in the vulvae, suggesting that ENPP-1 is transferred through EVs during mating. Furthermore, this study highlights the possibility that *C. elegans* also use EVs as a means of RNA-based extracellular communication.

Chapter 1.4 Research Statement

Animals must adapt to their surroundings to ensure survival. This adaptation is highly dependent on communication between the tissues that sense the environment and tissues that regulate development and reproductive capacity. Using the dauer stage of *C. elegans* as a model, the main objective of this study is to study how tissues communicate with each other to ensure that the physiological conditions are aligned with the available nutrients, and what occurs in the tissue after receiving such signal.

In *C. elegans*, during unfavourable conditions such as crowding, high temperature, or starvation, the animal can choose to halt reproductive development and instead enter an alternative life stage termed the “dauer” stage (Fielenbach and Antebi, 2008). Upon entering this stage, the germline stem cells arrest at the G2 cell cycle stage and remain quiescent throughout the diapause. This establishment of quiescence is dependent on LBK1/AMPK signalling (Narbonne and Roy, 2006). The deletion of either LKB1 or AMPK signalling results in germline hyperplasia and a loss of germ cell integrity during the dauer stage. Many animals will die during this diapause and those that recover exhibit a highly penetrant post-dauer sterility (Kadekar and Roy, 2019).

Previously, it has been shown that neuronal AMPK is sufficient for restoring germ cell integrity in AMPK mutants, however, the mechanisms that are engaged downstream of AMPK activation remains unclear (Kadekar and Roy, 2019). Thus, in chapter 2, we conducted an EMS-based forward genetic screen to identify additional regulators of germline stem cell quiescence during the dauer stage (Wong et al., 2023). The results of this screen revealed additional components in the AMPK pathway that are required for the timely establishment of quiescence. In chapter 3, further characterization of the genes from the genetic screen and their interacting proteins will provide an exact mechanism in which a pro-quiescent signal is transmitted from the neurons to the germ line. It has been previously implied that small RNAs are involved in this process, where blocking the biosynthesis of siRNAs or the entry of these siRNAs into the germ line can suppress the AMPK-dependent germline defects (Kadekar and Roy, 2019). Thus, in chapter 3, we also explore how small RNAs might play a role in the regulation of germ cell integrity and germline quiescence in response to environmental stress. Lastly, small RNAs post-

transcriptionally regulate gene expression. Therefore, in chapter 4, we will identify mRNA targets of these small RNAs, so that we can characterize what occurs in the germ line downstream of neuronal AMPK signalling.

The outcome of this research will elucidate some of the mechanisms governing the regulation of germline stem cell divisions. Furthermore, it will uncover a novel mechanism of how RNAs are transported between distant cells and tissues to facilitate intercellular communication. RNA is an inherently unstable molecule that is prone to degradation. Thus, it might be bound and protected by RNA-binding proteins until it is loaded into an Argonaute. The findings of these studies would provide insight into a naturally occurring lipid-based delivery mechanism for RNA, which would allow for the further development of RNA-based therapies to treat various diseases.

Figures

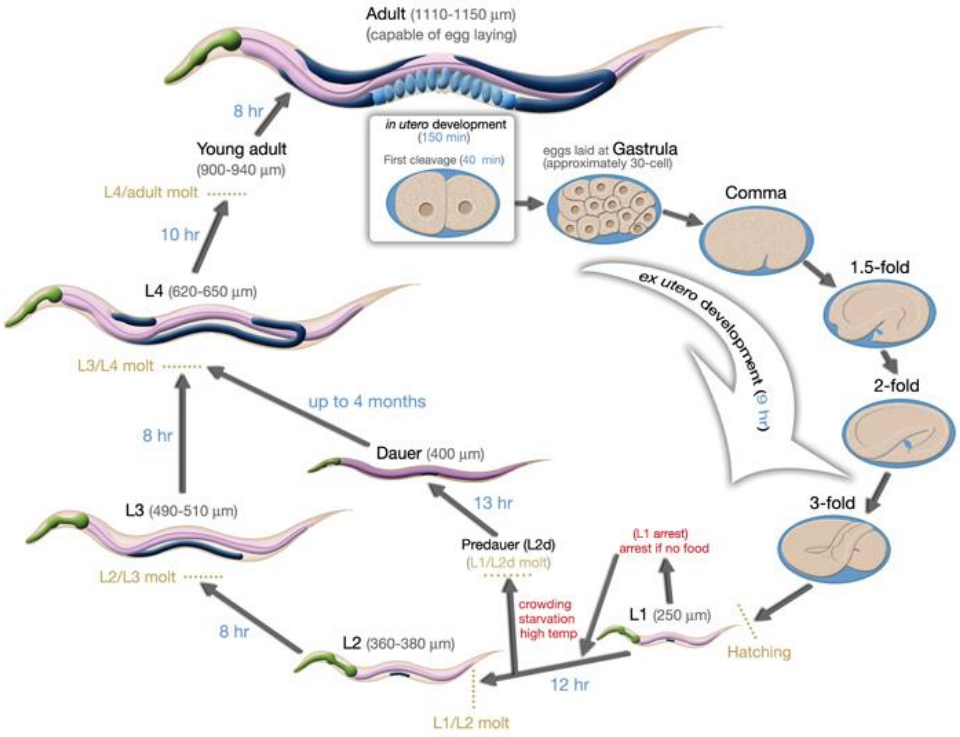

Figure 1.1. *C. elegans* can enter an alternative developmental pathway in response to unfavorable growth conditions. Under optimal conditions, *C. elegans* progresses through four larval stages and molts into a reproductive adult. However, if the organism encounters adverse conditions, such as high temperatures, crowding, or starvation, at the end of the L1 larval stage, it can enter the developmentally quiescent dauer stage. In this state, it can remain for several months. When conditions improve, the dauer larva can exit this stage and resume normal development at the L4 larval stage. Figure used with permission from WormAtlas. Altun, Z. F., Herndon, L. A., Wolkow, C. A., Crocker, C., Lints, R., and Hall, D. H. 2002-2024.

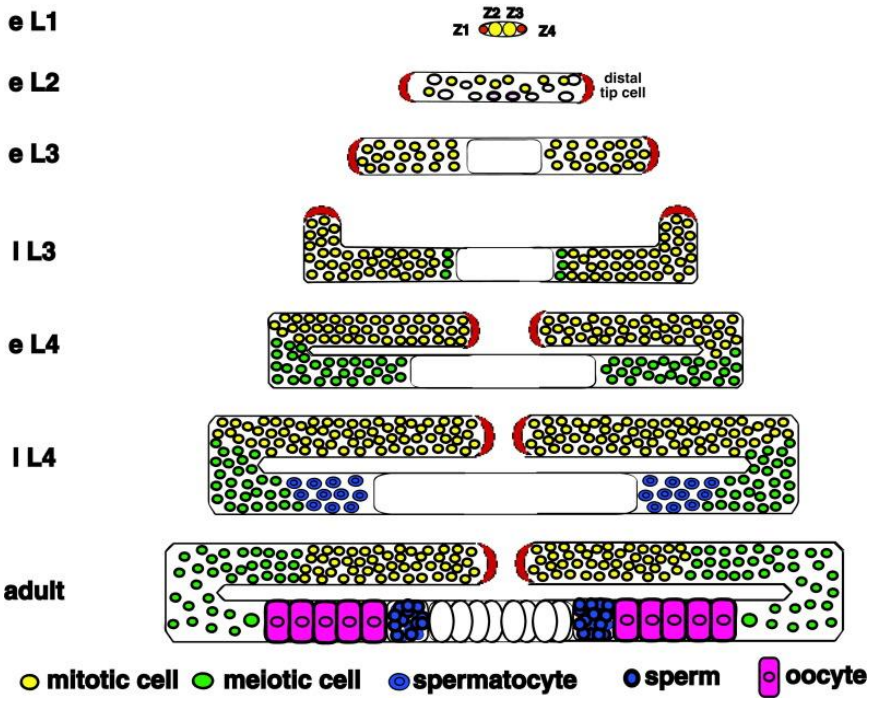

Figure 1.2. The *C. elegans* germ line will develop uninterrupted in replete conditions. The gonad of the L1 larvae consists of two primordial germ cells (Z2 and Z3) that are flanked by two somatic precursor cells (Z1 and Z4). Z2 and Z3 will divide uninterrupted to populate the gonad during development in replete conditions and will give rise to all the germ cells of the animal. Z1 and Z4 will undergo several rounds of cell division to give rise to the somatic gonad of the animal, including the distal tip cells (DTCs), gonadal sheath, spermatheca, spermatheca-uterine valve, and uterus. Unlike the Z2 and Z3 divisions, Z1 and Z4 will follow an invariant pattern of cell divisions, migrations, and differentiations. Figure used with permission from Pepper et al, *Dev Biology* 2003.

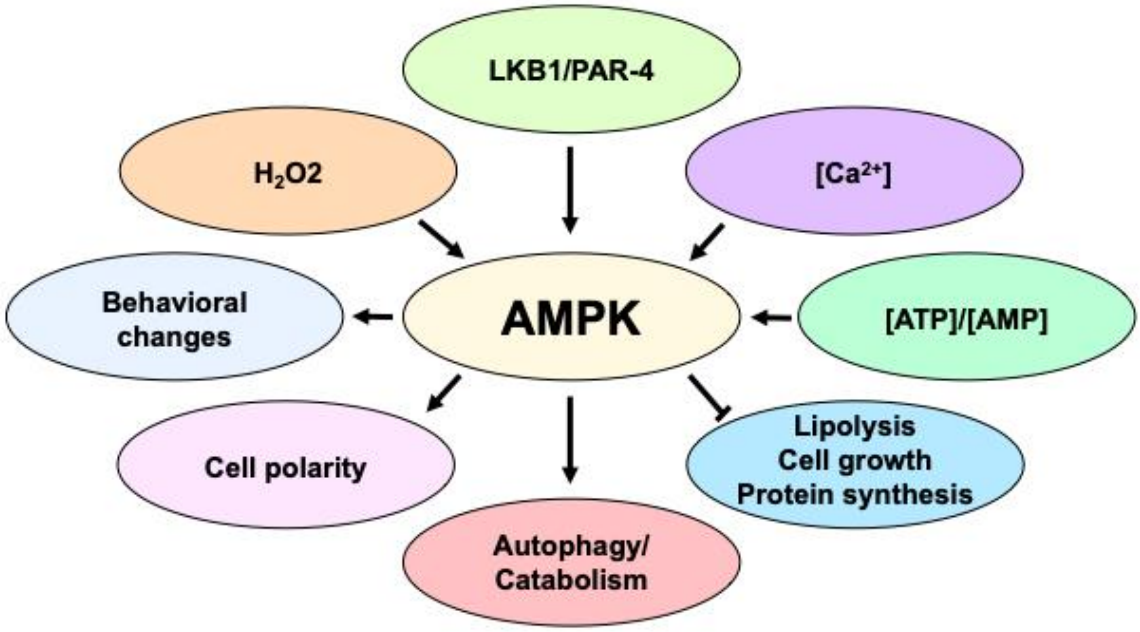

Figure 1.3. Regulation and activity of AMP-activated protein kinase (AMPK). AMPK is a critical energy sensor in cells that is activated in response to low cellular energy levels. AMP and ADP bind to the γ-subunit of AMPK, causing a conformational change that allows the β- and α-subunits to interact more effectively. This binding activates AMPK through phosphorylation by upstream kinases such as LKB1 (liver kinase B1) and CaMKKβ (calcium/calmodulin-dependent protein kinase kinase β). The activated AMPK then phosphorylates a variety of downstream targets to restore energy balance by inducing behavioral changes in *C. elegans*, cell polarity, and autophagy/catabolism, while inhibiting lipolysis, cell growth, and protein synthesis.

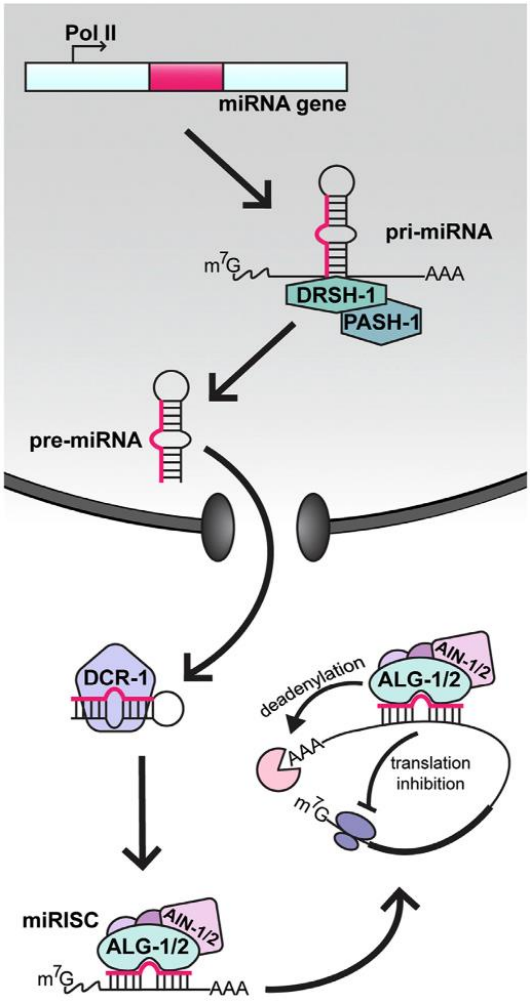

Figure 1.4. microRNA biogenesis and function in *C. elegans*. In the nucleus, RNA polymerase II (Pol II) transcribes miRNA genes into long primary transcripts known as pri-miRNAs. These pri-miRNAs are then processed by Drosha (DRSH-1) in conjunction with the RNA-binding protein Pasha (PASH-1), resulting in precursor miRNAs (pre-miRNAs) that form hairpin structures. The pre-miRNAs are transported to the cytoplasm, where Dicer (DCR-1) further processes them into a double-stranded heteroduplex containing the mature miRNA and the passenger strand. The mature miRNA is incorporated into an Argonaute protein (ALG-1 or ALG-2), creating the core microRNA-Induced Silencing Complex (miRISC). This complex binds to a target mRNA through

partial base-pairing, and the recruitment of AIN-1/2 and other factors leads to the repression of the target by deadenylation and/or inhibition of translation. Figure used with permission from Elder and Pasquinelli, Frontiers in Aging 2022.

References

Abdulkareem, I.H., and Blair, M. (2013). Phosphatase and tensin homologue deleted on chromosome 10. Niger Med J *54*, 79-86.

Abukhdeir, A.M., and Park, B.H. (2008). P21 and p27: roles in carcinogenesis and drug resistance. Expert Rev Mol Med *10*, e19.

Ahmadi, M., and Roy, R. (2016). AMPK acts as a molecular trigger to coordinate glutamatergic signals and adaptive behaviours during acute starvation. Elife *5*.

Alarcón, C.R., Lee, H., Goodarzi, H., Halberg, N., and Tavazoie, S.F. (2015). N 6-methyladenosine marks primary microRNAs for processing. Nature *519*, 482-485.

Albacete-Albacete, L., Navarro-Lérida, I., López, J.A., Martín-Padura, I., Astudillo, A.M., Ferrarini, A., Van-Der-Heyden, M., Balsinde, J., Orend, G., Vázquez, J.*, et al.* (2020). ECM deposition is driven by caveolin-1-dependent regulation of exosomal biogenesis and cargo sorting. J Cell Biol *219*.

Alberti, S., Gladfelter, A., and Mittag, T. (2019). Considerations and challenges in studying liquid-liquid phase separation and biomolecular condensates. Cell *176*, 419-434.

Alers, S., Löffler, A.S., Wesselborg, S., and Stork, B. (2012). Role of AMPK-mTOR-Ulk1/2 in the regulation of autophagy: cross talk, shortcuts, and feedbacks. Mol Cell Biol *32*, 2-11.

Alnaas, A.A., Watson-Siriboe, A., Tran, S., Negussie, M., Henderson, J.A., Osterberg, J.R., Chon, N.L., Harrott, B.M., Oviedo, J., Lyakhova, T.*, et al.* (2021). Multivalent lipid targeting by the calcium-independent C2A domain of synaptotagmin-like protein 4/granuphilin. J Biol Chem *296*, 100159.

Anderson, K.A., Ribar, T.J., Lin, F., Noeldner, P.K., Green, M.F., Muehlbauer, M.J., Witters, L.A., Kemp, B.E., and Means, A.R. (2008). Hypothalamic CaMKK2 contributes to the regulation of energy balance. Cell Metab *7*, 377-388.

Andres, D.A., Seabra, M.C., Brown, M.S., Armstrong, S.A., Smeland, T.E., Cremers, F.P., and Goldstein, J.L. (1993). cDNA cloning of component A of Rab geranylgeranyl transferase and demonstration of its role as a Rab escort protein. Cell *73*, 1091-1099.

Angelo, G., and Van Gilst, M.R. (2009). Starvation protects germline stem cells and extends reproductive longevity in *C. elegans*. Science *326*, 954-958.

Antebi, A., Yeh, W.H., Tait, D., Hedgecock, E.M., and Riddle, D.L. (2000). *daf-12* encodes a nuclear receptor that regulates the dauer diapause and developmental age in *C. elegans*. Genes Dev *14*, 1512-1527.

Arena, J.P., Liu, K.K., Paress, P.S., Frazier, E.G., Cully, D.F., Mrozik, H., and Schaeffer, J.M. (1995). The mechanism of action of avermectins in *Caenorhabditis elegans*: correlation between activation of glutamate-sensitive chloride current, membrane binding, and biological activity. J Parasitol *81*, 286-294.

Arighi, C.N., Hartnell, L.M., Aguilar, R.C., Haft, C.R., and Bonifacino, J.S. (2004). Role of the mammalian retromer in sorting of the cation-independent mannose 6-phosphate receptor. J Cell Biol *165*, 123-133.

Arya, S.B., Chen, S., Jordan-Javed, F., and Parent, C.A. (2022). Ceramide-rich microdomains facilitate nuclear envelope budding for non-conventional exosome formation. Nature Cell Biology *24*, 1019-1028.

Austin, J., and Kimble, J. (1987). *glp-1* Is required in the germ line for regulation of the decision between mitosis and meiosis in *C. elegans*. Cell *51*, 589-599.

Baas, A.F., Kuipers, J., van der Wel, N.N., Batlle, E., Koerten, H.K., Peters, P.J., and Clevers, H.C. (2004). Complete polarization of single intestinal epithelial cells upon activation of LKB1 by STRAD. Cell *116*, 457-466.

Baietti, M.F., Zhang, Z., Mortier, E., Melchior, A., Degeest, G., Geeraerts, A., Ivarsson, Y., Depoortere, F., Coomans, C., Vermeiren, E.*, et al.* (2012). Syndecan-syntenin-ALIX regulates the biogenesis of exosomes. Nat Cell Biol *14*, 677-685.

Barstead, R., Belfiore, M., Kimble, J., Mathies, L.D., Moulder, G., Pugnale, P., and Puoti, A. (2002). The MEP-1 zinc-finger protein acts with MOG DEAH box proteins to control gene expression via the *fem-3* 3′ untranslated region in *Caenorhabditis elegans*. RNA *8*, 725-739.

Batchelder, C., Dunn, M.A., Choy, B., Suh, Y., Cassie, C., Shim, E.Y., Shin, T.H., Mello, C., Seydoux, G., and Blackwell, T.K. (1999). Transcriptional repression by the *Caenorhabditis elegans* germ-line protein PIE-1. Genes Dev *13*, 202-212.

Baugh, L.R., and Sternberg, P.W. (2006). DAF-16/FOXO regulates transcription of *cki-1*/Cip/Kip and repression of *lin-4* during *C. elegans* L1 arrest. Curr Biol *16*, 780-785.

Beghein, E., Devriese, D., Van Hoey, E., and Gettemans, J. (2018). Cortactin and fascin-1 regulate extracellular vesicle release by controlling endosomal trafficking or invadopodia formation and function. Sci Rep *8*, 15606.

Behm-Ansmant, I., Rehwinkel, J., Doerks, T., Stark, A., Bork, P., and Izaurralde, E. (2006). mRNA degradation by miRNAs and GW182 requires both CCR4: NOT deadenylase and DCP1: DCP2 decapping complexes. Genes & development *20*, 1885-1898.

Behrends, C., Sowa, M.E., Gygi, S.P., and Harper, J.W. (2010). Network organization of the human autophagy system. Nature *466*, 68-76.

Bender, L.B., Cao, R., Zhang, Y., and Strome, S. (2004). The MES-2/MES-3/MES-6 Complex and Regulation of Histone H3 Methylation in *C. elegans*. Current Biology *14*, 1639-1643.

Berry, L.W., Westlund, B., and Schedl, T. (1997). Germ-line tumor formation caused by activation of *glp-1*, a *Caenorhabditis elegans* member of the Notch family of receptors. Development *124*, 925-936.

Binder, B., and Holzhütter, H.-G. (2012). A hypothetical model of cargo-selective rab recruitment during organelle maturation. Cell biochemistry and biophysics *63*, 59-71.

Blelloch, R., Anna-Arriola, S.S., Gao, D., Li, Y., Hodgkin, J., and Kimble, J. (1999). The *gon-1* Gene Is Required for Gonadal Morphogenesis in *Caenorhabditis elegans*. Developmental Biology *216*, 382-393.

Boswell, K.L., James, D.J., Esquibel, J.M., Bruinsma, S., Shirakawa, R., Horiuchi, H., and Martin, T.F. (2012). Munc13-4 reconstitutes calcium-dependent SNARE-mediated membrane fusion. J Cell Biol *197*, 301-312.

Boyd, L., Guo, S., Levitan, D., Stinchcomb, D.T., and Kemphues, K.J. (1996). PAR-2 is asymmetrically distributed and promotes association of P granules and PAR-1 with the cortex in *C. elegans* embryos. Development *122*, 3075-3084.

Braun, J.E., Truffault, V., Boland, A., Huntzinger, E., Chang, C.-T., Haas, G., Weichenrieder, O., Coles, M., and Izaurralde, E. (2012). A direct interaction between DCP1 and XRN1 couples mRNA decapping to 5′ exonucleolytic degradation. Nature structural & molecular biology *19*, 1324-1331.

Brenner, J.L., and Schedl, T. (2016). Germline Stem Cell Differentiation Entails Regional Control of Cell Fate Regulator GLD-1 in *Caenorhabditis elegans*. Genetics *202*, 1085-1103.

Brett, C.L., Plemel, R.L., Lobingier, B.T., Vignali, M., Fields, S., and Merz, A.J. (2008). Efficient termination of vacuolar Rab GTPase signaling requires coordinated action by a GAP and a protein kinase. J Cell Biol *182*, 1141-1151.

Broday , L., Kolotuev , I., Didier , C., Bhoumik , A., Podbilewicz , B., and Ronai , Z.e. (2004). The LIM domain protein UNC-95 is required for the assembly of muscle attachment structures and is regulated by the RING finger protein RNF-5 in *C. elegans*. Journal of Cell Biology *165*, 857-867.

Bungard, D., Fuerth, B.J., Zeng, P.-Y., Faubert, B., Maas, N.L., Viollet, B., Carling, D., Thompson, C.B., Jones, R.G., and Berger, S.L. (2010). Signaling Kinase AMPK Activates Stress-Promoted Transcription via Histone H2B Phosphorylation. Science *329*, 1201-1205.

Büssing, I., Yang, J.S., Lai, E.C., and Grosshans, H. (2010). The nuclear export receptor XPO-1 supports primary miRNA processing in *C. elegans* and Drosophila. EMBO J *29*, 1830-1839.

Cai, Q., Qiao, L., Wang, M., He, B., Lin, F.-M., Palmquist, J., Huang, S.-D., and Jin, H. (2018). Plants send small RNAs in extracellular vesicles to fungal pathogen to silence virulence genes. Science *360*, 1126-1129.

Cantalupo, G., Alifano, P., Roberti, V., Bruni, C.B., and Bucci, C. (2001). Rab-interacting lysosomal protein (RILP): the Rab7 effector required for transport to lysosomes. EMBO J *20*, 683-693.

Cao, R., and Zhang, Y. (2004). The functions of E(Z)/EZH2-mediated methylation of lysine 27 in histone H3. Curr Opin Genet Dev *14*, 155-164.

Capowski, E.E., Martin, P., Garvin, C., and Strome, S. (1991). Identification of grandchildless loci whose products are required for normal germ-line development in the nematode *Caenorhabditis elegans*. Genetics *129*, 1061-1072.

Cardoso-Moreira, M., Halbert, J., Valloton, D., Velten, B., Chen, C., Shao, Y., Liechti, A., Ascenção, K., Rummel, C., Ovchinnikova, S.*, et al.* (2019). Gene expression across mammalian organ development. Nature *571*, 505-509.

Casey, P.J., and Seabra, M.C. (1996). Protein prenyltransferases. J Biol Chem *271*, 5289-5292.

Cassani, M., and Seydoux, G. (2022). Specialized germline P-bodies are required to specify germ cell fate in *Caenorhabditis elegans* embryos. Development *149*.

Chapman, R.D., Conrad, M., and Eick, D. (2005). Role of the mammalian RNA polymerase II C-terminal domain (CTD) nonconsensus repeats in CTD stability and cell proliferation. Mol Cell Biol *25*, 7665-7674.

Chase, D., Serafinas, C., Ashcroft, N., Kosinski, M., Longo, D., Ferris, D.K., and Golden, A. (2000). The polo-like kinase PLK-1 is required for nuclear envelope breakdown and the completion of meiosis in *Caenorhabditis elegans*. Genesis *26*, 26-41.

Chason, R.J., Csokmay, J., Segars, J.H., DeCherney, A.H., and Armant, D.R. (2011). Environmental and epigenetic effects upon preimplantation embryo metabolism and development. Trends Endocrinol Metab *22*, 412-420.

Chen, C., Luo, Y., He, W., Zhao, Y., Kong, Y., Liu, H., Zhong, G., Li, Y., Li, J., Huang, J., *et al.* (2020a). Exosomal long noncoding RNA LNMAT2 promotes lymphatic metastasis in bladder cancer. J Clin Invest *130*, 404-421.

Chen, C., Yu, H., Han, F., Lai, X., Ye, K., Lei, S., Mai, M., Lai, M., and Zhang, H. (2022). Tumor-suppressive circRHOBTB3 is excreted out of cells via exosome to sustain colorectal cancer cell fitness. Mol Cancer *21*, 46.

Chen, C.Y., Chen, J., He, L., and Stiles, B.L. (2018). PTEN: Tumor Suppressor and Metabolic Regulator. Front Endocrinol (Lausanne) *9*, 338.

Chen, J., Mohammad, A., Pazdernik, N., Huang, H., Bowman, B., Tycksen, E., and Schedl, T. (2020b). GLP-1 Notch-LAG-1 CSL control of the germline stem cell fate is mediated by transcriptional targets *lst-1* and *sygl-1*. PLoS Genet *16*, e1008650.

Chen, L., Jiao, Z.H., Zheng, L.S., Zhang, Y.Y., Xie, S.T., Wang, Z.X., and Wu, J.W. (2009). Structural insight into the autoinhibition mechanism of AMP-activated protein kinase. Nature *459*, 1146-1149.

Chen, W., Dong, J., Haiech, J., Kilhoffer, M.C., and Zeniou, M. (2016). Cancer Stem Cell Quiescence and Plasticity as Major Challenges in Cancer Therapy. Stem Cells Int *2016*, 1740936.

Cheung, T.H., and Rando, T.A. (2013). Molecular regulation of stem cell quiescence. Nature Reviews Molecular Cell Biology *14*, 329-340.

Chevillet, J.R., Kang, Q., Ruf, I.K., Briggs, H.A., Vojtech, L.N., Hughes, S.M., Cheng, H.H., Arroyo, J.D., Meredith, E.K., Gallichotte, E.N., *et al.* (2014). Quantitative and stoichiometric analysis of the microRNA content of exosomes. Proceedings of the National Academy of Sciences of the United States of America *111*, 14888-14893.

Chien, S.C., Brinkmann, E.M., Teuliere, J., and Garriga, G. (2013). *Caenorhabditis elegans* PIG-1/MELK acts in a conserved PAR-4/LKB1 polarity pathway to promote asymmetric neuroblast divisions. Genetics *193*, 897-909.

Chotard, L., Mishra, A.K., Sylvain, M.A., Tuck, S., Lambright, D.G., and Rocheleau, C.E. (2010). TBC-2 regulates RAB-5/RAB-7-mediated endosomal trafficking in *Caenorhabditis elegans*. Molecular biology of the cell *21*, 2285-2296.

Christie, M., Boland, A., Huntzinger, E., Weichenrieder, O., and Izaurralde, E. (2013). Structure of the PAN3 pseudokinase reveals the basis for interactions with the PAN2 deadenylase and the GW182 proteins. Molecular cell *51*, 360-373.

Clay, M.R., and Sherwood, D.R. (2015). Basement Membranes in the Worm: A Dynamic Scaffolding that Instructs Cellular Behaviors and Shapes Tissues. Curr Top Membr *76*, 337-371.

Collins, R.N. (2003). "Getting it on"--GDI displacement and small GTPase membrane recruitment. Mol Cell *12*, 1064-1066.

Conte, D., Jr., MacNeil, L.T., Walhout, A.J.M., and Mello, C.C. (2015). RNA Interference in *Caenorhabditis elegans*. Curr Protoc Mol Biol *109*, 26.23.21-26.23.30.

Cook, S.J., Jarrell, T.A., Brittin, C.A., Wang, Y., Bloniarz, A.E., Yakovlev, M.A., Nguyen, K.C.Q., Tang, L.T.H., Bayer, E.A., Duerr, J.S.*, et al.* (2019). Whole-animal connectomes of both *Caenorhabditis elegans* sexes. Nature *571*, 63-71.

Corden, J.L., Cadena, D.L., Ahearn, J.M., Jr., and Dahmus, M.E. (1985). A unique structure at the carboxyl terminus of the largest subunit of eukaryotic RNA polymerase II. Proceedings of the National Academy of Sciences of the United States of America *82*, 7934-7938.

Corradetti, M.N., Inoki, K., Bardeesy, N., DePinho, R.A., and Guan, K.L. (2004). Regulation of the TSC pathway by LKB1: evidence of a molecular link between tuberous sclerosis complex and Peutz-Jeghers syndrome. Genes Dev *18*, 1533-1538.

Crittenden, S.L., Bernstein, D.S., Bachorik, J.L., Thompson, B.E., Gallegos, M., Petcherski, A.G., Moulder, G., Barstead, R., Wickens, M., and Kimble, J. (2002). A conserved RNA-binding protein controls germline stem cells in *Caenorhabditis elegans*. Nature *417*, 660-663.

Crittenden, S.L., Eckmann, C.R., Wang, L., Bernstein, D.S., Wickens, M., and Kimble, J. (2003). Regulation of the mitosis/meiosis decision in the *Caenorhabditis elegans* germline. Philos Trans R Soc Lond B Biol Sci *358*, 1359-1362.

Dalley, B.K., and Golomb, M. (1992). Gene expression in the *Caenorhabditis elegans* dauer larva: developmental regulation of Hsp90 and other genes. Dev Biol *151*, 80-90.

Davies, S.P., Helps, N.R., Cohen, P.T., and Hardie, D.G. (1995). 5'-AMP inhibits dephosphorylation, as well as promoting phosphorylation, of the AMP-activated protein kinase. Studies using bacterially expressed human protein phosphatase-2C alpha and native bovine protein phosphatase-2AC. FEBS Lett *377*, 421-425.

Dawson, G. (2021). Isolation of Lipid Rafts (Detergent-Resistant Microdomains) and Comparison to Extracellular Vesicles (Exosomes). Methods Mol Biol *2187*, 99-112.

Day, P., Sharff, A., Parra, L., Cleasby, A., Williams, M., Hörer, S., Nar, H., Redemann, N., Tickle, I., and Yon, J. (2007). Structure of a CBS-domain pair from the regulatory gamma1 subunit of human AMPK in complex with AMP and ZMP. Acta Crystallogr D Biol Crystallogr *63*, 587-596.

De Antoni, A., Schmitzová, J., Trepte, H.H., Gallwitz, D., and Albert, S. (2002). Significance of GTP hydrolysis in Ypt1p-regulated endoplasmic reticulum to Golgi transport revealed by the analysis of two novel Ypt1-GAPs. J Biol Chem *277*, 41023-41031.

De Rie, D., Abugessaisa, I., Alam, T., Arner, E., Arner, P., Ashoor, H., Åström, G., Babina, M., Bertin, N., and Burroughs, A.M. (2017). An integrated expression atlas of miRNAs and their promoters in human and mouse. Nature biotechnology *35*, 872-878.

Demoinet, E., Li, S., and Roy, R. (2017). AMPK blocks starvation-inducible transgenerational defects in *Caenorhabditis elegans*. Proceedings of the National Academy of Sciences *114*, E2689-E2698.

Denli, A.M., Tops, B.B., Plasterk, R.H., Ketting, R.F., and Hannon, G.J. (2004). Processing of primary microRNAs by the Microprocessor complex. Nature *432*, 231-235.

Desnoyers, L., Anant, J.S., and Seabra, M.C. (1996). Geranylgeranylation of Rab proteins. Biochem Soc Trans *24*, 699-703.

Dores, M.R., Grimsey, N.J., Mendez, F., and Trejo, J. (2016). ALIX Regulates the Ubiquitin-Independent Lysosomal Sorting of the P2Y1 Purinergic Receptor via a YPX3L Motif. PLoS One *11*, e0157587.

Du, L.L., and Novick, P. (2001). Purification and properties of a GTPase-activating protein for yeast Rab GTPases. Methods Enzymol *329*, 91-99.

Duan, Y., Veksler-Lublinsky, I., and Ambros, V. (2022). Critical contribution of 3′ non-seed base pairing to the in vivo function of the evolutionarily conserved *let-7*a microRNA. Cell Reports *39*, 110745.

Duguet, T.B., Soichot, J., Kuzyakiv, R., Malmström, L., and Tritten, L. (2020). Extracellular Vesicle-Contained microRNA of *C. elegans* as a Tool to Decipher the Molecular Basis of Nematode Parasitism. Frontiers in Cellular and Infection Microbiology *10*.

Duwat, P., Sourice, S., Cesselin, B., Lamberet, G., Vido, K., Gaudu, P., Le Loir, Y., Violet, F., Loubière, P., and Gruss, A. (2001). Respiration capacity of the fermenting bacterium Lactococcus lactis and its positive effects on growth and survival. J Bacteriol *183*, 4509-4516.

Eden, E.R., Sanchez-Heras, E., Tsapara, A., Sobota, A., Levine, T.P., and Futter, C.E. (2016). Annexin A1 Tethers Membrane Contact Sites that Mediate ER to Endosome Cholesterol Transport. Dev Cell *37*, 473-483.

Ellwanger, D.C., Büttner, F.A., Mewes, H.-W., and Stümpflen, V. (2011). The sufficient minimal set of miRNA seed types. Bioinformatics *27*, 1346-1350.

Fabbiano, F., Corsi, J., Gurrieri, E., Trevisan, C., Notarangelo, M., and D'Agostino, V.G. (2020). RNA packaging into extracellular vesicles: An orchestra of RNA-binding proteins? J Extracell Vesicles *10*, e12043.

Fabbri, M., Paone, A., Calore, F., Galli, R., Gaudio, E., Santhanam, R., Lovat, F., Fadda, P., Mao, C., Nuovo, G.J.*, et al.* (2012). MicroRNAs bind to Toll-like receptors to induce prometastatic inflammatory response. Proceedings of the National Academy of Sciences of the United States of America *109*, E2110-2116.

Fan, H.-Y., and Sun, Q.-Y. (2019). Chapter 12 - Oocyte Meiotic Maturation. In The Ovary (Third Edition), P.C.K. Leung, and E.Y. Adashi, eds. (Academic Press), pp. 181-203.

Fan, S.J., Kroeger, B., Marie, P.P., Bridges, E.M., Mason, J.D., McCormick, K., Zois, C.E., Sheldon, H., Khalid Alham, N., Johnson, E.*, et al.* (2020). Glutamine deprivation alters the origin and function of cancer cell exosomes. EMBO J *39*, e103009.

Fei, X., Li, Z., Yang, D., Kong, X., Lu, X., Shen, Y., Li, X., Xie, S., Wang, J., Zhao, Y.*, et al.* (2021). Neddylation of Coro1a determines the fate of multivesicular bodies and biogenesis of extracellular vesicles. J Extracell Vesicles *10*, e12153.

Ferreira, J.V., da Rosa Soares, A., Ramalho, J., Máximo Carvalho, C., Cardoso, M.H., Pintado, P., Carvalho, A.S., Beck, H.C., Matthiesen, R., Zuzarte, M.*, et al.* (2022). LAMP2A regulates the loading of proteins into exosomes. Sci Adv *8*, eabm1140.

Fielenbach, N., and Antebi, A. (2008). *C. elegans* dauer formation and the molecular basis of plasticity. Genes Dev *22*, 2149-2165.

Fong, Y., Bender, L., Wang, W., and Strome, S. (2002). Regulation of the Different Chromatin States of Autosomes and X Chromosomes in the Germ Line of *C. elegans*. Science *296*, 2235-2238.

Frasa, M.A., Maximiano, F.C., Smolarczyk, K., Francis, R.E., Betson, M.E., Lozano, E., Goldenring, J., Seabra, M.C., Rak, A., Ahmadian, M.R.*, et al.* (2010). Armus is a Rac1 effector that inactivates Rab7 and regulates E-cadherin degradation. Curr Biol *20*, 198-208.

Friedland, A.E., Tzur, Y.B., Esvelt, K.M., Colaiácovo, M.P., Church, G.M., and Calarco, J.A. (2013). Heritable genome editing in *C. elegans* via a CRISPR-Cas9 system. Nature Methods *10*, 741-743.

Fukuda, M. (2011). TBC proteins: GAPs for mammalian small GTPase Rab? Biosci Rep *31*, 159-168.

Fukuyama, M., Rougvie, A.E., and Rothman, J.H. (2006). *C. elegans* DAF-18/PTEN Mediates Nutrient-Dependent Arrest of Cell Cycle and Growth in the Germline. Current Biology *16*, 773-779.

Gallegos, M.E., Balakrishnan, S., Chandramouli, P., Arora, S., Azameera, A., Babushekar, A., Bargoma, E., Bokhari, A., Chava, S.K., Das, P.*, et al.* (2012). The *C. elegans* rab family: identification, classification and toolkit construction. PLoS One *7*, e49387.

Garcia-Martin, R., Wang, G., Brandão, B.B., Zanotto, T.M., Shah, S., Kumar Patel, S., Schilling, B., and Kahn, C.R. (2022). MicroRNA sequence codes for small extracellular vesicle release and cellular retention. Nature *601*, 446-451.

Geiser, F. (2013). Hibernation. Curr Biol *23*, R188-193.

Géminard, C., De Gassart, A., Blanc, L., and Vidal, M. (2004). Degradation of AP2 during reticulocyte maturation enhances binding of hsc70 and Alix to a common site on TFR for sorting into exosomes. Traffic *5*, 181-193.

Gerisch, B., Weitzel, C., Kober-Eisermann, C., Rottiers, V., and Antebi, A. (2001). A Hormonal Signaling Pathway Influencing *C. elegans* Metabolism, Reproductive Development, and Life Span. Developmental Cell *1*, 841-851.

González, A., Hall, M.N., Lin, S.C., and Hardie, D.G. (2020). AMPK and TOR: The Yin and Yang of Cellular Nutrient Sensing and Growth Control. Cell Metab *31*, 472-492.

Gottlieb, S., and Ruvkun, G. (1994). *daf-2, daf-16* and *daf-23*: genetically interacting genes controlling Dauer formation in *Caenorhabditis elegans*. Genetics *137*, 107-120.

Gowans, G.J., Hawley, S.A., Ross, F.A., and Hardie, D.G. (2013). AMP is a true physiological regulator of AMP-activated protein kinase by both allosteric activation and enhancing net phosphorylation. Cell Metab *18*, 556-566.

Grant, B., and Hirsh, D. (1999). Receptor-mediated Endocytosis in the *Caenorhabditis elegans* Oocyte. Molecular biology of the cell *10*, 4311-4326.

Grishok, A. (2005). RNAi mechanisms in *Caenorhabditis elegans*. FEBS Letters *579*, 5932-5939.

Gruidl, M.E., Smith, P.A., Kuznicki, K.A., McCrone, J.S., Kirchner, J., Roussell, D.L., Strome, S., and Bennett, K.L. (1996). Multiple potential germ-line helicases are components of the germ-line-specific P granules of *Caenorhabditis elegans*. Proceedings of the National Academy of Sciences *93*, 13837-13842.

Gu, X., Yan, Y., Novick, S.J., Kovach, A., Goswami, D., Ke, J., Tan, M.H.E., Wang, L., Li, X., de Waal, P.W*., et al.* (2017). Deconvoluting AMP-activated protein kinase (AMPK) adenine nucleotide binding and sensing. J Biol Chem *292*, 12653-12666.

Gulbins, E., and Kolesnick, R. (2003). Raft ceramide in molecular medicine. Oncogene *22*, 7070-7077.

Guo, B.B., Bellingham, S.A., and Hill, A.F. (2015). The neutral sphingomyelinase pathway regulates packaging of the prion protein into exosomes. J Biol Chem *290*, 3455-3467.

Gwinn, D.M., Shackelford, D.B., Egan, D.F., Mihaylova, M.M., Mery, A., Vasquez, D.S., Turk, B.E., and Shaw, R.J. (2008). AMPK phosphorylation of raptor mediates a metabolic checkpoint. Mol Cell *30*, 214-226.

Ha, M., and Kim, V.N. (2014). Regulation of microRNA biogenesis. Nature reviews Molecular cell biology *15*, 509-524.

Hall, D.H., Winfrey, V.P., Blaeuer, G., Hoffman, L.H., Furuta, T., Rose, K.L., Hobert, O., and Greenstein, D. (1999). Ultrastructural Features of the Adult Hermaphrodite Gonad of *Caenorhabditis elegans*: Relations between the Germ Line and Soma. Developmental Biology *212*, 101-123.

Han, J., Lee, Y., Yeom, K.-H., Kim, Y.-K., Jin, H., and Kim, V.N. (2004). The Drosha-DGCR8 complex in primary microRNA processing. Genes & development *18*, 3016-3027.

Han, J., Pluhackova, K., and Böckmann, R.A. (2017). The Multifaceted Role of SNARE Proteins in Membrane Fusion. Front Physiol *8*, 5.

Han, Q.-F., Li, W.-J., Hu, K.-S., Gao, J., Zhai, W.-L., Yang, J.-H., and Zhang, S.-J. (2022). Exosome biogenesis: Machinery, regulation, and therapeutic implications in cancer. Molecular Cancer *21*, 1-26.

Handa, N., Takagi, T., Saijo, S., Kishishita, S., Takaya, D., Toyama, M., Terada, T., Shirouzu, M., Suzuki, A., Lee, S.*, et al.* (2011). Structural basis for compound C inhibition of the human AMP-activated protein kinase α2 subunit kinase domain. Acta Crystallogr D Biol Crystallogr *67*, 480-487.

Hardie, D.G. (2011). AMP-activated protein kinase: an energy sensor that regulates all aspects of cell function. Genes Dev *25*, 1895-1908.

Harding, C., and Stahl, P. (1983). Transferrin recycling in reticulocytes: pH and iron are important determinants of ligand binding and processing. Biochem Biophys Res Commun *113*, 650-658.

Harding, C.V., Heuser, J.E., and Stahl, P.D. (2013). Exosomes: looking back three decades and into the future. J Cell Biol *200*, 367-371.

Hawley, S.A., Boudeau, J., Reid, J.L., Mustard, K.J., Udd, L., Mäkelä, T.P., Alessi, D.R., and Hardie, D.G. (2003). Complexes between the LKB1 tumor suppressor, STRAD alpha/beta and MO25 alpha/beta are upstream kinases in the AMP-activated protein kinase cascade. J Biol *2*, 28.

Hawley, S.A., Pan, D.A., Mustard, K.J., Ross, L., Bain, J., Edelman, A.M., Frenguelli, B.G., and Hardie, D.G. (2005). Calmodulin-dependent protein kinase kinase-beta is an alternative upstream kinase for AMP-activated protein kinase. Cell Metab *2*, 9-19.

Hawley, S.A., Ross, F.A., Gowans, G.J., Tibarewal, P., Leslie, N.R., and Hardie, D.G. (2014). Phosphorylation by Akt within the ST loop of AMPK-α1 down-regulates its activation in tumour cells. Biochem J *459*, 275-287.

He, J., Johnson, J.L., Monfregola, J., Ramadass, M., Pestonjamasp, K., Napolitano, G., Zhang, J., and Catz, S.D. (2016). Munc13-4 interacts with syntaxin 7 and regulates late endosomal maturation, endosomal signaling, and TLR9-initiated cellular responses. Molecular biology of the cell *27*, 572-587.

He, M., Zhang, T., Yang, Y., and Wang, C. (2021). Mechanisms of Oocyte Maturation and Related Epigenetic Regulation. Front Cell Dev Biol *9*, 654028.

Henderson, S.T., Gao, D., Christensen, S., and Kimble, J. (1997). Functional domains of LAG-2, a putative signaling ligand for LIN-12 and GLP-1 receptors in *Caenorhabditis elegans*. Molecular biology of the cell *8*, 1751-1762.

Henderson, S.T., Gao, D., Lambie, E.J., and Kimble, J. (1994). *lag-2* may encode a signaling ligand for the GLP-1 and LIN-12 receptors of *C. elegans*. Development *120*, 2913-2924.

Hilbi, H., and Haas, A. (2012). Secretive bacterial pathogens and the secretory pathway. Traffic *13*, 1187-1197.

Hird, S.N., Paulsen, J.E., and Strome, S. (1996). Segregation of germ granules in living *Caenorhabditis elegans* embryos: cell-type-specific mechanisms for cytoplasmic localisation. Development *122*, 1303-1312.

Hirsh, D., Oppenheim, D., and Klass, M. (1976). Development of the reproductive system of *Caenorhabditis elegans*. Developmental Biology *49*, 200-219.

Holdeman, R., Nehrt, S., and Strome, S. (1998). MES-2, a maternal protein essential for viability of the germline in *Caenorhabditis elegans*, is homologous to a Drosophila Polycomb group protein. Development *125*, 2457-2467.

Hong, Y., Roy, R., and Ambros, V. (1998). Developmental regulation of a cyclin-dependent kinase inhibitor controls postembryonic cell cycle progression in *Caenorhabditis elegans*. Development *125*, 3585-3597.

Huang, C.C., Hall, D.H., Hedgecock, E.M., Kao, G., Karantza, V., Vogel, B.E., Hutter, H., Chisholm, A.D., Yurchenco, P.D., and Wadsworth, W.G. (2003). Laminin alpha subunits and their role in *C. elegans* development. Development *130*, 3343-3358.

Hubbard, E.J., and Greenstein, D. (2000). The *Caenorhabditis elegans* gonad: a test tube for cell and developmental biology. Dev Dyn *218*, 2-22.

Hubbard, E.J.A., and Schedl, T. (2019). Biology of the *Caenorhabditis elegans* Germline Stem Cell System. Genetics *213*, 1145-1188.

Hurley, J.H., Boura, E., Carlson, L.A., and Różycki, B. (2010). Membrane budding. Cell *143*, 875-887.

Hurley, R.L., Anderson, K.A., Franzone, J.M., Kemp, B.E., Means, A.R., and Witters, L.A. (2005). The Ca^{2+}/calmodulin-dependent protein kinase kinases are AMP-activated protein kinase kinases. J Biol Chem *280*, 29060-29066.

Hurley, R.L., Barré, L.K., Wood, S.D., Anderson, K.A., Kemp, B.E., Means, A.R., and Witters, L.A. (2006). Regulation of AMP-activated protein kinase by multisite phosphorylation in response to agents that elevate cellular cAMP. J Biol Chem *281*, 36662-36672.

Hutagalung, A.H., and Novick, P.J. (2011). Role of Rab GTPases in membrane traffic and cell physiology. Physiological reviews *91*, 119-149.

Hutter, H., Vogel, B.E., Plenefisch, J.D., Norris, C.R., Proenca, R.B., Spieth, J., Guo, C., Mastwal, S., Zhu, X., Scheel, J.*, et al.* (2000). Conservation and novelty in the evolution of cell adhesion and extracellular matrix genes. Science *287*, 989-994.

Hyenne, V., Apaydin, A., Rodriguez, D., Spiegelhalter, C., Hoff-Yoessle, S., Diem, M., Tak, S., Lefebvre, O., Schwab, Y., Goetz, J.G.*, et al.* (2015). RAL-1 controls multivesicular body biogenesis and exosome secretion. J Cell Biol *211*, 27-37.

Hyttinen, J.M., Niittykoski, M., Salminen, A., and Kaarniranta, K. (2013). Maturation of autophagosomes and endosomes: a key role for Rab7. Biochimica et Biophysica Acta (BBA)-Molecular Cell Research *1833*, 503-510.

Iavello, A., Frech, V.S., Gai, C., Deregibus, M.C., Quesenberry, P.J., and Camussi, G. (2016). Role of Alix in miRNA packaging during extracellular vesicle biogenesis. Int J Mol Med *37*, 958-966.

Imai, A., Ishida, M., Fukuda, M., Nashida, T., and Shimomura, H. (2013). MADD/DENN/Rab3GEP functions as a guanine nucleotide exchange factor for Rab27 during granule exocytosis of rat parotid acinar cells. Arch Biochem Biophys *536*, 31-37.

Itoh, T., and Fukuda, M. (2006). Identification of EPI64 as a GTPase-activating protein specific for Rab27A. J Biol Chem *281*, 31823-31831.

Itoh, T., Satoh, M., Kanno, E., and Fukuda, M. (2006). Screening for target Rabs of TBC (Tre-2/Bub2/Cdc16) domain-containing proteins based on their Rab-binding activity. Genes Cells *11*, 1023-1037.

Jeppesen, D.K., Fenix, A.M., Franklin, J.L., Higginbotham, J.N., Zhang, Q., Zimmerman, L.J., Liebler, D.C., Ping, J., Liu, Q., Evans, R.*, et al.* (2019). Reassessment of Exosome Composition. Cell *177*, 428-445.e418.

Jia, D., Zhang, J.S., Li, F., Wang, J., Deng, Z., White, M.A., Osborne, D.G., Phillips-Krawczak, C., Gomez, T.S., Li, H.*, et al.* (2016). Structural and mechanistic insights into regulation of the retromer coat by TBC1d5. Nat Commun *7*, 13305.

Jia, K., Albert, P.S., and Riddle, D.L. (2002). DAF-9, a cytochrome P450 regulating *C. elegans* larval development and adult longevity. Development *129*, 221-231.

Jimenez-Orgaz, A., Kvainickas, A., Nägele, H., Denner, J., Eimer, S., Dengjel, J., and Steinberg, F. (2018). Control of RAB7 activity and localization through the retromer-TBC1D5 complex enables RAB7-dependent mitophagy. EMBO J *37*, 235-254.

Jo, M.H., Shin, S., Jung, S.-R., Kim, E., Song, J.-J., and Hohng, S. (2015). Human Argonaute 2 has diverse reaction pathways on target RNAs. Molecular cell *59*, 117-124.

Jonas, S., and Izaurralde, E. (2015). Towards a molecular understanding of microRNA-mediated gene silencing. Nature reviews genetics *16*, 421-433.

Jongsma, M.L.M., Bakker, J., Cabukusta, B., Liv, N., van Elsland, D., Fermie, J., Akkermans, J.L.L., Kuijl, C., van der Zanden, S.Y., Janssen, L.*, et al.* (2020). SKIP-HOPS recruits TBC1D15 for a Rab7-to-Arl8b identity switch to control late endosome transport. EMBO J *39*, e102301.

Joshi, P.M., Riddle, M.R., Djabrayan, N.J., and Rothman, J.H. (2010). *Caenorhabditis elegans* as a model for stem cell biology. Dev Dyn *239*, 1539-1554.

Ju, J., Aoyama, T., Yashiro, Y., Yamashita, S., Kuroyanagi, H., and Tomita, K. (2023). Structure of the *Caenorhabditis elegans* m6A methyltransferase METT10 that regulates SAM homeostasis. Nucleic Acids Research *51*, 2434-2446.

Jurczak, E.M., Christopher, W., Shaolin, L., Fabian, B., Ahilya, N.S., Thomas, F.D., Eric, A.M., and Richard, R. (2023). AMPK regulates small RNA pathway prevalence to mediate soma-to-germ line communication and establish germline stem cell quiescence. bioRxiv, 2023.2011.2015.567172.

Kadekar, P., Chaouni, R., Clark, E., Kazanets, A., and Roy, R. (2018). Genome-wide surveys reveal polarity and cytoskeletal regulators mediate LKB1-associated germline stem cell quiescence. BMC Genomics *19*, 462.

Kadekar, P., and Roy, R. (2019). AMPK regulates germline stem cell quiescence and integrity through an endogenous small RNA pathway. PLoS Biol *17*, e3000309.

Kalluri, R., and LeBleu, V.S. (2020). The biology, function, and biomedical applications of exosomes. Science *367*.

Kamath, R.S., and Ahringer, J. (2003). Genome-wide RNAi screening in *Caenorhabditis elegans*. Methods *30*, 313-321.

Kamath, R.S., Martinez-Campos, M., Zipperlen, P., Fraser, A.G., and Ahringer, J. (2000). Effectiveness of specific RNA-mediated interference through ingested double-stranded RNA in *Caenorhabditis elegans*. Genome Biology *2*, research0002.0001.

Kawamata, T., and Tomari, Y. (2010). Making risc. Trends in biochemical sciences *35*, 368-376.

Kawasaki, I., Amiri, A., Fan, Y., Meyer, N., Dunkelbarger, S., Motohashi, T., Karashima, T., Bossinger, O., and Strome, S. (2004). The PGL family proteins associate with germ granules and function redundantly in *Caenorhabditis elegans* germline development. Genetics *167*, 645-661.

Kawasaki, I., Shim, Y.H., Kirchner, J., Kaminker, J., Wood, W.B., and Strome, S. (1998). PGL-1, a predicted RNA-binding component of germ granules, is essential for fertility in *C. elegans*. Cell *94*, 635-645.

Kazan, J.M., Desrochers, G., Martin, C.E., Jeong, H., Kharitidi, D., Apaja, P.M., Roldan, A., St Denis, N., Gingras, A.C., Lukacs, G.L.*, et al.* (2021). Endofin is required for HD-PTP and ESCRT-0 interdependent endosomal sorting of ubiquitinated transmembrane cargoes. iScience *24*, 103274.

Kemphues, K.J., Priess, J.R., Morton, D.G., and Cheng, N.S. (1988). Identification of genes required for cytoplasmic localization in early *C. elegans* embryos. Cell *52*, 311-320.

Keniry, M., and Parsons, R. (2008). The role of PTEN signaling perturbations in cancer and in targeted therapy. Oncogene *27*, 5477-5485.

Kenyon, C. (1988). The nematode *Caenorhabditis elegans*. Science *240*, 1448-1453.

Kershner, A.M., and Kimble, J. (2010). Genome-wide analysis of mRNA targets for *Caenorhabditis elegans* FBF, a conserved stem cell regulator. Proceedings of the National Academy of Sciences of the United States of America *107*, 3936-3941.

Khvorova, A., Reynolds, A., and Jayasena, S.D. (2003). Functional siRNAs and miRNAs exhibit strand bias. Cell *115*, 209-216.

Killian, D.J., and Hubbard, E.J.A. (2004). *C. elegans pro-1* activity is required for soma/germline interactions that influence proliferation and differentiation in the germ line. Development *131*, 1267-1278.

Kim, Y.K., Bourgeois, C.F., Isel, C., Churcher, M.J., and Karn, J. (2002). Phosphorylation of the RNA polymerase II carboxyl-terminal domain by CDK9 is directly responsible for human immunodeficiency virus type 1 Tat-activated transcriptional elongation. Mol Cell Biol *22*, 4622-4637.

Kim, Y.K., and Kim, V.N. (2007). Processing of intronic microRNAs. EMBO J *26*, 775-783.

Kimble, J., and Crittenden, S.L. (2007). Controls of germline stem cells, entry into meiosis, and the sperm/oocyte decision in *Caenorhabditis elegans*. Annu Rev Cell Dev Biol *23*, 405-433.

Kimble, J., and Hirsh, D. (1979). The postembryonic cell lineages of the hermaphrodite and male gonads in *Caenorhabditis elegans*. Dev Biol *70*, 396-417.

Kimble, J., and Simpson, P. (1997). THE LIN-12/Notch SIGNALING PATHWAY AND ITS REGULATION. Annual Review of Cell and Developmental Biology *13*, 333-361.

Kimble, J.E., and White, J.G. (1981). On the control of germ cell development in *Caenorhabditis elegans*. Developmental Biology *81*, 208-219.

Kimura, K.D., Tissenbaum, H.A., Liu, Y., and Ruvkun, G. (1997). *daf-2*, an insulin receptor-like gene that regulates longevity and diapause in *Caenorhabditis elegans*. Science *277*, 942-946.

Kinchen, J.M., and Ravichandran, K.S. (2010). Identification of two evolutionarily conserved genes regulating processing of engulfed apoptotic cells. Nature *464*, 778-782.

Kjøbsted, R., Roll, J.L.W., Jørgensen, N.O., Birk, J.B., Foretz, M., Viollet, B., Chadt, A., Al-Hasani, H., and Wojtaszewski, J.F.P. (2019). AMPK and TBC1D1 Regulate Muscle Glucose Uptake After, but Not During, Exercise and Contraction. Diabetes *68*, 1427-1440.

Klass, M., and Hirsh, D. (1976). Non-ageing developmental variant of *Caenorhabditis elegans*. Nature *260*, 523-525.

Knoblich, J.A. (2008). Mechanisms of Asymmetric Stem Cell Division. Cell *132*, 583-597.

Korf, I., Fan, Y., and Strome, S. (1998). The Polycomb group in *Caenorhabditis elegans* and maternal control of germline development. Development *125*, 2469-2478.

Kornev, A.P., Haste, N.M., Taylor, S.S., and Eyck, L.F. (2006). Surface comparison of active and inactive protein kinases identifies a conserved activation mechanism. Proceedings of the National Academy of Sciences of the United States of America *103*, 17783-17788.

Kornev, A.P., and Taylor, S.S. (2015). Dynamics-Driven Allostery in Protein Kinases. Trends Biochem Sci *40*, 628-647.

Kostić, I., Li, S., and Roy, R. (2003). *cki-1* links cell division and cell fate acquisition in the *C. elegans* somatic gonad. Dev Biol *263*, 242-252.

Kostić, I., and Roy, R. (2002). Organ-specific cell division abnormalities caused by mutation in a general cell cycle regulator in *C. elegans*. Development *129*, 2155-2165.

Kowal, J., Arras, G., Colombo, M., Jouve, M., Morath, J.P., Primdal-Bengtson, B., Dingli, F., Loew, D., Tkach, M., and Théry, C. (2016). Proteomic comparison defines novel markers to characterize heterogeneous populations of extracellular vesicle subtypes. Proceedings of the National Academy of Sciences of the United States of America *113*, E968-977.

Kucharczyk, R., Hoffman-Sommer, M., Piekarska, I., Von Mollard, G.F., and Rytka, J. (2009). The Saccharomyces cerevisiae protein Ccz1p interacts with components of the endosomal fusion machinery. FEMS yeast research *9*, 565-573.

Kummer, D., Steinbacher, T., Schwietzer, M.F., Thölmann, S., and Ebnet, K. (2020). Tetraspanins: integrating cell surface receptors to functional microdomains in homeostasis and disease. Med Microbiol Immunol *209*, 397-405.

Kuznicki, K.A., Smith, P.A., Leung-Chiu, W.M., Estevez, A.O., Scott, H.C., and Bennett, K.L. (2000). Combinatorial RNA interference indicates GLH-4 can compensate for GLH-1; these two P granule components are critical for fertility in *C. elegans*. Development *127*, 2907-2916.

L'Hernault, S.W. (2009). The genetics and cell biology of spermatogenesis in the nematode *C. elegans*. Molecular and Cellular Endocrinology *306*, 59-65.

Lafourcade, C., Sobo, K., Kieffer-Jaquinod, S., Garin, J., and van der Goot, F.G. (2008). Regulation of the V-ATPase along the Endocytic Pathway Occurs through Reversible Subunit Association and Membrane Localization. PLOS ONE *3*, e2758.

Lee, H.Y., Zhou, K., Smith, A.M., Noland, C.L., and Doudna, J.A. (2013a). Differential roles of human Dicer-binding proteins TRBP and PACT in small RNA processing. Nucleic Acids Res *41*, 6568-6576.

Lee, J.M., Seo, W.Y., Song, K.H., Chanda, D., Kim, Y.D., Kim, D.K., Lee, M.W., Ryu, D., Kim, Y.H., Noh, J.R.*, et al.* (2010a). AMPK-dependent repression of hepatic gluconeogenesis via disruption of CREB.CRTC2 complex by orphan nuclear receptor small heterodimer partner. J Biol Chem *285*, 32182-32191.

Lee, J.O., Lee, S.K., Kim, N., Kim, J.H., You, G.Y., Moon, J.W., Jie, S., Kim, S.J., Lee, Y.W., Kang, H.J.*, et al.* (2013b). E3 ubiquitin ligase, WWP1, interacts with AMPKα2 and down-regulates its expression in skeletal muscle C2C12 cells. J Biol Chem *288*, 4673-4680.

Lee, J.W., Park, S., Takahashi, Y., and Wang, H.G. (2010b). The association of AMPK with ULK1 regulates autophagy. PLoS One *5*, e15394.

Lee, M.T., Mishra, A., and Lambright, D.G. (2009). Structural mechanisms for regulation of membrane traffic by rab GTPases. Traffic *10*, 1377-1389.

Lee, R.C., Feinbaum, R.L., and Ambros, V. (1993). The *C. elegans* heterochronic gene lin-4 encodes small RNAs with antisense complementarity to lin-14. Cell *75*, 843-854.

Leidal, A.M., Huang, H.H., Marsh, T., Solvik, T., Zhang, D., Ye, J., Kai, F., Goldsmith, J., Liu, J.Y., Huang, Y.H.*, et al.* (2020). The LC3-conjugation machinery specifies the loading of RNA-binding proteins into extracellular vesicles. Nat Cell Biol *22*, 187-199.

Letunic, I., Doerks, T., and Bork, P. (2015). SMART: recent updates, new developments and status in 2015. Nucleic Acids Res *43*, D257-260.

Li, G., and Marlin, M.C. (2015). Rab family of GTPases. Methods Mol Biol *1298*, 1-15.

Li, X., Wang, L., Zhou, X.E., Ke, J., de Waal, P.W., Gu, X., Tan, M.H., Wang, D., Wu, D., Xu, H.E.*, et al.* (2015). Structural basis of AMPK regulation by adenine nucleotides and glycogen. Cell Res *25*, 50-66.

Littleton, J.T., Barnard, R.J.O., Titus, S.A., Slind, J., Chapman, E.R., and Ganetzky, B. (2001). SNARE-complex disassembly by NSF follows synaptic-vesicle fusion. Proceedings of the National Academy of Sciences *98*, 12233-12238.

Liu, J.J. (2016). Retromer-Mediated Protein Sorting and Vesicular Trafficking. J Genet Genomics *43*, 165-177.

Liu, T.-T., Gomez, T.S., Sackey, B.K., Billadeau, D.D., and Burd, C.G. (2012). Rab GTPase regulation of retromer-mediated cargo export during endosome maturation. Molecular biology of the cell *23*, 2505-2515.

Liu, X.M., Ma, L., and Schekman, R. (2021). Selective sorting of microRNAs into exosomes by phase-separated YBX1 condensates. Elife *10*.

Lizcano, J.M., Göransson, O., Toth, R., Deak, M., Morrice, N.A., Boudeau, J., Hawley, S.A., Udd, L., Mäkelä, T.P., Hardie, D.G.*, et al.* (2004). LKB1 is a master kinase that activates 13 kinases of the AMPK subfamily, including MARK/PAR-1. EMBO J *23*, 833-843.

Lötvall, J., Hill, A.F., Hochberg, F., Buzás, E.I., Di Vizio, D., Gardiner, C., Gho, Y.S., Kurochkin, I.V., Mathivanan, S., Quesenberry, P.*, et al.* (2014). Minimal experimental requirements for definition of extracellular vesicles and their functions: a position statement from the International Society for Extracellular Vesicles. J Extracell Vesicles *3*, 26913.

Ludewig, A.H., Kober-Eisermann, C., Weitzel, C., Bethke, A., Neubert, K., Gerisch, B., Hutter, H., and Antebi, A. (2004). A novel nuclear receptor/coregulator complex controls *C. elegans* lipid metabolism, larval development, and aging. Genes Dev *18*, 2120-2133.

Luo, H., Li, X., Li, T., Zhao, L., He, J., Zha, L., Qi, Q., and Yu, Z. (2019). microRNA-423-3p exosomes derived from cardiac fibroblasts mediates the cardioprotective effects of ischaemic post-conditioning. Cardiovasc Res *115*, 1189-1204.

M, H.R., Bayraktar, E., G, K.H., Abd-Ellah, M.F., Amero, P., Chavez-Reyes, A., and Rodriguez-Aguayo, C. (2017). Exosomes: From Garbage Bins to Promising Therapeutic Targets. Int J Mol Sci *18*.

Ma, J., Wang, Y.T., Chen, L.H., Yang, B.Y., Jiang, Y.Z., Wang, L.X., Chen, Z.Q., Ma, G.R., Fang, L.Q., and Wang, Z.B. (2023). Dauer larva-derived extracellular vesicles extend the life of *Caenorhabditis elegans*. Biogerontology *24*, 581-592.

Mafakheri, S., Flörke, R.R., Kanngießer, S., Hartwig, S., Espelage, L., De Wendt, C., Schönberger, T., Hamker, N., Lehr, S., Chadt, A.*, et al.* (2018). AKT and AMP-activated protein kinase regulate TBC1D1 through phosphorylation and its interaction with the cytosolic tail of insulin-regulated aminopeptidase IRAP. J Biol Chem *293*, 17853-17862.

Mahla, R.S. (2016). Stem Cells Applications in Regenerative Medicine and Disease Therapeutics. Int J Cell Biol *2016*, 6940283.

Manning, G., Whyte, D.B., Martinez, R., Hunter, T., and Sudarsanam, S. (2002). The protein kinase complement of the human genome. Science *298*, 1912-1934.

Marin, T.L., Gongol, B., Zhang, F., Martin, M., Johnson, D.A., Xiao, H., Wang, Y., Subramaniam, S., Chien, S., and Shyy, J.Y. (2017). AMPK promotes mitochondrial biogenesis and function by phosphorylating the epigenetic factors DNMT1, RBBP7, and HAT1. Sci Signal *10*.

Marsin, A.S., Bertrand, L., Rider, M.H., Deprez, J., Beauloye, C., Vincent, M.F., Van den Berghe, G., Carling, D., and Hue, L. (2000). Phosphorylation and activation of heart PFK-

2 by AMPK has a role in the stimulation of glycolysis during ischaemia. Current Biology *10*, 1247-1255.

Marz, K.E., Lauer, J.M., and Hanson, P.I. (2003). Defining the SNARE Complex Binding Surface of α-SNAP: IMPLICATIONS FOR SNARE COMPLEX DISASSEMBLY. Journal of Biological Chemistry *278*, 27000-27008.

Mathivanan, S., Ji, H., and Simpson, R.J. (2010). Exosomes: extracellular organelles important in intercellular communication. Journal of proteomics *73*, 1907-1920.

McCarter, J., Bartlett, B., Dang, T., and Schedl, T. (1997). Soma–Germ Cell Interactions in *Caenorhabditis elegans*: Multiple Events of Hermaphrodite Germline Development Require the Somatic Sheath and Spermathecal Lineages. Developmental Biology *181*, 121-143.

McGough, I.J., and Cullen, P.J. (2011). Recent advances in retromer biology. Traffic *12*, 963-971.

McNally, K.L., and McNally, F.J. (2005). Fertilization initiates the transition from anaphase I to metaphase II during female meiosis in *C. elegans*. Developmental Biology *282*, 218-230.

Meharena, H.S., Chang, P., Keshwani, M.M., Oruganty, K., Nene, A.K., Kannan, N., Taylor, S.S., and Kornev, A.P. (2013). Deciphering the structural basis of eukaryotic protein kinase regulation. PLoS Biol *11*, e1001680.

Mehenni, H., Gehrig, C., Nezu, J., Oku, A., Shimane, M., Rossier, C., Guex, N., Blouin, J.L., Scott, H.S., and Antonarakis, S.E. (1998). Loss of LKB1 kinase activity in Peutz-Jeghers syndrome, and evidence for allelic and locus heterogeneity. Am J Hum Genet *63*, 1641-1650.

Mehlmann, L.M. (2005). Stops and starts in mammalian oocytes: recent advances in understanding the regulation of meiotic arrest and oocyte maturation. Reproduction *130*, 791-799.

Mello, C.C., Draper, B.W., Krause, M., Weintraub, H., and Priess, J.R. (1992). The *pie-1* and *mex-1* genes and maternal control of blastomere identity in early *C. elegans* embryos. Cell *70*, 163-176.

Mello, C.C., Schubert, C., Draper, B., Zhang, W., Lobel, R., and Priess, J.R. (1996). The PIE-1 protein and germline specification in *C. elegans* embryos. Nature *382*, 710-712.

Miller, M.A., Nguyen, V.Q., Lee, M.-H., Kosinski, M., Schedl, T., Caprioli, R.M., and Greenstein, D. (2001a). A Sperm Cytoskeletal Protein That Signals Oocyte Meiotic Maturation and Ovulation. Science *291*, 2144-2147.

Miller, M.A., Nguyen, V.Q., Lee, M.H., Kosinski, M., Schedl, T., Caprioli, R.M., and Greenstein, D. (2001b). A sperm cytoskeletal protein that signals oocyte meiotic maturation and ovulation. Science *291*, 2144-2147.

Miller, M.A., Ruest, P.J., Kosinski, M., Hanks, S.K., and Greenstein, D. (2003). An Eph receptor sperm-sensing control mechanism for oocyte meiotic maturation in *Caenorhabditis elegans*. Genes Dev *17*, 187-200.

Mizuno, K., Kitamura, A., and Sasaki, T. (2003). Rabring7, a novel Rab7 target protein with a RING finger motif. Molecular biology of the cell *14*, 3741-3752.

Morrison, S.J., Shah, N.M., and Anderson, D.J. (1997). Regulatory Mechanisms in Stem Cell Biology. Cell *88*, 287-298.

Morton, D.G., Shakes, D.C., Nugent, S., Dichoso, D., Wang, W., Golden, A., and Kemphues, K.J. (2002). The *Caenorhabditis elegans par-5* gene encodes a 14-3-3 protein required for cellular asymmetry in the early embryo. Dev Biol *241*, 47-58.

Motola, D.L., Cummins, C.L., Rottiers, V., Sharma, K.K., Li, T., Li, Y., Suino-Powell, K., Xu, H.E., Auchus, R.J., Antebi, A.*, et al.* (2006). Identification of ligands for DAF-12 that govern dauer formation and reproduction in *C. elegans*. Cell *124*, 1209-1223.

Nakano, A., Kato, H., Watanabe, T., Min, K.-D., Yamazaki, S., Asano, Y., Seguchi, O., Higo, S., Shintani, Y., Asanuma, H.*, et al.* (2010). AMPK controls the speed of microtubule polymerization and directional cell migration through CLIP-170 phosphorylation. Nature Cell Biology *12*, 583-590.

Nakano, A., and Takashima, S. (2012). LKB1 and AMP-activated protein kinase: regulators of cell polarity. Genes Cells *17*, 737-747.

Narbonne, P., Hyenne, V., Li, S., Labbé, J.-C., and Roy, R. (2010). Differential requirements for STRAD in LKB1-dependent functions in *C. elegans*. Development *137*, 661-670.

Narbonne, P., and Roy, R. (2006). Inhibition of germline proliferation during *C. elegans* dauer development requires PTEN, LKB1 and AMPK signalling. Development *133*, 611-619.

Narbonne, P., and Roy, R. (2009). *Caenorhabditis elegans* dauers need LKB1/AMPK to ration lipid reserves and ensure long-term survival. Nature *457*, 210-214.

Nielsen, E., Cheung, A.Y., and Ueda, T. (2008). The regulatory RAB and ARF GTPases for vesicular trafficking. Plant Physiol *147*, 1516-1526.

Nikonorova, I.A., Wang, J., Cope, A.L., Tilton, P.E., Power, K.M., Walsh, J.D., Akella, J.S., Krauchunas, A.R., Shah, P., and Barr, M.M. (2022). Isolation, profiling, and tracking of extracellular vesicle cargo in *Caenorhabditis elegans*. Curr Biol *32*, 1924-1936.e1926.

O'Brien, J., Hayder, H., Zayed, Y., and Peng, C. (2018). Overview of MicroRNA Biogenesis, Mechanisms of Actions, and Circulation. Front Endocrinol (Lausanne) *9*, 402.

Oakhill, J.S., Steel, R., Chen, Z.P., Scott, J.W., Ling, N., Tam, S., and Kemp, B.E. (2011). AMPK is a direct adenylate charge-regulated protein kinase. Science *332*, 1433-1435.

Ogata-Kawata, H., Izumiya, M., Kurioka, D., Honma, Y., Yamada, Y., Furuta, K., Gunji, T., Ohta, H., Okamoto, H., and Sonoda, H. (2014). Circulating exosomal microRNAs as biomarkers of colon cancer. PloS one *9*, e92921.

Ogg, S., and Ruvkun, G. (1998). The *C. elegans* PTEN homolog, DAF-18, acts in the insulin receptor-like metabolic signaling pathway. Mol Cell *2*, 887-893.

Okada, C., Yamashita, E., Lee, S.J., Shibata, S., Katahira, J., Nakagawa, A., Yoneda, Y., and Tsukihara, T. (2009). A high-resolution structure of the pre-microRNA nuclear export machinery. Science *326*, 1275-1279.

Okamura, K., Ishizuka, A., Siomi, H., and Siomi, M.C. (2004). Distinct roles for Argonaute proteins in small RNA-directed RNA cleavage pathways. Genes Dev *18*, 1655-1666.

Onoue, K., Jofuku, A., Ban-Ishihara, R., Ishihara, T., Maeda, M., Koshiba, T., Itoh, T., Fukuda, M., Otera, H., Oka, T.*, et al.* (2013). Fis1 acts as a mitochondrial recruitment factor for TBC1D15 that is involved in regulation of mitochondrial morphology. J Cell Sci *126*, 176-185.

Ostrowski, M., Carmo, N.B., Krumeich, S., Fanget, I., Raposo, G., Savina, A., Moita, C.F., Schauer, K., Hume, A.N., Freitas, R.P.*, et al.* (2010). Rab27a and Rab27b control different steps of the exosome secretion pathway. Nature Cell Biology *12*, 19-30.

Pan, B.T., and Johnstone, R.M. (1983). Fate of the transferrin receptor during maturation of sheep reticulocytes in vitro: selective externalization of the receptor. Cell *33*, 967-978.

Pan, X., Eathiraj, S., Munson, M., and Lambright, D.G. (2006). TBC-domain GAPs for Rab GTPases accelerate GTP hydrolysis by a dual-finger mechanism. Nature *442*, 303-306.

Pan, Z., Zhao, R., Li, B., Qi, Y., Qiu, W., Guo, Q., Zhang, S., Zhao, S., Xu, H., Li, M.*, et al.* (2022). EWSR1-induced circNEIL3 promotes glioma progression and exosome-mediated macrophage immunosuppressive polarization via stabilizing IGF2BP3. Mol Cancer *21*, 16.

Paradis, S., and Ruvkun, G. (1998). *Caenorhabditis elegans* Akt/PKB transduces insulin receptor-like signals from AGE-1 PI3 kinase to the DAF-16 transcription factor. Genes Dev *12*, 2488-2498.

Pawelec, A., Arsić, J., and Kölling, R. (2010). Mapping of Vps21 and HOPS binding sites in Vps8 and effect of binding site mutants on endocytic trafficking. Eukaryotic cell *9*, 602-610.

Pazdernik, N., and Schedl, T. (2013). Introduction to germ cell development in *Caenorhabditis elegans*. Adv Exp Med Biol *757*, 1-16.

Pedersen, N.M., Wenzel, E.M., Wang, L., Antoine, S., Chavrier, P., Stenmark, H., and Raiborg, C. (2020). Protrudin-mediated ER-endosome contact sites promote MT1-MMP exocytosis and cell invasion. J Cell Biol *219*.

Pereira-Leal, J.B., and Seabra, M.C. (2001). Evolution of the Rab family of small GTP-binding proteins. J Mol Biol *313*, 889-901.

Pfeffer, S.R. (2001). Rab GTPases: specifying and deciphering organelle identity and function. Trends Cell Biol *11*, 487-491.

Pfeffer, S.R. (2005). Structural clues to Rab GTPase functional diversity. J Biol Chem *280*, 15485-15488.

Pfitzner, A.K., Mercier, V., Jiang, X., Moser von Filseck, J., Baum, B., Šarić, A., and Roux, A. (2020). An ESCRT-III Polymerization Sequence Drives Membrane Deformation and Fission. Cell *182*, 1140-1155.e1118.

Phuyal, S., Hessvik, N.P., Skotland, T., Sandvig, K., and Llorente, A. (2014). Regulation of exosome release by glycosphingolipids and flotillins. The FEBS Journal *281*, 2214-2227.

Platta, H.W., and Stenmark, H. (2011). Endocytosis and signaling. Current Opinion in Cell Biology *23*, 393-403.

Polekhina, G., Gupta, A., van Denderen, B.J., Feil, S.C., Kemp, B.E., Stapleton, D., and Parker, M.W. (2005). Structural basis for glycogen recognition by AMP-activated protein kinase. Structure *13*, 1453-1462.

Popovic, D., Akutsu, M., Novak, I., Harper, J.W., Behrends, C., and Dikic, I. (2012). Rab GTPase-activating proteins in autophagy: regulation of endocytic and autophagy pathways by direct binding to human ATG8 modifiers. Mol Cell Biol *32*, 1733-1744.

Poteryaev, D., Datta, S., Ackema, K., Zerial, M., and Spang, A. (2010). Identification of the switch in early-to-late endosome transition. Cell *141*, 497-508.

Poteryaev, D., Fares, H., Bowerman, B., and Spang, A. (2007). *Caenorhabditis elegans* SAND-1 is essential for RAB-7 function in endosomal traffic. EMBO J *26*, 301-312.

Qiao, L., Lan, C., Capriotti, L., Ah-Fong, A., Nino Sanchez, J., Hamby, R., Heller, J., Zhao, H., Glass, N.L., Judelson, H.S.*, et al.* (2021). Spray-induced gene silencing for disease control is dependent on the efficiency of pathogen RNA uptake. Plant Biotechnol J *19*, 1756-1768.

Rabas, N., Palmer, S., Mitchell, L., Ismail, S., Gohlke, A., Riley, J.S., Tait, S.W.G., Gammage, P., Soares, L.L., Macpherson, I.R.*, et al.* (2021). PINK1 drives production of mtDNA-containing extracellular vesicles to promote invasiveness. J Cell Biol *220*.

Rak, A., Fedorov, R., Alexandrov, K., Albert, S., Goody, R.S., Gallwitz, D., and Scheidig, A.J. (2000). Crystal structure of the GAP domain of Gyp1p: first insights into interaction with Ypt/Rab proteins. EMBO J *19*, 5105-5113.

Rak, A., Pylypenko, O., Niculae, A., Pyatkov, K., Goody, R.S., and Alexandrov, K. (2004). Structure of the Rab7:REP-1 complex: insights into the mechanism of Rab prenylation and choroideremia disease. Cell *117*, 749-760.

Raposo, G., Nijman, H.W., Stoorvogel, W., Liejendekker, R., Harding, C.V., Melief, C.J., and Geuze, H.J. (1996). B lymphocytes secrete antigen-presenting vesicles. J Exp Med *183*, 1161-1172.

Rashid, S., Wong, C., and Roy, R. (2021). Developmental plasticity and the response to nutrient stress in *Caenorhabditis elegans*. Dev Biol *475*, 265-276.

Reinhart, B.J., Slack, F.J., Basson, M., Pasquinelli, A.E., Bettinger, J.C., Rougvie, A.E., Horvitz, H.R., and Ruvkun, G. (2000). The 21-nucleotide *let-7* RNA regulates developmental timing in *Caenorhabditis elegans*. Nature *403*, 901-906.

Ren, P., Lim, C.S., Johnsen, R., Albert, P.S., Pilgrim, D., and Riddle, D.L. (1996). Control of *C. elegans* larval development by neuronal expression of a TGF-beta homolog. Science *274*, 1389-1391.

Richardson, P.M., and Zon, L.I. (1995). Molecular cloning of a cDNA with a novel domain present in the tre-2 oncogene and the yeast cell cycle regulators BUB2 and cdc16. Oncogene *11*, 1139-1148.

Riddle, D.L., Swanson, M.M., and Albert, P.S. (1981). Interacting genes in nematode dauer larva formation. Nature *290*, 668-671.

Rimel, J.K., and Taatjes, D.J. (2018). The essential and multifunctional TFIIH complex. Protein Sci *27*, 1018-1037.

Rink, J., Ghigo, E., Kalaidzidis, Y., and Zerial, M. (2005). Rab conversion as a mechanism of progression from early to late endosomes. Cell *122*, 735-749.

Rittershaus, E.S., Baek, S.H., and Sassetti, C.M. (2013). The normalcy of dormancy: common themes in microbial quiescence. Cell Host Microbe *13*, 643-651.

Robinson, H., Ruelcke, J.E., Lewis, A., Bond, C.S., Fox, A.H., Bharti, V., Wani, S., Cloonan, N., Lai, A., Margolin, D*., et al.* (2021). Caveolin-1-driven membrane remodelling regulates hnRNPK-mediated exosomal microRNA sorting in cancer. Clin Transl Med *11*, e381.

Roden, C., and Gladfelter, A.S. (2021). RNA contributions to the form and function of biomolecular condensates. Nat Rev Mol Cell Biol *22*, 183-195.

Ross, F.A., MacKintosh, C., and Hardie, D.G. (2016). AMP-activated protein kinase: a cellular energy sensor that comes in 12 flavours. Febs j *283*, 2987-3001.

Russell, J.C., Kim, T.K., Noori, A., Merrihew, G.E., Robbins, J.E., Golubeva, A., Wang, K., MacCoss, M.J., and Kaeberlein, M. (2020). Composition of *Caenorhabditis elegans* extracellular vesicles suggests roles in metabolism, immunity, and aging. Geroscience *42*, 1133-1145.

Ryan, V.H., Dignon, G.L., Zerze, G.H., Chabata, C.V., Silva, R., Conicella, A.E., Amaya, J., Burke, K.A., Mittal, J., and Fawzi, N.L. (2018). Mechanistic View of hnRNPA2 Low-Complexity Domain Structure, Interactions, and Phase Separation Altered by Mutation and Arginine Methylation. Mol Cell *69*, 465-479.e467.

Samaj, J., Baluska, F., Voigt, B., Schlicht, M., Volkmann, D., and Menzel, D. (2004). Endocytosis, actin cytoskeleton, and signaling. Plant Physiol *135*, 1150-1161.

Sanders, M.J., Ali, Z.S., Hegarty, B.D., Heath, R., Snowden, M.A., and Carling, D. (2007). Defining the mechanism of activation of AMP-activated protein kinase by the small molecule A-769662, a member of the thienopyridone family. J Biol Chem *282*, 32539-32548.

Sato, K., Norris, A., Sato, M., and Grant, B.D. (2014). *C. elegans* as a model for membrane traffic. WormBook, 1-47.

Savina, A., Fader, C.M., Damiani, M.T., and Colombo, M.I. (2005). Rab11 promotes docking and fusion of multivesicular bodies in a calcium-dependent manner. Traffic *6*, 131-143.

Savio, L.E.B., de Andrade Mello, P., Santos, S., de Sousa, J.C., Oliveira, S.D.S., Minshall, R.D., Kurtenbach, E., Wu, Y., Longhi, M.S., Robson, S.C.*, et al.* (2020). P2X7 receptor activation increases expression of caveolin-1 and formation of macrophage lipid rafts, thereby boosting CD39 activity. J Cell Sci *133*.

Schackwitz, W.S., Inoue, T., and Thomas, J.H. (1996). Chemosensory neurons function in parallel to mediate a pheromone response in *C. elegans*. Neuron *17*, 719-728.

Schmeisser, K., Kaptan, D., Raghuraman, B.K., Shevchenko, A., Rodenfels, J., Penkov, S., and Kurzchalia, T.V. (2024). Mobilization of cholesterol induces the transition from quiescence to growth in *Caenorhabditis elegans* through steroid hormone and mTOR signaling. Communications Biology *7*, 121.

Schöneberg, J., Lee, I.H., Iwasa, J.H., and Hurley, J.H. (2017). Reverse-topology membrane scission by the ESCRT proteins. Nat Rev Mol Cell Biol *18*, 5-17.

Schulze, U., Vollenbröker, B., Braun, D.A., Van Le, T., Granado, D., Kremerskothen, J., Fränzel, B., Klosowski, R., Barth, J., Fufezan, C.*, et al.* (2014). The Vac14-interaction network is linked to regulators of the endolysosomal and autophagic pathway. Mol Cell Proteomics *13*, 1397-1411.

Scott, A., Willis, C.R.G., Muratani, M., Higashitani, A., Etheridge, T., Szewczyk, N.J., and Deane, C.S. (2023). *Caenorhabditis elegans* in microgravity: An omics perspective. iScience *26*, 107189.

Scott, C.C., and Gruenberg, J. (2011). Ion flux and the function of endosomes and lysosomes: pH is just the start: the flux of ions across endosomal membranes influences endosome function not only through regulation of the luminal pH. Bioessays *33*, 103-110.

Scott, C.C., Vacca, F., and Gruenberg, J. (2014). Endosome maturation, transport and functions. Paper presented at: Seminars in cell & developmental biology (Elsevier).

Scott, J.W., Hawley, S.A., Green, K.A., Anis, M., Stewart, G., Scullion, G.A., Norman, D.G., and Hardie, D.G. (2004). CBS domains form energy-sensing modules whose

binding of adenosine ligands is disrupted by disease mutations. J Clin Invest *113*, 274-284.

Seaman, M.N., Harbour, M.E., Tattersall, D., Read, E., and Bright, N. (2009). Membrane recruitment of the cargo-selective retromer subcomplex is catalysed by the small GTPase Rab7 and inhibited by the Rab-GAP TBC1D5. J Cell Sci *122*, 2371-2382.

Sendinc, E., Valle-Garcia, D., Jiao, A., and Shi, Y. (2020). Analysis of m6A RNA methylation in *Caenorhabditis elegans*. Cell Discovery *6*, 47.

Sengupta, P., and Samuel, A.D. (2009). *Caenorhabditis elegans*: a model system for systems neuroscience. Curr Opin Neurobiol *19*, 637-643.

Seydoux, G., and Dunn, M.A. (1997). Transcriptionally repressed germ cells lack a subpopulation of phosphorylated RNA polymerase II in early embryos of *Caenorhabditis elegans* and Drosophila melanogaster. Development *124*, 2191-2201.

Seydoux, G., Mello, C.C., Pettitt, J., Wood, W.B., Priess, J.R., and Fire, A. (1996). Repression of gene expression in the embryonic germ lineage of *C. elegans*. Nature *382*, 713-716.

Seydoux, G., and Schedl, T. (2001). The germline in *C. elegans*: origins, proliferation, and silencing. Int Rev Cytol *203*, 139-185.

Shackelford, D.B., and Shaw, R.J. (2009). The LKB1-AMPK pathway: metabolism and growth control in tumour suppression. Nat Rev Cancer *9*, 563-575.

Shaffer, J.M., and Greenwald, I. (2022). SALSA, a genetically encoded biosensor for spatiotemporal quantification of Notch signal transduction in vivo. Dev Cell *57*, 930-944.e936.

Sherr, C.J., and Roberts, J.M. (1999). CDK inhibitors: positive and negative regulators of G1-phase progression. Genes Dev *13*, 1501-1512.

Sheta, M., Taha, E.A., Lu, Y., and Eguchi, T. (2023). Extracellular Vesicles: New Classification and Tumor Immunosuppression. Biology (Basel) *12*.

Shin, H., Haupt, K.A., Kershner, A.M., Kroll-Conner, P., Wickens, M., and Kimble, J. (2017). SYGL-1 and LST-1 link niche signaling to PUF RNA repression for stem cell maintenance in *Caenorhabditis elegans*. PLoS Genet *13*, e1007121.

Shin, H.-W., Hayashi, M., Christoforidis, S., Lacas-Gervais, S., Hoepfner, S., Wenk, M.R., Modregger, J., Uttenweiler-Joseph, S., Wilm, M., and Nystuen, A. (2005). An enzymatic cascade of Rab5 effectors regulates phosphoinositide turnover in the endocytic pathway. The Journal of cell biology *170*, 607-618.

Shin, T.H., and Mello, C.C. (2003). Chromatin regulation during *C. elegans* germline development. Current Opinion in Genetics & Development *13*, 455-462.

Sievers, F., and Higgins, D.G. (2018). Clustal Omega for making accurate alignments of many protein sequences. Protein Sci *27*, 135-145.

Skotland, T., Hessvik, N.P., Sandvig, K., and Llorente, A. (2019). Exosomal lipid composition and the role of ether lipids and phosphoinositides in exosome biology. J Lipid Res *60*, 9-18.

Smythe, C.D.W., Greenall, M., and Kealey, T. (1998). The Activity of HMG-CoA Reductase and Acetyl-CoA Carboxylase in Human Apocrine Sweat Glands, Sebaceous Glands, and Hair Follicles Is Regulated by Phosphorylation and by Exogenous Cholesterol. Journal of Investigative Dermatology *111*, 139-148.

Song, L., Tang, S., Han, X., Jiang, Z., Dong, L., Liu, C., Liang, X., Dong, J., Qiu, C., Wang, Y.*, et al.* (2019). KIBRA controls exosome secretion via inhibiting the proteasomal degradation of Rab27a. Nat Commun *10*, 1639.

Soni, P., Anupom, T., Lesanpezeshki, L., Rahman, M., Hewitt, J.E., Vellone, M., Stodieck, L., Blawzdziewicz, J., Szewczyk, N.J., and Vanapalli, S.A. (2022). Microfluidics-integrated spaceflight hardware for measuring muscle strength of *Caenorhabditis elegans* on the International Space Station. npj Microgravity *8*, 50.

Stroupe, C. (2018). This Is the End: Regulation of Rab7 Nucleotide Binding in Endolysosomal Trafficking and Autophagy. Front Cell Dev Biol *6*, 129.

Sulston, J.E., Schierenberg, E., White, J.G., and Thomson, J.N. (1983). The embryonic cell lineage of the nematode *Caenorhabditis elegans*. Developmental Biology *100*, 64-119.

Suzuki, T., Bridges, D., Nakada, D., Skiniotis, G., Morrison, S.J., Lin, J.D., Saltiel, A.R., and Inoki, K. (2013). Inhibition of AMPK catabolic action by GSK3. Mol Cell *50*, 407-419.

Takahashi, A., Okada, R., Nagao, K., Kawamata, Y., Hanyu, A., Yoshimoto, S., Takasugi, M., Watanabe, S., Kanemaki, M.T., Obuse, C.*, et al.* (2017). Exosomes maintain cellular homeostasis by excreting harmful DNA from cells. Nat Commun *8*, 15287.

Tanzer, A., and Stadler, P.F. (2004). Molecular evolution of a microRNA cluster. Journal of molecular biology *339*, 327-335.

Taylor, S.S., and Kornev, A.P. (2011). Protein kinases: evolution of dynamic regulatory proteins. Trends Biochem Sci *36*, 65-77.

Théry, C., Witwer, K.W., Aikawa, E., Alcaraz, M.J., Anderson, J.D., Andriantsitohaina, R., Antoniou, A., Arab, T., Archer, F., Atkin-Smith, G.K.*, et al.* (2018). Minimal information for

studies of extracellular vesicles 2018 (MISEV2018): a position statement of the International Society for Extracellular Vesicles and update of the MISEV2014 guidelines. J Extracell Vesicles *7*, 1535750.

Thomas, J.H., Birnby, D.A., and Vowels, J.J. (1993). Evidence for parallel processing of sensory information controlling dauer formation in *Caenorhabditis elegans*. Genetics *134*, 1105-1117.

Tibaut, M., Mekis, D., and Petrovic, D. (2017). Pathophysiology of Myocardial Infarction and Acute Management Strategies. Cardiovasc Hematol Agents Med Chem *14*, 150-159.

Trajkovic, K., Hsu, C., Chiantia, S., Rajendran, L., Wenzel, D., Wieland, F., Schwille, P., Brügger, B., and Simons, M. (2008). Ceramide triggers budding of exosome vesicles into multivesicular endosomes. Science *319*, 1244-1247.

Umezu, T., Ohyashiki, K., Kuroda, M., and Ohyashiki, J.H. (2013). Leukemia cell to endothelial cell communication via exosomal miRNAs. Oncogene *32*, 2747-2755.

Unhavaithaya, Y., Shin, T.H., Miliaras, N., Lee, J., Oyama, T., and Mello, C.C. (2002). MEP-1 and a Homolog of the NURD Complex Component Mi-2 Act Together to Maintain Germline-Soma Distinctions in *C. elegans*. Cell *111*, 991-1002.

Updike, D., and Strome, S. (2010). P granule assembly and function in *Caenorhabditis elegans* germ cells. J Androl *31*, 53-60.

Urbán, N., and Cheung, T.H. (2021). Stem cell quiescence: the challenging path to activation. Development *148*.

van Balkom, B.W., de Jong, O.G., Smits, M., Brummelman, J., den Ouden, K., de Bree, P.M., van Eijndhoven, M.A., Pegtel, D.M., Stoorvogel, W., Würdinger, T.*, et al.* (2013). Endothelial cells require miR-214 to secrete exosomes that suppress senescence and

induce angiogenesis in human and mouse endothelial cells. Blood *121*, 3997-4006, s3991-3915.

van den Heuvel, S., and Kipreos, E.T. (2012). *C. elegans* cell cycle analysis. Methods Cell Biol *107*, 265-294.

van Niel, G., Charrin, S., Simoes, S., Romao, M., Rochin, L., Saftig, P., Marks, M.S., Rubinstein, E., and Raposo, G. (2011). The tetraspanin CD63 regulates ESCRT-independent and -dependent endosomal sorting during melanogenesis. Dev Cell *21*, 708-721.

Vanlandingham, P.A., and Ceresa, B.P. (2009). Rab7 regulates late endocytic trafficking downstream of multivesicular body biogenesis and cargo sequestration. J Biol Chem *284*, 12110-12124.

Vieira, O.V., Bucci, C., Harrison, R.E., Trimble, W.S., Lanzetti, L., Gruenberg, J., Schreiber, A.D., Stahl, P.D., and Grinstein, S. (2003). Modulation of Rab5 and Rab7 recruitment to phagosomes by phosphatidylinositol 3-kinase. Molecular and cellular biology *23*, 2501-2514.

Vietri, M., Radulovic, M., and Stenmark, H. (2020). The many functions of ESCRTs. Nat Rev Mol Cell Biol *21*, 25-42.

Villarroya-Beltri, C., Gutiérrez-Vázquez, C., Sánchez-Cabo, F., Pérez-Hernández, D., Vázquez, J., Martin-Cofreces, N., Martinez-Herrera, D.J., Pascual-Montano, A., Mittelbrunn, M., and Sánchez-Madrid, F. (2013). Sumoylated hnRNPA2B1 controls the sorting of miRNAs into exosomes through binding to specific motifs. Nature Communications *4*, 2980.

Vollmer, P., Will, E., Scheglmann, D., Strom, M., and Gallwitz, D. (1999). Primary structure and biochemical characterization of yeast GTPase-activating proteins with substrate preference for the transport GTPase Ypt7p. Eur J Biochem *260*, 284-290.

Vowels, J.J., and Thomas, J.H. (1992). Genetic analysis of chemosensory control of dauer formation in *Caenorhabditis elegans*. Genetics *130*, 105-123.

Vowels, J.J., and Thomas, J.H. (1994). Multiple chemosensory defects in *daf-11* and *daf-21* mutants of *Caenorhabditis elegans*. Genetics *138*, 303-316.

Wadsworth, W.G., and Riddle, D.L. (1989). Developmental regulation of energy metabolism in *Caenorhabditis elegans*. Dev Biol *132*, 167-173.

Wandinger-Ness, A., and Zerial, M. (2014). Rab proteins and the compartmentalization of the endosomal system. Cold Spring Harb Perspect Biol *6*, a022616.

Wang, C.-W., Stromhaug, P.E., Shima, J., and Klionsky, D.J. (2002). The Ccz1-Mon1 protein complex is required for the late step of multiple vacuole delivery pathways. Journal of biological chemistry *277*, 47917-47927.

Wang, J.T., and Seydoux, G. (2014). P granules. Curr Biol *24*, R637-r638.

Wang, R., Cao, L., Thorne, R.F., Zhang, X.D., Li, J., Shao, F., Zhang, L., and Wu, M. (2021). LncRNA GIRGL drives CAPRIN1-mediated phase separation to suppress glutaminase-1 translation under glutamine deprivation. Sci Adv *7*.

Wang, W., Zheng, Y., Wang, M., Yan, M., Jiang, J., and Li, Z. (2019). Exosomes derived miR-126 attenuates oxidative stress and apoptosis from ischemia and reperfusion injury by targeting ERRFI1. Gene *690*, 75-80.

Waterhouse, A., Bertoni, M., Bienert, S., Studer, G., Tauriello, G., Gumienny, R., Heer, F.T., de Beer, T.A.P., Rempfer, C., Bordoli, L.*, et al.* (2018). SWISS-MODEL: homology modelling of protein structures and complexes. Nucleic Acids Res *46*, W296-w303.

Watts, J.L., Morton, D.G., Bestman, J., and Kemphues, K.J. (2000). The *C. elegans par-4* gene encodes a putative serine-threonine kinase required for establishing embryonic asymmetry. Development *127*, 1467-1475.

Watts, J.L., and Ristow, M. (2017). Lipid and Carbohydrate Metabolism in *Caenorhabditis elegans*. Genetics *207*, 413-446.

Wei, D., Zhan, W., Gao, Y., Huang, L., Gong, R., Wang, W., Zhang, R., Wu, Y., Gao, S., and Kang, T. (2021). RAB31 marks and controls an ESCRT-independent exosome pathway. Cell Res *31*, 157-177.

Weiberg, A., Wang, M., Lin, F.-M., Zhao, H., Zhang, Z., Kaloshian, I., Huang, H.-D., and Jin, H. (2013). Fungal Small RNAs Suppress Plant Immunity by Hijacking Host RNA Interference Pathways. Science *342*, 118-123.

Wen, S.W., Lima, L.G., Lobb, R.J., Norris, E.L., Hastie, M.L., Krumeich, S., and Möller, A. (2019). Breast Cancer-Derived Exosomes Reflect the Cell-of-Origin Phenotype. Proteomics *19*, e1800180.

Wilson, J.M., de Hoop, M., Zorzi, N., Toh, B.H., Dotti, C.G., and Parton, R.G. (2000). EEA1, a tethering protein of the early sorting endosome, shows a polarized distribution in hippocampal neurons, epithelial cells, and fibroblasts. Molecular biology of the cell *11*, 2657-2671.

Wilson, R.C., Tambe, A., Kidwell, M.A., Noland, C.L., Schneider, C.P., and Doudna, J.A. (2015). Dicer-TRBP complex formation ensures accurate mammalian microRNA biogenesis. Mol Cell *57*, 397-407.

Wong, C., Kadekar, P., Jurczak, E., and Roy, R. (2023). Germline stem cell integrity and quiescence are controlled by an AMPK-dependent neuronal trafficking pathway. PLoS Genet *19*, e1010716.

Wong, Y.C., Ysselstein, D., and Krainc, D. (2018). Mitochondria-lysosome contacts regulate mitochondrial fission via RAB7 GTP hydrolysis. Nature *554*, 382-386.

Woo, S.S., James, D.J., and Martin, T.F. (2017). Munc13-4 functions as a Ca^{2+} sensor for homotypic secretory granule fusion to generate endosomal exocytic vacuoles. Molecular biology of the cell *28*, 792-808.

Woods, A., Dickerson, K., Heath, R., Hong, S.P., Momcilovic, M., Johnstone, S.R., Carlson, M., and Carling, D. (2005). Ca^{2+}/calmodulin-dependent protein kinase kinase-beta acts upstream of AMP-activated protein kinase in mammalian cells. Cell Metab *2*, 21-33.

Woods, A., Johnstone, S.R., Dickerson, K., Leiper, F.C., Fryer, L.G., Neumann, D., Schlattner, U., Wallimann, T., Carlson, M., and Carling, D. (2003). LKB1 is the upstream kinase in the AMP-activated protein kinase cascade. Curr Biol *13*, 2004-2008.

Wu, Y., and Griffin, E.E. (2017). Regulation of Cell Polarity by PAR-1/MARK Kinase. Curr Top Dev Biol *123*, 365-397.

Wurmser, A.E., Sato, T.K., and Emr, S.D. (2000a). New component of the vacuolar class C-Vps complex couples nucleotide exchange on the Ypt7 GTPase to SNARE-dependent docking and fusion. The Journal of cell biology *151*, 551-562.

Wurmser, A.E., Sato, T.K., and Emr, S.D. (2000b). New component of the vacuolar class C-Vps complex couples nucleotide exchange on the Ypt7 GTPase to SNARE-dependent docking and fusion. J Cell Biol *151*, 551-562.

Xiao, B., Sanders, M.J., Underwood, E., Heath, R., Mayer, F.V., Carmena, D., Jing, C., Walker, P.A., Eccleston, J.F., Haire, L.F.*, et al.* (2011). Structure of mammalian AMPK and its regulation by ADP. Nature *472*, 230-233.

Xie, M., Li, M., Vilborg, A., Lee, N., Shu, M.-D., Yartseva, V., Šestan, N., and Steitz, J.A. (2013). Mammalian 5′-capped microRNA precursors that generate a single microRNA. Cell *155*, 1568-1580.

Xu, L., Fong, Y., and Strome, S. (2001). The *Caenorhabditis elegans* maternal-effect sterile proteins, MES-2, MES-3, and MES-6, are associated in a complex in embryos. Proceedings of the National Academy of Sciences *98*, 5061-5066.

Yamano, K., Fogel, A.I., Wang, C., van der Bliek, A.M., and Youle, R.J. (2014). Mitochondrial Rab GAPs govern autophagosome biogenesis during mitophagy. Elife *3*, e01612.

Yan, Y., Mukherjee, S., Harikumar, K.G., Strutzenberg, T.S., Zhou, X.E., Suino-Powell, K., Xu, T.-H., Sheldon, R.D., Lamp, J., Brunzelle, J.S.*, et al.* (2021). Structure of an AMPK complex in an inactive, ATP-bound state. Science *373*, 413-419.

Yan, Y., Zhou, X.E., Xu, H.E., and Melcher, K. (2018). Structure and Physiological Regulation of AMPK. Int J Mol Sci *19*.

Yang, J.-S., Maurin, T., Robine, N., Rasmussen, K.D., Jeffrey, K.L., Chandwani, R., Papapetrou, E.P., Sadelain, M., O'Carroll, D., and Lai, E.C. (2010). Conserved vertebrate

mir-451 provides a platform for Dicer-independent, Ago2-mediated microRNA biogenesis. Proceedings of the National Academy of Sciences *107*, 15163-15168.

Yin, X., Murphy, S.J., Wilkes, M.C., Ji, Y., and Leof, E.B. (2013). Retromer maintains basolateral distribution of the type II TGF-β receptor via the recycling endosome. Molecular biology of the cell *24*, 2285-2298.

Yoda, M., Kawamata, T., Paroo, Z., Ye, X., Iwasaki, S., Liu, Q., and Tomari, Y. (2010). ATP-dependent human RISC assembly pathways. Nature structural & molecular biology *17*, 17-23.

Yokoi, A., Villar-Prados, A., Oliphint, P.A., Zhang, J., Song, X., De Hoff, P., Morey, R., Liu, J., Roszik, J., Clise-Dwyer, K.*, et al.* (2019). Mechanisms of nuclear content loading to exosomes. Sci Adv *5*, eaax8849.

Yoon, T.Y., and Munson, M. (2018). SNARE complex assembly and disassembly. Curr Biol *28*, R397-r401.

Young, A.R., Chan, E.Y., Hu, X.W., Köchl, R., Crawshaw, S.G., High, S., Hailey, D.W., Lippincott-Schwartz, J., and Tooze, S.A. (2006). Starvation and ULK1-dependent cycling of mammalian Atg9 between the TGN and endosomes. J Cell Sci *119*, 3888-3900.

Yuan, J., and Horvitz, H.R. (1992). The *Caenorhabditis elegans* cell death gene *ced-4* encodes a novel protein and is expressed during the period of extensive programmed cell death. Development *116*, 309-320.

Zavodszky, E., Vicinanza, M., and Rubinsztein, D.C. (2013). Biology and trafficking of ATG9 and ATG16L1, two proteins that regulate autophagosome formation. FEBS Lett *587*, 1988-1996.

Zhang, C.S., Hawley, S.A., Zong, Y., Li, M., Wang, Z., Gray, A., Ma, T., Cui, J., Feng, J.W., Zhu, M.*, et al.* (2017). Fructose-1,6-bisphosphate and aldolase mediate glucose sensing by AMPK. Nature *548*, 112-116.

Zhang, C.S., Jiang, B., Li, M., Zhu, M., Peng, Y., Zhang, Y.L., Wu, Y.Q., Li, T.Y., Liang, Y., Lu, Z.*, et al.* (2014). The lysosomal v-ATPase-Ragulator complex is a common activator for AMPK and mTORC1, acting as a switch between catabolism and anabolism. Cell Metab *20*, 526-540.

Zhang, F., Barboric, M., Blackwell, T.K., and Peterlin, B.M. (2003). A model of repression: CTD analogs and PIE-1 inhibit transcriptional elongation by P-TEFb. Genes Dev *17*, 748-758.

Zhang, H., Kolb, F.A., Jaskiewicz, L., Westhof, E., and Filipowicz, W. (2004). Single processing center models for human Dicer and bacterial RNase III. Cell *118*, 57-68.

Zhang, L., Li, J., Young, L.H., and Caplan, M.J. (2006). AMP-activated protein kinase regulates the assembly of epithelial tight junctions. Proceedings of the National Academy of Sciences *103*, 17272-17277.

Zhang, L., Ward, J.D., Cheng, Z., and Dernburg, A.F. (2015). The auxin-inducible degradation (AID) system enables versatile conditional protein depletion in *C. elegans*. Development *142*, 4374-4384.

Zhang, S., Li, F., Zhou, T., Wang, G., and Li, Z. (2020a). *Caenorhabditis elegans* as a Useful Model for Studying Aging Mutations. Front Endocrinol (Lausanne) *11*, 554994.

Zhang, S., Wang, C., Ma, B., Xu, M., Xu, S., Liu, J., Tian, Y., Fu, Y., and Luo, Y. (2020b). Mutant p53 Drives Cancer Metastasis via RCP-Mediated Hsp90α Secretion. Cell Rep *32*, 107879.

Zhang, X.-M., Walsh, B., Mitchell, C.A., and Rowe, T. (2005). TBC domain family, member 15 is a novel mammalian Rab GTPase-activating protein with substrate preference for Rab7. Biochemical and biophysical research communications *335*, 154-161.

Zhao, Y.G., Codogno, P., and Zhang, H. (2021). Machinery, regulation and pathophysiological implications of autophagosome maturation. Nat Rev Mol Cell Biol *22*, 733-750.

Zheng, D., Huo, M., Li, B., Wang, W., Piao, H., Wang, Y., Zhu, Z., Li, D., Wang, T., and Liu, K. (2021). The role of exosomes and exosomal microRNA in cardiovascular disease. Frontiers in cell and developmental biology *8*, 616161.

Zhong, L., Liao, D., Li, J., Liu, W., Wang, J., Zeng, C., Wang, X., Cao, Z., Zhang, R., Li, M.*, et al.* (2021). Rab22a-NeoF1 fusion protein promotes osteosarcoma lung metastasis through its secretion into exosomes. Signal Transduction and Targeted Therapy *6*, 59.

Zhou, M., Halanski, M.A., Radonovich, M.F., Kashanchi, F., Peng, J., Price, D.H., and Brady, J.N. (2000). Tat modifies the activity of CDK9 to phosphorylate serine 5 of the RNA polymerase II carboxyl-terminal domain during human immunodeficiency virus type 1 transcription. Mol Cell Biol *20*, 5077-5086.

Zhou, Q., Lai, Y., Bacaj, T., Zhao, M., Lyubimov, A.Y., Uervirojnangkoorn, M., Zeldin, O.B., Brewster, A.S., Sauter, N.K., Cohen, A.E.*, et al.* (2015). Architecture of the synaptotagmin-SNARE machinery for neuronal exocytosis. Nature *525*, 62-67.

Zhou, W., Fong, M.Y., Min, Y., Somlo, G., Liu, L., Palomares, M.R., Yu, Y., Chow, A., O'Connor, S.T., Chin, A.R.*, et al.* (2014). Cancer-secreted miR-105 destroys vascular endothelial barriers to promote metastasis. Cancer Cell *25*, 501-515.

Zhu, H., Zhu, G., Liu, J., Liang, Z., Zhang, X.C., and Li, G. (2007). Rabaptin-5-independent membrane targeting and Rab5 activation by Rabex-5 in the cell. Molecular biology of the cell *18*, 4119-4128.

Zonies, S., Motegi, F., Hao, Y., and Seydoux, G. (2010). Symmetry breaking and polarization of the *C. elegans* zygote by the polarity protein PAR-2. Development *137*, 1669-1677.

Chapter 2: Germline stem cell integrity and quiescence are controlled by an AMPK-dependent neuronal trafficking pathway

Christopher Wong[1], Pratik Kadekar[1], Elena Jurczak[1], Richard Roy[1]

[1]Department of Biology, McGill University; Montreal, H3A 1B1, Canada.

Adapted from PLOS Genetics 19, no. 4

Abstract

During periods of energetic stress, *Caenorhabditis elegans* can execute a developmentally quiescent stage called “dauer”, during which all germline stem cells undergo a G2 cell cycle arrest. In animals that lack AMP-activated protein kinase (AMPK) signalling, the germ cells fail to arrest, undergo uncontrolled proliferation, and lose their reproductive capacity upon recovery from this quiescent stage. These germline defects are accompanied by, and likely result from, an altered chromatin landscape and gene expression program. Through genetic analysis we identified an allele of *tbc-7*, a predicted RabGAP protein that functions in the neurons, which when compromised, suppresses the germline hyperplasia in the dauer larvae, as well as the post-dauer sterility and somatic defects characteristic of AMPK mutants. This mutation also corrects the abundance and aberrant distribution of transcriptionally activating and repressive chromatin marks in animals that otherwise lack all AMPK signalling. We identified RAB-7 as one of the potential RAB proteins that is modulated by *tbc-7* and show that the activity of RAB-7 is critical for the maintenance of germ cell integrity during the dauer stage. We reveal that TBC-7 is regulated by AMPK through two mechanisms when the animals enter the dauer stage. Acutely, the AMPK-mediated phosphorylation of TBC-7 reduces its activity, potentially by autoinhibition, thereby preventing the inactivation of RAB-7. In the more long term, AMPK regulates the miRNAs *mir-1* and *mir-44* to attenuate *tbc-7* expression. Consistent with this, animals lacking *mir-1* and *mir-44* are post-dauer sterile, phenocopying the germline defects of AMPK mutants. Altogether, we have uncovered an AMPK-dependent and microRNA-regulated cellular trafficking pathway that is initiated in

the neurons, and is critical to control germline gene expression cell non-autonomously in response to adverse environmental conditions.

Authors' summary

During environmental challenges many organisms possess the ability to forego reproduction temporarily to enter a diapause stage only to resume reproduction when growing conditions improve. In *C. elegans*, the dauer stage is associated with a general developmental quiescence that is essential to preserve the reproductive competence of the germ cells following recovery, and this is controlled by AMPK signalling. However, we show that AMPK activation need not occur in all cells, but is critical in those cells that are likely most sensitive to such changes, namely in the neurons. Using genetic analysis, we revealed that the activation of AMPK in the neurons engages changes in RAB-7 trafficking, which are the result of a two-pronged AMPK-dependent regulation of a predicted RabGAP protein called TBC-7. By first modulating the activity of TBC-7, AMPK enhances RAB-7 activation, while later in the diapause, AMPK promotes the activity of two microRNAs that impinge on the *tbc-7* transcript, thereby blocking its expression. This results in a cell non-autonomous pro-quiescent signal that instructs the germ cells to modify their chromatin landscape and associated gene expression, ensuring that the germ cells remain reproductively competent for the duration of the diapause stage.

Introduction

For many organisms, development unravels as a successive series of growth, quiescence, and phases of cell differentiation that proceed according to an organism-specific program. This is particularly true for closed systems, such as during embryonic development, where events often unfold independently of external resource availability due to maternal provisioning for the developing organism.

This situation changes dramatically as animals emerge from the embryo, and juveniles are subject to dramatic fluctuations in growth conditions. These challenges can be detrimental to continuous development and thus have driven the emergence of diverse mechanisms of adaptation that have evolved to enhance survival. One common means to circumvent these challenges is the programmed ability to undergo a period of developmental quiescence, or a diapause. In microbial cells, like bacteria and yeast, rapid growth and divisions arrest when resources are exhausted, while cells remain viable and poised to resume proliferation when growth conditions improve [1-3].

But this kind of quiescence is not unique to microbes. Mammalian cells in culture arrest their cell divisions and enter a G_0 state if they are deprived of growth factors (serum), glucose, or when they become confluent [4]. Moreover, cells that no longer appropriately execute quiescence in response to these cues, can often demonstrate other rogue behaviours, typical of transformed cells [3]. It is therefore highly advantageous to appropriately respond to these adverse environmental signals and execute a quiescent state as an adaptive means of protecting the cell and its invaluable genetic material.

Multicellular organisms also employ various states of quiescence to ensure survival during periods of environmental stress [5-7]. However, not all cells in the

organism are capable of sensing these cues and therefore depend on specialized cells to communicate information to their distant neighbours to protect them against these challenges.

These specialized cells often express molecular sensors that are capable of both gauging external fluctuations and initiating the appropriate adaptive cellular/organismal changes to enhance survival during difficult environmental circumstances. Among the most widely studied of these cellular/molecular sensors is the stress-responsive AMP-activated protein kinase (AMPK). During periods of stress, it phosphorylates critical targets to block energy-consuming anabolic processes and activate pathways that will enhance the cellular energy pool. For example, many animals, including humans, forego reproduction during periods of excess stress or starvation [5, 8]. Both starved *C. elegans* or mutants that lack insulin signalling when exposed to high temperatures during the L4 larval or early adult stages are infertile and do not produce oocytes [9]. This is presumably because gametogenesis is very energy demanding and the resulting progeny would not fare well in a resource-depleted or unfavourable environment [9]. However, this oogenesis defect can be bypassed in these mutants by eliminating AMPK activity [8, 10].

Activation of AMPK in *C. elegans* larvae that execute the highly-resistant, diapause-like dauer stage results in germline quiescence, while other somatic cell divisions are arrested through a parallel pathway [10, 11]. In the absence of AMPK signalling, mutant germ cells continue to proliferate despite a lack of resources, resulting in sterility following recovery [8, 10].

Animals can survive for months in the non-feeding dauer stage, yet when animals exit this diapause they are fully fertile with little or no negative reproductive consequence

[12, 13]. On the other hand, mutants that lack all AMPK signalling die prematurely during the dauer stage, and if they do recover they exhibit highly penetrant sterility [10]. The AMPK-mediated quiescence that occurs during the dauer stage is therefore protective and is critical to preserve germ cell integrity during this period of prolonged stress. Consistent with this, wild-type animals that transit through the dauer stage exhibit differences in their gene expression compared to animals that never encountered the stresses associated with dauer development [14, 15]. These changes persist in the post-dauer animals as a molecular memory stored in the form of epigenetic marks, which have been shown to influence post-dauer fertility.

Mutants that lack all AMPK signalling display significant changes in gene expression during the dauer stage and as post-dauer adult animals when compared to wild-type animals [10]. In addition, the levels of transcriptionally activating and repressive chromatin marks within the germ line are abnormally upregulated, while their distribution is also abnormal. This suggests that the differences in gene expression in AMPK mutants could be attributed to the misregulation of chromatin marks in the affected germ cells.

Recent studies have indicated that AMPK can act cell non-autonomously to regulate life span [16], while the restoration of AMPK in some somatic cells was sufficient to correct the germline defects in AMPK mutants [10, 17]. Namely, driving AMPK activity in the neurons and the excretory system was shown to suppress the AMPK germline defects [10]. Moreover, the post-dauer sterility and the germline hyperplasia typical of AMPK mutants are also partially suppressed when components of the endogenous small RNA pathway are compromised [10]. These findings suggest that several different pathways are likely to be involved in conveying the necessary signals to execute an

adaptive gene expression response in the germ line in response to dauer entry. This is most likely coordinated through the function of specialized sensing cells; a role very often fulfilled by neurons. In the context of dauer development, AMPK would activate these various events in response to the metabolic challenges associated with dauer development in order to protect the germ line throughout the duration of the diapause.

Here we describe how AMPK regulates germ cell homeostasis in response to energy stress. This role requires its activity not in the germ cells, but in the neurons. By performing a genetic screen designed to identify genes involved in the AMPK regulation of germ cell integrity and germline quiescence during the dauer stage, we isolated eight alleles that partially restore germ cell function in these mutants. One of these genes encodes a RabGAP that enhances the intrinsic GTP hydrolysis activity of one or more Rab proteins, converting it from its active RAB-GTP form to its inactivated RAB-GDP form [18]. This RabGAP functions in the neurons to negatively regulate its RAB target. Furthermore, we demonstrate that the RabGAP is subject to regulation both directly by AMPK-mediated phosphorylation in the short term, and then in later stages of the diapause, by regulating its expression by two microRNAs. Therefore, through the successive targeting of a single RabGAP in the neurons, AMPK signals cell non-autonomously to the germline stem cells to arrest their cell divisions and to maintain germ cell integrity at the onset of this period of developmental quiescence.

Results

Mutations that reverse the germline defects of AMPK mutants.

The *C. elegans* dauer stage is marked by a pervasive organismal developmental quiescence that is initiated as animals transit through the preparatory L2d stage. This is accompanied by a complete arrest in germ cell divisions mediated by the activity of the *C. elegans* orthologues of the human tumour suppressor genes PTEN (*daf-18*), LKB1 (*par-4*), and one of its many downstream targets, AMPK [8]. Animals that lack all AMPK signalling due to the deletion of both catalytic subunits *aak-1* and *aak-2* (referred to as *aak(0)*) undergo extensive germline hyperplasia during dauer formation and exhibit post-dauer sterility, in addition to a number of metabolic/somatic phenotypes [10, 17]. Curiously, the compromise of various components involved in the biogenesis and function of small RNAs can partially restore germ cell quiescence in AMPK mutant dauer larvae, in addition to the corresponding post-dauer fertility in these mutants.

To identify additional genes that converge either on these small RNA regulators or on AMPK targets in the germ line, we performed a forward genetic screen to obtain mutants that suppress the germline defects typical of AMPK mutants. Eight alleles were isolated that fall into five complementation groups (Table 1), each of which suppressed the germ cell hyperplasia and/or the post-dauer sterility in AMPK mutants to varying degrees (S1A-C Fig and S1 Table). All isolated alleles were able to lay viable embryos that gave rise to a fertile generation.

The *rr166* allele was the most effective in suppressing the AMPK germline and somatic defects (Fig 1A-C). When AMPK mutants recover from the dauer stage, many animals die prematurely. Those mutants that recover display diverse abnormalities in

vulval development, such as protruding vulva, burst vulva, or multivulva [10]. In addition to its effects on the germline hyperplasia, *rr166* suppressed most of the post-dauer somatic defects. This allele may therefore not be exclusively active in the germ line and could have a function in the soma during normal development and/or in the dauer stage. Alternatively, it could adjust cell divisions in somatic tissues through its effect on the germ line (S1 Table).

AMPK is also required for the typical long-term survival of the dauer larva by regulating triglyceride hydrolysis during the dauer stage [17]. Dauer larvae with intact AMPK signalling can survive for several weeks/months, while mutants with disrupted AMPK/LKB1 signalling die prematurely due to the inappropriate depletion of stored lipids important to sustain animals. Strikingly, neither *rr166* nor *rr267* improved the dauer survival of *aak(0)* mutants, suggesting that the *rr166* and *rr267* mutations do not affect other AMPK-regulated metabolic pathways and may be more specific to germ line/gonadal physiology (Fig 1D).

_rr166_ corrects the abnormal deposition of the chromatin marks in the germ line of AMPK mutant dauer larvae and post-dauer adults.

daf-2; aak(0) mutants not only have upregulated levels of both transcriptionally activating and repressive chromatin marks, but they also have an abnormal distribution of these epigenetic modifications across the germ line in both dauer and post-dauer animals [10]. This altered chromatin landscape is associated with a dramatic change in germline gene expression during the dauer stage, which remains unaltered upon dauer exit, persisting into the post-dauer adult. To better understand how *rr166* suppresses the

AMPK germline defects, we examined the levels of chromatin marks that were aberrant in the AMPK mutant dauer larvae to assess how these epigenetic modifications are affected in the *daf-2; aak(0); rr166* mutant. Western analysis revealed that both activating (H3K4me3) and repressive (H3K9me3) chromatin modifications were restored to nearly normal levels in the germ cell nuclei of *daf-2; aak(0); rr166* dauer larvae that lack all AMPK signalling (S2A-A'' Fig). In addition, the distribution of the chromatin marks was also corrected (S2B-C'' Fig).

Using the same approach, we confirmed that the *rr166* mutation was also able to suppress the increased abundance of the chromatin marks in the *daf-2; aak(0)* mutants during the post-dauer stage (S3A-A'' Fig). Immunofluorescence analysis against these histone modifications indicated that *rr166* could correct the abundance of each mark in individual nuclei, while also reestablishing the overall distribution pattern across the germ line (S3B-C'' Fig). Interestingly, while the levels of H3K9me3 in the *rr166* mutants were similar compared to *daf-2* control animals, the levels of H3K4me3 were not completely restored to *daf-2* control levels, albeit they were reduced compared to those of *daf-2; aak(0)* mutants (S3B-B'' Fig). Together, these data indicate that *rr166* corrects the abundance and distribution of chromatin marks in the germ line that presumably prime germline gene expression for a period of developmental quiescence, in animals that lack all AMPK signalling.

Misregulated RabGAP activity in neurons of AMPK mutants results in germline abnormalities during the dauer stage.

To identify relevant polymorphisms that could correspond to the affected gene responsible for the suppression of AMPK germline defects, genomic DNA from *daf-2; aak(0); rr166* mutants was subjected to next generation sequence analysis [19]. *rr166* was revealed to be a typical EMS-generated G->A transition mutation in a gene called *tbc-7* that encodes a predicted RabGAP protein.

To confirm that *rr166* is indeed an allele of *tbc-7*, we performed RNAi against *tbc-7* in the *daf-2; aak(0)* mutants. Fertility was partially restored in *daf-2; aak(0); tbc-7* (RNAi) animals, and they showed no significant difference in their post-dauer fertility when compared to *daf-2; aak(0); rr166* animals (Fig 2A). Furthermore, when *daf-2; aak(0); rr166* mutants were injected with a fosmid which contained a wild-type copy of *tbc-7*, the suppression of the AMPK mutant germline defects was reverted, suggesting that *rr166* is indeed an allele of *tbc-7* (Fig 2A).

The *rr166* allele is a missense mutation that results in a change from serine to phenylalanine at position 520, which corresponds to the predicted TLDc domain of *tbc-7*. From the same complementation group, the *rr267* allele corresponds to a missense mutation that alters a phenylalanine to leucine at position 156, which does not correspond to any predicted protein domain. The difference in the position of the mutations could account for the ability of each allele to suppress the AMPK germline defects; compromising the TLDc domain with the S520F mutation could have a greater impact on TBC-7 function compared to the F156L mutation.

Mutations that eliminate the entire *tbc-7* region are presumably non-viable, as no mutants that contain a large or complete deletion of *tbc-7* can be maintained as a homozygous animal, but *rr166* is viable. To determine if the *tbc-7(rr166)* point mutation is a hypomorphic allele of an essential gene, we crossed the *tbc-7(rr166)* mutation into a null mutant that contains a deletion of the entire *tbc-7* gene (*tm10766*). Our subsequent genetic analyses were consistent with *rr166* acting as a recessive, hypomorphic allele of *tbc-7* (S4A-B Fig and Materials and Methods).

Recent work demonstrated that AMPK can regulate germ cell integrity cell non-autonomously during the dauer stage [10]. Restoring AMPK function in the neurons and in the excretory system re-established germline quiescence and germ cell integrity in AMPK mutants [10]. Furthermore, the somatic expression of *aak-2* was able to correct both the abundance and distribution of chromatin marks in the dauer germ line, suggesting that the somatic function of AMPK controls the execution of germline quiescence in response to dauer cues.

tbc-7 encodes a RabGAP protein that is conserved in *Drosophila* and in humans, where it is critical for appropriate synaptic vesicle dynamics in neurons [20]. Because of this neuronal role, we wondered if *tbc-7* might regulate the germ line cell non-autonomously during the dauer stage. To better understand where *tbc-7* is expressed we generated a transgenic strain using a fosmid containing a TBC-7::GFP translational fusion protein. This fosmid contains the entire coding sequence of *tbc-7* as well as the 5'UTR, 3'UTR, and any potential upstream and downstream regulatory sequences (starts X: 5,120,813 and ends X:5,154,839) (See Materials and Methods). A previous report suggested that *tbc-7* might act predominantly in muscle to regulate autophagy, but this

may not be entirely accurate, since this expression analysis was based on a relatively small region of upstream sequence used to drive a transcriptional fusion transgene [21]. Fosmid-based reporter systems contain large genomic regions that are more likely to capture most, if not all, cis-regulatory information, therefore resulting in a more accurate representation of the expression of any given gene [22].

Imaging revealed that TBC-7 is highly expressed in the neurons of adult animals grown in replete conditions as well as in dauer larvae (Fig 2B-C). Moreover, the neuronal expression of *tbc-7* is critical for its function in this context, since the introduction of a wild-type copy of *tbc-7* cDNA driven by a pan-neuronal promoter in the *daf-2; aak(0); tbc-7* mutants reverted the suppression of AMPK germline defects (Fig 2D). Because of the claim that *tbc-7* might also function in the body wall muscles [21], a wild-type copy of *tbc-7* cDNA was driven by a muscle-specific promoter (*myo-3)* in *daf-2; aak(0); tbc-7* mutants to determine if this tissue contributes to the regulation of dauer germ line integrity. Unlike our findings using a neuron-specific *tbc-7* transgene, driving the expression of *tbc-7* exclusively in the muscles was unable to revert the suppression of the germline defects, suggesting that *tbc-7* does not regulate germ cell integrity from the body wall muscle, and its role in antagonizing germ cell quiescence during the dauer stage is dependent on its neuronal function (S5A Fig).

Our initial findings indicated that when AMPK function is restored in the excretory system, or in the nervous system, the post-dauer sterility and the germline hyperplasia are corrected, suggesting that AMPK may also work in the excretory system to regulate germ cell integrity during the dauer stage [10]. To determine if *tbc-7* expression in the excretory system may also contribute to this AMPK effect on the germ line, a wild-type

copy of *tbc-7* cDNA was driven by an excretory system-specific promoter (*sulp-5*) in *aak(0); tbc-7* mutants. Similar to the muscle-specific expression, this excretory-specific transgene had no effect on the *tbc-7*-associated suppression of the AMPK mutant phenotypes. Therefore, AMPK must somehow modulate *tbc-7* function in the neurons during the onset of the dauer stage to instruct the germ line to execute quiescence (S5B Fig).

To further confirm that *tbc-7* acts in the neurons, we used a tissue-specific RNAi strategy that allowed us to compromise the expression of *tbc-7* exclusively in one tissue at a time (see Materials and Methods) (S2 Table) [23, 24]. If *tbc-7* activity is required in the neurons, then *daf-2; aak(0)* mutants that are subjected to *tbc-7* RNAi exclusively in the neurons should phenocopy the *tbc-7(rr166)* mutation and suppress the AMPK germline defects. Using the neuronal RNAi strain, we found that *tbc-7* RNAi indeed suppressed the post-dauer sterility of *daf-2; aak(0)* mutants, while strains that had *tbc-7* compromised exclusively in the germ line showed no such suppression, although the RNAi was indeed effective (Figs 2E and S8). Taken together, these data indicate that TBC-7 functions in the neurons to antagonize AMPK-dependent germline quiescence and germ cell integrity during the dauer stage.

TBC-7 negatively regulates RAB-7 in the neurons to maintain germ cell integrity.

TBC-7 is a predicted RabGAP protein that could enhance the intrinsic GTP hydrolysis activity of Rab GTPases, presumably converting them from their active GTP-bound form into their inactive GDP-bound form. In AMPK mutants, the *tbc-7*-associated RAB(s) are most probably in their inactive GDP-bound form due to misregulated TBC-7

activity, while in *daf-2; aak(0); tbc-7* mutants, the *tbc-7*-associated RAB(s) may be in their active GTP-bound form (Fig 3A). Therefore, compromising the expression of the RAB(s) associated with *tbc-7* should revert the suppression conferred by the *tbc-7* mutation, causing a loss of germ cell integrity and post-dauer fertility. To identify which RAB protein is regulated by *tbc-7*, each predicted *rab* gene in the *C. elegans* genome was compromised using a hypomorphic RNAi strategy [25]. This RNAi survey of RAB proteins revealed that TBC-7 may regulate a large number of RAB effectors (Fig 3B and S3 Table). However, when *rab-7* was compromised in the *daf-2; aak(0); tbc-7* mutants, the post-dauer fertility was reduced to a level similar to that of post-dauer *daf-2; aak(0)* mutants (compare the fourth column in Fig 3B with the first column in Fig 2A). Furthermore, if *rab-7* acts downstream of AMPK signalling and *tbc-7* to regulate germline quiescence in the dauer stage, then disabling it should result in dauer phenotypes very similar or identical to AMPK mutants. Indeed, *rab-7* RNAi in the *daf-2; aak(0); tbc-7* mutant during the dauer stage caused post-dauer sterility (Fig 3B, fourth column). Taken together, these data strongly support a role for *rab-7* in the correct regulation of germline quiescence during the dauer stage.

The compromise of *rab-10* in the *daf-2; aak(0); tbc-7* mutants showed a similar phenotype to the loss of *rab-7* through RNAi. Therefore, to examine if RAB-10 could be a direct target of TBC-7, we employed our tissue-specific RNAi system in the *daf-2; aak(0); tbc-7* mutant to examine in which tissue RAB-10 functions during the dauer stage. When *rab-10* was compromised exclusively in the germ line, the animals were post-dauer sterile, while the compromise in the neurons had no observable effects on the post-dauer fertility, suggesting that *rab-10* functions in the germ line (S6 Fig). We therefore reasoned

that RAB-10 is most likely not a direct Rab target of TBC-7 in this context, since they function in different tissues.

To further confirm that RAB-7 is regulated by TBC-7 in the neurons, we once again used our tissue-specific RNAi system [23, 24] to attenuate *rab-7* activity exclusively in the neurons, which resulted in highly penetrant post-dauer sterility (S4 Table), while its compromise in the germ line had no observable effects on the reproductive output of the post-dauer animal (Fig 3C).

Rab proteins bind GTP and then hydrolyse it to GDP through their intrinsic GTPase activity, which is greatly enhanced by the activity of its corresponding RabGAP [18]. By using a mutated form of a Rab protein in which the GTPase activity has been disabled (GTP-locked), a constitutively active form of the Rab can be used to assess the various roles of the activated Rab protein [26, 27]. Using this strategy, we introduced a GTP-locked variant of RAB-7 in the neurons of the *daf-2; aak(0)* animals by introducing a point mutation Q68L in RAB-7 driven by the *rgef-1* neuronal promoter [26, 28]. In mammalian cells, the GTP-hydrolysis deficient mutants Rab7 Q67L are locked in its GTP-bound form, resulting in constitutive activity [28]. The orthologous mutation in *C. elegans* RAB-7 Q68L results in a GTP-locked variant of RAB-7 that when expressed in the intestine, results in larger intestinal vesicles [26]. If RAB-7 is involved in establishing or maintaining germline quiescence and is misregulated by TBC-7 when AMPK is no longer functional, then the presence of a GTP-locked variant in this context should result in the suppression of the post-dauer sterility presumably caused by misregulated TBC-7 activity in the absence of AMPK signalling. Indeed, the expression of the GTP-locked RAB-7 variant improved post-dauer fertility (average of 56%) in the AMPK mutant dauer larvae (Fig 3D). Taken

altogether, our analyses indicate that misregulated TBC-7 blocks RAB-7 activation in the neurons of dauer larvae, thereby allowing germ cell divisions to continue, eventually resulting in the germline hyperplasia typical of AMPK mutants.

mir-1 and _mir-44_ negatively regulate _tbc-7_ downstream of AMPK activation to promote germline quiescence.

The RabGAP *tbc-7* has been previously reported to be regulated by *mir-1* [21, 29], whereby *mir-1* binds directly to the 3'UTR of *tbc-7* to silence its expression. The loss of the *mir-1* binding site or the loss of *mir-1* itself results in an overexpression of *tbc-7*, causing impaired autophagy and proteotoxic stress [21]. In a separate study that sequenced miRNA-target sites bound by ALG-1, *mir-1* was found to bind the 3'UTR of *tbc-7* directly, further suggesting that *mir-1* could be a direct regulator of *tbc-7* expression [30]. microRNA production is critical for entering the dauer stage and genetic mutants that are deficient in producing specific microRNAs, or do not possess the machinery necessary for microRNA production, are dauer deficient [31]. However, it is possible that in addition to their critical role in dauer formation, microRNAs may also be involved in regulating multiple key targets that are necessary for various aspects of the diapause, including the maintenance of germ cell integrity.

To determine if any potential small RNAs could impinge on *tbc-7* function, we analysed the predicted *tbc-7* transcript using TargetScanWorm (version 6.2), a program designed to measure the biological relevance between predicted miRNAs and seed sequences. We identified two highly conserved seed sequences for *mir-1* and one highly conserved seed sequence for *mir-44* in the 3' UTR of *tbc-7* (S5 Table). *mir-1* is one of 32

conserved microRNAs throughout the Bilateria and is important for many functions including autophagy, muscle development, and sarcomere and mitochondrial integrity [32, 33]. The *mir-44* family modulates the germline sex determination pathway in *C. elegans* by promoting the production of sperm in the hermaphrodite germ line [34].

If *mir-1* and *mir-44* regulate the expression of *tbc-7* directly, then the loss of either or both of them during the dauer stage should result in the misregulation of *tbc-7*. This increase in TBC-7 activity would further enhance the hydrolysis of RAB-7 GTP into RAB-7 GDP, resulting in the same post-dauer phenotypes seen in *daf-2; aak(0)* mutants. Curiously, when mutants that contain deletions of the *mir-1* microRNA (*mir-1(gk276)*) and deletions of the entire *mir-44* microRNA family (*nDf49* allele: *mir-44, ZK930.12, mir-42, ZK930.15, mir-43*) were allowed to spend 24 hours in the dauer stage, there were no observable defects in the post-dauer fertility (Fig 4B). However, if the duration of dauer is prolonged to 7 days, *mir-1; daf-2* and *mir-44; daf-2* mutants exhibited varying degrees of post-dauer sterility, while *daf-2* control animals were unaffected (Fig 4B). After allowing *mir-1; daf-2* and *mir-44; daf-2* mutants to recover after 7 days in the dauer stage, the mutants were found to recover at normal rates compared to *daf-2* control animals and AMPK mutants, but their fertility was greatly decreased, such that they resembled AMPK mutants. This finding suggests that the germ cells may lose their integrity after a prolonged duration in the dauer stage in the *mir-1; daf-2* and *mir-44; daf-2* mutants, presumably due to the inappropriate regulation of *tbc-7*. Furthermore, when the activity of the TBC-7 target RAB-7 was further reduced by performing *rab-7* RNAi, the *mir-1; daf-2* and *mir-44; daf-2* mutants exhibited post-dauer sterility after only 24 hours in the dauer stage (Fig 4C). Moreover, *mir-1; mir-44; daf-2* mutants exhibited similar post-dauer

germline defects after spending 7 days in the dauer stage or after 24 hours after being subjected to *rab-7* RNAi (S7A-B Fig). This enhancement of the *mir-1* and *mir-44* post-dauer sterility following *rab-7* RNAi is consistent with a role of *mir-1* and *mir-44* in the regulation of *tbc-7*. Our findings suggest that as the animal spends an extended period of time in the dauer stage, the loss of *mir-1* and *mir-44* presumably allows for *tbc-7* transcripts to be actively expressed. TBC-7 can then continually enhance the hydrolysis of RAB-7 GTP into RAB-7 GDP, decreasing the neuronal pool of available active RAB-7. It is this depletion of active RAB-7 in its GTP-bound state that is most likely responsible for the observed germ cell hyperplasia and the loss of germ cell integrity, rendering the post-dauer animals sterile.

If *mir-1* and *mir-44* do indeed bind to the 3'UTR of *tbc-7* to negatively regulate its expression during the dauer stage, then the deletion of these sequences should lead to increased *tbc-7* expression, thereby reducing the levels of GTP-bound RAB-7 and a consequent loss of post-dauer fertility. In *daf-2* control animals that harbour wild-type AMPK function, but possess a deletion of the *mir-1* and *mir-44* seed sequences in the *tbc-7* 3'UTR, the recovered post-dauer adults exhibited a marked sterility compared to identical animals with an unmodified wild-type 3'UTR (Fig 4D). This underscores the importance of these miRNA binding sites and the need to block TBC-7 activity during the dauer stage to preserve germline integrity (Fig 4D). Furthermore, to complement these findings, we reasoned that the enhanced neuronal expression of *mir-1* or *mir-44* in *daf-2; aak(0)* mutants should suppress the AMPK germline defects by reducing the levels of *tbc-7*. Consistent with this, increased *mir-1* or *mir-44* expression in *daf-2; aak(0)* mutants suppressed the post-dauer sterility of AMPK mutants (Fig 4E). Together these results

suggest that *mir-1* and *mir-44* play an important role in regulating RAB-7 activity by directly binding to the *tbc-7* 3'UTR to control its expression during the dauer stage.

AMPK-mediated phosphorylation of TBC-7 could reduce its RabGAP activity.

Although we have described how microRNAs contribute to the regulation of *tbc-7* in the neurons in response to AMPK activation, the kinetics of the *mir-1* and *mir-44* inhibition are not consistent with the timing of the first changes that occur in the germ line following the initiation of dauer formation. *mir-1* and *mir-44* mutants only exhibit post-dauer sterility after remaining in dauer for a longer duration, suggesting that these microRNAs may not be the sole regulators of TBC-7 activity. We therefore questioned whether AMPK might play an additional role in the regulation of TBC-7, perhaps through a key post-translational modification that would act more immediately than the activation of the miRNA-mediated *tbc-7* inhibition. We noticed that TBC-7 possesses a high stringency AMPK phosphorylation motif on Ser115 [35], making it a prime target of AMPK upon activation of the kinase during dauer formation to negatively affect the function or stability of TBC-7.

Very often, AMPK phosphorylates its targets thereby generating a 14-3-3 recognition site that eventually leads to target degradation [35]. To confirm if this is how AMPK affects TBC-7, we first performed a Western analysis on TBC-7 in *daf-2* control and *daf-2; aak(0)* mutant dauer larvae to determine if AMPK could affect the stability of TBC-7 by targeting it for subsequent degradation. If this is the case, the abundance of TBC-7 should be significantly higher in mutant animals that lack all AMPK signalling. Our analysis indicated that this was not the case and the abundance of TBC-7 was not

significantly different between the two genotypes (Fig 5A). We then examined if the S520F mutation in *rr166* affected the stability of TBC-7. If the S520F mutation destabilized TBC-7, then we would expect a decrease in the levels of TBC-7 S520F compared to wild-type TBC-7. Western analysis showed that the S520F mutation did not affect the abundance of the TBC-7, suggesting that this mutation does not cause TBC-7 to be degraded at the onset of dauer in the absence of AMPK, but could disrupt its catalytic activity (Fig 5A'). These data indicate that neither AMPK nor the S520F mutation affects TBC-7 activity through targeted protein degradation, but rather that it must engage an alternative means of regulating TBC-7 activity prior to the onset of *mir-1* and *mir-44* expression/regulation (Fig 5A-A'). However, since the abundance of TBC-7 was measured solely in the neurons, we cannot exclude that the levels of TBC-7 may be affected in other tissues in animals that lack AMPK signalling.

AMPK has previously been shown to phosphorylate RabGAPs directly thereby inducing an intramolecular autoinhibition [37]. In mammalian cells, the AMPK-mediated phosphorylation of Ser168 near the N-terminus of TBC1D17 reduces its GAP activity toward its substrate Rab5 [37]. Due to the structural similarities between TBC1D17 and TBC-7, and the location of the AMPK phosphoacceptor sites, we questioned if the AMPK-mediated phosphorylation of TBC-7, like that of TBC1D17, could also reduce its GAP activity towards its target RAB-7. To examine the role of the predicted AMPK phosphorylation site Ser115 in the potential autoinhibition in TBC-7 (Fig 5B-C), we replaced the phosphoacceptor Ser115 with a non-phosphorylable alanine residue. Mutants expressing a non-phosphorylable variant of TBC-7 exhibited highly penetrant post-dauer sterility, consistent with this site being an important target of AMPK during the

onset of the dauer stage (Fig 5D). To complement these findings, we reasoned that expressing the reciprocal phosphomimetic mutation of TBC-7 in *daf-2; aak(0)* mutants might compensate for the loss of AMPK in mutant animals, and suppress the mutant germline defects typically observed in these animals. Consistent with this possibility, the introduction of a variant TBC-7 where Ser115 is replaced with a negatively charged phosphomimetic glutamic acid residue was sufficient to suppress the germline defects in AMPK mutants (Fig 5E). Together, our data indicate that the AMPK-dependent phosphorylation of Ser115 on TBC-7 is important to antagonize its GAP activity, most likely toward RAB-7, thereby allowing RAB-7 to instruct the germ cells to execute quiescence and to ensure post-dauer reproductive competence.

Discussion

Upon entry into the developmentally arrested dauer stage, AMPK modulates the germline cell cycle while also altering the chromatin landscape of these cells to instruct the appropriate changes in germline gene expression required to preserve germ cell integrity throughout the diapause [10]. In the absence of this master metabolic regulator, animals exhibit excessive germ cell hyperplasia during the dauer stage, while animals that are allowed to recover display highly penetrant sterility as well as various somatic defects [10]. This correlates with an increased abundance and abnormal distribution of both activating and repressive chromatin marks in the germ cells of these mutants. The modifications observed are likely responsible for the dramatic deviation from the normal expression of germline-expressed genes in AMPK mutant dauer larvae and this maladaptive expression program persists into the post-dauer animals [10].

Using genetic analysis to identify suppressors of this reproductive defect, we isolated 8 mutants that corresponded to 5 complementation groups. Two of these groups had multiple alleles suggesting that the screen was near saturation, while two of these mutations corresponded to a gene encoding a RabGAP protein called TBC-7. *tbc-7* null mutants are non-viable, underscoring once again the power of unbiased forward genetic approaches in the identification of highly specific point mutations.

The chromatin marks that are abnormally regulated in the germ line of AMPK mutant animals are corrected in the *rr166* background. Curiously, the *rr289* allele that we isolated also shows germline hyperplasia in the dauer larva when compared to *aak(0)* mutants, but it still shows 61% fertility. Although we have not yet characterised this gene product, this allele is good evidence that the loss of germ cell integrity may not be directly

linked to the germline hyperplasia. The germline phenotypes and the reduced dauer survival typical of AMPK mutants also appear unlinked. Although it has been hypothesized that the germ line hyperplasia may exhaust valuable lipid stores required for dauer survival, evidence suggests that this is unlikely. First, neither of the isolated *tbc-7* alleles suppress the premature dauer lethality that occurs in AMPK mutants. The timing of the two phenotypes is also very different; the hyperplasia happens during dauer formation, while the premature lethality occurs over a week later. Moreover, the reduced dauer survival of AMPK mutant dauer larvae was unaffected by restoring AMPK in the neurons [17]. Our data therefore suggest that the tissue-specific requirements for regulating germ cell integrity differ from those necessary for dauer survival, and that the neuronal activity of *tbc-7/rab-7* probably has no significant role in regulating triacylglyceride metabolism during the dauer stage.

tbc-7 activity must be regulated to ensure the proper maintenance of germ cells during this period of quiescence. When *tbc-7* activity is compromised in AMPK defective animals, the defects in the germline chromatin landscape are corrected to near wild-type levels. This pathway may therefore be one of the major effectors of germline quiescence and integrity that occurs during the dauer stage. Curiously, the orthologues of this gene product are important for vesicle formation in the neurons in *Drosophila* and in mammals. Consistent with this, TBC-7 is expressed almost exclusively in the neurons of *C. elegans* and not in the germ cells.

The nervous system constitutes the perfect early response system to mediate any organismal adaptation to environmental challenges. Since AMPK activity in these cells is sufficient to change gene expression in the germ line, this protein kinase likely acts as a

direct sensor for cellular ATP levels to transduce a signal from the neurons to vulnerable cell types dispersed throughout the organism [10, 38].

tbc-7 is expressed in many neurons in both dauer larvae and adult animals where it localizes to the late endosomal membrane to regulate the activity of RAB-7, a small *ras*-like GTPase involved in the positive regulation of the early to late endosome transition [26, 39]. Late endosomes are involved in recycling cargo back to the plasma membrane, trafficking towards the Golgi body, or fusion with lysosomes to create a lysosome/late endosome hybrid to degrade cargo [26, 39, 40]. Given this wide range of functions, the mechanistic details of how RAB-7 may communicate information between the neurons and the germ line remain unclear. Our observations support a role for RAB-7 in the cellular trafficking of a neuron-derived diffusible signal to the germ line to establish germ cell quiescence during the dauer stage, although the nature of this diffusible signal remains enigmatic.

We have recently shown that small RNAs are involved in maintaining germ cell integrity during the dauer stage [10]. Upon the inhibition of endogenous siRNA activity, both the post-dauer fertility and the upregulation of chromatin marks in AMPK mutants are partially corrected. Furthermore, the loss of the dsRNA channel *sid-1* partially restores post-dauer germ cell integrity in the AMPK mutants, implying that the transfer of endogenous siRNAs during the dauer stage is misregulated and maladaptive in the absence of AMPK.

Our analysis suggests that this role of small RNAs may not be the sole required functions of these critical regulators during the various changes in gene expression that are associated with dauer formation. By analysing the microRNA seed sequences present

within the 3'UTR of *tbc-7*, we were able to demonstrate how two microRNAs, *mir-1* and *mir-44*, are critical for the maintenance of germ cell integrity. Animals that lack *mir-1* or *mir-44* show the same germline defects as AMPK mutants, although these phenotypes are only visible after these mutants spend a longer period of time in the dauer stage. Moreover, these germline defects are further exacerbated upon the compromise of *rab-7* expression, suggesting that in the *mir-1* and *mir-44* mutants, *tbc-7* continually suppresses the activation of RAB-7. In other organisms, *mir-1* acts in a similar manner to regulate synaptic function at neuromuscular junctions [32]. These genetic data indicate that *mir-1* and *mir-44* are upstream negative regulators of *tbc-7* expression, thus they act indirectly as positive regulators of *rab-7* activity. Therefore, at the onset of dauer formation, AMPK activation might ultimately affect the formation of GTP-bound RAB-7, which in turn would be the major effector in the neurons by enabling communication with the germ cells to preserve their integrity over the long term.

It is however still unknown how or whether AMPK is able to regulate small RNA production or function, nor do we understand how this may bring about the observed changes in the chromatin modifications in the germ line. Interestingly, many components of the microRNA biogenesis machinery, including DRSH-1, PASH-1, and DCR-1, have multiple medium stringency AMPK phosphorylation motifs, which may suggest a role for AMPK in the direct regulation of the microRNA biogenesis machinery to ensure that microRNAs are produced in a timely manner. Alternatively, it is possible that microRNA production is regulated independently of AMPK/LKB1 signalling and these protein kinases impinge on components downstream of miRNA synthesis and processing to mediate these changes. Our initial identification of small RNA pathway involvement did not include

regulators of the miRNA pathway, but this was due to their critical role in various aspects of embryonic and post-embryonic development [41]. A conservative explanation for these findings is that AMPK may be acting in a parallel pathway with *mir-1* and *mir-44* to restrict the activity of TBC-7, meanwhile the endogenous siRNA pathway or other small RNA populations might act further downstream to regulate the germline chromatin landscape and gene expression during the dauer stage. Further work will be required to discern if there are direct interactions between the miRNA pathway and AMPK signalling, although because of the critical role of miRNAs in developmental timing, and hence dauer formation, these pathways will have to be teased out carefully with newly available genetic tools in order to accurately interpret their potential involvement in these processes.

As larvae enter the dauer stage, the frequency of germ cell division decreases dramatically to finally arrest during the diapause. The observed kinetics of *mir-1* inhibition are insufficient to account for the timing of the changes in the germ line following the initiation of dauer formation. By using non-phosphorylable and phosphomimetic transgenic TBC-7 variants we showed that the AMPK-mediated phosphorylation of TBC-7 likely attenuates its GAP activity without altering its stability/abundance. Through analogy with other RabGAP AMPK targets, the AMPK-mediated phosphorylation may induce a conformational change in TBC-7, resulting in its autoinhibition [37]. Consistent with this, the removal of the AMPK phosphoacceptor site on TBC-7 results in a loss of germ cell integrity after only 2 days in the dauer stage, compared to the 7 days required for the same change to occur in *mir-1* and *mir-44* mutants. Therefore, AMPK likely acts as a direct inhibitor of TBC-7 activity, but it also acts successively by activating *mir-1* and *mir-44*, thereby enabling prolonged RAB-7 activity throughout the entire dauer stage; from

onset to recovery. However, further experiments will need to be performed to confirm the direct phosphorylation of TBC-7 by AMPK. The AMPK-mediated phosphorylation of TBC-7 would account for the acute means of activating RAB-7 as animals begin to form dauer larvae, while the *mir-1* and *mir-44* regulation of the *tbc-7* transcript would act redundantly and later during the diapause to ensure that any remaining mRNA cannot be expressed to antagonize the critical RAB-7 activation necessary for germline integrity during the later stages of the diapause.

In summary, we have characterised an AMPK-dependent microRNA regulated *tbc-7/rab-7* pathway that acts cell non-autonomously in the neurons to establish quiescence in the germ line during periods of energetic stress. As the animals enter the dauer stage, AMPK phosphorylates Ser115 on TBC-7 to affect its GAP activity, thus allowing RAB-7 to remain in its GTP-bound active form and to perform its function, while later in the diapause, *mir-1* and *mir-44* bind to the 3'UTR of *tbc-7* to block its expression (Fig 6).

Although we have identified this *mir-1/mir-44/tbc-7/rab-7* pathway, we have yet to uncover which particular function of *rab-7* is responsible for transmitting this dauer signal from the neurons to the germ line. Nor do we understand how a *rab-7* pathway occurring in the neurons can alter the chromatin landscape in the germ cells of the dauer larva. Communication between the soma and the germ cells is a conserved phenomenon [42]. However, it remains undetermined whether this transfer of information is mediated through a RAB-7-dependent neuroendocrine pathway or via an alternative means of intertissue communication that has yet to be fully characterized.

Materials and Methods

C. elegans strains and maintenance

All *C. elegans* strains were maintained at 15°C on nematode growth medium petri plates and according to standard protocols unless otherwise indicated [43]. The strains used in this study are listed in S6 Table.

Transgenic lines and compound mutants were created in the laboratory using standard molecular genetics approaches. In this manuscript, we list *daf-2(e1370) aak-1(tm1944) III; aak-2(ok523) X* mutants as *daf-2; aak(0)* mutants to indicate a complete lack of AMPK catalytic activity. Since *aak(0)* is 'composed' of two genes on two different chromosomes, we keep it on a 'separate' chromosome when writing the genotype, detached from *daf-2(e1370)* on chromosome III and *tbc-7(rr166)* on chromosome X. All mutant strains isolated following mutagenesis were backcrossed at least 5 times prior to characterization and subsequent whole-genome sequencing. All transgenes were injected at 15 ng/μL unless specified otherwise. The transgene containing *pre-mir-1* driven by *rgef-1* promoter were injected at 1 ng/μL. The transgene containing *pre-mir-44* driven by *rgef-1* promoter was injected at 0.5 ng/μL. All injection mixes contained 120 ng/μL of pRF-4 (*rol-6D*) as a dominant injection marker and the concentration of DNA was made up to 200 ng/μL with an empty vector pSK.

Genetic suppressor screen

Animals were mutagenized as described elsewhere with some modifications [43]. P_0 L4 AMPK null (*daf-2; aak(0);* strain name MR1000) mutants were treated with 0.05 mM EMS. F_1 animals were isolated to separate the F_1 generation from the P_0 generation.

The F_1 generation was allowed to grow to become gravid adults before they were synchronized to obtain F_2 candidates that were homozygous for the EMS-generated mutation. The F_2 generation was assessed for their ability to suppress the AMPK germline defects. F_2 animals were switched to a restrictive 25°C temperature for 48 hours to induce dauer formation and kept for an additional 48 hours in the dauer stage for a total of 96 hours. All F_2 animals were subjected to 1% SDS in order to eliminate dauer-defective mutants. After, F_2 animals were switched into the permissive temperature of 15°C to trigger dauer recovery. The F_2 generation was screened for their ability to suppress germline defects typical of AMPK mutants; candidates were assessed on their % of egg-laying post-dauer animals, No. of germ cells in dauer larvae, post-dauer brood size, and % of adult animals with wild-type appearance (the lack of any vulval defects or premature death). In total, 8 independent alleles were isolated from approximately 7000 haploid mutagenized genomes.

Potential candidates that were able to suppress the AMPK germline defects were submitted for next-generation sequencing using Deep Sequencing Data Shotgun (Beads 360). Genomic DNA was extracted using the phenol-chloroform DNA isolation method. The integrity of the extracted DNA was examined on an agarose gel and through nanodrop spectrophotometer. Library preparation and quality check was done by the Génome Québec sequencing facility. Seven candidates were submitted for sequencing along with the starting mutagenesis strain *daf-2; aak(0)* (strain name: MR1000). The average number of reads per candidate is 58,268,582 reads. The sequencing results of each candidate and the starting strain *daf-2; aak(0)* were aligned to WBcel235 as a reference genome. After assembly of the genomes, all the candidates were compared

against *daf-2; aak(0)* to identify any potential mutations caused by the EMS. Variant calling was done using bcftools on each candidate after genome alignment. Each genetic variation was ranked using the Z-score from Wilcoxon rank sum test of mutant alleles vs. the reference genome sequence.

Complementation and other genetic analyses

Complementation analysis was conducted as previously described [44]. Each candidate was injected with a plasmid containing GFP driven by the pharyngeal promoter *myo-2p* and heat shocked at 30°C for 6 hours to induce males. Males expressing pharyngeal GFP were crossed with an EMS-generated mutant adult hermaphrodite (that did not express pharyngeal GFP) of a different genotype. Cross progeny was identified using the pharyngeal GFP marker. The F_1 cross progeny that were heterozygous for two EMS-induced alleles were made to transit through the dauer stage and the % of fertile post-dauer animals and the No. of germ cells in dauer larvae were assessed as a measure of complementation. All eight candidates generated from the EMS screen were crossed to each other in order to assign their complementation group. EMS-generated candidates that generated cross progeny that were post-dauer sterile or suffered from germline hyperplasia were categorized into different complementation groups, while those that were post-dauer fertile and could suppress their germline hyperplasia were categorized into the same complementation group.

To determine if *rr166* is a null allele of *tbc-7*, we crossed *rr166* into a known *tbc-7(tm10766)* null background. The *tbc-7(tm10766)* null mutation is embryonic lethal, so these mutants are balanced and maintained as heterozygotes. When *tm10766*

hermaphrodites were crossed with *tbc-7(rr166)* males, we were able to isolate viable F1 mutants that carried the *tbc-7(tm10766)* deletion and the *tbc-7(rr166)* point mutation, suggesting that *rr166* is a hypomorphic allele of *tbc-7* (S4 Fig).

Dauer recovery assay

Post-dauer fertility and somatic phenotypes were assayed and quantified as described elsewhere [10]. A population of genetically identical mutants were synchronized using alkaline hypochlorite. The resulting embryos were hatched in M9 buffer and then plated on NGM plates seeded with OP50. The resulting animals were incubated at 25°C for 96 hours so that the animals can spend at least 24 hours in the dauer stage. Afterwards, the animals were switched back to a permissive temperature of 15°C to trigger dauer recovery and allow for normal development. The animals were then singled onto NGM plates. The post-dauer fertility and brood size of each animal were assessed 7 days after switching into the permissive temperature. The brood size of each animal is the number of hatched progenies. The post-dauer adults were assessed visually for any post-dauer somatic defects.

DAPI staining and germ cell quantification

DAPI staining and germ cell quantification of the dauer larvae was conducted as described elsewhere [10]. A population of genetically identical animals were synchronized and allowed to hatch in M9 solution. The animals were then plated onto NGM seeded with OP50 and incubated at 25°C for 96 hours to allow the animals to spend at least 24 hours in the dauer stage. The resulting dauer larvae were washed off the plate and

soaked in Carnoy's solution (60% ethanol, 30% acetic acid, 10% chloroform) overnight on a shaker. Afterwards, the Carnoy's solution was removed and the dauer larvae was washed twice with 1x PBS + 0.1% Tween 20 (PBST). The dauer larvae were then stained with 0.1 mg/mL DAPI solution for 30 minutes on a shaker. Finally, the DAPI solution was removed, and the sample was washed four times with PBST (15 minutes for each wash on a shaker). The larvae were then mounted onto glass slides. Germ cells per dauer gonad was determined based on their position and their nuclear morphology. The number of germ cells in the dauer larvae were counted manually.

Dauer survival assay

Dauer survival assay was conducted as described elsewhere [8]. A population of genetically identical animals were synchronized and allowed to hatch in M9 solution. The animals were then plated onto NGM seeded with OP50 and incubated at 25°C for 48 hours to induce dauer formation. Then dauer larvae were singled into PCR strip tubes containing 10 μL of M9 buffer, one animal per well. Trapping the larvae in PCR tubes prevented the dauer larvae from crawling off the bacterial lawn and desiccating at the edge of the plate. Dauer survival was monitored daily and was scored based on their movement in response to exposure to a focused beam of 425-440 nm light.

Western blot analysis

Western blot analysis was conducted as described elsewhere [10]. *C. elegans* dauer larvae and adults were manually picked into 10 μL PBST. Then 10 μL of SDS loading buffer (5% β-mercaptoethanol, 0.02% bromophenol blue, 30% glycerol, 10%

sodium dodecyl sulfate, 250 mM pH 6.8 Tris-Cl) was added before the entire mixture was subjected to multiple rounds of freeze-thawing with liquid nitrogen and 100°C heat block. Nitrocellulose membranes were incubated with rabbit anti-GFP (homemade antibody), rabbit anti-H3K4me3 (1:1000 dilution, Abcam, ab8580), rabbit anti-H3K9me3 (1:1000 dilution, Cell Signalling Technology, 9754S), or mouse anti-α-tubulin (1:2000, Sigma-Aldrich, St. Louis, MO, USA). After SDS-PAGE and Western blotting, proteins were visualized using horseradish-peroxidase-conjugated anti-rabbit or anti-mouse secondary antibodies (1:2000, Bio-Rad, Hercules, CA, USA).

Fosmid preparation and injection

The fosmid containing a wild-type copy of *tbc-7* translationally fused to GFP is from the UBC N2 fosmid library (Don Moreman) that was ordered from the TransgeneOme Project *C. elegans*. The clone identification is: 3304493055384826 E02. This fosmid contains the entire sequence of the *tbc-7* gene, including exons and introns and the 5' and 3'UTRs. It also contains an additional upstream sequence (starts X: 5,120,813) that is 13,467 bp in size starting from the transcription start site and an additional downstream sequence (ends X: 5,154,839) that is 8,095 bp in size starting from the end of the last exon. The fosmid was extracted from *E. coli* using the EZ-10 Spin Column Plasmid DNA Miniprep Kit (Cat. #: BS513) from Bio Basic. The purified fosmid was co-injected with a transformation marker pRF-4 (plasmid containing a dominant negative variant of the *rol-6* gene). The fosmid was injected at a concentration of 1 ng/μL and the pRF-4 transformation marker was injected at a concentration of 120 ng/μL. The injections were

performed on *daf-2* mutants for the imaging of TBC-7::GFP in Fig 2B and 2C, and on *daf-2; aak(0); tbc-7* mutants to revert the suppression conferred by the *rr166* allele in Fig 2A.

Plasmid cloning and preparation

To generate the plasmid that drives a GTP-locked variant of RAB-7 in the neurons, the GTP-locked variant of RAB-7 Q68L was amplified from a pGEX-5X-2 vector containing RAB-7 Q68L (a generous gift from Dr. Christian Rocheleau). The sequences of the primers used to amplify *rab-7* are 5'-atggatgaactatacaaaatgtcgggaaccagaaagaa-3' and 3'-acacggttaacaattgcatcccgaattctgctggttctg-5'. The GTP-locked variant of RAB-7 Q68L was inserted between the neuronal promoter *rgef-1* and a wild-type *rab-7* 3'UTR in the pSK vector using Gibson assembly.

The 3'UTR deletions were generated by amplifying a wild-type copy of the *tbc-7* 3'UTR from genomic DNA and inserting it into an empty vector pMR377. The sequences of the primers used to amplify the 3'UTR are 5'-tcgtagaattccaactgagcgcattcactctgcccaag-3' and 3'-ccgtacggccgactagtaggttcaggctgcaagaaaaaca-5'. The *mir-1* and *mir-44* binding sites on the *tbc-7* 3'UTR were removed by linearizing the entire pMR377+3'UTR plasmid using a set of primers that flanked the *mir-1* and *mir-44* seed sequences in a PCR reaction. The linearized PCR product was phosphorylated by polynucleotide kinase for 30 minutes and ligated by DNA ligase overnight to generate a plasmid that contains the *tbc-7* 3'UTR with the *mir-1* and *mir-44* seed sequences removed. The sequences of primers used to delete the seed sequences are 5'- ctcctcgcctccaatgtttg-3' and 3'-ggcaatacttaagaatgaggaagg-5'. The deletion from the site directed mutagenesis was verified by sequencing the pMR377 plasmid with the mutant *tbc-7* 3'UTR. The mutant *tbc-*

7 3'UTR was amplified using the original set of primers for the 3'UTR and inserted using Gibson assembly behind a wild-type copy of *tbc-7* cDNA driven by the *rgef-1p* neuron-specific promoter in a modified pPD95.77 vector.

The amino acid substitutions to mutate the predicted AMPK phosphosite on TBC-7 was done by amplifying a wild-type copy of *tbc-7* from cDNA and inserting it into an empty vector pMR377. The sequences of the primers used to amplify *tbc-7* are 5'-ctttacattttgttttcagaatgacggaaaacgctggatc-3' and 3'-cagttggaattctacgaatgttagtcgctggaagtaacatgga-5'. Site directed mutagenesis was performed on the pMR377+*tbc-7* plasmid to replace the Ser115 residue with either Ala or Glu. Primers were designed around the AGT codon that encodes for Ser115. One primer contained overlaps with the GCC codon or CTC codon that encodes for Ala or Glu, respectively. The plasmid containing *tbc-7* was mutagenized using these primers to create a linearized PCR product. This product was phosphorylated by polynucleotide kinase for 30 minutes and ligated by DNA ligase overnight to generate a plasmid that contains a mutant variant of *tbc-7* that has its Ser115 replaced with either S115A or S115E. The primers used to create the S115A mutation are 5'-aattttgattgaaagaagtcggatc-3' and 3'-GGCgagcactccaccttcatctg-5'. The primers used to create the S115E mutation are 5'-aattttgattgaaagaagtcggatc-3' and 3'-CTCgagcactccaccttcatctg-5'. The mutant *tbc-7* gene was amplified using the original set of primers used to amplify the *tbc-7* cDNA sequence and was inserted using Gibson assembly between a *rgef-1p* neuron-specific promoter and wild-type *tbc-7* 3'UTR in a modified pPD95.77 vector.

All plasmids used in this manuscript were verified using restriction digestion analysis and sequencing analysis.

Immunostaining and quantification

C. elegans dauer larvae and post-dauer adult gonads were dissected, fixed, and stained as described elsewhere [45]. Extruded gonads were incubated with rabbit anti-H3K4me3 (1:500 dilution, Abcam, ab8580) or rabbit anti-H3K9me3 (1:500 dilution, Cell Signalling Technology, 9754S). Secondary antibodies were Alexa-Fluor-488–coupled goat anti-rabbit (1:500; Life Technologies, Carlsbad, CA, USA). Gonads were counterstained with DAPI (0.1 µg/mL dilution, Roche Diagnostics, 10236276001). Microscopy was performed as described elsewhere [10, 46]. Ratios for the fluorescence intensity across the germ line were determined using ImageJ. The ratio was calculated by dividing the immunofluorescence signal of either anti-H3K4me3 or anti-H3K9me3 by the fluorescence signal of DAPI per nucleus.

RNA interference by feeding

RNA interference was conducted as described elsewhere based on standard feeding protocols [10, 47]. Bacterial clones expressing dsRNA from the Ahringer *C. elegans* RNAi feeding library were grown in LB medium with ampicillin at 37°C overnight [48]. The bacterial culture was then seeded onto NGM plates containing ampicillin and IPTG (1 mM) and allowed to grow for 48 hours at room temperature to induce dsRNA expression. A population of genetically identical animals were synchronized and allowed to hatch in M9 buffer before they were plated onto NGM plates containing bacteria that expressed dsRNA. The animals were incubated at 25°C for 96 to allow the animals to spend at least 24 hours in the dauer stage. If the experiment required the animals to be

separated, individual animals were separated onto NGM plates containing bacteria that expressed dsRNA.

Generation of tissue-specific RNAi strains

All tissue-specific RNAi strains contain a *rde-1(mkc36)* mutation. *rde-1(mkc36)* contains a 67 bp insertion and a 4 bp deletion that creates three premature stop codons [24]. *rde-1(mkc36)* mutants do not respond to exogenous RNAi by feeding or injection [24]. A germline-specific RNAi strain was generated by expressing a single-copy of *rde-1* in the germ line driven by the *sun-1* promoter inserted on chromosome II using MosSCI [24]. To generate neuron-specific RNAi strains, *rde-1* and *sid-1* were expressed exclusively in the neurons of *rde-1(mkc36)* animals using the *rgef-1* promoter [49]. Neurons of *C. elegans* exhibit weak penetrance through feeding, thus extra copies of neuronal *sid-1* potentially serves as a dsRNA sink, allowing for a robust RNAi phenotype through feeding [23]. Tissue-specific RNAi strains do not exhibit any developmental defects when grown in replete conditions, when passed through the dauer stage on standard NGM plates, or when grown on L4440 empty vector control compared to their non-*rde* counterpart. The specificity and efficiency of these tissue-specific RNAi strains were examined by feeding animals expressing either neuronal or germline TBC-7::GFP with either empty vector control L4440 or dsRNA against GFP. The levels of TBC-7::GFP expression were quantified using Western blotting against GFP (S8A-B Fig).

Prediction of *mir-1* and *mir-44* seed sequence

mir-1 and *mir-44* were identified as a potential regulator of *tbc-7* through TargetScanWorm release 6.2 (S5 Table). Two highly conserved *mir-1* seed sequences and one highly conserved *mir-44* seed sequence were identified in the 3'UTR of *tbc-7*. The P_{CT} and conserved branch length are measures of the biological relevance of the predicted miRNA and target interaction, with greater values being more likely to have detectable biological function [50, 51].

Acknowledgements

We thank the members of the Roy and Zetka laboratories for their thoughtful discussions and comments on the manuscript. We acknowledge Anja Boskovic for help with the bioinformatics and Julian Moran for technical assistance during the screen. We also acknowledge the *Caenorhabditis elegans* Genetics Center and the National BioResource Project: *Caenorhabditis elegans* Shigen for *C. elegans* strains.

Figures and Tables

Allele(s)	Complementation Group	Dominance/ Recessiveness	Penetrance		
			% egg laying post-dauer animals	No. of germ cells in dauer larvae	% wild type-like
daf-2	-	-	100	35	100
daf-2; aak(0)	-	-	0	153	68
rr166	Group 1	Recessive	83	68	92
rr249	Group 2	Semi-dominant	78	97	84
rr256	Group 3	Recessive	67	85	84
rr261	Group 4	Recessive	67	90	76
rr266	Group 3	Recessive	63	66	84
rr267	Group 1	Recessive	67	97	80
rr268	Group 5	Recessive	68	75	76
rr289	Group 3	Recessive	61	112	72

Table 2.1. Mutants that suppress the sterility of post-dauer AMPK mutants fall into five complementation groups. Eight EMS-generated alleles were isolated from a genetic screen designed to identify genes involved in the AMPK regulation of germ cell integrity and germline quiescence during the dauer stage. All eight alleles were able to lay viable embryos that gave rise to a fertile generation. Through cross complementation analysis they were found to fall into five complementation groups, two of which had

multiple independent alleles; Group 1 - *rr166, rr267* and Group 3 - *rr256, rr266, rr289.* Based on our F_1 and F_2 cross-complementation analysis, all the alleles behave recessively, with the exception of *rr249*, which acts semi-dominantly. Wild type-like indicates the lack of any post-dauer somatic phenotypes associated with the loss of AMPK signalling, such as protruding vulva, burst vulva, multivulva, or premature death during the recovery period from the dauer stage. The values for % egg laying post-dauer animals, no. of germ cells in dauer larvae, and % wild type-like are presented as means. All strains contain the *daf-2(e1370)* allele. All EMS mutant strains are *daf-2; aak(0)*. Each assay was repeated three times with 50 animals in each trial. n = 50.

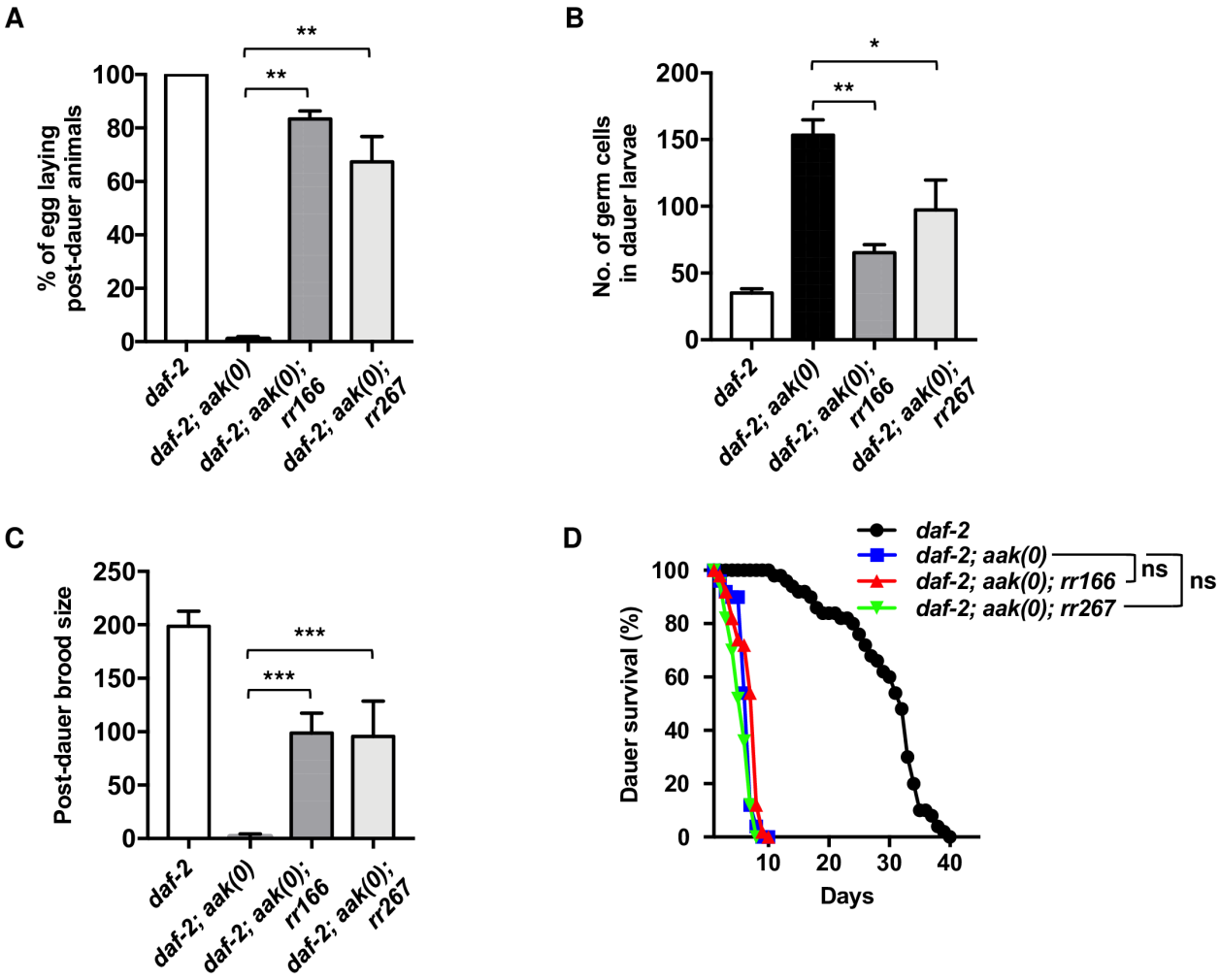

Fig 2.1. *rr166* and *rr267* partially suppress the post-dauer sterility and dauer germline hyperplasia of AMPK mutants. (A-C) *rr166* and *rr267* suppress the (A) post-dauer sterility, (B) dauer germline hyperplasia, and (C) brood size defects in animals that lack all AMPK signalling. (D) *rr166* and *rr267* do not suppress the reduced dauer survival typical of *aak(0)* mutants. ***P < 0.0001 when compared to *daf-2; aak(0)* using ordinary one-way ANOVA for post-dauer brood size and no. of germ cells in dauer larvae. Data are represented as mean ± SD. ***P < 0.0001 when compared to *daf-2; aak(0)* using Marascuilo procedure for % egg laying post-dauer animals (% total). No significant difference (ns) was observed when compared to *daf-2; aak(0)* using a log-rank test for

dauer survival. All animals carry the *daf-2(e1370)* allele. The values for % egg laying post-dauer animals, no. of germ cells in dauer larvae, and post-dauer brood size are presented as means. Each assay was repeated three times with 50 animals in each trial. n = 50.

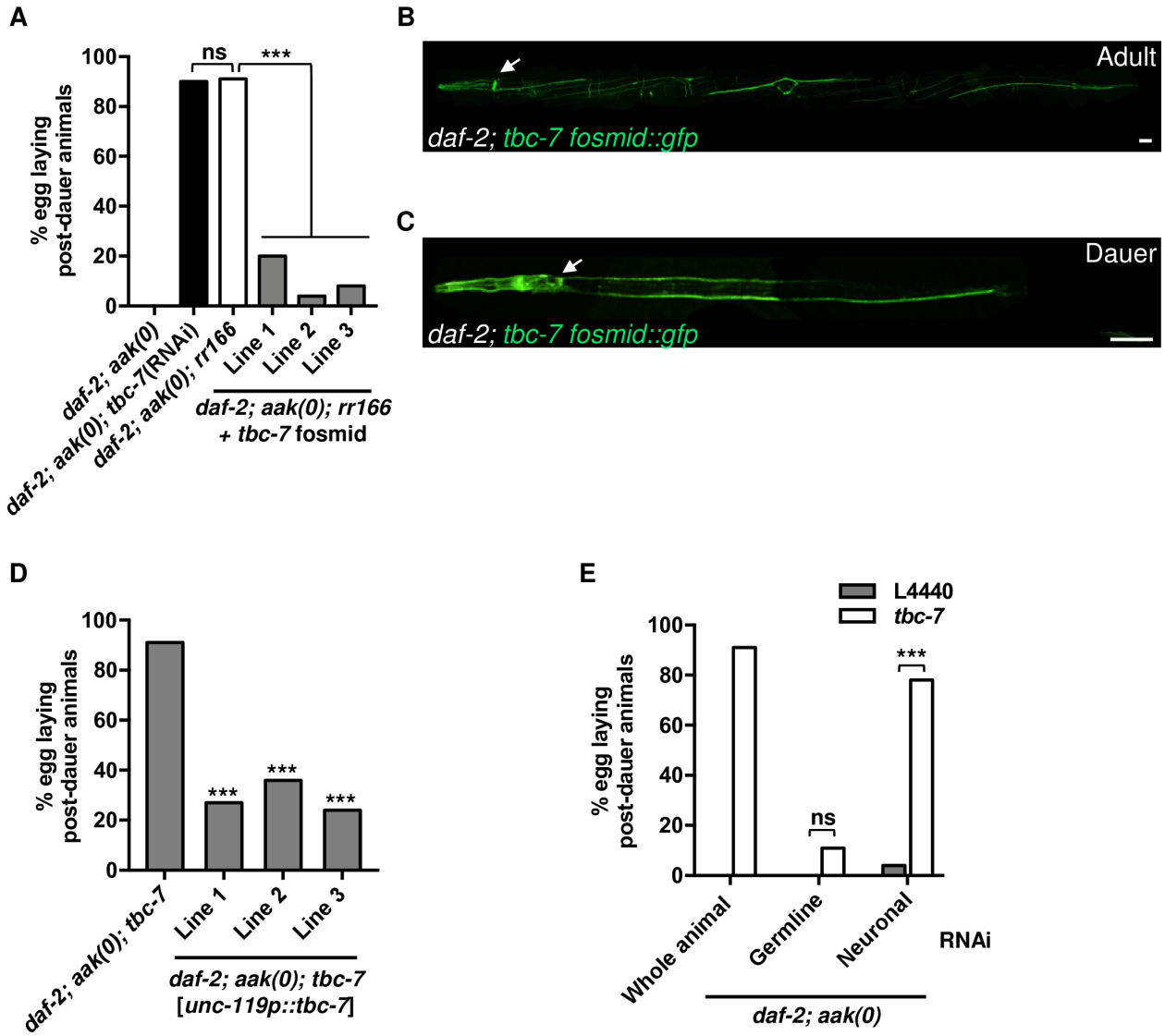

Fig 2.2. *tbc-7* functions in the neurons to maintain germ cell integrity during the dauer stage. (A) *rr166* is an allele of the RabGAP *tbc-7.* RNAi against *tbc-7* in *daf-2; aak(0)* suppresses the post-dauer sterility. Injection of a fosmid containing a wild-type copy of *tbc-7* (C31H2.1) into *daf-2; aak(0); tbc-7* mutants partially reverts the *tbc-7*-associated suppression of the *aak(0)* germline defects. ***P < 0.0001 when comparing *daf-2; aak(0); rr166* and *daf-2; aak(0); rr166* + *tbc-7* fosmid based on Marascuilo procedure for % egg laying post-dauer animals. ns when comparing *daf-2; aak(0); tbc-7(RNAi)* and *daf-2; aak(0); rr166* based on Marascuilo procedure for % egg laying post-

dauer animals. (B-C) The expression of a fosmid containing *tbc-7* translationally fused to GFP is shown in (B) wild-type adult animals and in (C) dauer larvae. White arrows indicate the nerve ring. Scale bars: 25 μm. Note that the morphological abnormality visible in the image is a result of the *rol-6D* co-transformation marker. (D) A wild-type copy of *tbc-7* cDNA expressed exclusively in the neurons by the *unc-119* promoter in the *tbc-7*-suppressed mutants reverts the suppression of the AMPK germline phenotypes. ***P < 0.0001 when compared to *daf-2; aak(0); tbc-7* based on Marascuilo procedure for % egg laying post-dauer animals. (E) Tissue-specific RNAi experiments reveal that the compromise of *tbc-7* expression exclusively in the neurons (Neuronal) is sufficient to suppress the AMPK germline defects. ***P < 0.0001 when compared to L4440 empty vector based on Marascuilo procedure for % egg laying post-dauer animals. All animals carry the *daf-2(e1370)* allele. The values for % egg laying post-dauer animals are presented as means. Each assay was repeated three times with 50 animals in each trial. n = 50.

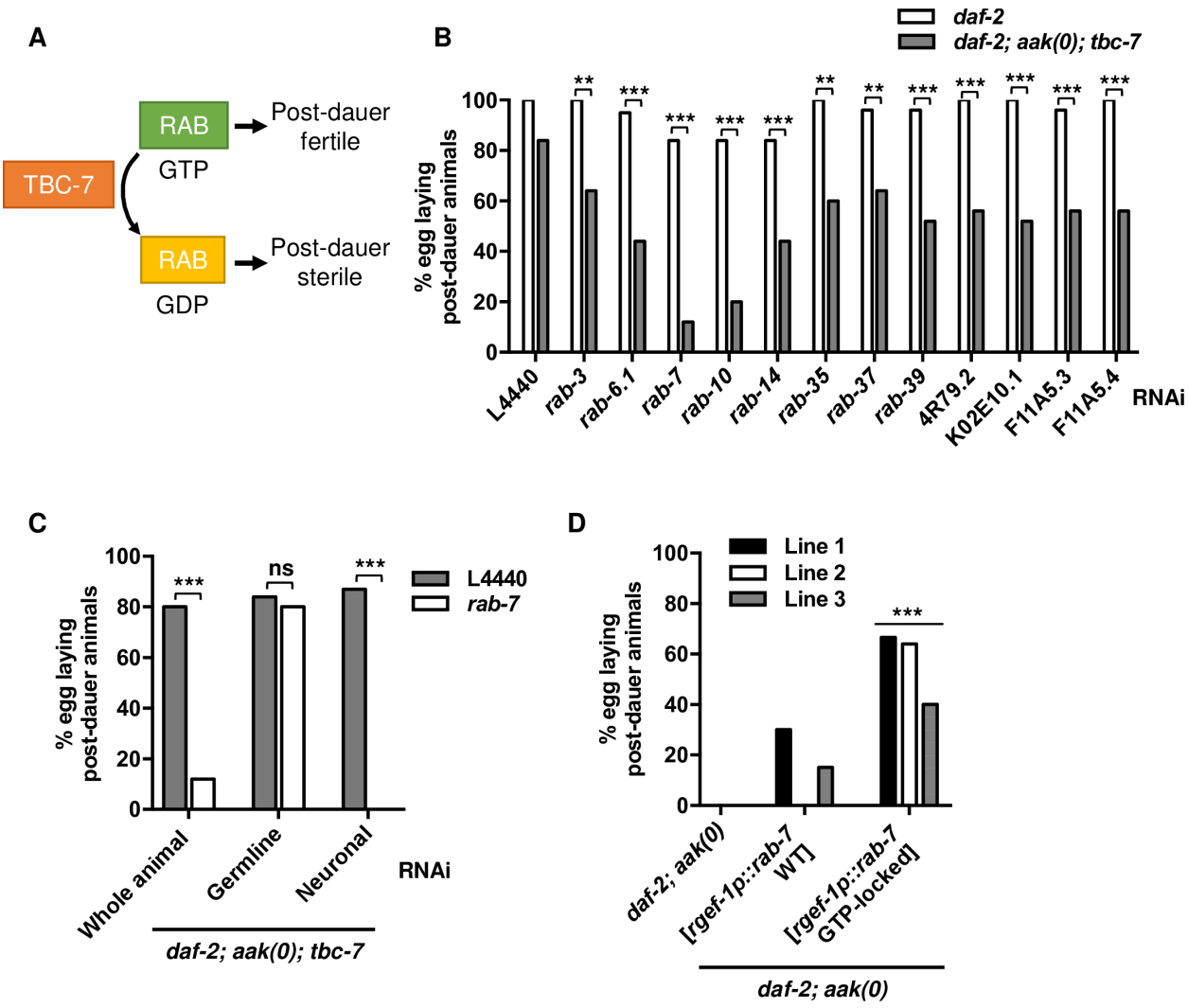

Fig 2.3. TBC-7 regulates RAB-7 in the neurons to maintain germ cell integrity during the dauer stage. (A) Graphical figure illustrating the regulation of RAB activity by TBC-7. In *daf-2; aak(0); tbc-7* mutants, TBC-7 is inactive, allowing its RAB protein to be active in its GTP-bound state. By compromising the expression of this RAB protein using RNAi, the suppression of post-dauer sterility is lost. (B) By subjecting each predicted known *rab* gene in the *C. elegans* genome to RNAi, several RAB proteins were identified as potential RAB partners of TBC-7. All of the RNAi treatments were performed in animals with the *daf-2(e1370)* background. ***P < 0.0001, **P < 0.001 when compared to *daf-2* with the same RNAi treatment using Marascuilo procedure for % of egg laying animals. (C)

Tissue-specific RNAi experiments reveal that *rab-7* expression is required in the neurons and not the germ line for the *tbc-7* suppression of AMPK germline phenotypes. ***P < 0.0001, **P < 0.001 when compared to L4440 empty vector using Marascuilo procedure for % of egg laying animals. (D) Introduction of a GTP-locked variant of RAB-7 (Q68L) [26, 27] into *daf-2; aak(0)* mutants partially suppresses the post-dauer sterility. ***P < 0.0001 when compared to *daf-2; aak(0)* mutants expressing neuronal wild-type *rab-7* using Marascuilo procedure for % of egg laying animals. All animals carry the *daf-2(e1370)* allele. The values for % egg laying post-dauer animals are presented as means. Each assay was repeated three times with 50 animals in each trial. n = 50.

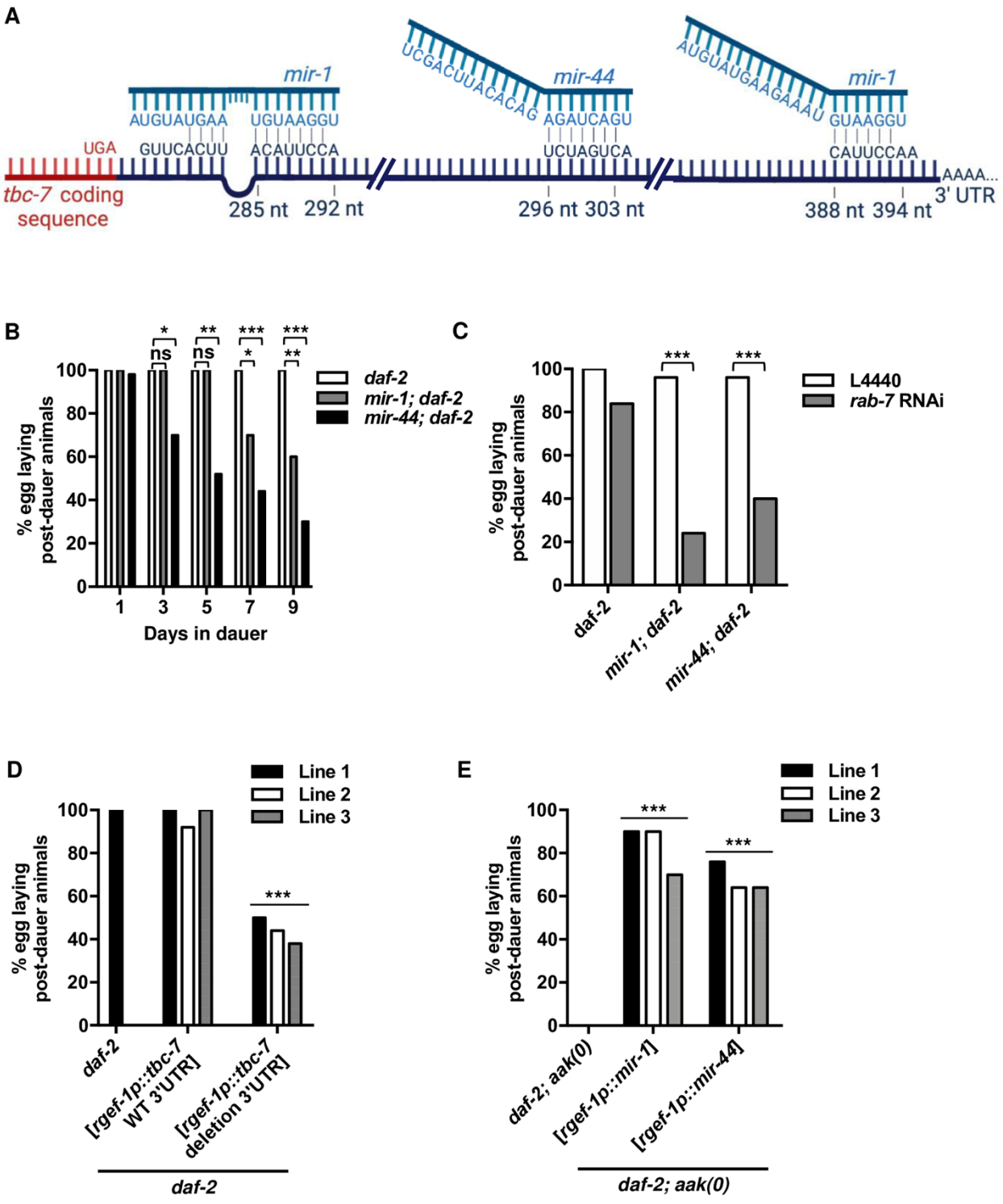

Fig 2.4. *mir-1* and *mir-44* are required to maintain germ cell integrity during the dauer stage. (A) A model illustrating the binding of *mir-1* to the two predicted seed

sequences and *mir-44* to the one predicted seed sequence on the 3' UTR of the *tbc-7* transcript. Lines indicate predicted binding between the microRNAs and *tbc-7* 3' UTR. (B) *mir-1; daf-2* and *mir-44; daf-2* mutants exhibit post-dauer sterility after 7 days in the dauer stage. ***P < 0.0001, **P < 0.001, *P < 0.01 when compared to *daf-2* that spent an identical duration in the dauer stage using Marascuilo procedure for % egg laying post-dauer animals. (C) Reducing *rab-7* levels greatly enhances/accelerates the post-dauer sterility associated with a loss of *mir-1* or *mir-44*. ***P < 0.0001 when compared to L4440 empty vector using Marascuilo procedure for % egg laying post-dauer animals. (D) Mutants with a deletion of the *mir-1* and *mir-44* seed sequence on the 3'UTR of *tbc-7* exhibit post-dauer sterility after 1 day in the dauer stage. ***P < 0.0001 when compared to *daf-2* expressing a wild-type *tbc-7* 3'UTR using Marascuilo procedure for % egg laying post-dauer animals. (E) Increased *mir-1* or *mir-44* expression in *daf-2; aak(0)* mutants suppresses post-dauer sterility. ***P < 0.0001 when compared to *daf-2; aak(0)* using Marascuilo procedure for % egg laying post-dauer animals. All animals carry the *daf-2(e1370)* allele. The values for % egg laying post-dauer animals are presented as means. Each assay was repeated three times with 50 animals in each trial. n = 50.

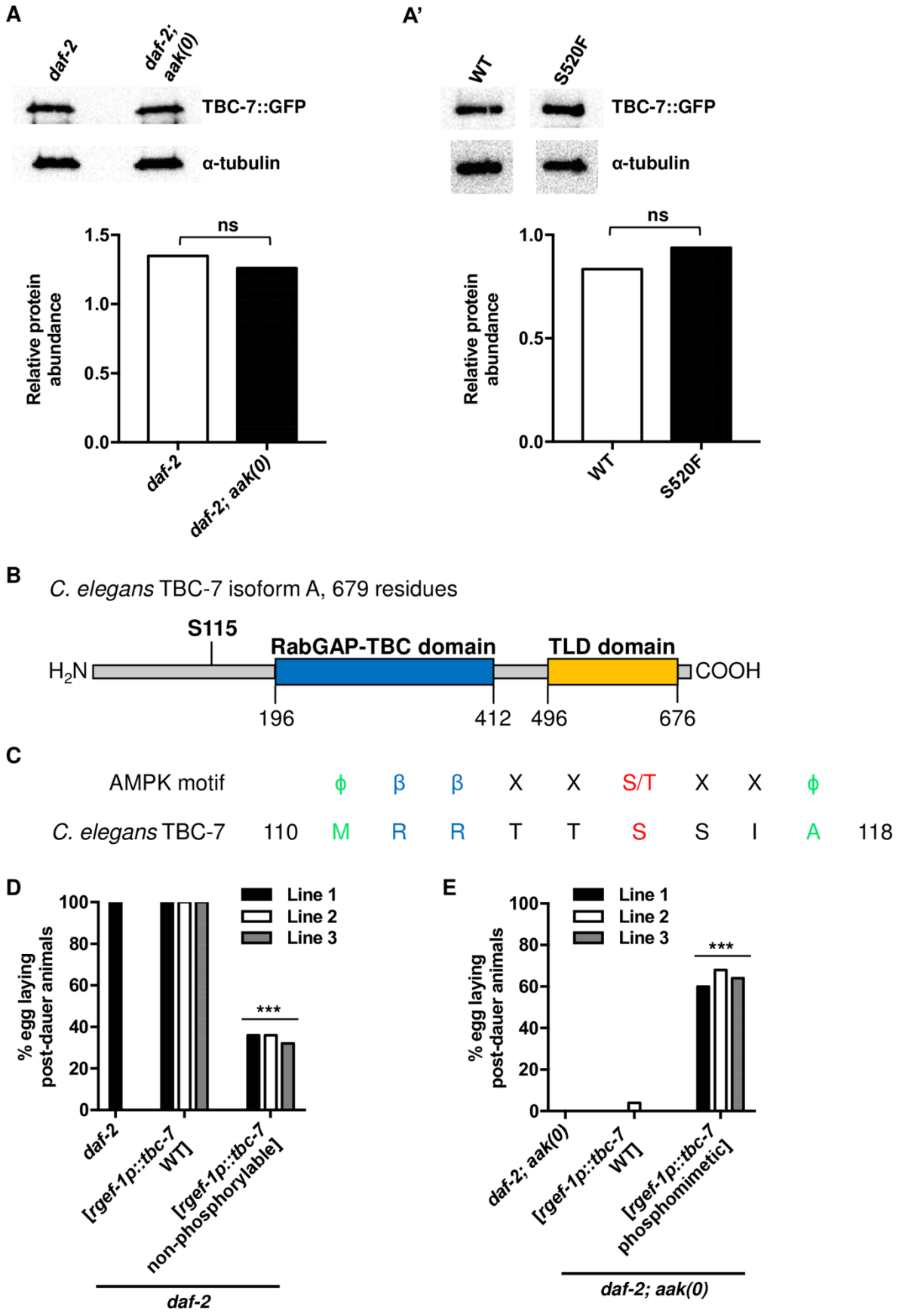
A
daf-2
daf-2; aak(0)
TBC-7::GFP
α-tubulin
ns
Relative protein abundance
1.5
1.0
0.5
0.0
daf-2
daf-2; aak(0)
A'
WT
S520F
TBC-7::GFP
α-tubulin
ns
Relative protein abundance
1.0
0.5
0.0
WT
S520F
B
C. elegans TBC-7 isoform A, 679 residues
S115
RabGAP-TBC domain
TLD domain
H2N
COOH
196
412
496
676
C
AMPK motif
ϕ β β X X S/T X X ϕ
C. elegans TBC-7
110 M R R T T S S I A 118
D
Line 1
Line 2
Line 3
% egg laying post-dauer animals
100
80
60
40
20
0
***
daf-2
[rgef-1p::tbc-7 WT]
[rgef-1p::tbc-7 non-phosphorylable]
daf-2
E
Line 1
Line 2
Line 3
% egg laying post-dauer animals
100
80
60
40
20
0
***
daf-2; aak(0)
[rgef-1p::tbc-7 WT]
[rgef-1p::tbc-7 phosphomimetic]
daf-2; aak(0)

Fig 2.5. AMPK-mediated phosphorylation of Ser115 attenuates TBC-7 activity. (A) Western blot analysis of TBC-7 abundance shows no significant difference in the protein levels between the *daf-2* control and *daf-2; aak(0)* mutant backgrounds. TBC-7 expression was quantified and normalized to α-tubulin using ImageJ software. ns when compared to *daf-2* using Student's t-test. (A') Western blot analysis shows no significant difference in the protein levels between wild type and S520F TBC-7. TBC-7 expression was quantified and normalized to α-tubulin using ImageJ software. ns when compared to *daf-2* using Student's t-test. (B) A model showing the predicted domains and the consensus AMPK phosphorylation site of TBC-7. The RabGAP-TBC domain and TLD domain are shown in blue and yellow, respectively. The predicted AMPK phosphorylation site at Ser115 is indicated in bold [36]. (C) The amino acid sequence of TBC-7 was analyzed to identify any potential AMPK phosphorylation motifs. The alignment of the sequence around Ser115 is shown with analogous sites to the AMPK phosphorylation motif sequence. Hydrophobic residues, green; hydrophilic residues, blue; phosphosite acceptor, red. (D) Animals expressing a S115A non-phosphorylable mutation of TBC-7 exhibit post-dauer sterility following recovery. ***P < 0.0001 when compared to *daf-2* animals and *daf-2* animals that express a wild-type version of *tbc-7* using Marascuilo procedure for % egg laying post-dauer animals. (E) A S115E phosphomimetic mutation of TBC-7 in *daf-2; aak(0)* mutants suppresses the post-dauer sterility. ***P < 0.0001 when compared to *daf-2* and *daf-2; aak(0)* mutants that express a wild-type variant of *tbc-7* using Marascuilo procedure for % egg laying post-dauer animals. All animals carry the *daf-2(e1370)* allele. The values for % egg laying post-dauer animals are presented as means. Each assay was repeated three times with 50 animals in each trial. n = 50.

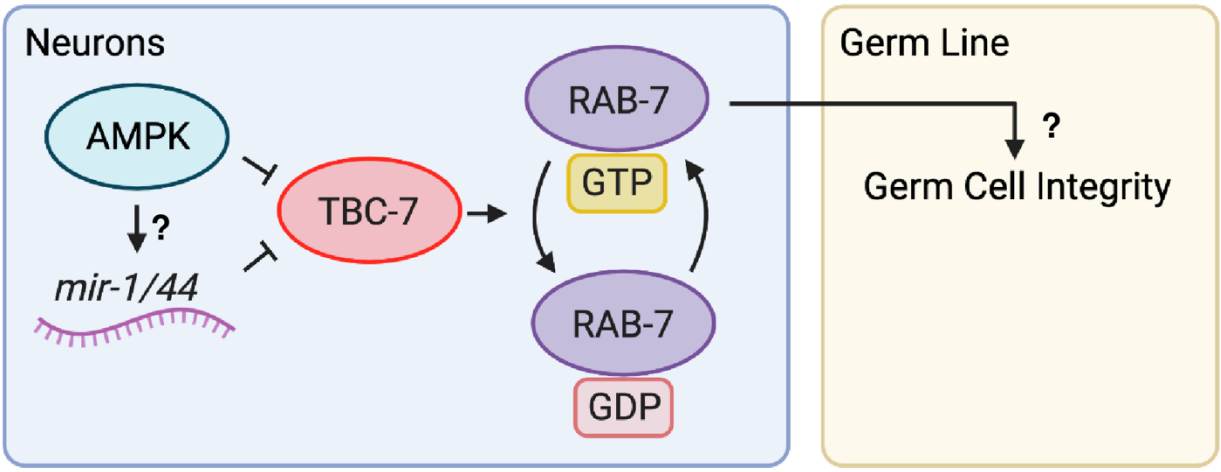

Fig 2.6. AMPK regulates *rab-7* activity in neurons to establish germline quiescence and preserve germ cell integrity during the dauer stage. When animals enter the dauer stage, AMPK, *mir-1*, and *mir-44* negatively regulate TBC-7 activity in the neurons. *mir-1* and mir-44 are able to bind to the *tbc-7* 3'UTR to negatively regulate its expression. AMPK-mediated phosphorylation of TBC-7 negatively regulates its activity. In parallel, it may be possible that AMPK could act directly on the miRNA biogenesis machinery to promote the production of *mir-1* and *mir-44*, as suggested by the presence of phosphorylation motifs on microRNA biogenesis components. It is still unknown which particular neuronal *rab-7* pathway alters the chromatin landscape in the germ cells of the dauer larva downstream of this mechanism. Reducing TBC-7 activity allows RAB-7 to remain in its active GTP-bound form to mediate changes in the dauer germ line to preserve germ cell integrity and post-dauer reproductive fitness.

Supporting information figures and tables

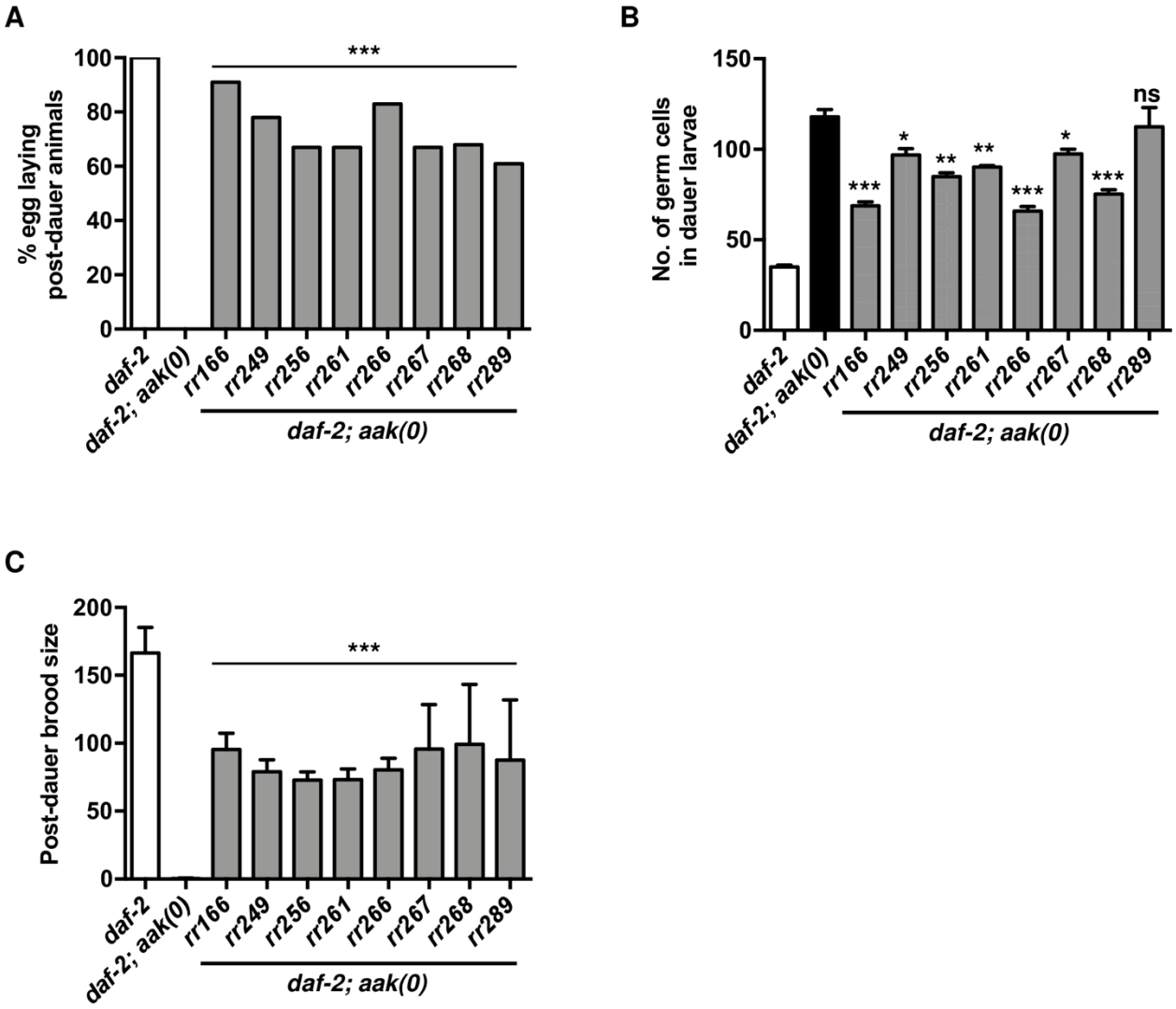

Fig. S2.1. Mutants partially suppress the dauer germline hyperplasia and post-dauer sterility associated with loss of AMPK. (A-C) Mutants isolated from an EMS suppressor screen partially suppress the (A) post-dauer sterility, (B) dauer germline hyperplasia, and (C) brood size defects associated with a lack of AMPK signalling. ***P < 0.0001, **P < 0.001, *P < 0.05 when compared to *daf-2; aak(0)* using ordinary one-way ANOVA for post-dauer brood size and no. of germ cells in dauer larvae. ***P < 0.0001 when compared to *daf-2; aak(0)* using Marascuilo procedure for % egg laying post-dauer

animals. All animals isolated from the screen include *daf-2; aak(0)* in the background. The values for % egg laying post-dauer animals, no. of germ cells in dauer larvae, and post-dauer brood size are presented as means. Each assay was repeated three times with 50 animals in each trial. n = 50.

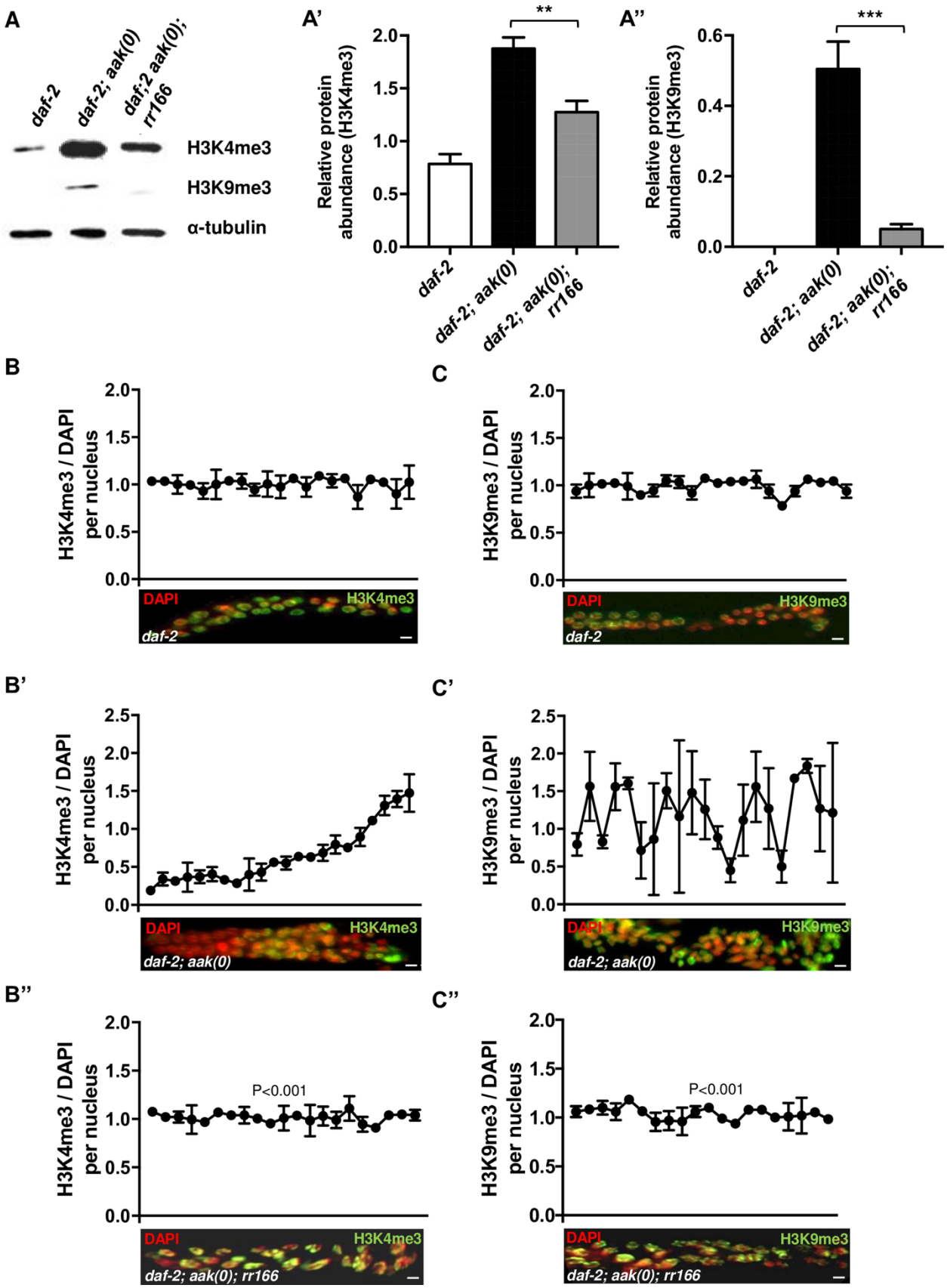
A
daf-2
daf-2; aak(0)
daf;2 aak(0); rr166
H3K4me3
H3K9me3
α-tubulin
A'
Relative protein abundance (H3K4me3)
**
2.0
1.5
1.0
0.5
0.0
daf-2
daf-2; aak(0)
daf-2; aak(0); rr166
A''
Relative protein abundance (H3K9me3)
***
0.6
0.4
0.2
0.0
daf-2
daf-2; aak(0)
daf-2; aak(0); rr166
B
H3K4me3 / DAPI per nucleus
DAPI
H3K4me3
daf-2
C
H3K9me3 / DAPI per nucleus
DAPI
H3K9me3
daf-2
B'
H3K4me3 / DAPI per nucleus
DAPI
H3K4me3
daf-2; aak(0)
C'
H3K9me3 / DAPI per nucleus
DAPI
H3K9me3
daf-2; aak(0)
B''
H3K4me3 / DAPI per nucleus
P<0.001
DAPI
H3K4me3
daf-2; aak(0); rr166
C''
H3K9me3 / DAPI per nucleus
P<0.001
DAPI
H3K9me3
daf-2; aak(0); rr166

Fig. S2.2. The abnormal abundance and distribution of chromatin marks typical of dauer larvae that lack AMPK is corrected in *rr166* mutants. (A) Global levels of H3K4me3 and H3K9me3 were quantified by performing whole-animal western analysis on dauer larvae. (A'-A'') Levels of chromatin marks were quantified and normalized to α-tubulin using ImageJ software. ***P < 0.0001 when compared to *daf-2; aak(0)* using Student's t-test. (B-C'') The distribution and abundance of activating and repressive chromatin marks are corrected in the *daf-2; aak(0); rr166* mutants. The top row (*daf-2*), middle row (*daf-2; aak(0)*), and bottom row (*daf-2; aak(0); rr166*) show (B, B', B'') H3K4me3 (green), (C, C', C'') H3K9me3 (green), and DAPI (red). The graphs represent the average immunofluorescence signal of anti-H3K4me3 and anti-H3K9me3 normalized to DAPI in each nucleus across the dissected germ line. All images are merged, condensed Z stacks and are aligned such that distal is left and proximal is right. Due to technical difficulties, only single gonadal arms were analyzed (distal, proximal). **P < 0.001 using the F-test for variance when compared to *daf-2; aak(0)*. All animals carry the *daf-2(e1370)* allele. Scale bar: 4 μm. n = 15.

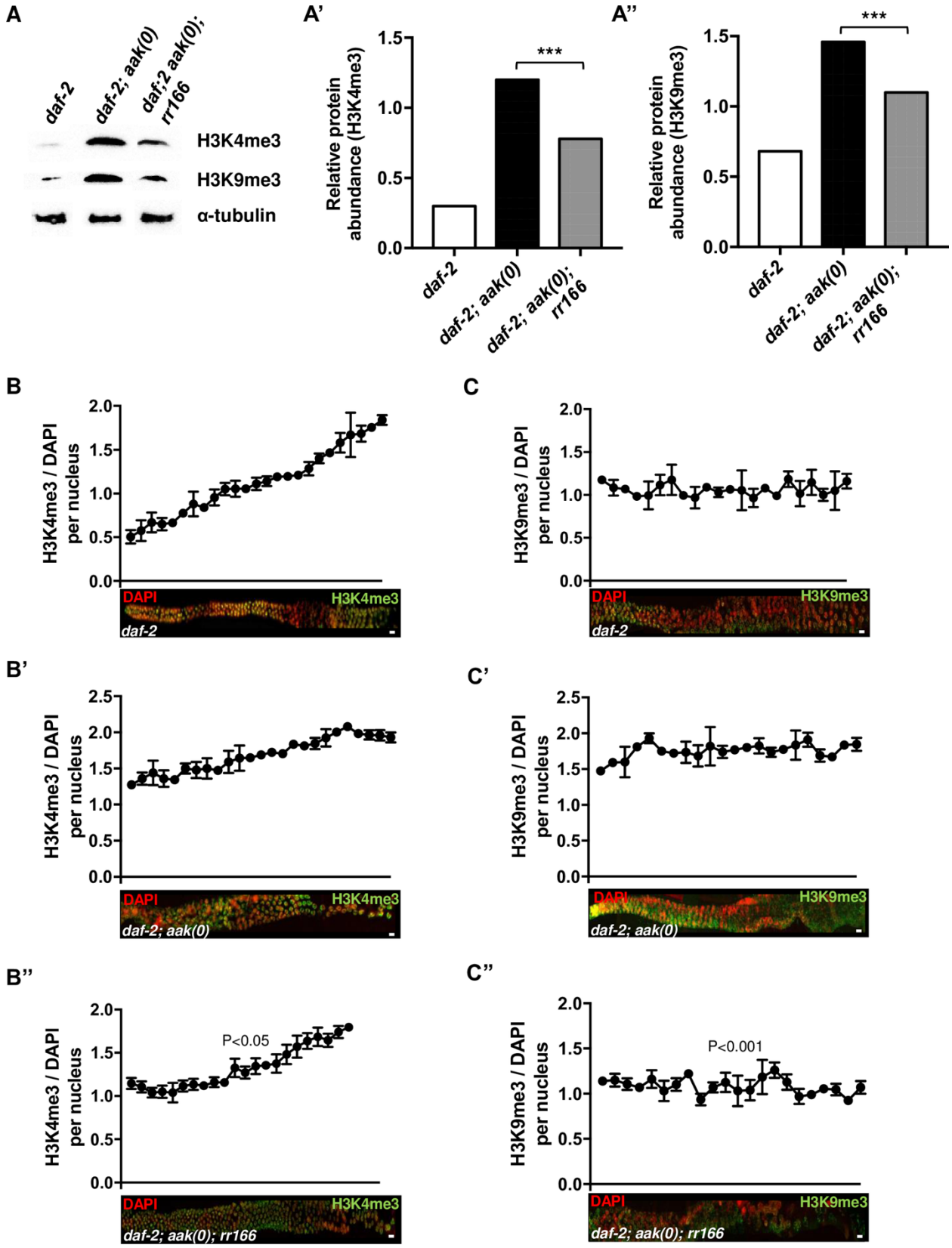
A
daf-2
daf-2; aak(0)
daf;2 aak(0); rr166
H3K4me3
H3K9me3
α-tubulin
A'
Relative protein abundance (H3K4me3)
***
daf-2
daf-2; aak(0)
daf-2; aak(0); rr166
A''
Relative protein abundance (H3K9me3)
***
daf-2
daf-2; aak(0)
daf-2; aak(0); rr166
B
H3K4me3 / DAPI per nucleus
DAPI
H3K4me3
daf-2
C
H3K9me3 / DAPI per nucleus
DAPI
H3K9me3
daf-2
B'
H3K4me3 / DAPI per nucleus
DAPI
H3K4me3
daf-2; aak(0)
C'
H3K9me3 / DAPI per nucleus
DAPI
H3K9me3
daf-2; aak(0)
B''
H3K4me3 / DAPI per nucleus
P<0.05
DAPI
H3K4me3
daf-2; aak(0); rr166
C''
H3K9me3 / DAPI per nucleus
P<0.001
DAPI
H3K9me3
daf-2; aak(0); rr166

Fig. S2.3. The *rr166* mutation restores appropriate chromatin remodeling in post-dauer AMPK mutants. (A) Global levels of H3K4me3 and H3K9me3 were quantified by performing whole-animal western analysis of dauer larvae. (B) Chromatin marks were quantified and normalized to α-tubulin using ImageJ software. ***P < 0.0001 when compared to *daf-2; aak(0)* using Student's t-test. (B-C'') The aberrant distribution and abundance of activating (H3K4me3) and repressive (H3K9me3) chromatin marks observed in post-dauer adults that lack AMPK signalling are corrected in the *daf-2; aak(0); rr166* mutants. The top row (*daf-2*), middle row (*daf-2; aak(0)*), and bottom row (*daf-2; aak(0); rr166*) show (B, B', B'') H3K4me3 (green), (C, C', C'') H3K9me3 (green), and DAPI (red). The graphs represent the average immunofluorescence signal of anti-H3K4me3 and anti-H3K9me3 normalized to DAPI across the dissected germ line. All images are merged, condensed Z stacks that are aligned such that distal is left and proximal is right. Due to technical difficulties, only single gonadal arms were analyzed (distal, proximal). **P < 0.001 using the F-test for variance when compared to *daf-2; aak(0)*. All animals carry the *daf-2(e1370)* allele. Scale bar: 4 μm. n = 15.

A

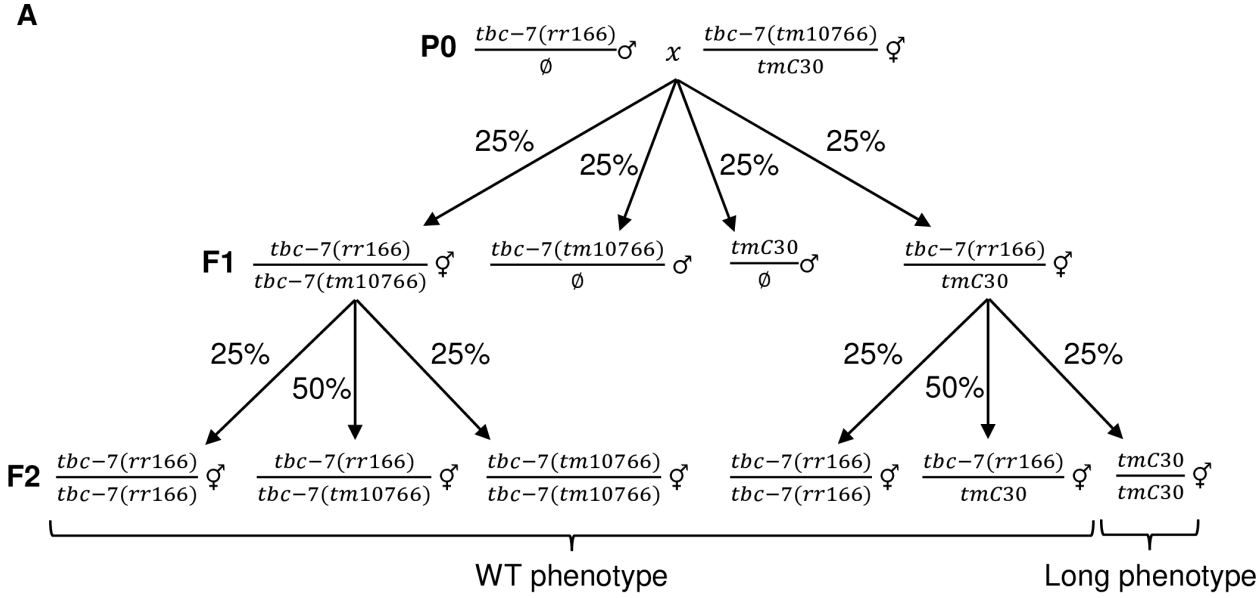

B

Genotype of F1 generation	Trial 1	Trial 2	Average Ratio
$\frac{tbc-7(rr166)}{tbc-7(tm10766)}$	43%	53%	48%
$\frac{tbc-7(rr166)}{tmC30}$	57%	47%	52%

Fig. S2.4. *tbc-7(rr166)* is a hypomorphic allele. (A) Schematic showing the cross with *tbc-7(rr166)* with *tbc-7(tm10766)*, which contains a 21,846 bp deletion that completely removes *tbc-7*. Homozygous *tbc-7(tm10766)* is lethal and is balanced with *tmC30*, which is a balancer that has a recessive Long (Lon) phenotype. To confirm if *tbc-7(rr166)* is a hypomorphic allele, *tbc-7(rr166)* was crossed with *tbc-7(tm10766)* and the F_2 cross progeny were examined in order to identify F_1 heterozygous *tbc-7(rr166)/tbc-7(tm10766)* hermaphrodites. F_1 heterozygous *tbc-7(rr166)/tbc-7(tm10766)* hermaphrodites should yield no Lon phenotype progeny, while F_1 heterozygous *tbc-7(rr166)/tmC30* should yield 25% Lon phenotype progeny. (B) Table showing the percentage of F_1 genotypes over

two independent crosses. The F_2 progeny of every F_1 was assessed. F_1 genotypes assessed per cross $n \geq 150$.

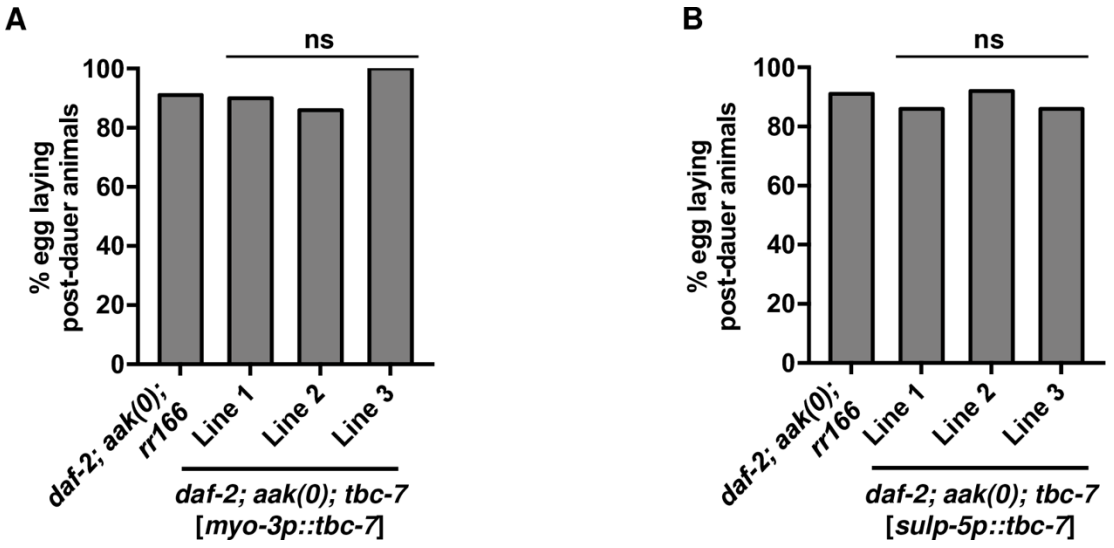

Fig. S2.5. TBC-7 does not work in the body wall muscle or excretory system to regulate germ cell integrity. A wild-type copy of *tbc-7* cDNA expressed exclusively in the (A) muscles by the *myo-3* promoter or the (B) excretory system by the *sulp-5* promoter in the *tbc-7*-suppressed mutants does not revert the suppression of the AMPK germline phenotypes. ns when compared to *daf-2; aak(0); tbc-7* based on Marascuilo procedure for % egg laying animals. All animals carry the *daf-2(e1370)* allele. The values for % egg laying post-dauer animals are presented as means. Each assay was repeated three times with 50 animals in each trial. n = 50.

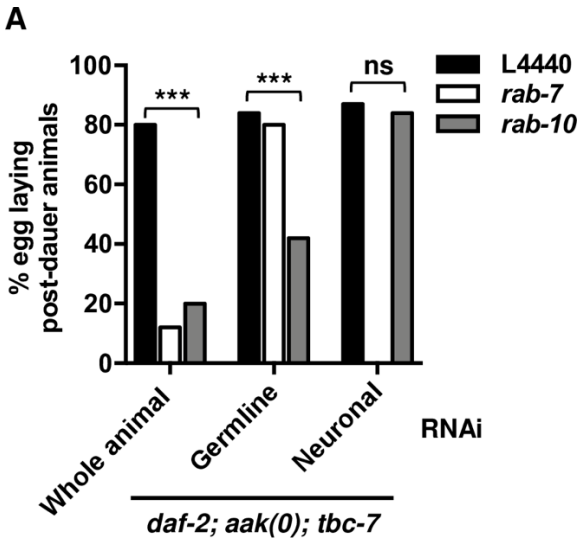

Fig. S2.6. *rab-7* functions in the neurons while *rab-10* functions in the germ line. (A) Tissue-specific RNAi experiments in the *daf-2; aak(0); tbc-7* mutant show that *rab-7* functions in the neurons while *rab-10* functions in the germ line. ***P < 0.0001 when compared to L4440 empty vector using Marascuilo procedure for % of egg laying post-dauer animals. The values for % egg laying post-dauer animals are presented as means. Each assay was repeated three times with 50 animals in each trial. n = 50.

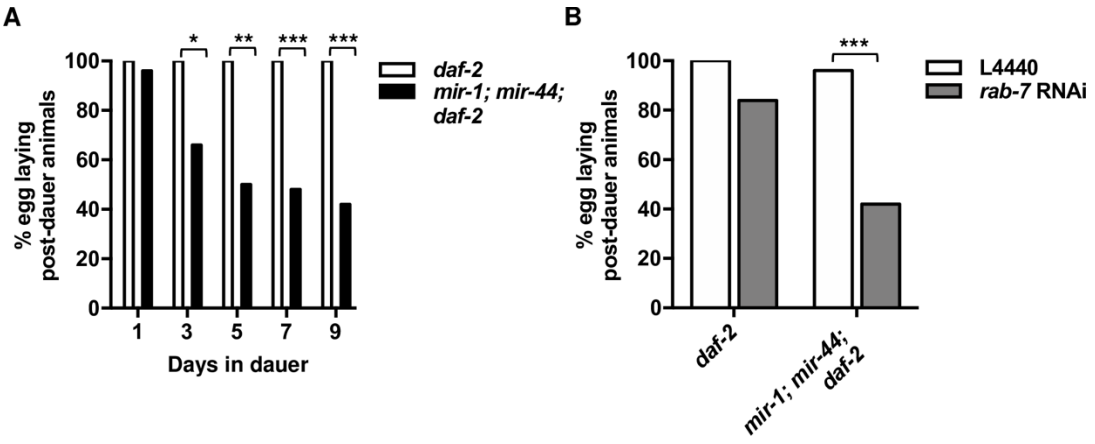

Fig. S2.7. *mir-1; mir-44; daf-2* double mutants display the same post-dauer germline defects. (A) *mir-1*; *mir-44; daf-2* mutants exhibit post-dauer sterility after 7 days in the dauer stage. ***P < 0.0001, **P < 0.001, *P < 0.01 when compared to *daf-2* animals that spent an identical duration in the dauer stage using Marascuilo procedure for % egg laying animals. (B) Reducing *rab-7* levels greatly enhances/accelerates the post-dauer sterility associated with a loss of *mir-1* and *mir-44*. ***P < 0.0001 when compared to L4440 empty vector using Marascuilo procedure for % egg laying animals. All animals carry the *daf-2(e1370)* allele. The values for % egg laying post-dauer animals are presented as means. Each assay was repeated three times with 50 animals in each trial. n = 50.

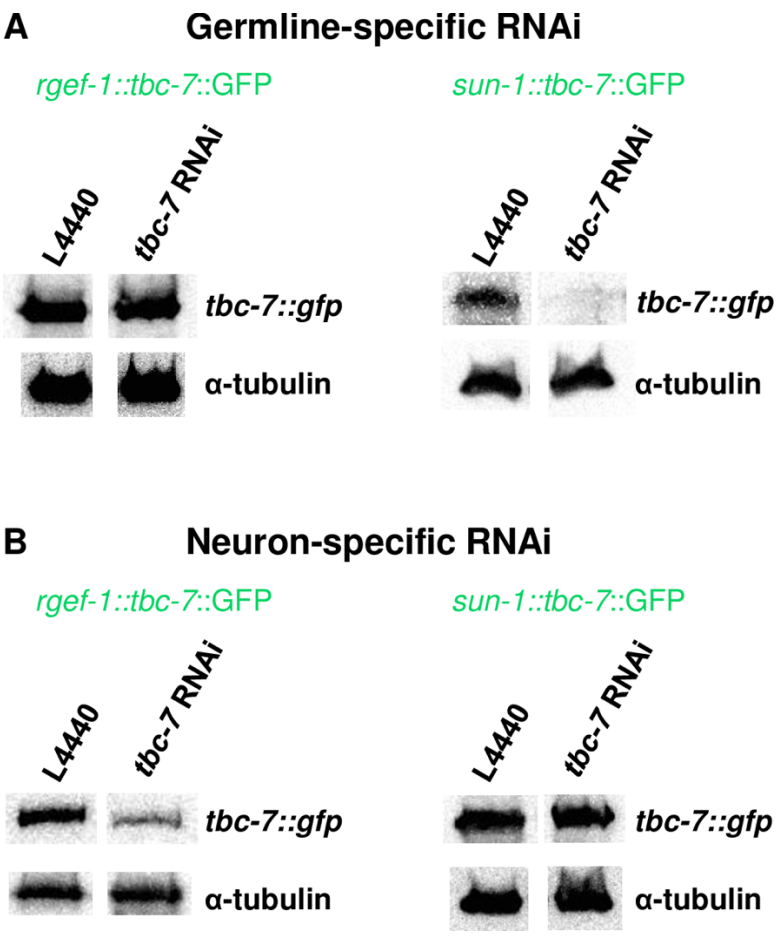

Fig. S2.8. Tissue-specific TBC-7::GFP used as a sensor for RNAi efficiency and specificity in the neurons and the germ line. TBC-7::GFP was expressed in either the neurons (*rgef-1* promoter) or the in the germ line (*sun-1* promoter) of animals with (A) germline-specific RNAi and (B) neuron-specific RNAi. Tissue-specific RNAi animals were treated with either empty vector control L4440 or with dsRNA against *tbc-7*. The levels of TBC-7::GFP protein expression were quantified using Western blotting against GFP. α-tubulin was used as a loading control.

Genotype	WT-like (%)	Protruding vulva (%)	Multivulva (%)	Burst vulva (%)	PD lethality (%)
daf-2	100	0	0	0	0
daf-2; aak(0)	68	8	4	4	16
rr166	92	4	0	0	4
rr249	84	12	0	0	4
rr256	84	0	0	12	4
rr261	76	12	0	12	0
rr266	84	4	0	8	4
rr267	80	8	0	8	4
rr268	76	12	4	4	4
rr289	72	8	0	16	4

Table S2.1. Mutants isolated from an EMS suppressor screen partially suppress the post-dauer somatic defects of AMPK mutants. Mutants were allowed to transit through the dauer stage and recover. The post-dauer somatic defects were assessed seven days after the recovery period. All animals carry the *daf-2(e1370)* allele. Mutants isolated from the EMS screen are *daf-2; aak(0)*. The values are presented as means. Each assay was repeated three times with 50 animals in each trial. n = 50.

Gene targeted by RNAi	Tissue investigated	RNAi phenotype	Mutants showing RNAi phenotype (%)			
			daf-2	*daf-2; aak(0)*	Germline-specific	Neuron-specific
dpy-10	Hypodermis	Dumpy	96	80	0	0
egg-5	Germ line	Embryonic lethal	64	88	100	10
unc-13	Nervous system	Paralysis	64	56	0	80

Table S2.2. *daf-2; aak(0); rde-1* mutants with tissue-specific expression of *rde-1* exhibit tissue-specific RNAi phenotypes. To create a tissue-specific RNAi strain in the *daf-2; aak(0); rde-1* background, *rde-1* was driven exclusively in the neurons using a *rgef-1* promoter or in the germ line using a *sun-1* promoter to create a neuron-specific or germline-specific RNAi strain, respectively. To confirm that *daf-2; aak(0); rde-1* mutants with tissue-specific expression of *rde-1* exhibit tissue-specific RNAi phenotypes, mutants were fed dsRNA against *dpy-10* (hypodermis), *egg-5* (germ line), or *unc-13* (neurons) and the phenotypes were scored. Each dsRNA treatment exhibits a unique phenotype, such as dumpy (*dpy-10* RNAi), embryonic lethal (*egg-5* RNAi), or paralysis (*unc-13* RNAi). *daf-2* control, *daf-2; aak(0)*, or the tissue-specific RNAi strains were synchronized and plated on bacteria expressing one of three dsRNAs. These animals transited through the dauer stage, and their RNAi phenotype was scored as post-dauer adults. Only mutants expressing *rde-1* in the same tissues targeted by the dsRNA should exhibit the RNAi phenotype. All mutants are *daf-2; aak(0)* except the *daf-2* control. The values are presented as means. Each assay was repeated three times with 50 animals in each trial. n = 50.

	% egg laying post-dauer animals	
RNAi	***daf-2***	***daf-2; aak(0); tbc-7***
L4440	100	84
rab-1	0	0
rab-2	60	40
rab-3	100	64
rab-5	24	0
rab-6.1	95	44
rab-6.2	86	84
rab-7	84	12
rab-8	83	64
rab-10	84	20
rab-11.1	68	40
rab-11.2	7	8
rab-14	84	44
rab-21	85	88
rab-27	100	84
rab-28	80	92
rab-35	100	60
rab-37	96	64
rab-39	96	52
R07B1.12	100	84
4R79.2	100	56
K02E10.1	100	52
F11A5.3	96	56
F11A5.4	100	56
C33D12.6	100	84
C33E6.22	100	84

Table S2.3. Post-dauer fertility after RNAi treatment against *rab* genes. *daf-2* control and *daf-2; aak(0); tbc-7* mutants were fed dsRNA against all known and predicted *rab*

genes then allowed to transit through the dauer stage. L4440 empty vector was used as a control. All animals have the *daf-2(e1370)* allele. The values for % egg laying post-dauer animals are presented as means. Each assay was repeated three times with 50 animals in each trial. n = 50.

Gene targeted by RNAi	Tissue investigated	RNAi phenotype	Mutants showing RNAi phenotype (%)			
			daf-2	*daf-2; aak(0); tbc-7*	Germline-specific	Neuron-specific
dpy-10	Hypodermis	Dumpy	96	84	0	0
egg-5	Germ line	Embryonic lethal	64	72	100	0
unc-13	Nervous system	Paralysis	64	68	0	80

Table S2.4. *daf-2; aak(0); rde-1; tbc-7* mutants with tissue-specific expression of *rde-1* exhibit tissue-specific RNAi phenotypes. To create a tissue-specific RNAi strain in the *daf-2; aak(0); rde-1; tbc-7* background, *rde-1* was driven exclusively in the neurons using a *rgef-1* promoter or in the germ line using a *sun-1* promoter to create a neuron-specific or germline-specific RNAi strain, respectively. To confirm that *daf-2; aak(0); rde-1; tbc-7* mutants with tissue-specific expression of *rde-1* exhibit tissue-specific RNAi phenotypes, mutants were fed dsRNA against *dpy-10* (hypodermis), *egg-5* (germ line), or *unc-13* (neurons) and the phenotypes were scored. Each dsRNA treatment exhibits a unique phenotype, such as dumpy (*dpy-10* RNAi), embryonic lethal (*egg-5* RNAi), or paralysis (*unc-13* RNAi). *daf-2* control, *daf-2; aak(0)*, or the tissue-specific RNAi strains were synchronized and plated on bacteria expressing one of three dsRNAs. These animals transited through the dauer stage, and their RNAi phenotype was scored as post-dauer adults. Only mutants expressing *rde-1* in the same tissues targeted by the dsRNA should exhibit the RNAi phenotype. All mutants are *daf-2; aak(0); tbc-7* except the *daf-2* control. The values are presented as means. Each assay was repeated three times with 50 animals in each trial. n = 50.

Position		Predicted consensus sequence	Conserved branch length	Preferentially conserved targeting (P_{CT})
mir-1	Position 285-292 of *tbc-7* 3' UTR	5'...UCACUUAUUUUCU**ACAUUCCA**...3' 3' AUGUAUGAAGAAA---**UGUAAGG**U 5'	0.995	0.94
	Position 388-394 of *tbc-7* 3' UTR	5'...UAAUCAGAAGCU**CAUUCCAA**...3' 3' AUGUAUGAAGAAAU**GUAAGG**U 5'	0.759	0.69
mir-44	Position 296-303 of *tbc-7* 3' UTR	5'…UUCUACAUUCCAACU**UCUAGUCA**…3' 3' UCGACUUACACAG**AGAUCAG**U 5'	0.637	0.84

Table S2.5. Predicted *mir-1* and *mir-44* seed sequences in the 3' UTR of *tbc-7*. Two highly conserved *mir-1* seed sequences (bold) and one highly conserved *mir-44* seed sequence (bold) were identified in the 3' UTR of *tbc-7* (TargetScanWorm release 6.2), suggesting that *mir-1* and *mir-44* directly regulates *tbc-7* expression. The P_{CT} and conserved branch length are measures of the biological relevance of the predicted miRNA and target interaction, with greater values being more likely to have detectable biological function [50, 51].

References

1. Brauer MJ, Huttenhower C, Airoldi EM, Rosenstein R, Matese JC, Gresham D, et al. Coordination of growth rate, cell cycle, stress response, and metabolic activity in yeast. Molecular biology of the cell. 2008;19(1):352-67.

2. Rittershaus ES, Baek SH, Sassetti CM. The normalcy of dormancy: common themes in microbial quiescence. Cell Host Microbe. 2013;13(6):643-51.

3. Valcourt JR, Lemons JM, Haley EM, Kojima M, Demuren OO, Coller HA. Staying alive: metabolic adaptations to quiescence. Cell Cycle. 2012;11(9):1680-96.

4. Gospodarowicz D, Moran JS. Growth factors in mammalian cell culture. Annu Rev Biochem. 1976;45:531-58.

5. Heijmans BT, Tobi EW, Stein AD, Putter H, Blauw GJ, Susser ES, et al. Persistent epigenetic differences associated with prenatal exposure to famine in humans. Proceedings of the National Academy of Sciences of the United States of America. 2008;105(44):17046-9.

6. Wong C, Roy R. AMPK Regulates Developmental Plasticity through an Endogenous Small RNA Pathway in *Caenorhabditis elegans*. Int J Mol Sci. 2020;21(6).

7. Yao G. Modelling mammalian cellular quiescence. Interface Focus. 2014;4(3):20130074.

8. Narbonne P, Roy R. Inhibition of germline proliferation during C. elegans dauer development requires PTEN, LKB1 and AMPK signalling. Development. 2006;133(4):611-9.

9. Tissenbaum HA, Ruvkun G. An insulin-like signaling pathway affects both longevity and reproduction in *Caenorhabditis elegans*. Genetics. 1998;148(2):703-17.

10. Kadekar P, Roy R. AMPK regulates germline stem cell quiescence and integrity through an endogenous small RNA pathway. PLoS Biol. 2019;17(6):e3000309.

11. Hong Y, Roy R, Ambros V. Developmental regulation of a cyclin-dependent kinase inhibitor controls postembryonic cell cycle progression in *Caenorhabditis elegans*. Development. 1998;125(18):3585-97.

12. Cassada RC, Russell RL. The dauerlarva, a post-embryonic developmental variant of the nematode *Caenorhabditis elegans*. Developmental biology. 1975;46(2):326-42.

13. Fielenbach N, Antebi A. C. elegans dauer formation and the molecular basis of plasticity. Genes & development. 2008;22(16):2149-65.

14. Hall SE, Chirn GW, Lau NC, Sengupta P. RNAi pathways contribute to developmental history-dependent phenotypic plasticity in C. elegans. RNA (New York, NY). 2013;19(3):306-19.

15. Hall SE, Beverly M, Russ C, Nusbaum C, Sengupta P. A cellular memory of developmental history generates phenotypic diversity in C. elegans. Current biology : CB. 2010;20(2):149-55.

16. Burkewitz K, Morantte I, Weir HJM, Yeo R, Zhang Y, Huynh FK, et al. Neuronal CRTC-1 governs systemic mitochondrial metabolism and lifespan via a catecholamine signal. Cell. 2015;160(5):842-55.

17. Narbonne P, Roy R. *Caenorhabditis elegans* dauers need LKB1/AMPK to ration lipid reserves and ensure long-term survival. Nature. 2009;457(7226):210-4.

18. Dumas JJ, Zhu Z, Connolly JL, Lambright DG. Structural basis of activation and GTP hydrolysis in Rab proteins. Structure. 1999;7(4):413-s2.

19. Doitsidou M, Jarriault S, Poole RJ. Next-Generation Sequencing-Based Approaches for Mutation Mapping and Identification in *Caenorhabditis elegans*. Genetics. 2016;204(2):451-74.

20. Uytterhoeven V, Kuenen S, Kasprowicz J, Miskiewicz K, Verstreken P. Loss of skywalker reveals synaptic endosomes as sorting stations for synaptic vesicle proteins. Cell. 2011;145(1):117-32.

21. Nehammer C, Ejlerskov P, Gopal S, Handley A, Ng L, Moreira P, et al. Interferon-β-induced miR-1 alleviates toxic protein accumulation by controlling autophagy. eLife. 2019;8.

22. Tursun B, Cochella L, Carrera I, Hobert O. A toolkit and robust pipeline for the generation of fosmid-based reporter genes in C. elegans. PloS one. 2009;4(3):e4625.

23. Calixto A, Chelur D, Topalidou I, Chen X, Chalfie M. Enhanced neuronal RNAi in C. elegans using SID-1. Nat Methods. 2010;7(7):554-9.

24. Zou L, Wu D, Zang X, Wang Z, Wu Z, Chen D. Construction of a germline-specific RNAi tool in C. elegans. Sci Rep. 2019;9(1):2354.

25. Gallegos ME, Balakrishnan S, Chandramouli P, Arora S, Azameera A, Babushekar A, et al. The C. elegans rab family: identification, classification and toolkit construction. PloS one. 2012;7(11):e49387.

26. Chotard L, Mishra AK, Sylvain MA, Tuck S, Lambright DG, Rocheleau CE. TBC-2 regulates RAB-5/RAB-7-mediated endosomal trafficking in *Caenorhabditis elegans*. Molecular biology of the cell. 2010;21(13):2285-96.

27. Der CJ, Finkel T, Cooper GM. Biological and biochemical properties of human rasH genes mutated at codon 61. Cell. 1986;44(1):167-76.

28. Méresse S, Gorvel JP, Chavrier P. The rab7 GTPase resides on a vesicular compartment connected to lysosomes. J Cell Sci. 1995;108 (Pt 11):3349-58.

29. Gutiérrez-Pérez P, Santillán EM, Lendl T, Wang J, Schrempf A, Steinacker TL, et al. miR-1 sustains muscle physiology by controlling V-ATPase complex assembly. Sci Adv. 2021;7(42):eabh1434.

30. Broughton JP, Lovci MT, Huang JL, Yeo GW, Pasquinelli AE. Pairing beyond the Seed Supports MicroRNA Targeting Specificity. Molecular cell. 2016;64(2):320-33.

31. Alvarez-Saavedra E, Horvitz HR. Many families of C. elegans microRNAs are not essential for development or viability. Current biology : CB. 2010;20(4):367-73.

32. Simon DJ, Madison JM, Conery AL, Thompson-Peer KL, Soskis M, Ruvkun GB, et al. The microRNA miR-1 regulates a MEF-2-dependent retrograde signal at neuromuscular junctions. Cell. 2008;133(5):903-15.

33. Takane K, Fujishima K, Watanabe Y, Sato A, Saito N, Tomita M, et al. Computational prediction and experimental validation of evolutionarily conserved microRNA target genes in bilaterian animals. BMC Genomics. 2010;11(1):101.

34. Maniates KA, Olson BS, Abbott AL. Sperm fate is promoted by the mir-44 microRNA family in the *Caenorhabditis elegans* hermaphrodite germline. Genetics. 2021;217(1):1-14.

35. Gwinn DM, Shackelford DB, Egan DF, Mihaylova MM, Mery A, Vasquez DS, et al. AMPK phosphorylation of raptor mediates a metabolic checkpoint. Molecular cell. 2008;30(2):214-26.

36. Obenauer JC, Cantley LC, Yaffe MB. Scansite 2.0: Proteome-wide prediction of cell signaling interactions using short sequence motifs. Nucleic acids research. 2003;31(13):3635-41.

37. Rao XS, Cong XX, Gao XK, Shi YP, Shi LJ, Wang JF, et al. AMPK-mediated phosphorylation enhances the auto-inhibition of TBC1D17 to promote Rab5-dependent glucose uptake. Cell Death Differ. 2021;28(12):3214-34.

38. Ahmadi M, Roy R. AMPK acts as a molecular trigger to coordinate glutamatergic signals and adaptive behaviours during acute starvation. eLife. 2016;5.

39. Poteryaev D, Fares H, Bowerman B, Spang A. *Caenorhabditis elegans* SAND-1 is essential for RAB-7 function in endosomal traffic. The EMBO journal. 2007;26(2):301-12.

40. Bucci C, Thomsen P, Nicoziani P, McCarthy J, van Deurs B. Rab7: a key to lysosome biogenesis. Molecular biology of the cell. 2000;11(2):467-80.

41. Grishok A, Pasquinelli AE, Conte D, Li N, Parrish S, Ha I, et al. Genes and mechanisms related to RNA interference regulate expression of the small temporal RNAs that control C. elegans developmental timing. Cell. 2001;106(1):23-34.

42. Conine CC, Rando OJ. Soma-to-germline RNA communication. Nat Rev Genet. 2022;23(2):73-88.

43. Brenner S. The genetics of *Caenorhabditis elegans*. Genetics. 1974;77(1):71-94.

44. Yook, K. Complementation. Wormbook. 2005;1.24.1. Available from: http://www.wormbook.org.

45. Arduengo PM, Appleberry OK, Chuang P, L'Hernault SW. The presenilin protein family member SPE-4 localizes to an ER/Golgi derived organelle and is required for

proper cytoplasmic partitioning during *Caenorhabditis elegans* spermatogenesis. J Cell Sci. 1998;111 (Pt 24):3645-54.

46. Kostić I, Li S, Roy R. Cki-1 links cell division and cell fate acquisition in the C. elegans somatic gonad. Developmental biology. 2003;263(2):242-52.

47. Kamath RS, Fraser AG, Dong Y, Poulin G, Durbin R, Gotta M, et al. Systematic functional analysis of the *Caenorhabditis elegans* genome using RNAi. Nature. 2003;421(6920):231-7.

48. Fraser AG, Kamath RS, Zipperlen P, Martinez-Campos M, Sohrmann M, Ahringer J. Functional genomic analysis of C. elegans chromosome I by systematic RNA interference. Nature. 2000;408(6810):325-30.

49. Stefanakis N, Carrera I, Hobert O. Regulatory Logic of Pan-Neuronal Gene Expression in C. elegans. Neuron. 2015;87(4):733-50.

50. Friedman RC, Farh KK, Burge CB, Bartel DP. Most mammalian mRNAs are conserved targets of microRNAs. Genome research. 2009;19(1):92-105.

51. Jan CH, Friedman RC, Ruby JG, Bartel DP. Formation, regulation and evolution of *Caenorhabditis elegans* 3'UTRs. Nature. 2011;469(7328):97-101.

Bridging statement between chapters 2 and 3

In chapter 2, we described a mechanism in which AMPK regulates the germ line non-autonomously in the neurons. Through an EMS-based forward genetic screen, we identified two alleles of a RabGAP protein *tbc-7*. RabGAP proteins enhance the inherent hydrolysis ability of Rab GTPases to convert the GTPase from its active GTP-bound form to its inactive GDP-bound form. AMPK mutants, during the dauer stage, exhibit somatic and germline defects, such as germline hyperplasia and post-dauer sterility. By compromising *tbc-7* function, whether through an EMS-induced lesion or through RNAi knockdown, we can suppress these germline defects. The *rr166* allele of *tbc-7* can also suppress the abnormal increase and misregulated distribution of histone marks in the germ line as well. We also showed through genetic analyses and confocal imaging that TBC-7 primarily functions in the neurons. Interestingly, while *tbc-7* can cell non-autonomously regulate the germ line during the dauer stage, it still suffers from the reduced dauer survival typically seen in AMPK mutants, suggesting that *tbc-7* does not play a role in regulating lipid supplies.

Through phospho-mimetic and -null experiments, we showed that AMPK directly phosphorylates TBC-7 in the neurons in order to shut down its RabGAP activity. In addition, we showed that two miRNAs, *mir-1* and *mir-44*, bind directly to the 3'UTR of the *tbc-7* transcript in order to suppress its expression, demonstrating two levels of regulation for *tbc-7*. Genetic analyses reveals that RAB-7 could be one Rab target of TBC-7. When TBC-7 is active, RAB-7 is converted from its active RAB-GTP form into its inactive RAB-GDP form. Through tissue-specific RNAi experiments, we show that TBC-7 regulates RAB-7 activity in the neurons.

In the following chapter, I examined the role of RAB-7 in endosomal maturation and exosome biogenesis to better understand how it might be regulating the germ line from the neurons during the dauer stage. This study revealed that the miRNA Argonautes, ALG-1 and ALG-2, and miRNAs are loaded into exosomes derived from RAB-7 activity in the neurons. These exosomal miRISC regulate germline gene expression to ensure appropriate germline quiescence in response to environmental stress. We also demonstrate that the loading of these miRNAs are dependent on short sequence motifs called EXOmotifs found on the mature miRNA sequence.

Chapter 3: Neuronal exosomes transport a miRISC cargo to preserve stem cell integrity during energy stress

Christopher Wong[1], Elena M. Jurczak[1], Richard Roy[1]*

[1]Department of Biology, McGill University; Montreal, H3A 1B1, Canada.

Manuscript in review

Abstract

During periods of nutrient scarcity, many animals undergo germline quiescence to preserve reproductive capacity, and neurons are often necessary for this adaptation. We show here that starvation causes the release of neuronal miRNA/Argonaute-loaded exosomes following AMPK-regulated trafficking changes within serotonergic neurons. This neuron-to-germ line communication is independent of classical serotonergic neurotransmission, but instead relies on endosome-derived vesicles that carry a pro-quiescent miRNA cargo to modify germline gene expression. Using a miRNA activity sensor, we show that neuronally-expressed miRNAs can extinguish the expression of germline-mRNA targets in an exosome-dependent manner. Our findings demonstrate how an adaptive neuronal response can change gene expression at a distance by re-directing intracellular trafficking to release neuronal exosomes with specific miRNA cargos capable of tracking to their appropriate destinations.

Introduction

Despite their shared ability to self-renew following division, many types of stem cells remain quiescent unless they receive specific signals to proliferate. This quiescence is likely a conserved means of protecting their invaluable genomic information. By using *C. elegans*, we sought to elucidate the genetic pathways that dictate the various events involved in establishing quiescence in the germline stem cells. During periods of environmental challenge, *C. elegans* larvae can enter a non-ageing "dauer" stage, where development is halted and the germline stem cells arrest[1]. The AMP-activated protein kinase (AMPK) and its upstream activator, the LKB1 tumour-suppressor orthologue *par-4*, are essential to establish this quiescence[2]. Not surprisingly, mutants that lack all AMPK signalling are completely sterile following recovery from this stage[3,4].

As animals enter the dauer stage, neuronally-expressed AMPK blocks the activity of a RabGAP protein called TBC-7 to ensure that the conserved GTPase RAB-7, the putative Rab target of TBC-7, remains GTP-bound in order to preserve the reproductive capacity of the germ cells during the dauer stage[4]. RAB-7 is essential for early-to-late endosome maturation and the generation of exosomes[5-7]. Recently, this class of extracellular vesicles has attracted attention due to their potential roles in cell-cell communication in both physiological and pathological processes[8]. However, due to the heterogeneity of these extracellular vesicles and the cargos that they transport, it is still unclear whether their release from cells is part of a regulated pathway, or alternatively, a routine shedding of cellular material.

We describe here how the neuronal activation of AMPK in response to starvation results in the formation and secretion of exosomes that carry instructions in the form of

miRNAs, from the neurons to the stem cells present in the germ line. Following their internalization, these cargo-containing vesicles then transmit a pro-quiescent signal that instructs the germline stem cells to arrest their cell divisions and modify their gene expression to preserve reproductive fitness throughout the course of a potentially lengthy period of energy stress.

Results

Neuronal RAB-7 localizes to the germ line.

We previously identified RAB-7 as a putative target of TBC-7, a gene that when disabled can suppress the germline defects associated with loss of AMPK signalling (Figure 1A)[4]. Animals with intact AMPK signalling (*daf-2*) or compromised *tbc-7* function (*daf-2; aak(0); tbc-7*) maintain active (GTP-bound) RAB-7 during this quiescent period, allowing them to pass through the dauer stage with no reproductive consequences. AMPK mutants (*daf-2; aak(0)*) that lack both catalytic subunits of AMPK, *aak-1* and *aak-2* (*aak(0)*), on the other hand, are completely sterile following recovery from this quiescent stage (post-dauer sterile). Curiously, this sterility can be reversed following the expression of a single catalytic AMPK subunit (*aak-2*) in the neurons, suggesting that AMPK can affect changes in the neurons that are required to maintain reproductive competence following this quiescence, and this feature is mediated through RAB-7 and presumably its role in endosomal trafficking[3,4].

RAB-7 has multiple roles in cellular trafficking, but its role in the formation of multivesicular bodies and endosomally-derived secreted vesicles could account for the cell non-autonomous effects we observe in these post-dauer animals. To determine if RAB-7 is involved in the production of neuronal extracellular vesicles that could transmit information to the germ line during the dauer stage, we expressed a translational fusion protein GFP::RAB-7 exclusively in the neurons and subsequently monitored RAB-7 localization in the resulting dauer larvae.

Based on germ cell transcriptome analyses *rab-7* is presumably not expressed in the germ cells[9]. However, RAB-7 protein was detected in the germ cells using

antibodies[10]. We detected GFP in both the neurons and the germ cells of *daf-2* and *daf-2; aak(0); tbc-7* mutant dauer larvae, but not in *daf-2; aak(0)* (AMPK) mutants (Figure 1B-D), suggesting that neuronal GFP::RAB-7 localization to the germ line may be necessary for post-dauer fertility (see Table S1 for quantification of the GFP::RAB-7 signal in the germ line) (Table S1). The GFP::RAB-7 localization to the perinuclear region is consistent with recipient cells treated with exogenous exosomes that have accumulated endosomal trafficking components[11]. No GFP signal could be detected in the germ lines of animals that did not transit through the dauer stage, regardless of their genotype, suggesting that the release and subsequent mobility of these neuronal GFP::RAB-7-associated structures is specific to this physiological response (Figure S1A-C). The GFP::RAB-7 signal was still visible in the germ cells of *daf-2; aak(0); tbc-7* mutant animals that recovered from this stage (Figure S1D and S1F), while no GFP signal was detected in post-dauer *daf-2; aak(0)* mutants (Figure S1E).

There are multiple pathways that govern entry into the dauer stage, including insulin-like signalling/IGF, TGF-β, cGMP signalling, serotonergic neurotransmission, and steroid hormone signal transduction (see Figure 3 in Biglous et al, 2021)[12,13]. All of these pathways result in the arrest of germline cell cycle and the establishment of dauer-typical metabolism and morphology. To examine if this mechanism of neuron to germ line communication through RAB-7 is conserved in other modes of dauer entry, neuronal GFP::RAB-7 was expressed in *daf-7* mutants and wild-type N2 dauer larvae induced through dauer pheromone or starvation, and image analysis was performed on the resultant dauer larvae. DAF-7 encodes the TGF-β superfamily ligand and is required for continuous development under favourable conditions; thus, the loss of DAF-7 function

results in constitutive dauer formation[14]. Similar to our initial observations in the *daf-2* (insulin-like receptor) mutants, the GFP signal was also detected in the germ lines of *daf-7* and N2 dauer larvae induced through exposure to dauer pheromone or by starvation, suggesting that the transfer of neuronal GFP::RAB-7 to the germ cells at the onset of dauer development is a general, conserved feature that is shared among the best characterized pathways associated with dauer formation (Figure S2A-C).

To confirm that the GFP detected in the germ line is of neuronal origin, we drove the expression of GFP::RAB-7 using the pan-neuronal *rgef-1p* promoter in animals where RNAi activity was restricted to either the neurons or the germ line[4]. We then fed these animals bacteria that expressed dsRNA against *gfp*, or with an empty vector control L4440 and imaged the resultant dauer larvae. Feeding germline-restricted RNAi animals with dsRNA against *gfp* should prevent the accumulation of GFP mRNA in the germ line. Therefore, any GFP protein signal detected in the germ cells would have to be of neuronal origin due to the neuron-specific expression conferred by the pan-neuronal promoter (*rgef-1p*). In these germline-restricted RNAi animals, we were still able to detect GFP in the germ cells, even after feeding with dsRNA against *gfp* and L4440, suggesting that the GFP detected must be from the *gfp* expressed from the transgene expressed in the neurons from the pan-neuronal promoter (Figure S3A and S3B). We repeated this experiment in animals where RNAi is only active in the neurons, and we did not detect GFP in the germ cells of these animals fed with dsRNA against *gfp* (Figure S3C), while the GFP was still detectable in animals fed with empty vector L4440 (Figure S3D). Because we eliminate any possibility that the germ cell might make GFP autonomously through these tissue-restricted RNAi experiments, we conclude that GFP::RAB-7 is made

in the neurons in response to dauer and AMPK signalling, and is subsequently released and incorporated into the germ cells.

We initially chose to drive GFP::RAB-7 expression using an extrachromosomal array-based transgene because the germ cells actively repress these types of transgenes. This would allow us to conclude that any observed GFP expression in the germ line could be attributed to transgene expression in the soma. However, we could not exclude that the genetic background might influence the de-silencing of the transgenes in the germ line allowing the germ cells to express the pan-neuronal GFP::RAB-7[15]. Therefore, to assess whether these extrachromosomal transgenes are ectopically expressed in the germ line in addition to the neurons, we drove the expression of mKate and GFP::RAB-7 in the neurons, while separating the two transgenic sequences by a T2A ribosomal skipper element, and imaged the resulting dauer larvae[16]. If the extrachromosomal transgene is expressed in the germ line during the dauer stage, then both the mKate and GFP::RAB-7 should be visible in the germ cells. Consistent with our previous observations, image analysis shows strong mKate expression exclusively in the neurons, while GFP::RAB-7 is observed in both the neurons and germ line (Figure S3E).

Moreover, to further control for any potential artifacts that could arise to the additional copies of GFP::RAB-7 in the context of an extrachromosomal array context, we expressed a single-copy insertion of our neuronal GFP::RAB-7 using a single-copy MosSCI insertion. We crossed these mutants with animals expressing a mCherry::HIS-11 germline marker and into our control dauer animals (*daf-2)*, AMPK mutant dauer animals (*daf-2; aak(0)*), and the fertile, suppressed AMPK mutants (*daf-2; aak(0); tbc-7)*. We imaged dauer larvae from each of these mutant genotypes and, similar to our findings

with the extrachromosomal arrays, we observed GFP signal in the germ lines of the post-dauer fertile strains that expressed the single-copy insertions (Figure S3F-H).

To better define the localization of the GFP::RAB-7 signal within the germ line, we showed the image analysis of this single-copy transgene in *daf-2* animals as a single confocal slice rather than a compressed z-stack image (Figure S3I). The single confocal slice clearly indicates that the GFP::RAB-7 is indeed within the germ cells proper. No signal was detected in the germ cells of the AMPK null mutants (*daf-2; aak(0)*). All of these data taken together collectively support our conclusion that the GFP protein detected in the germ line does not arise from mRNA produced in the germ line, but is rather from a neuronal origin.

If the localization of GFP::RAB-7 to the germ cells is a result of classical neurotransmitter release, then disabling the release of these critical signals from the neurons should impact post-dauer fertility. We therefore assessed the effects on fertility in the suppressed (fertile) AMPK mutants after either synaptic vesicle (*unc-13*) or dense-core vesicle secretion (*unc-31*) had been abolished[17,18]. The post-dauer fertility of these mutants was however unaffected by either of these mutations (Figure S4A), suggesting that these GFP::RAB-7 structures are unlikely to be generated by pathways involved in vesicle-mediated peptide secretion or synaptic vesicle release.

In addition, because of the previously described role of RAB-7 in endosome to lysosome trafficking and autophagy[19], we also determined whether autophagy was affected in mutants with altered RAB-7 activity (*daf-2; aak(0); tbc-7*), and this might contribute to the restored fertility and/or the observed movement of GFP::RAB-7 to the germ cells. As autophagy progresses, the *C. elegans* orthologue of Atg8/LC3, LGG-1 is

lipidated to become LGG-1 phosphatidylethanolamine (PE), then subsequently cleaved to eventually contribute to the formation of the autolysosome[19]. Using a GFP-tagged LGG-1 transgene, we assessed autophagic flux through Western analysis to conclude that autophagy is unaffected in *tbc-7*-compromised mutants (Figure S4B and S4C).

Because RAB-7 functions both in endosomal maturation and exosome production, we characterized these GFP-containing structures by immunogold labelling TEM following their purification from dauer larvae. GFP::RAB-7 localized to the membrane of these isolated vesicles (Figure 1E), which were 30-150 nm (Figure 1F), within the diameter range typical of small extracellular vesicles (sEVs) derived from the endosomal pathway[20]. Immunogold labelling TEM analysis also indicated that approximately 54% of exosomes contained RAB-7 on their membranes (Figure 1G). To assess if these sEVs could be exosomes specifically from the endosomal route, we performed immunoprecipitation using an anti-HA antibody against HA::GFP::RAB-7 on the vesicle sample and performed Western analysis against known markers CD63/TSP-7, Tsg101/TSG-101, Rab5/RAB-5, and Alix/ALX-1[21-24]. As these antibodies were raised against human, mouse, and rat, we verified their cross-reactivity with their *C. elegans* orthologues by subjecting their associated gene products to RNAi in *daf-2* control animals (Figure 1H-K). Moreover, our analysis of the expression pattern of a TSP-7::GFP fusion protein in dauer larvae is consistent with its potential role in the formation of exosomes in the neurons (Figure S4D) and with the pattern observed in adult animals[25-27]. Our Western analysis indicated that TSP-7, TSG-101, RAB-5, and ALX-1 were indeed associated with our GFP-containing RAB-7 structures, consistent with the possibility that these vesicle-like structures could indeed be exosomes derived from the endosomal pathway (Figure

1L and 1M). Our data therefore support a role for RAB-7 in contributing to the formation of specialized neuronal vesicles following AMPK activation[4]. These RAB-7-associated exosomes exit the neurons and thereafter translocate to the germ cells during the dauer stage, where RAB-7 remains up to 24h after recovery from the dauer stage.

If these GFP::RAB-7 vesicles are indeed exosomes, then interfering with exosome biogenesis should have an impact on the localization of GFP::RAB-7 to the germ line during the dauer stage. We therefore assessed the post-dauer fertility of *daf-2; aak(0); tbc-7* mutants after feeding them with either control RNAi bacteria (L4440) or bacteria that express dsRNA against *ral-1*, a GTPase involved in multivesicular body formation and fusion with the plasma membrane[28]. The loss of *ral-1* reduced the post-dauer fertility (Figure S4E), but in addition, animals fed with dsRNA against *ral-1* blocked the secretion of RAB-7-containing exosomes from the neurons (Figure S4F and S4G), suggesting that a direct disruption of the exosome biogenesis or secretion pathway interferes with germ cell integrity.

In contrast to our *ral-1* RNAi results, other non-exosomal secretory pathways do not appear to have any role in this process. TAT-5 is a conserved P4-ATPase that represses phosphatidylethanolamine externalization on the plasma membrane and ectosome production[29]. Loss of TAT-5 results in the large-scale budding of vesicles from the plasma membrane during the embryonic stage. These vesicles are independent from the endosomal pathway and lead to defects in cell adhesion and cell shape, ultimately resulting in sterility. Thus, introducing extra copies of TAT-5 in the neurons of our post-dauer fertile animals (*daf-2; aak(0); tbc-7*) should prevent the localization of GFP::RAB-7 to the germ line during the dauer stage if these RAB-7 vesicles are derived from

spontaneous budding of the plasma membrane. Consistent with our previous findings, introducing extra copies of TAT-5 in the neurons did not affect the post-dauer fertility, nor disrupt the localization of GFP::RAB-7 to the germ cells (Figure S4H-I), suggesting that this alternative secretory pathway does not contribute to the secretion of GFP::RAB-7 from the neurons.

In *C. elegans*, the nervous system uses an array of conserved neurotransmitters, similar to mammals, in order to influence the activity of molecular pathways in post-synaptic neurons. Since these neurons have specialized functions in signalling, it is possible that *tbc-7* functions in only one class of neurons that is critical for responding to the energy stress associated with dauer formation. To determine in which neurons *tbc-7* might function, we drove the expression of wild-type *tbc-7* under neuron class-specific promoters in *daf-2; aak(0); tbc-7* mutants and assessed the resultant post-dauer fertility of these transgenic animals, whereby the re-introduction of a wild-type copy of *tbc-7* in the relevant neurons should restore the wild-type function of the RabGAP and render the post-dauer animals sterile. The expression of wild-type *tbc-7* exclusively in serotonergic neurons (*tph-1p*) reverted the suppression of the AMPK germline defects (Figure 1N), while driving the expression of GFP::RAB-7 in the serotonergic neurons was sufficient to detect GFP signal in the germ cells of these dauer larvae (Figure 1O). These data suggest that the serotonergic neurons could be the major, but potentially not the only, class of neurons that produce and secrete exosomes in response to energy stress through the activity of the AMPK/TBC-7/RAB-7 signalling axis during the dauer stage.

Because we observed neuronally-derived GFP::RAB-7 in the germ cells we questioned whether RAB-7 alone was sufficient to navigate all RAB-7-associated

exosomes to the germ cells. We therefore expressed GFP::RAB-7 in multiple cell types using tissue-specific promoters, but despite visible GFP signal in each of the tissues assayed, no GFP could be detected in the germ cells of the transgene-expressing dauer larvae (Figure S5A-C). These data indicate that although neuronal RAB-7 is critical for the formation and release of these exosomes, it does not function alone. An additional navigator component must be required to direct the neuronal RAB-7-associated exosomes to the germ line.

miRNAs regulate germline gene expression.

The neuronal RAB-7-associated exosomes could provide a pro-quiescent signal that instructs the stem cells to modify their chromatin and adjust their gene expression in anticipation of a potentially lengthy environmental challenge. We have shown that small RNA pathways are important effectors downstream of AMPK[3,30-32], while miRNAs and other RNAs have been identified in the cargo of several types of exosomes[33]. Therefore, to determine if the AMPK-dependent germline quiescence is regulated through a small RNA-based mechanism, we soaked *daf-2; aak(0)* mutants in a solution that contained RNA extracted from *daf-2* dauer larvae (see Materials and Methods). Surprisingly, this RNA was sufficient to suppress the post-dauer sterility of the AMPK mutants (Figure 2A), indicating that one or more RNA species in this mixture acts downstream of AMPK and was capable of restoring quiescence to the germline stem cells in the AMPK animals. Furthermore, this RNA-mediated suppression did not require the miRNAs *mir-1* and *mir-44*, both of which have been shown to regulate *tbc-7* activity during the dauer stage[4] (Figure 2A).

To examine if the suppression of the germline defects might act through an mRNA-based mechanism, we repeated the RNA soaking experiment, but prior to soaking, we separated the RNA mixture using oligo $d(T)_{25}$ beads to create one fraction with only mRNA and another that was poly(A) mRNA depleted (flowthrough). When the *daf-2; aak(0)* animals were incubated with the mRNA fraction, these animals remained post-dauer sterile (Figure 2B). However, when the *daf-2; aak(0)* mutants were incubated with the flowthrough fraction containing all small non-coding RNAs (Figure 2B), the animals were post-dauer fertile.

To further determine what type of RNA is responsible for the suppression of germline defects and consequent restoration of fertility, we separated the RNA mixture to create one fraction with RNAs larger than 200 nucleotides (>200 nts) and another with RNAs smaller than 200 nucleotides (<200 nts), then incubated each fraction with *daf-2; aak(0)* mutants and assessed their post-dauer fertility in each case. Remarkably, only when the *daf-2; aak(0)* mutants were incubated with the fraction containing the RNAs smaller than 200 nucleotides, could post-dauer fertility be restored (Figure 2C).

To further test what RNAs might be involved in the RNA-mediated restoration of germline competence, we digested the RNA extracts with RNase A. RNase A digests all RNA efficiently at 0 M NaCl, but at 0.3 M NaCl or higher, RNase A selectively digests single-stranded RNA, leaving double-stranded RNAs intact[34,35]. When *daf-2; aak(0)* mutants were incubated with RNA previously treated with RNase A without NaCl, the animals were completely sterile (Figure 2D). However, when the RNA solution was treated with RNase A in 0.5 M NaCl prior to incubation with *daf-2; aak(0)* mutants, the post-dauer sterility was completely suppressed (Figure 2D). These data suggest that the

rescuing component of our RNA solution was not mRNA, but was more likely a double-stranded RNA(s) that can be processed into small RNAs (less than 200 nucleotides). These would then be responsible for the maintenance of germ cell quiescence/integrity during the dauer stage.

Lastly, we wanted to examine if we could reproduce these results by soaking the *daf-2; aak(0)* mutants with RAB-7-containing exosomes that were isolated through immunoprecipitation. We determined the concentration of the exosomes using nanoparticle tracking analysis and incubated *daf-2; aak(0)* mutants with a range of concentrations previously shown to elicit a physiological effect[36]. When incubated with RAB-7-containing exosomes at a concentration of 10^7 vesicles/mL, we were able to restore fertility to the *daf-2; aak(0)* mutants (Figure 2E). To assess if the RNA cargo within these exosomes alone could suppress the germline defects, we purified the RNA contents from these exosomes and incubated the resulting RNA with *daf-2; aak(0)* mutants. Animals incubated with the exosomal RNA were post-dauer fertile compared to animals incubated with M9 buffer or *gfp* dsRNA produced through *in vitro* transcription (Figure 2F). These results indicate that these exosomes and their RNA contents are sufficient to preserve germ cell integrity during the dauer stage.

From these and other data, we know that small RNAs affect germline quiescence[3,4], but whether the role of small RNAs could be dependent on the release of neuronal exosomes has not been experimentally established. By performing directed or unbiased RNAi surveys in fertile AMPK mutant animals that have activated RAB-7 (*daf-2; aak(0); tbc-7)* and assessing the post-dauer fertility after treatment with dsRNA, we sought to identify components that are required for this process; gene products potentially

involved in a) the production and trafficking of the exosomal cargo, b) transporting the exosomes between tissues, and even c) effecting the chromatin changes in the germline stem cells.

DCR-1 is an endoribonuclease III-like enzyme that is essential for the production of all small RNAs, with the exception of piRNAs[37]. RNAi of *dcr-1* in *daf-2; aak(0); tbc-7* mutants resulted in post-dauer sterile animals (Figure 2G), indicating that it, and/or its small RNA products, are required for germline integrity (germline quiescence and post-dauer fertility) during this stage. We then performed RNAi to compromise each of the hingepin biosynthetic enzymes for every class of small RNAs that require *dcr-1* activity. From this analysis we noted that when the components required for miRNA biogenesis were disabled, the mutants became post-dauer sterile, while the loss of other factors required for siRNA production or function had no effect on post-dauer fertility (Figure 2G and S6A), suggesting that only miRNAs are involved in preserving germ cell integrity during or after the dauer stage. Since the entire miRNA repertoire is dramatically reduced in AMPK mutants[38], this would explain why the RNA extracts from these animals could not rescue the AMPK mutant defects following our soaking experiments (Figure 2A).

Because AMPK and TBC-7/RAB-7 function together in the neurons to regulate germline integrity during the dauer stage, we used a previously verified tissue-specific RNAi strategy to confirm where miRNA biogenesis is required to provide the pro-quiescent signal to the germline stem cells[4]. Our findings indicated that when miRNA biogenesis was compromised exclusively in the neurons, we reproduced the same post-dauer sterility described above, while disabling these same factors in the germ line had no effect (Figure 2H). These data are consistent with a model where miRNAs that are

produced in the neurons are responsible for the gene expression changes required in the germline stem cells downstream of RAB-7 activation.

Following the formation of a mature miRNA, multiple components are required to eventually bind to their mRNA targets and modify expression. Complete loss of many of these gene products result in lethality or dauer defective phenotypes, but hypomorphic RNAi, particularly when carried out in a tissue-specific manner, can reveal if indeed such components are necessary. Perhaps more importantly, it can inform us about where their function is required to preserve germline integrity over the course of the dauer stage. We therefore performed RNAi on the Argonautes and RISC components of every class of small RNAs that required DCR-1 activity in *daf-2; aak(0); tbc-7* mutants. Our whole animal RNA indicated that the loss of the miRNA Argonautes, ALG-1 and ALG-2, as well as some of the RISC components resulted in the loss of post-dauer fertility (Figure S6B). However, the loss of the 26G, 21U, and 22G Argonautes and RISC components had no effect on the post-dauer fertility of these animals (Figure S6C-E). We repeated this experiment, but this time using tissue-specific RNAi mutants. Both the loss of the miRNA Argonautes in the neurons, and alternatively, the loss of some of the other RISC components in the germ line, resulted in the loss of post-dauer fertility (Figure S6F and S6G).

Neuronal miRISC translocates to the germ line with RAB-7.

The neuronal exosomes could potentially transport pre-miRNAs, which would require assembly into a miRISC complex in the germ cells. Alternatively, the miRNAs could be expressed and pre-assembled with their cognate miRISC Argonaute proteins poised to act upon delivery. To distinguish between these possibilities, we expressed the

miRNA Argonautes ALG-1 and ALG-2 fused to mKate in the neurons and imaged the transgenic dauer larvae to assess whether the Argonautes remained within the neurons, or like the RAB-7-containing exosomes, they could be detected in both the neurons and in the germ cells. For both ALG-1 and ALG-2, fluorescent signal was detected in the germ cells of *daf-2* control and in the suppressed, fertile AMPK mutant (*daf-2; aak(0); tbc-7)* dauer larvae (Figure 3A, Figure S7A, S7C, and S7E), but not in the germ cells of AMPK mutant (*daf-2; aak(0)*) dauer larvae, or animals expressing neuronal mKate alone, thus exhibiting a similar expression pattern to GFP::RAB-7 (Figure S7B, S7D, and S7F). Furthermore, the localization of ALG-1/-2 mKate signal in the germ line was dependent on *rab-7*, although the mKate signal remained strong in the neurons of the *rab-7(RNAi)* animals (Figure 3B and 3C). Consistent with this observation, neuronal GFP::RAB-7 and mKate::ALG-1 localized to germ cells during the dauer stage. (Figure S7G). To ensure that this observation was not due to the extrachromosomal array-based expression of our transgene, we expressed a single-copy MosSCI insertion of our neuronal mKate::ALG-1 and then crossed these mutants with animals expressing a HIS-15::GFP germline marker and into our control dauer strain (*daf-2)*, the AMPK mutants (*daf-2; aak(0))*, and the fertile, suppressed AMPK mutant animals (*daf-2; aak(0); tbc-7)*. We then imaged the dauer larvae of each genotype and observed mKate signal in the germ cells of animals with single-copy insertions (Figure S7H-J), which yielded results that were essentially identical to our observations with the extrachromosomal transgenes.

If the Argonautes are complexed with their miRNA cargo within exosomes they should also purify with our exosome preparations. Western analysis indicated that ALG-1 was present in samples of purified exosomes (Figure 3D). Moreover, ALG-1 is

associated with its miRNA cargo on the interior of the exosome and not non-specifically bound to the exosomal outer surface. We were still able to detect ALG-1 following treatment of the exosomes with Proteinase K alone, indicating that the lipid bilayer of the exosome protects ALG-1 from proteolytic degradation. However, when the exosomes were treated with detergent, then with the protease, ALG-1 was no longer detectable (Figure 3E). This indicates that the solubilization of the exosomal membrane permitted Proteinase K to digest ALG-1 that was initially protected by the lipid barrier. These data suggest that ALG-1 is incorporated into the neuronal exosomes, potentially bound to its miRNA cargo, in a regulated manner. The miRISC complex is then released from the neurons within the RAB-7-containing vesicles; these entities home specifically to the gonad, where following internalization, the miRNAs can instruct the germline stem cells to execute quiescence in response to the environmental cues associated with dauer development.

Neuronal miRNAs require EXOmotifs to silence germline targets.

To evaluate if the neuronally-produced miRNAs could affect gene expression in the germ line through a RAB-7/exosome-dependent mechanism, we developed a miRNA activity sensor that would be responsive to neuronally-expressed miRNAs. We recently revealed that the levels of many miRNAs are dramatically decreased by the loss of AMPK[38]. Among them, *mir-51* seems to be among the most significantly affected[38]. However, when *mir-51* levels were increased in the neurons, post-dauer fertility was restored significantly (Figure 4A). This could be explained if *mir-51* was able to interact with its mRNA targets in the germ cells.

Using a fluorescent germline miRNA activity sensor created by driving HIS-15::GFP that contains three binding sites for *mir-51* in its 3'UTR (hereafter referred to as "sensor"), we tested whether the GFP (sensor) could be silenced in a *mir-51*-dependent manner (Figure 4B). In replete conditions, GFP was expressed at similar levels in the adult stage in both control animals (*daf-2*) and AMPK mutants (*daf-2; aak(0)*) mutants (Figure 4C-E). However, during the dauer stage, control *daf-2* animals silenced the sensor in the germ cells, while the expression of the sensor was unaffected in dauer larvae that lacked AMPK (Figure 4F-H). To show that this effect is specific to the activity of *mir-51*, we expressed *mir-51* exclusively in the neurons of *mir-51* deletion mutants and found that the transgenic mutant animals nevertheless silenced the sensor (Figure 4I-J and 4L). Next, we scrambled the *mir-51* seed sequences in the sensor of control *daf-2* animals, preventing *mir-51* from binding to the 3'UTR (Figure 4K and 4L) (see Methods and Materials). These sequence changes in the *mir-51* target site resulted in the full restoration of HIS-15::GFP expression in the germ cells (Figure 4K and 4L). Taken together, these data suggest that miRNAs, such as *mir-51*, that are expressed in the neurons, can silence germline mRNA targets that possess its target site, and that this regulation is both specific and AMPK-dependent during the dauer stage.

Because neuronally-expressed *mir-51* can act cell non-autonomously to silence germline targets and RAB-7-containing exosomes exit the neurons to ensure germline quiescence, it seemed plausible that these exosomes carry a miRNA cargo that provides a pro-quiescent signal to the germline stem cells in anticipation of the dauer stage. To determine if the silencing of the sensor we observed with *mir-51* involves the RAB-7-associated exosomes, we compromised the production of exosomes by RNAi and

compared the levels of the sensor with that of control animals. Inhibiting the production of exosomes by *rab-7* RNAi completely abrogated the silencing of the sensor by *mir-51*, while empty vector RNAi controls remained fully capable of silencing the GFP expression (Figure 4M-O). Therefore, the neuronal miRNA-dependent silencing of germline targets we observed in dauer larvae is entirely dependent on *rab-7*, most likely through its role in the formation of exosomes.

The loading of miRNA cargos into exosomes relies on a number of factors, including short nucleotide stretches called EXOmotifs that act as sorting sequences for miRNAs and determine whether the miRNA will be retained within the cell or packaged into exosomes[39]. Any disruption of these motifs results in the exclusion of the miRNA from exosomes[39]. *mir-51* possesses three of these motifs, consistent with its potential incorporation in RAB-7-associated exosomes. To examine if these EXOmotifs contribute to the sorting of neuronally-produced *mir-51* into exosomes to target the germ line, we expressed a *mir-51* variant with scrambled EXOmotifs in the neurons of animals that lack *mir-51* and assessed its ability to silence the sensor. *In silico* modeling predicts that scrambling of the EXOmotifs in *mir-51* would not affect its synthesis or secondary structure (Figure 5A-C), yet the scrambled mutant *mir-51* variant failed to silence the germline sensor (Figure 5D and 5E). Consistent with our imaging results, mutants with the scrambled EXOmotif *mir-51* variant could no longer suppress the post-dauer sterility (Figure 5F), suggesting that *mir-51* is likely to be sorted into exosomes through the recognition of its EXOmotifs in order to ultimately reach its germline targets.

To examine if the disruption of the EXOmotifs of *mir-51* affects its loading into the exosomes, we conducted qPCR using specialized TaqMan probes on whole animals and

exosomes purified through immunoprecipitation against HA::GFP::RAB-7 to quantify the levels of *mir-51* (Figure 5G). We detected *mir-51* in the whole animal RNA extracts and in exosomes purified from control dauer larvae that were deleted for endogenous *mir-51,* but expressed wild-type *mir-51* from a transgene that is driven exclusively in the neurons (Figure 5H). Next, we expressed a variant of *mir-51* with scrambled EXOmotifs using the same promoter in the neurons of the same dauer animals that lacked endogenous *mir-51*. We detected the scrambled EXOmotif variant of *mir-51* in the whole animal RNA extracts, however, we could not detect any *mir-51* in the purified exosomes extracted from these animals (Figure 5I). Furthermore, our probes are highly specific to their targets and there is little to no cross recognition between the miRNA substrates (wt *mir-51* and scrambled EXOmotif *mir-51*) (Figure 5J and 5K). This experiment therefore indicates that the EXOmotifs of *mir-51* are essential for the loading of the miRNA into the neuronal exosomes.

In addition to showing that a neuronally produced miRNA can regulate an artificially expressed germline sensor, we wanted to determine if the same miRNA expression could regulate the germline chromatin landscape and consequent change in gene expression previously shown to be misregulated in AMPK mutants. To show that these neuronally-derived exosomes play a role in regulating the germline gene expression program during the dauer stage, we first assessed the levels of chromatin marks in *daf-2; aak(0)* mutants expressing neuronal *mir-51*. In *daf-2; aak(0)* dauer larvae with no additional transgenes, the levels of all the chromatin marks we assessed were upregulated[3]. However, in *daf-2; aak(0)* mutants that express neuronal *mir-51*, the abundance of both activating and

repressive chromatin marks were partially restored to near wild-type levels (Figure 6A and 6B).

Since the aberrant chromatin landscape presumably contributes to the abnormal gene expression observed in AMPK mutant dauer larvae, we questioned whether the modifications that were observed downstream of *mir-51* expression were correlated with corrective changes in germline gene expression. We therefore performed RT-qPCR to quantify the levels of germline-expressed genes that are differentially expressed during the dauer stage in *daf-2; aak(0)* mutants as compared to *daf-2* mutants[3,40]. Our analysis revealed that the mRNA levels of these selected germline genes largely resemble those measured in *daf-2* mutants (Figure 6C), suggesting that the defects in germline gene expression typical of AMPK mutants that occur during the dauer stage can be corrected by expressing *mir-51* in the neurons.

The effect of *mir-51* expression likely impinges on one or more mRNA targets in the germ line. We identified at least 66 genes that are expressed in the germ cells and possess complementary sequences that could be bound by *mir-51* (or *mir-51* family members). If the effects of *mir-51* expression are being mediated by the downregulation of one or more of its mRNA targets, then the compromise of the predicted *mir-51* targets in the germ line could suppress the germline defects seen in AMPK mutant dauer animals. We therefore subjected each of the germline-expressed genes with *mir-51* binding sites in their 3'UTRs, as predicted by TargetScanWorm 6.2, to RNAi analysis and assessed their effect on the sterility that arises following dauer recovery. Of the 66 genes tested, RNAi of 9 genes could individually, partially suppress the post-dauer sterility (Table S2).

Altogether, our data suggest that miRNAs synthesized in the neurons, like *mir-51*, are incorporated into RAB-7 exosomes, likely through the presence of cis-acting EXOmotifs. As we have shown, *mir-51* affects its target mRNAs through its loading into exosomes and its eventual physical binding to its sites in the 3'UTR of its germline targets. However, we have shown that the expression of one miRNA such as *mir-51*, is sufficient to increase the expression of multiple miRNAs, including the *tbc-7* regulators *mir-1* and *mir-44*, and even other *mir-51* family members, by re-prioritizing DCR-1 activity to upregulate miRNA synthesis (Jurczak et al., 2023). Following their synthesis and loading into exosomes, the miRNA-containing vesicles are then released, and subsequently make their way to the germ line where they adjust gene expression to promote quiescence in the germline stem cells.

Small RNA regulators act at distinct stages.

In order to determine if additional known small RNA regulatory components might be involved in the transport of the exosomal miRNAs from the neurons to the germ line, we employed a hypomorphic RNAi strategy in *daf-2; aak(0); tbc-7* (AMPK mutant animals with active RAB-7) to survey the effects of compromising individual genes involved in dsRNA transport on post-dauer fertility. RNAi of *sid-3*, *sid-5*, and *rme-8* in these mutants reduced post-dauer fertility significantly, indicating that their effects are required for the appropriate changes in germline gene expression mediated by the RAB-7-associated exosomes (Figure 7A and 7B). SID-5 is a single-pass transmembrane RNA channel and has been shown to localize with endosomal components like RAB-7 and LMP-1, thus linking RNA mobility to vesicular transport[41]. RME-8 is a conserved protein required for

endocytosis, and similarly to SID-5, localizes to endosomal membranes[42]. Because SID-5 has been shown to function in a cell non-autonomous manner as a dsRNA exporter rather than importer[41], we examined in which tissues these RNA transport proteins could be required by using strains where RNAi activity is restricted to either the neurons or the germ line[41,42]. These RNAi experiments indicated that *sid-5* and *rme-8* are required exclusively in the neurons, consistent with their known roles in RNA export and endocytic maturation, respectively (Figure 7C).

On the other hand, the conserved non-receptor tyrosine kinase *sid-3,* was required in the germ line (Figure 7C). SID-3 is required for the efficient uptake of dsRNA in *C. elegans*[43], while its mammalian orthologue (ACK) was initially identified as a binding partner of Cdc42, a small GTPase that promotes endocytosis[44]. A kinase-dead SID-3 variant is unable to import dsRNA into *C. elegans* cells[43]. Therefore, to examine if the kinase domain of SID-3 is required for the maintenance of germ cell integrity, we expressed a kinase-dead variant of SID-3 in the *daf-2; aak(0); tbc-7* mutants[43]. Unlike animals with wild-type SID-3, the *daf-2; aak(0); tbc-7* mutants that expressed a kinase-dead SID-3 variant could no longer suppress the germline defects associated with a lack of AMPK signalling during the dauer stage or following recovery (Figure 7D and 7E). Moreover, mutants with compromised *sid-3* expression or a kinase-dead SID-3 variant blocked the miRNA-dependent silencing of the miRNA sensor in the germ cells (Figure 7F-H), similar to *daf-2; aak(0)* mutants.

Following the incorporation of the exosomes, the germ cells undergo a concerted cell cycle arrest associated with a general modification of the chromatin[3]. This invokes the possibility of an amplification mechanism, whereby the pro-quiescent instructions

conveyed by the miRNAs must be uniformly distributed throughout the entire germ line. The RNAi spreading defective (*rsd*) genes have been shown to regulate both the import of dsRNA into cells and the propagation of the small RNA-based signals[45,46]. *rsd-2* and *rsd-3* encode proteins that associate with intracellular trafficking components and endomembranes, where the loss of either one of these gene products results in silencing defects, not only in the tissue where the dsRNA is acting, but also in adjacent cells and tissues[46]. Consistent with their implication in this endosome-mediated process, the loss of *rsd-3* and *rsd-6* expression resulted in extensive post-dauer sterility, while further interrogation indicated that these two genes are only required in the germ line (Figure 7I and 7J). Like SID-3, RSD-3 has a conserved ENTH domain that is required for RNA import into somatic and germ cells[46], and although RSD-6 does not have an ENTH domain, it does possess a Tudor domain, which has known roles in transposon silencing through RNAi activity[45,47,48]. Therefore, like SID-3, RSD-3 and RSD-6 could be required for exosomal miRNA uptake and/or to propagate or amplify small RNA signals uniformly throughout the germ line. Nevertheless, following internalization of RAB-7 containing exosome, the contents of this vesicle, miRNA, and perhaps other constituents, will transmit a pro-quiescent signal that must be propagated throughout the entire germ line to adjust germline gene expression accordingly. This is essential to preserve germ cell integrity throughout the potentially lengthy energy stress associated with the dauer diapause.

Discussion

The emergence of exosomes as critical extracellular agents capable of delivering biologically relevant signalling molecules to target tissues has been fuelled by numerous studies in various models. Their purification and subsequent analysis have indicated that these vesicles carry a diverse macromolecular cargo that can include DNA, proteins, mRNA, miRNAs, and other RNA fragments[33,39,49]. Yet, despite the identification of these important molecules, the effects of releasing intracellular contents to neighbouring cells or tissues have yet to be fully elucidated due to the large heterogenicity of extracellular vesicles and their many biogenesis and loading pathways.

In *C. elegans*, double-stranded RNA produced in the neurons has been previously shown to enter the gonad to affect germline gene expression[50]. These double-stranded RNAs are likely processed into small RNAs and can presumably pair with matching complementary sequences in germ cells, that can lead to, at least in some cases, transgenerational gene silencing. Indeed, small RNAs present in neurons have been demonstrated to modify behaviour transgenerationally in an RDE-4/PACT-dependent manner[51], demonstrating how these small mobile RNAs move around the animal to direct various cellular processes. This is further demonstrated in animals that have no germ cells, yet they have an extended lifespan through increased DAF-16/FoxO activity in the intestine. This lifespan extension is entirely dependent on the activity of neuronal *mir-71*, thus revealing an RNA-mediated signalling network that exists between the neurons, the gut, and the germ line, which influences the lifespan of the entire organism[52]. But despite these demonstrations of how neurons and neuronal small RNAs can act to regulate changes in germline gene expression in *C. elegans*, a genetic, mechanistically defined

pathway that could account for this intertissue movement/communication has not yet been described.

Using an unbiased genetic approach, we have shown how the formation and release of RAB-7-containing exosomes from the neurons is required to signal non-autonomously to the *C. elegans* germ line (Figure 7K). These exosomes carry pro-quiescent instructions in the form of miRNAs that are required to adjust gene expression in the germline stem cells to block their cell divisions, while preparing the genome for an extended period of stress that would otherwise compromise reproductive fitness.

The extensive energy stress associated with starvation could presumably affect the levels of critical macromolecular building blocks, and/or the energy-dependent quality control mechanisms that monitor their synthesis in the germ cells. That the serotonergic neurons have evolved a role in adjusting germline gene expression in response to energy stress via AMPK activation is a particularly efficient means of protecting genome integrity in the "immortal" germ lineage. These neurons are highly sensitive to intracellular changes in energy levels, eliciting adaptive modifications to foraging behaviours to correct any perceived energy deficit[53].

Although the function of AMPK in this subclass of neurons has already been described for its role in behavioural modification in response to starvation[54], our data indicate that AMPK activation in the serotonergic neurons acts at multiple levels. In addition to its critical role in altering feeding strategies, its activation also initiates a specific trafficking process that culminates with the incorporation of not only *mir-51*, but a select group of miRNAs, among probably additional molecules, into RAB-7-associated exosomes earmarked for release and targeting to the germ line.

Using our miRNA sensor, we confirmed the importance of EXOmotifs in the packaging of miRNAs into exosomes, while also demonstrating that their expression in neurons results in the efficient silencing of their cognate transcripts in a distant tissue. Whether this requires nascent transcription of EXOmotif-harbouring miRNAs remains to be resolved, but either the expression or the selection of these transcripts is dependent on neuronal AMPK. Alternatively, perhaps all EXOmotif-containing miRNAs and their bound Argonautes are indiscriminately incorporated into the maturing neuronal exosomes. The exosomes would then carry a constant miRNA cargo, and following internalization, only relevant mRNA targets expressed in the target tissue would be affected. In this scenario, the AMPK-dependent activation of RAB-7 would be sufficient to initiate the process.

The molecular basis of the germline translocation of the exosomes and the role of the dsRNA transporter SID-3 in their internalization is still unclear. Nevertheless, our genetic analysis indicates that the miRNA-containing exosomes access the germline stem cells to effect changes in their gene expression. However, to ensure that all the germline stem cells respond uniformly, the miRNA signal must be amplified and spread throughout the entire germ line. This is not consistent with the current model of miRNA action, whereby miRNAs act stoichiometrically. It therefore invokes the possibility of an intermediate that is responsible for either amplifying or relaying the signal throughout the germ line.

The pro-quiescent function of these exosomes relies on RAB-7 to generate the appropriate vesicles, but other factors provide the navigational function responsible for germline homing. In the developmental context we describe here, the exosomes deliver

pro-quiescent instructions in the form of miRNAs to the germline stem cells, but it is unlikely that such an elaborate mechanism of cell non-autonomous regulation would be exclusive to the dauer stage. In *C. elegans*, the transfer of vesicles between organisms, rather than between different tissues of one animal to induce a physiological effect has been previously documented. Exosomes have been shown to regulate the formation of alae and the life span of adult animals[28,36], while extracellular vesicles containing RNA- and nucleotide-binding proteins can be transferred from males via the cilia of male-specific sensory neurons into hermaphrodites during mating[55]. It is not yet clear how these examples of exosome-mediated communication might be regulated, but at least some components of the pathways are likely conserved at the most fundamental level.

Moreover, some of the described transgenerational phenomena that implicate the neurons in the generation of a small RNA trigger could also function through exosome-mediated targeting to the germ line. However, once these small RNAs arrive at their destination, they must then affect specific modifications at the chromatin level, many of which are mediated by the nuclear Argonaute protein HRDE-1 in *C. elegans*[51]. Similarly, alterations in the chromatin landscape and the associated changes in gene expression observed in post-dauer adult animals might also be dependent on these neuronal exosomes[40]. It is therefore quite plausible that exosomal small RNAs could establish these epigenetic changes by altering the expression of the germline histone writers to not only maintain germ cell integrity, but also contribute to the altered gene expression observed in post-dauer animals.

The packaging of RNA into exosomes has more recently become a useful diagnostic tool due to their remarkable stability[56]. In addition, critical miRNAs have been

found in exosomes associated with breast cancer, leukemia, and endothelial cancer cell lines[57-59]. However, with the exception of a few cases, how or whether the presence of these RNAs contributes to the metastatic potential, or other features of the growing tumour, still remains to be established in most cases[60,61].

In other contexts, exosomal miRNAs have positive roles and are implicated in more healthy outcomes. Most notably, exosomal miR-126, which is secreted by cardiac fibroblasts, reduces the severity of myocardial ischemia reperfusion injury[62]. Indeed, since the first description of the effects of exosomal miRNAs, the potential therapeutic benefits of these miRNA carriers has expanded, improving the prognosis of multiple sclerosis and other central nervous system diseases[63,64].

By exploiting the EXOmotif-based incorporation of selected RNA molecules into these vesicles, virtually any miRNA, or potentially any RNA, may be internalized into these vectors for precise tissue-specific targeting. The key factors involved in directing these vesicles to desired tissue locations will ultimately come from purification and characterization of the neuronal exosome-associated constituents that are responsible for the navigator function. While understanding what gene products are involved and how the miRNA cargo is released from these exosomes following internalization may provide invaluable information to improve the development of effective RNA therapeutics.

Our work highlights the function of these neuronal exosomes in the epigenetic modification of germ cell gene expression. Although we did not demonstrate if or how these vesicles might contribute to any transgenerational epigenetic phenomena, past work has shown that neuron-specific small RNAs can communicate with the germ line to adaptively modify behaviours transgenerationally[51]. Curiously, in the late 19th century

Darwin proposed a role for "gemmules" in the transmission of heritable traits[65]. Our findings underscore a role for neuronal vesicles that bring about epigenetic change in the germ line to adapt gene expression to protect the reproductive competence of the germ cells. We do not yet know if these, or related vesicles, might also act as vectors to convey heritable epigenetic modifications, but if that bears true, Darwin's "gemmule" hypothesis may not have been so far removed from the actual mechanisms that drive these changes.

Acknowledgments: The Canadian Institutes of Health Research (Project Grant, CIHR PJT-180267) supported this work. We acknowledge the *Caenorhabditis elegans* Genetics Center (CGC) for providing *C. elegans* strains. We are grateful to Michael Strauss and the Facility for Electron Microscopy Research at McGill University for help with sample preparation and microscope operation. We thank Monique Zetka for providing the anti-HA antibody. We thank Abigail Gerhold for providing a strain containing a mCherry germline marker. We are also grateful to Shaolin Li and Ryan Dawson for technical assistance, Ehab Abouheif for discussion, and Chris Rocheleau and Artur Kania for their comments on the manuscript.

Author contributions: C.W. and R.R. conceptualized the study and designed the methodology. C.W. and E.M.J. conducted the investigation. C.W. analyzed the data. R.R. acquired the funding and supervised the study. C.W. and R.R. wrote the original draft. C.W., E.M.J., and R.R. reviewed and edited this manuscript.

Declaration of interests: The authors declare no competing interests.

Data and materials availability: All data are available in the main text or the supplementary materials.

Supplemental Information

Figure S1. Neuronal RAB-7 that localizes to the germ line during the dauer stage persists into the post-dauer germ line, Related to Figure 1.

Figure S2. The mechanism of neuron to germ line transfer of GFP::RAB-7 is conserved across different modes of dauer formation, Related to Figure 1.

Figure S3. GFP signal detected in the germ line is of neuronal origin, Related to Figure 1.

Figure S4. GFP signal detected in the germ line is dependent on exosome biogenesis and secretion, Related to Figure 1.

Figure S5. The localization of the RAB-7-associated exosomes to the germ line requires that they be formed in the neurons, Related to Figure 1.

Figure S6. Other classes of small RNAs are not required to maintain germ cell integrity in post-dauer AMPK mutants, Related to Figure 2.

Figure S7. Neuronally-expressed miRNA Argonautes are incorporated into exosomes in a RAB-7-dependent manner, Related to Figure 3.

Table S1. Quantification of relative fluorescence intensity of whole animal imaging, Related to Figure 1, 3, S1, S2, S3, S4, S5, S7.

Table S2. Post-dauer fertility of *daf-2; aak(0)* mutants fed with bacteria expressing dsRNA against *mir-51* targets, Related to Figure 6.

Table S3. Experimental Model: *Caenorhabditis elegans* Strains, Related to STAR Methods.

Table S4. Cloning and Construct Assembly Primers, Related to STAR Methods.

Table S5. RT-qPCR primers, Related to STAR Methods.

Figures

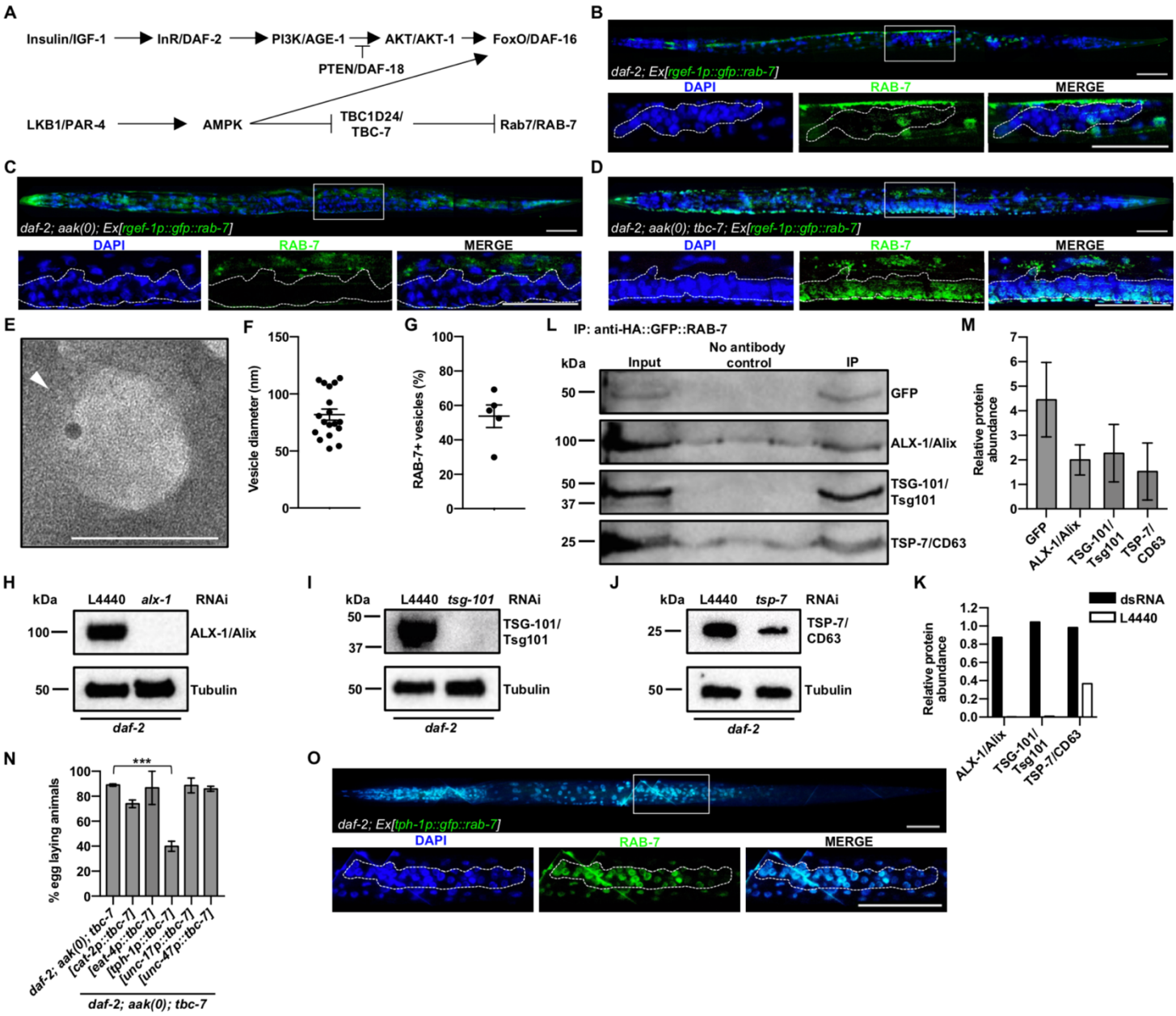

Figure 3.1. Neuronal RAB-7 is associated with exosomes that localize to the germ line during energy stress.

(A) Genetic pathway of insulin-like signalling and AMPK signalling with mammalian/*C. elegans* orthologues.

(B-D) Confocal images of neuronal GFP::RAB-7 expression in dauer larvae in (A) *daf-2*, (B) *daf-2; aak(0)*, and (C) *daf-2; aak(0); tbc-7* mutants.

(E) Negative stain TEM on isolated exosomes from *daf-2* mutants that express neuronal HA::RAB-7 with 6 nm immunogold against HA. White arrowhead indicates gold particle bound to exosome. White arrow indicates lipid bilayer. Scale bar, 50 nm. Representative of three independent exosome purifications.

(F) Vesicle diameter (nm) of purified vesicles containing HA::GFP::RAB-7 determined through Velox software (Thermo Scientific). Representative of three independent exosome purifications. n = 20 measurements.

(G) Percentage of vesicles with RAB-7 in a pan-exosome purification as determined by immunogold TEM analysis using anti-HA antibodies. Each percentage represents one biological replicate. For each replicate, 50-100 vesicles were quantified.

(H-J) Western analysis with (J) anti-Alix/ALX-1, (K) anti-Tsg101/TSG-101, and (L) anti-CD63/TSP-7 antibodies on animals fed with either L4440 empty vector control or dsRNA against (J) *alx-1*, (K) *tsg-101*, or (L) *tsp-7*, respectively.

(K) Levels of Alix/ALX-1, Tsg101/TSG-101, and CD63/TSP-7 were quantified and normalized to tubulin using ImageJ software.

(L) An immunoprecipitation using an anti-HA antibody to isolate HA::GFP::RAB-7 containing exosomes. Western analysis with anti-GFP, anti-ALX-1/Alix, anti-TSG-101/Tsg101, and anti-TSP-7/CD63 antibodies. The input is purified pan-exosomes from *daf-2* mutants expressing neuronal HA::GFP::RAB-7.

(M) Levels of GFP, ALX-1/Alix, TSG-101/Tsg101, and TSP-7/CD63 in the IP lane were quantified using ImageJ software and normalized to the input. Representative of three independent experiments.

(N) Post-dauer fertility of *daf-2; aak(0); tbc-7* mutants with wild-type *tbc-7* expressed in dopaminergic (*cat-2p*), glutaminergic (*eat-4p*), serotonergic (*tph-1p*), cholinergic (*unc-17p*), and GABAergic (*unc-47p*) neurons.

(O) Confocal images of GFP::RAB-7 expression in *daf-2* dauer larvae expressed in serotonergic neurons (*tph-1p*).

For (B-D, O), solid white frame indicates position of the higher magnification insets (below). Dotted white lines outline the gonad. Scale bars, 50 μm. Representative of three independently-generated transgenic lines. All images show anterior to the left; dorsal up.

For (N), data is mean ± SEM. ***P < 0.0001; Marascuilo procedure. n = 50 animals. Post-dauer fertility data are representative of three independent experiments. See also Figures S1, S2, S3, S4, and S5.

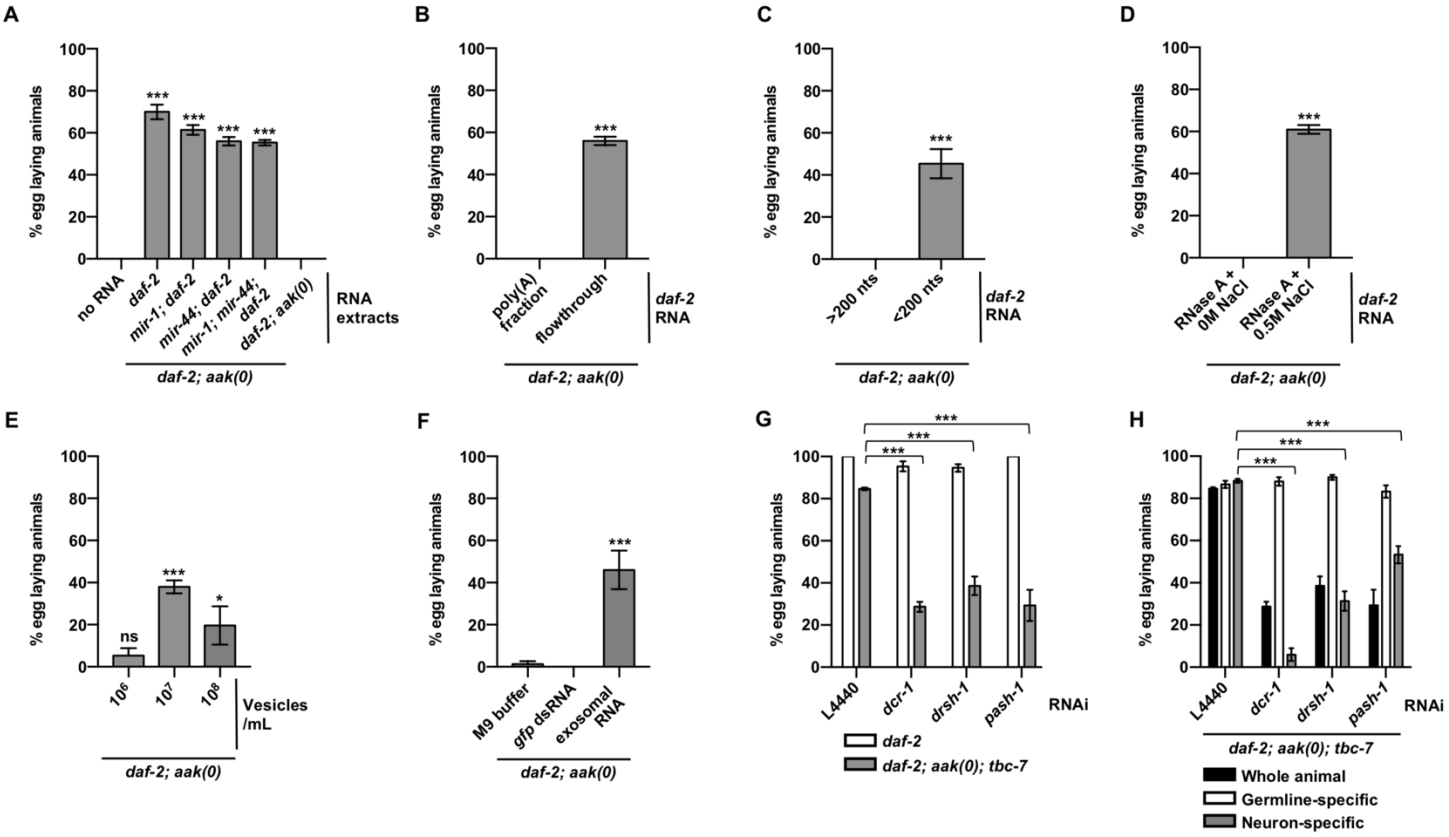

Figure 3.2. Neuronal miRNA synthesis is required to preserve germ cell integrity.

(A-C) Post-dauer fertility of *daf-2; aak(0)* mutants soaked in (A) RNA extracted from animals of indicated genotypes, (B) either the poly(A) fraction or a poly(A)-depleted fraction (flowthrough) of total RNA extracted from *daf-2* mutants, (C) fractions containing either RNAs larger than 200 nts (>200 nts) or less than 200 nts (<200 nts) extracted from *daf-2* mutants, and (D) RNA extracted from *daf-2* dauer larvae that were treated with RNase A in either 0 M or 0.5 M NaCl.

(E and F) Post-dauer fertility of *daf-2; aak(0)* mutants soaked in (E) isolated HA::GFP::RAB-7-containing exosomes and (F) RNA purified from HA::GFP::RAB-7-containing exosomes.

(G and H) Post-dauer fertility of *daf-2; aak(0); tbc-7* mutants fed with bacteria expressing dsRNA corresponding to components involved in miRNA biogenesis in (G) whole animal or (H) assessed using tissue-specific RNAi mutants.

For (A-H), data is mean ± SEM. ***P < 0.0001; *P < 0.01; ns, not significant; Marascuilo procedure. n = 50 animals. Post-dauer fertility data are representative of three independent experiments. See also Figure S6.

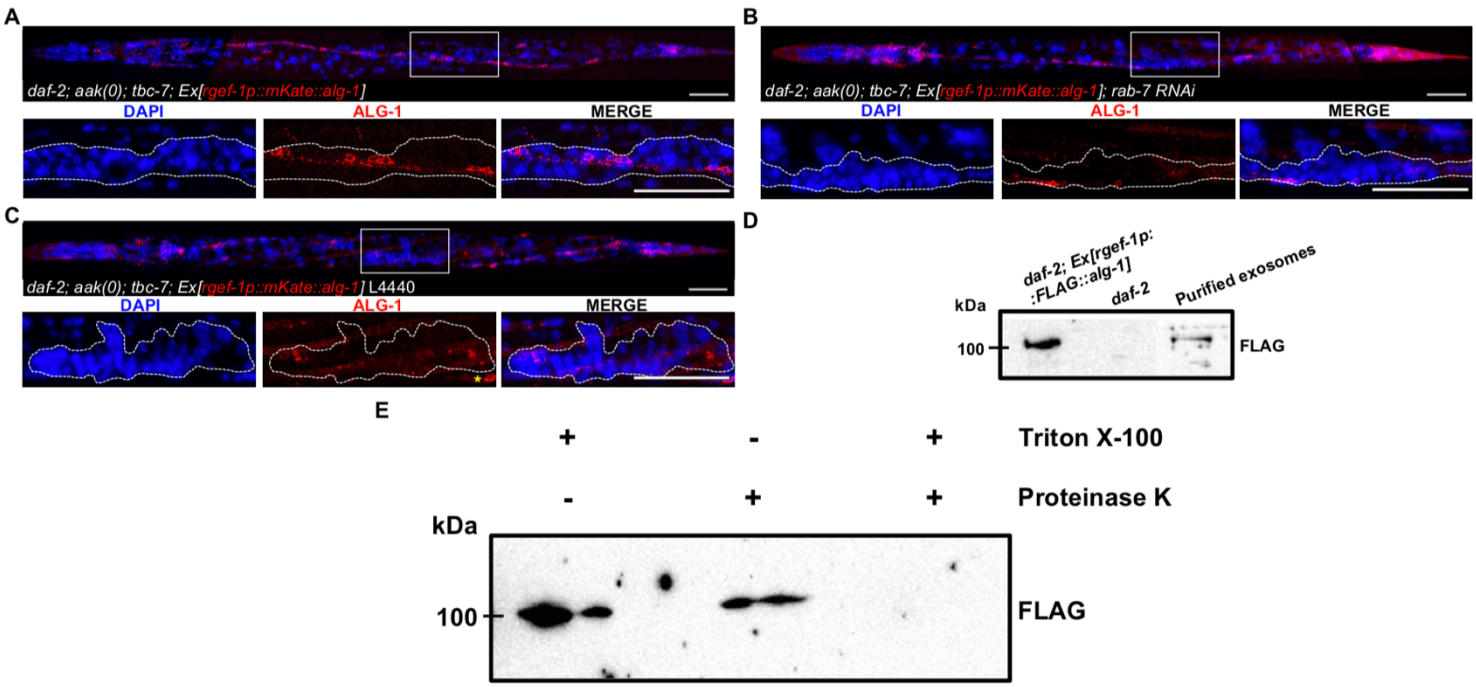

Figure 3.3. miRNA Argonautes are incorporated into neuron-derived exosomes and subsequently localize to the germ line.

(A) Confocal images of neuronal mKate::ALG-1 expression in *daf-2; aak(0); tbc-7* dauer larvae.

(B and C) Confocal images of neuronal mKate::ALG-1 expression in *daf-2; aak(0); tbc-7* dauer larvae fed with bacteria that express (B) empty vector L4440 or (C) dsRNA that corresponds to *rab-7*. Yellow asterisks indicate mKate signal from the nerve cord.

(D) Western analysis performed with anti-FLAG antibodies on exosomes isolated from mutants expressing neuronal FLAG::ALG-1. Western blots were spliced together due to differences in exposure times. Representative of two independent experiments.

(E) Western analysis performed with anti-FLAG antibodies on exosomes isolated from mutants expressing neuronal FLAG::ALG-1 that have been treated with either Triton X-100, Proteinase K, or both. Representative of two independent experiments.

For (A-C), solid white frame indicates position of the higher magnification insets (below). Dotted white lines outline the gonad. Scale bars, 50 μm. Representative of three independently generated transgenic lines. All images show anterior to the left; dorsal up. See also Figure S7.

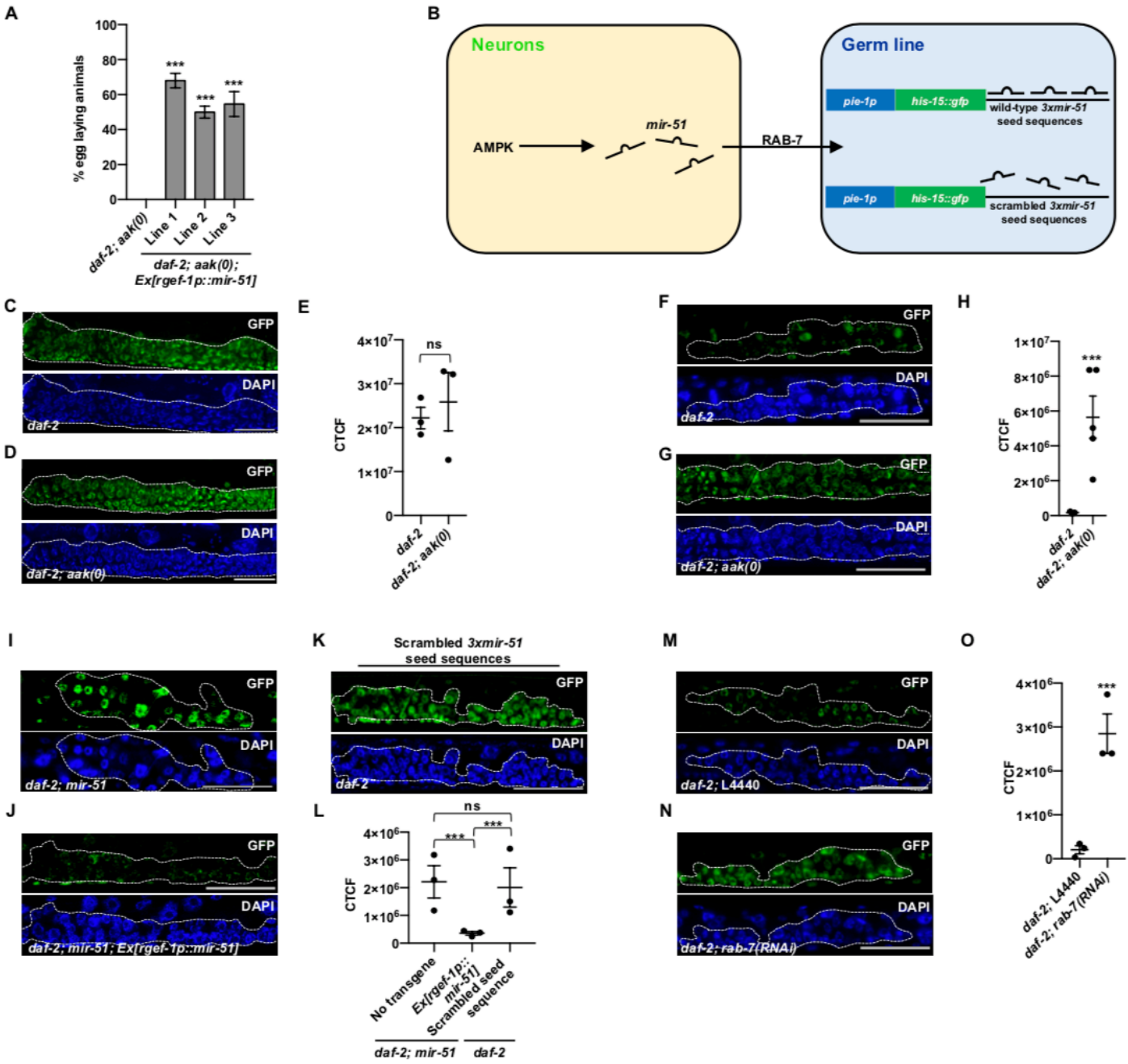

Figure 3.4. Neuronally-expressed miRNAs silence germ cell targets in a RAB-7-dependent manner.

(A) Post-dauer fertility of *daf-2; aak(0)* mutants expressing neuronal *mir-51*.

(B) Graphic description of the *mir-51*-specifc germline miRNA sensor.

(C and D) Confocal images of the miRNA sensor in (C) *daf-2* and (D) *daf-2; aak(0)* adult animals grown in replete conditions.

(E) Corrected total cell fluorescence (CTCF) of GFP intensity by genotype as described in C and D.

(F and G) Confocal images of the miRNA sensor containing three wild-type *mir-51* seed sequences in (F) *daf-2* and (G) *daf-2; aak(0)* dauer larvae.

(H) Corrected total cellular fluorescence (CTCF) of GFP intensity by genotype as described in F and G.

(I and J) Confocal images of the miRNA sensor containing three wild-type *mir-51* seed sequences in (I) *daf-2; mir-51* and (J) *daf-2; mir-51* that express a *mir-51* transgene driven by a pan-neuronal promoter (*rgef-1p::mir-51*) dauer larvae.

(K) Confocal image of the miRNA sensor containing three scrambled *mir-51* seed sequences in *daf-2* dauer larvae.

(L) Corrected total cellular fluorescence (CTCF) of GFP intensity by genotype as described in I, J, and K.

(M and N) Confocal images of the *mir-51*-specific miRNA sensor in *daf-2* dauer larvae fed with bacteria that express (M) empty vector L4440 or (N) dsRNA that corresponds to *rab-7*.

(O) Corrected total cell fluorescence (CTCF) of GFP intensity by genotype and RNAi condition as described in M and N.

For (A), data is mean ± SEM. ***P < 0.0001; ns, not significant; Marascuilo procedure. n = 50 animals. Post-dauer fertility data are representative of three independent experiments. For (C-D, F-G, I-J, K, M-N), dotted white lines outline the gonad. Scale bars, 50 μm. Representative of three independently-generated transgenic lines. For (E, H, L, O), data is mean ± SEM. ***P < 0.0001; Student's t-test. n = 3 trials.

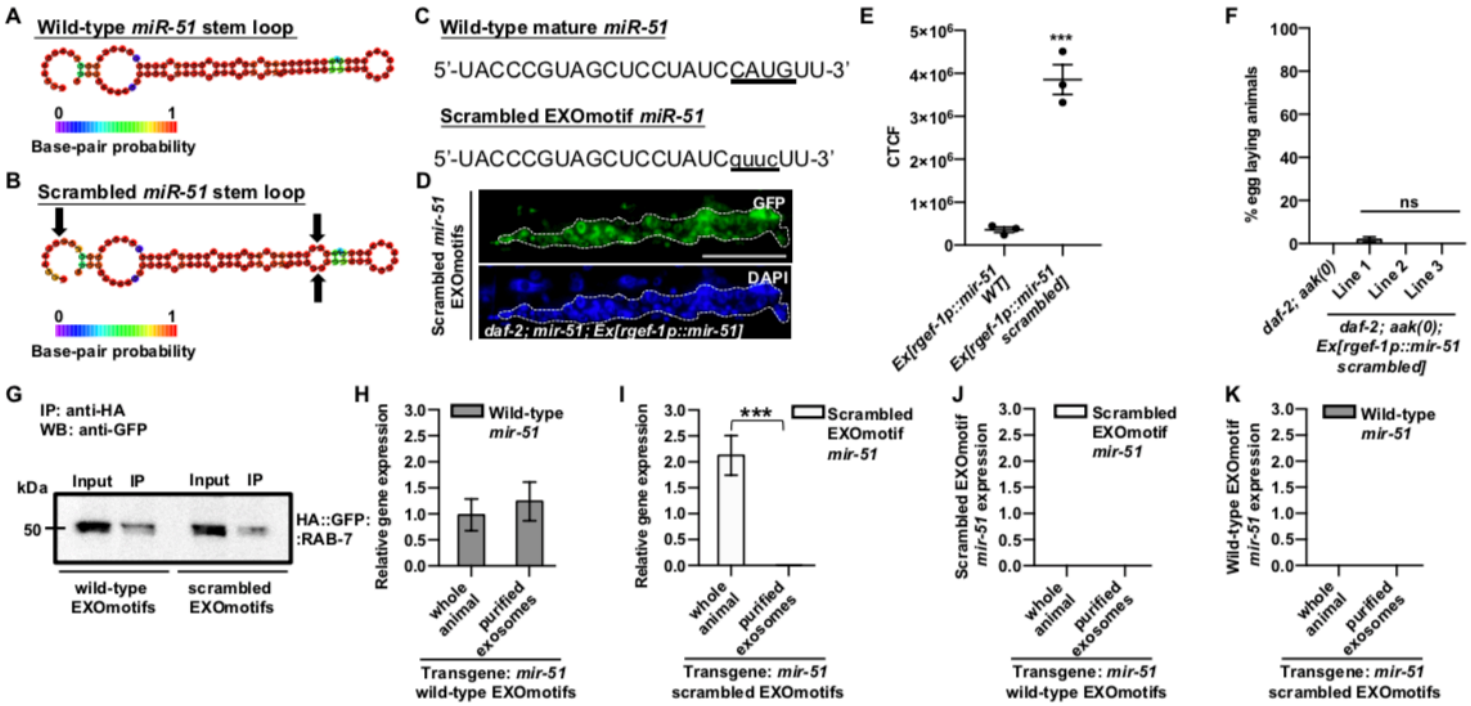

Figure 3.5. Neuronally-expressed miRNAs are loaded into exosomes through EXOmotifs to regulate germ cell integrity non-autonomously.

(A and B) Predicted structure for the hairpin miRNA for (A) wild-type or (B) EXOmotif scrambled *mir-51* by RNAfold Webserver software. Red or blue colouring indicate a high or low probability of pairing, respectively. Black arrows indicate the location of the mutated EXOmotif.

(C) The sequence of the wild-type and scrambled EXOmotif variants of mature *mir-51*.

(D) Confocal image of the miRNA sensor in *daf-2; mir-51* mutants expressing neuronal *mir-51* with three scrambled EXOmotifs.

(E) Corrected total cell fluorescence (CTCF) of GFP intensity by genotype.

(F) Post-dauer fertility of *daf-2; aak(0)* mutants expressing neuronal *mir-51* with scrambled EXOmotifs.

(G) Western analysis using anti-GFP antibodies on HA::GFP::RAB-7-containing exosomes purified from an immunoprecipitation using anti-HA antibodies conjugated with protein G beads to verify the specificity of the immunoprecipitation. The input is purified pan-exosomes from *daf-2* mutants expressing neuronal HA::GFP::RAB-7. Representative of three independent experiments.

(H) Relative gene expression of wild-type *mir-51* on whole animals and exosomes purified from *daf-2; mir-51* mutants expressing neuronal *mir-51* with wild-type EXOmotifs.

(I) Relative gene expression of scrambled EXOmotifs *mir-51* on whole animals and exosomes purified from *daf-2; mir-51* mutants expressing neuronal *mir-51* with scrambled EXOmotifs.

(J) Level of wild-type *mir-51* detected using a scrambled EXOmotif *mir-51* probe in whole animals and exosomes purified from *daf-2; mir-51* mutants expressing neuronal *mir-51* that possesses wild-type EXOmotifs.

(K) Level of scrambled EXOmotif *mir-51* detected using a wild-type *mir-51* EXOmotif probe in whole animals and exosomes purified from *daf-2; mir-51* mutants expressing neuronal *mir-51* with scrambled EXOmotifs.

For (D), dotted white lines outline the gonad. Scale bars, 50 μm. Representative of three independently-generated transgenic lines. For (F), data is mean ± SEM. ***P < 0.0001; ns, not significant; Marascuilo procedure. n = 50 animals. Post-dauer fertility data are representative of three independent experiments. For (H-K), Gene expression was normalized to the expression of *mir-235*. Data is mean ± SEM. ***P < 0.0001; two-way ANOVA. RT-qPCR data are representative of three independent experiments. For (E), data is mean ± SEM. ***P < 0.0001; Student's t-test. n = 3 trials.

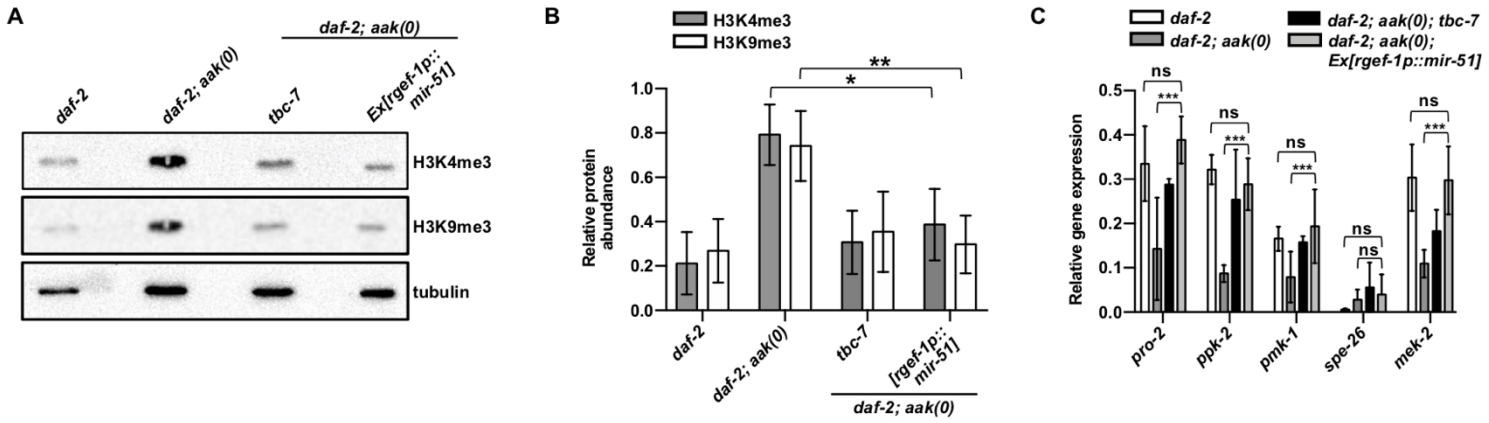

Figure 3.6. Neuronally-expressed miRNAs regulate germline gene expression and dauer-specific chromatin remodeling.

(A) Global levels of H3K4me3 and H3K9me3 were quantified by performing whole-animal western analysis on dauer larvae.

(B) Levels of chromatin marks were quantified and normalized to tubulin using ImageJ software. **P < 0.001, *P < 0.01 using Student's t-test. Representative of four independent experiments.

(C) RT-qPCR was conducted on *daf-2; aak(0); Ex[rgef-1p::mir-51]* mutants to quantify the levels of germline genes that were previously shown to be differentially expressed in the dauer stage. The expression between genotypes were normalized to *tba-1*. ***P < 0.001, ns, not significant using two-way ANOVA. Data is mean ± SEM. RT-qPCR data are representative of three independent experiments.

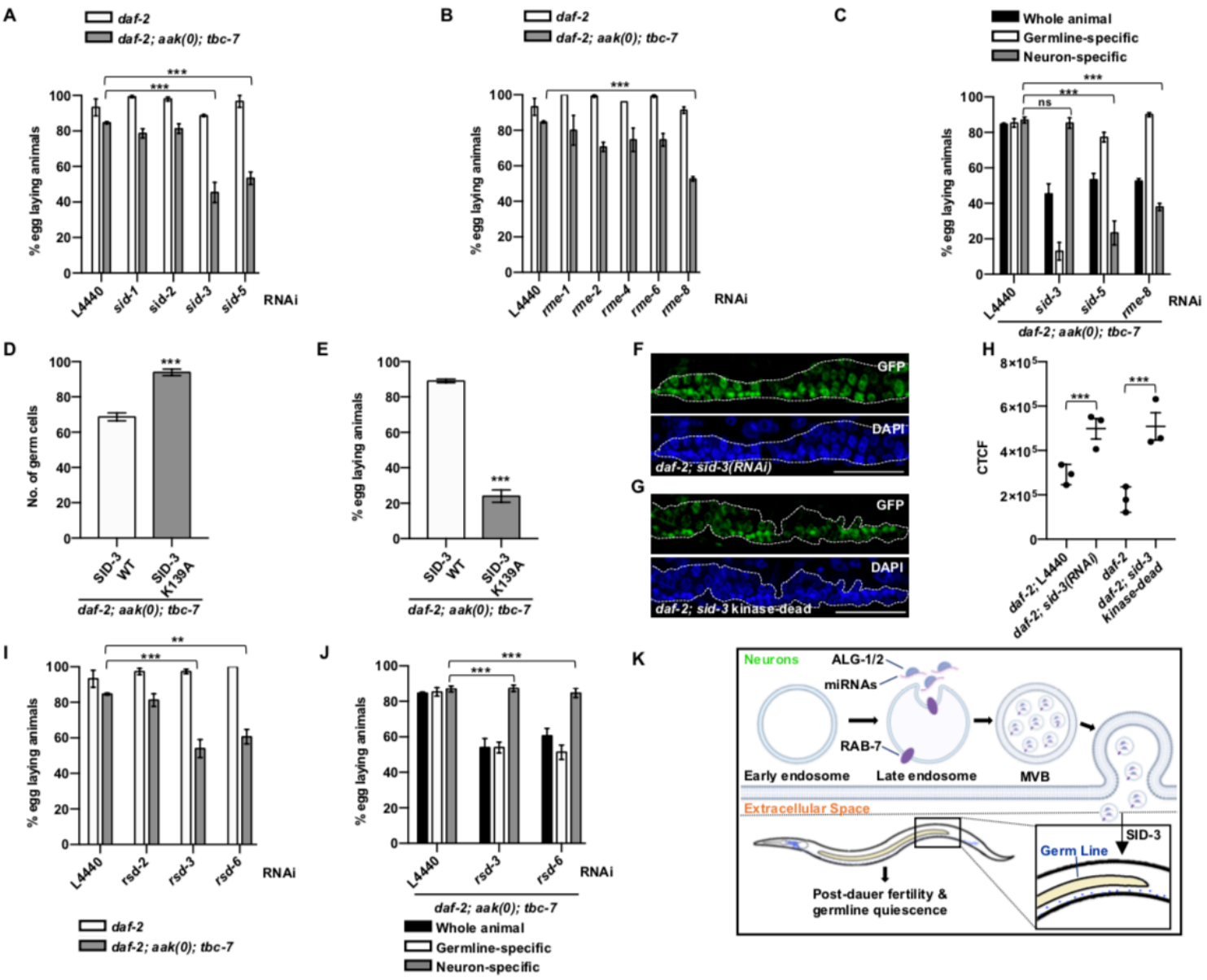

Figure 3.7. miRNA-containing exosomes require dsRNA transport proteins to efficiently transmit pro-quiescent signals to the germline stem cells.

(A-C) Post-dauer fertility of *daf-2; aak(0); tbc-7* mutants fed with bacteria expressing dsRNA that corresponds to various small RNA transporters in animals subjected to (A and B) whole animal RNAi or (C) tissue-specific RNAi.

(D and E) The (D) number of germ cell sin the dauer larvae and (E) post-dauer fertility of *daf-2; aak(0); tbc-7* mutants with a kinase-dead variant of SID-3.

(F and G) Confocal images of the miRNA sensor containing three wild-type *mir-51* seed sequences in *daf-2* dauer larvae (I) fed with bacteria expressing dsRNA that corresponds to *sid-3* or (J) with a CRISPR-engineered kinase-dead SID-3 K139A variant. Dotted white lines outline the gonad. Scale bars, 50 μm. Representative of three independently-generated transgenic lines.

(H) Corrected total cell fluorescence (CTCF) of GFP intensity by genotype.

(I and J) Post-dauer fertility of *daf-2; aak(0); tbc-7* mutants fed with bacteria expressing dsRNA that corresponds to RNAi spreading components in animals subjected to (I) whole animal RNAi or (J) tissue-specific RNAi.

(K) Proposed model of the secretion of neuronal exosomes containing miRNAs to protect germline integrity.

For (A-E, I-J), data is mean ± SEM. ***P < 0.0001; ns, not significant; Marascuilo procedure. n = 50 animals. For (H), data is mean ± SEM. ***P < 0.0001; one-way ANOVA. n = 25 animals. Post-dauer fertility and number of germ cells data is representative of three independent experiments. For (H), data is mean ± SEM. ***P < 0.0001; Student's t-test. n = 3 trials.

Supplementary Information

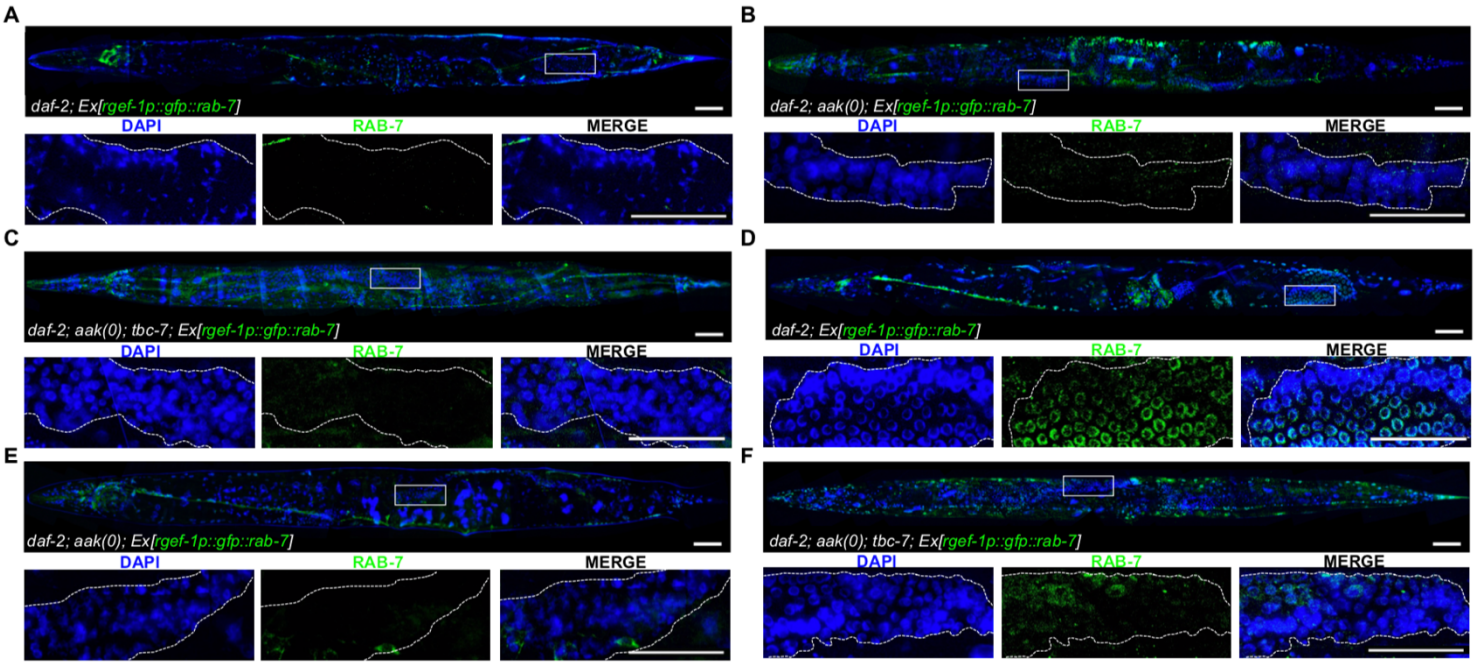

Figure S3.1. Neuronal RAB-7 that localizes to the germ line during the dauer stage persists into the post-dauer germ line, Related to Figure 1.

(A-C) Confocal images of neuronal GFP::RAB-7 expression in (A) *daf-2*, (B) *daf-2; aak(0)*, and (C) *daf-2; aak(0); tbc-7* adults that did not transit through the dauer stage.

(D-F) Confocal images of neuronal GFP::RAB-7 expression in post-dauer adults in (D) *daf-2*, (E) *daf-2; aak(0)*, and (F) *daf-2; aak(0); tbc-7* mutants.

For (A-F), solid white frame indicates position of the higher magnification insets (below). Dotted white lines outline the gonad. Scale bars, 50 μm. Representative of three independently generated transgenic lines. All images show anterior to the left; dorsal up.

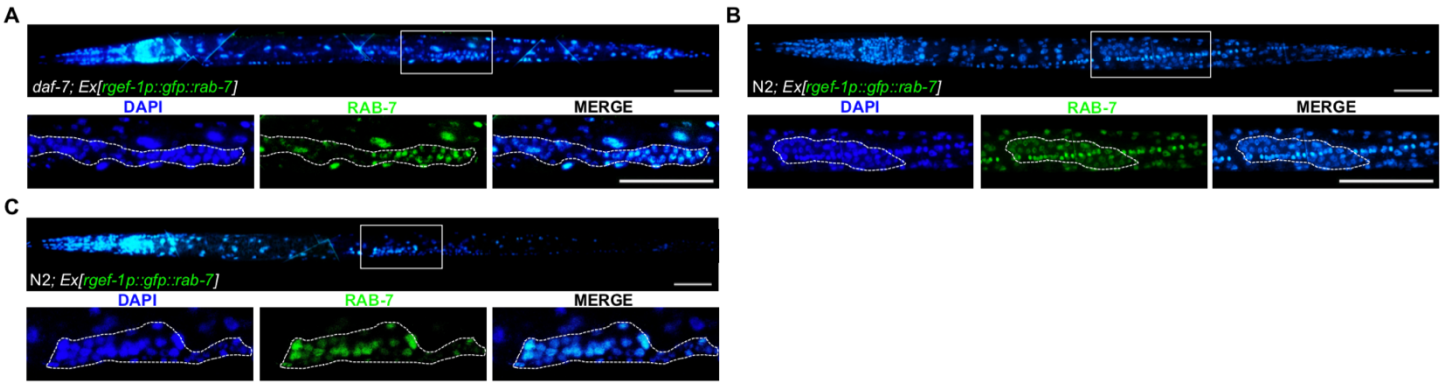

Figure S3.2. The mechanism of neuron to germ line transfer of GFP::RAB-7 is conserved across different modes of dauer formation, Related to Figure 1.

(A-C) Confocal images of neuronal GFP::RAB-7 expression in (A) *daf-7* mutants and wild type N2 dauer larvae induced through (B) dauer pheromone and (C) starvation. Solid white frame indicates position of the higher magnification insets (below). Dotted white lines outline the gonad. Scale bars, 50 μm. Representative of three independently-generated transgenic lines. All images show anterior to the left; dorsal up.

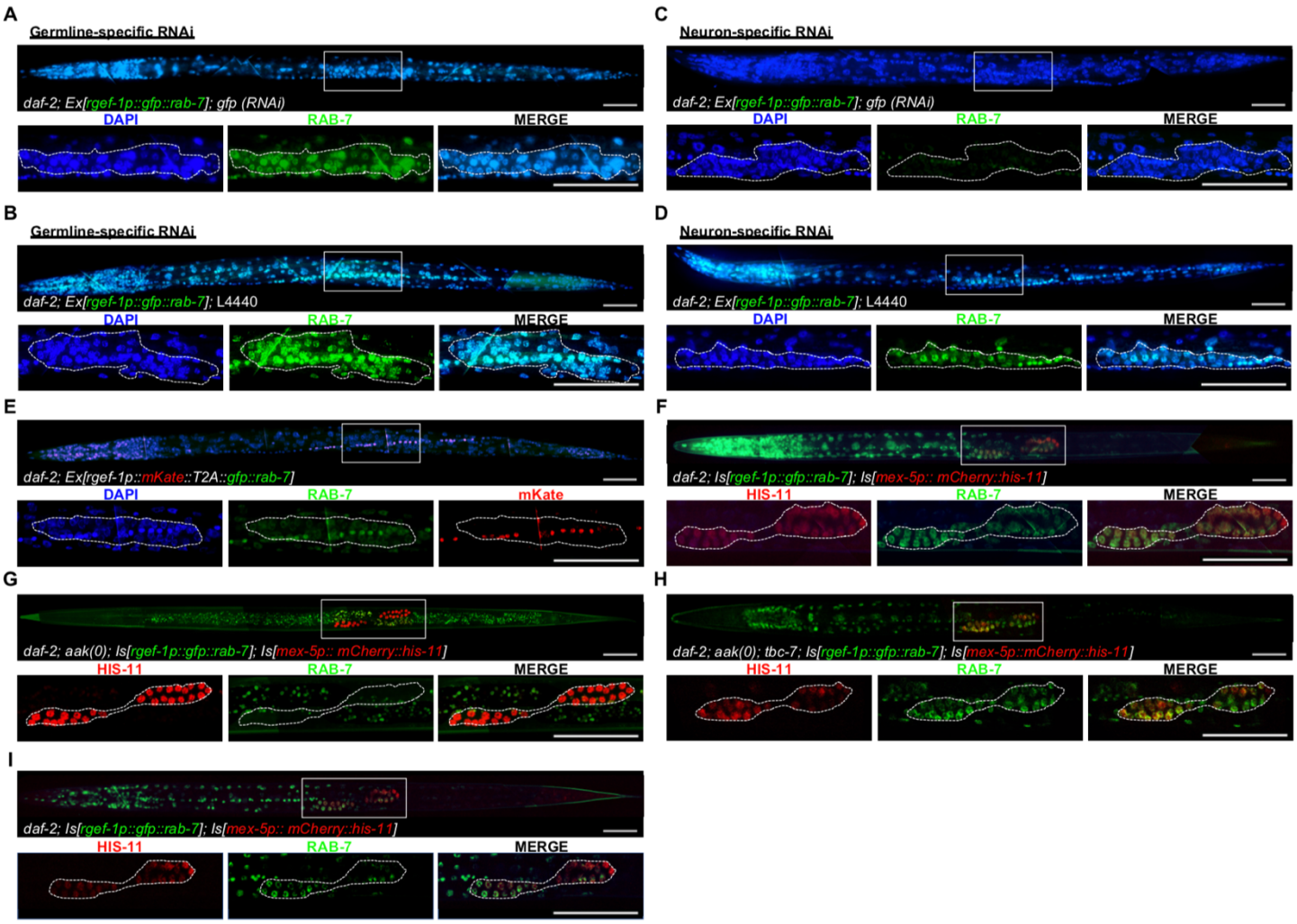

Figure S3.3. GFP signal detected in the germ line is of neuronal origin, Related to Figure 1.

(A and B) Confocal images of *daf-2* mutants with RNAi activity restricted to the germline tissue expressing neuronal GFP::RAB-7 fed with bacteria expressing (A) dsRNA against *gfp* or (B) control empty vector L4440.

(C and D) Confocal images of *daf-2* mutants with RNAi activity restricted to the neuronal tissue expressing neuronal GFP::RAB-7 fed with bacteria expressing (A) dsRNA against *gfp* or (B) control empty vector L4440.

(E) Confocal images of *daf-2* mutants expressing neuronal mKate::T2A::GFP::RAB-7.

(F-H) Confocal images of (F) *daf-2*, (G) *daf-2; aak(0)*, and (H) *daf-2; aak(0); tbc-7* mutants expressing a single-copy insertions of neuronal GFP::RAB-7 and germline mCherry::HIS-11.

(I) Single confocal slice of *daf-2* animals expressing a single-copy insertions of neuronal GFP::RAB-7 and germline mCherry::HIS-11.

For (A-I), solid white frame indicates position of the higher magnification insets (below). Dotted white lines outline the gonad. Scale bars, 50 μm. Representative of three independently-generated transgenic lines. All images show anterior to the left; dorsal up.

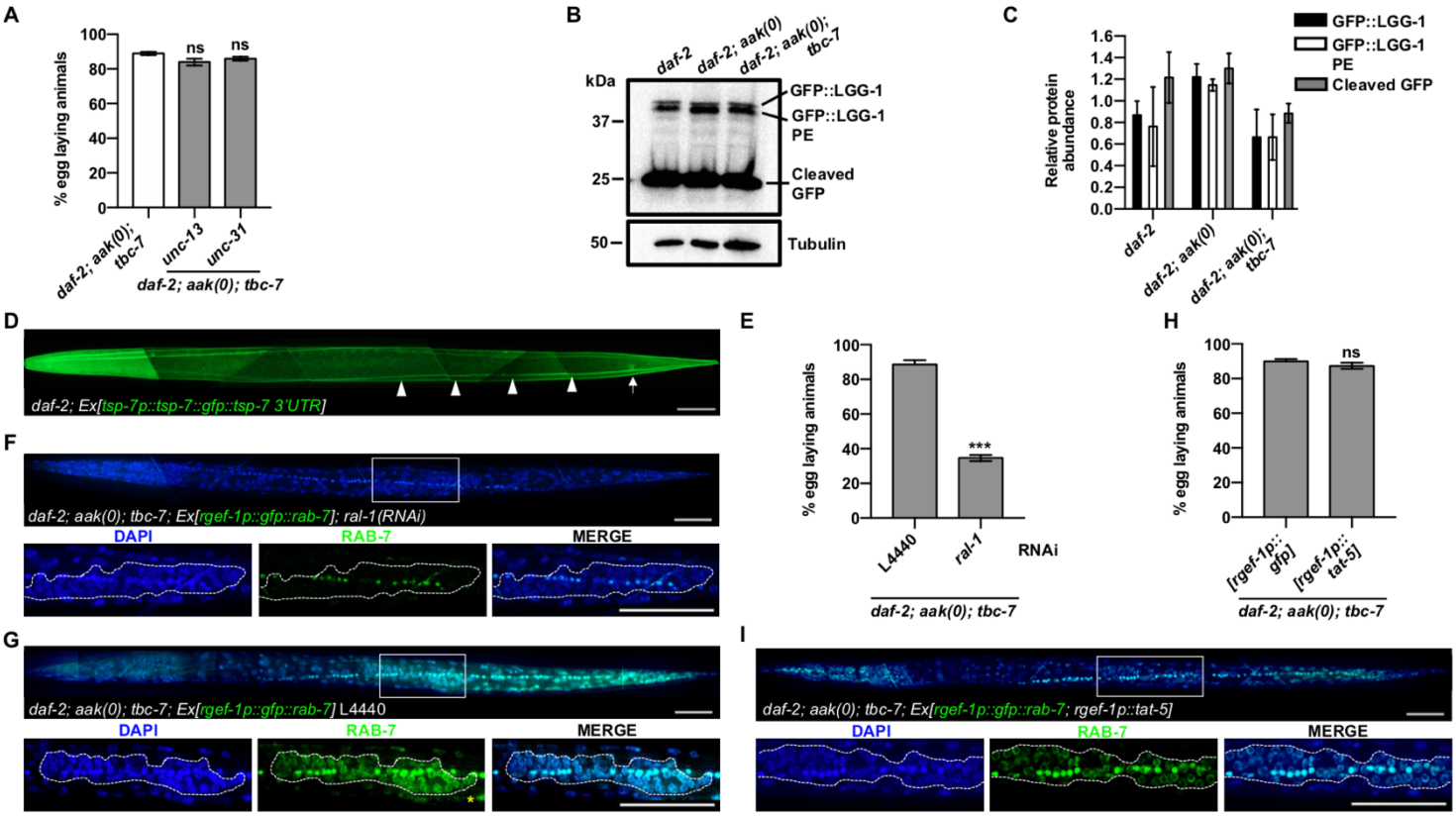

Figure S3.4. GFP signal detected in the germ line is dependent on exosome biogenesis and secretion, Related to Figure 1.

(A) Post-dauer fertility of *daf-2; aak(0); tbc-7* mutants that contain either a variant of *unc-13* (synaptic vesicle) with a premature stop codon or a deletion of *unc-31* (dense-core vesicle).

(B) Western analysis with anti-GFP antibodies on whole protein lysate of *daf-2*, *daf-2; aak(0)*, and *daf-2; aak(0); tbc-7* mutants expressing a GFP::LGG-1 transgene. The phosphatidylethanolamine (PE) conjugated LGG-1 variant and cleaved GFP are readouts of autophagic flux. Representative of two independent experiments.

(C) Levels of GFP::LGG-1, GFP::LGG-1 PE, and GFP were quantified and normalized to tubulin using ImageJ software. Representative of three independent experiments.

(D) Confocal images of TSP-7::GFP expression driven by the *tsp-7* promoter in dauer larvae. Arrowheads indicate the nerve chord. Arrow indicates the anus. Images show anterior to the left; dorsal up. Scale bar, 50 μm.

(E) Post-dauer fertility of *daf-2; aak(0); tbc-7* mutants fed with bacteria expressing dsRNA that corresponds to r*al-1*.

(F and G) Confocal images of neuronal GFP::RAB-7 expression in dauer larvae in *daf-2; aak(0); tbc-7* mutants fed with bacteria expressing (E) empty vector L4440 or (F) dsRNA that corresponds to *ral-1*. Yellow asterisks indicate GFP signal from the nerve cord.

(H) Post-dauer fertility of *daf-2; aak(0); tbc-7* mutants fed with bacteria expressing either neuronal GFP or TAT-5.

(I) Confocal images of neuronal GFP::RAB-7 expression in dauer larvae in *daf-2; aak(0); tbc-7* mutants expressing neuronal TAT-5.

For (A, E, H), data is mean ± SEM. ns, not significant; Marascuilo procedure. n = 50 animals. Post-dauer fertility data are representative of three independent experiments. For (F, G, I), solid white frame indicates position of the higher magnification insets (below).

Dotted white lines outline the gonad. Scale bars, 50 μm. Representative of three independently-generated transgenic lines.

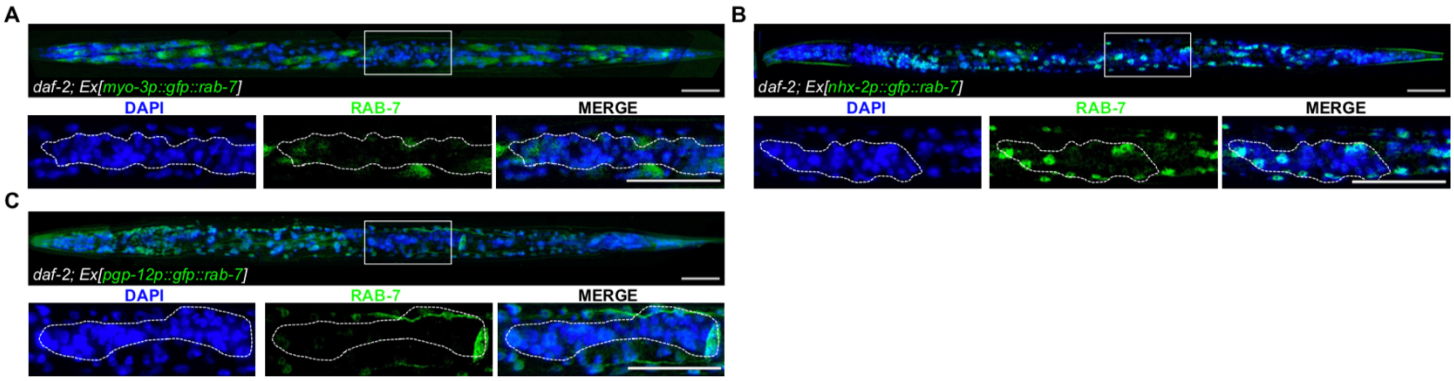

Figure S3.5. The localization of the RAB-7-associated exosomes to the germ line requires that they be formed in the neurons, Related to Figure 1.

(A-C) Confocal images of GFP::RAB-7 expression in dauer larvae expressed in the (A) muscle (*myo-3p*), (B) intestine (*nhx-2p*), or (C) the excretory system (*pgp-12p*). Solid white frame indicates position of the higher magnification insets (below). Dotted white lines outline the gonad. Scale bars, 50 μm. Representative of three independently generated transgenic lines. All images show anterior to the left; dorsal up.

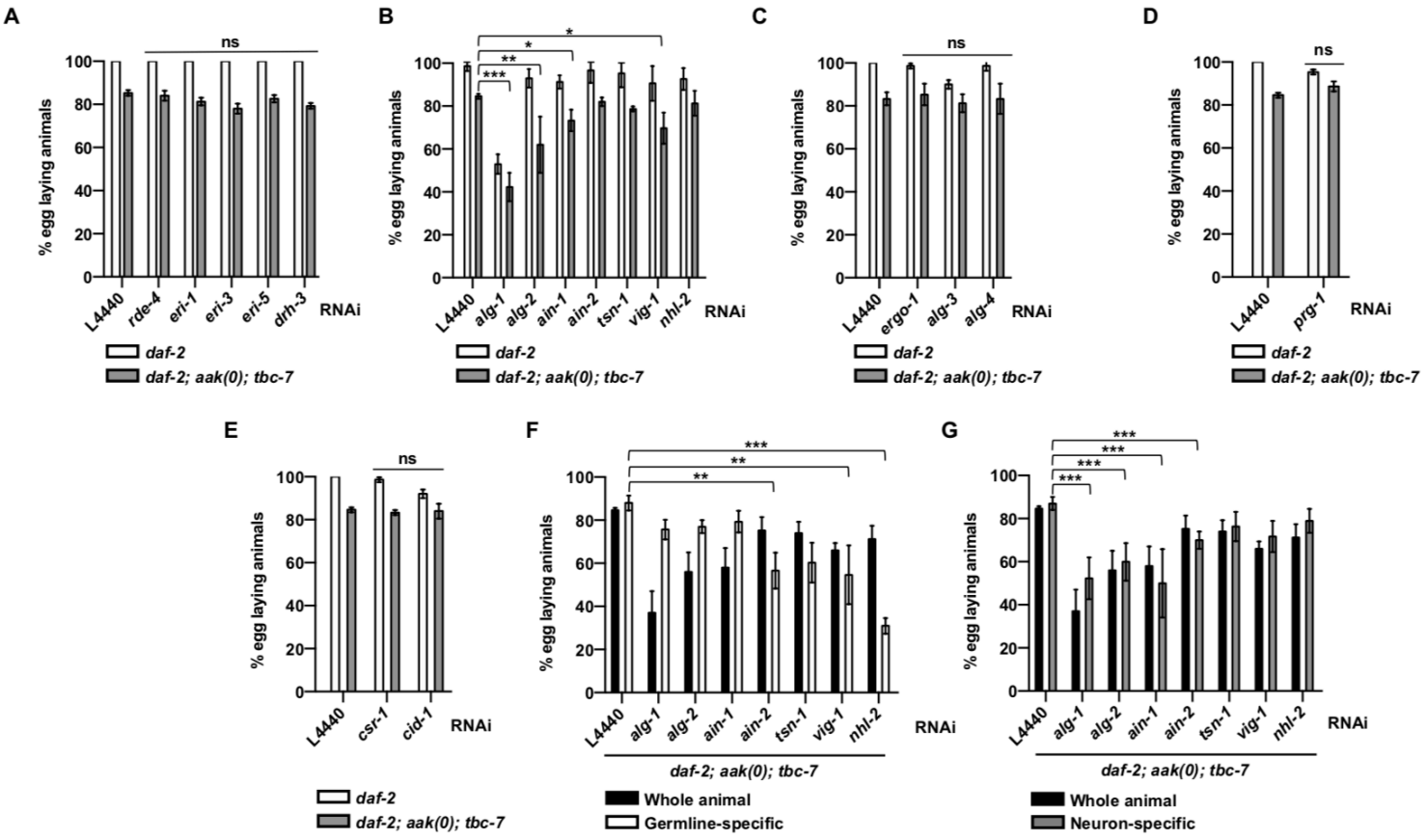

Figure S3.6. Other classes of small RNAs are not required to maintain germ cell integrity in post-dauer AMPK mutants, Related to Figure 2.

(A) Post-dauer fertility of *daf-2; aak(0)* mutants fed with bacteria expressing dsRNA that corresponds to components involved in siRNA biogenesis.

(B) Post-dauer fertility of *daf-2; aak(0); tbc-7* mutants fed with bacteria expressing dsRNA corresponding to miRISC components.

(C-E) Post-dauer fertility of *daf-2; aak(0); tbc-7* mutants fed with bacteria expressing dsRNA that corresponds to (C) 26G, (D) 21U, and (E) 22G Argonautes and RISC components.

(F and G) Post-dauer fertility of *daf-2; aak(0); tbc-7* mutants fed with bacteria expressing dsRNA that corresponds to miRISC components in (F) germline-specific or (G) neuron-specific RNAi mutants.

For (A-G), data is mean ± SEM. ***P < 0.0001; **P < 0.001; *P < 0.01; ns, not significant; Marascuilo procedure. n = 50 animals. Post-dauer fertility data are representative of three independent experiments.

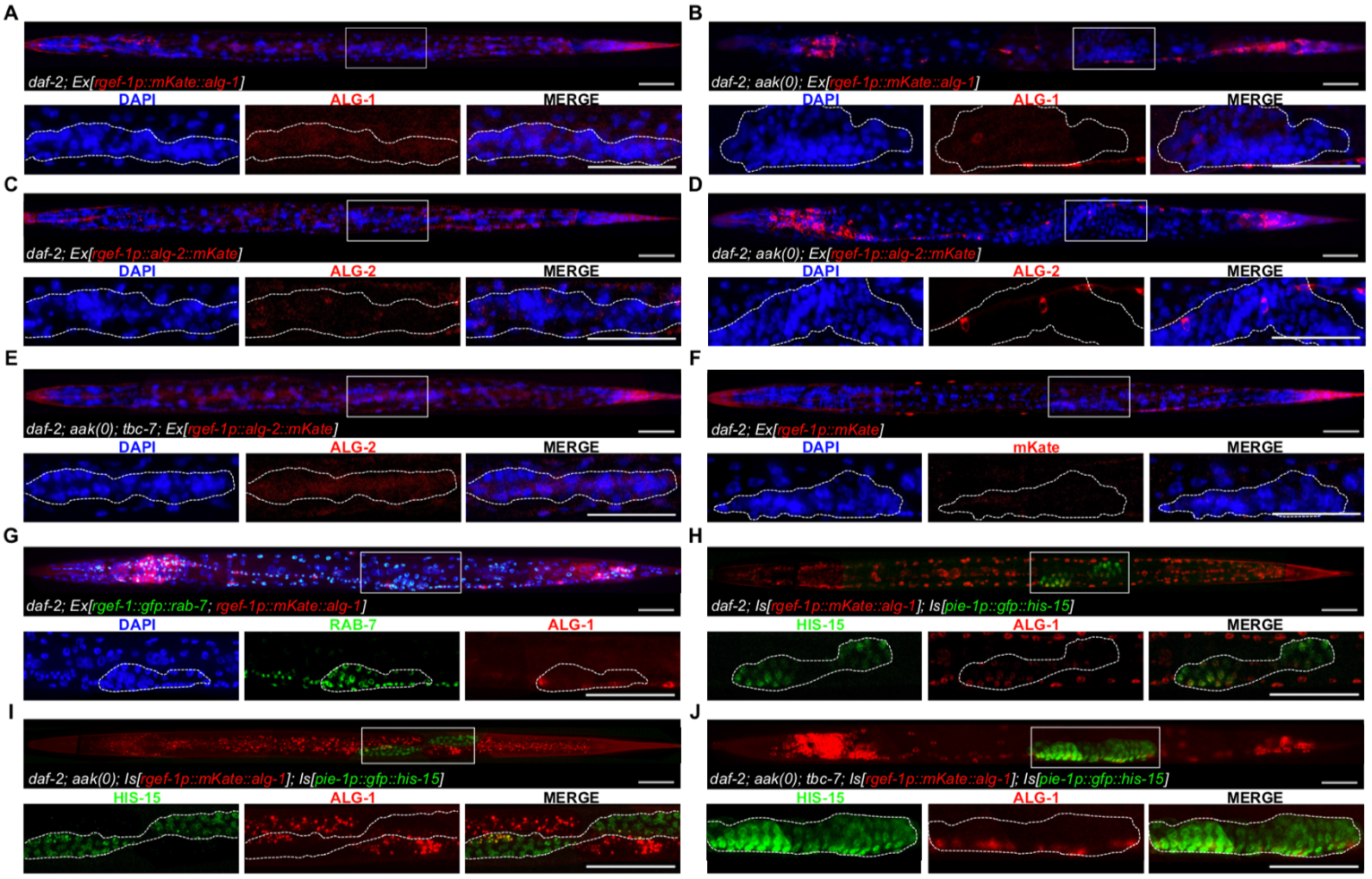

Figure S3.7. Neuronally-expressed miRNA Argonautes are incorporated into exosomes in a RAB-7-dependent manner, Related to Figure 3.

(A and B) Confocal images of neuronal mKate::ALG-1 expression in dauer larvae in (A) *daf-2* and (B) *daf-2; aak(0)* mutants.

(C and E) Confocal images of neuronal ALG-2::mKate expression in dauer larvae in (C) *daf-2*, (D) *daf-2; aak(0)*, and (E) *daf-2; aak(0); tbc-7* mutants.

(F) Confocal image of neuronal mKate expression in *daf-2* dauer larvae.

(G) Confocal images of neuronal mKate::ALG-1 and GFP::RAB-7 expression in dauer larvae in *daf-2* mutants.

(H-J) Confocal images of (H) *daf-2*, (I) *daf-2; aak(0)*, and (J) *daf-2; aak(0); tbc-7* mutants expressing a single-copy insertions of neuronal mKate::ALG-1 and germline HIS-15::GFP.

For (A-J), solid white frame indicates position of the higher magnification insets (below). Dotted white lines outline the gonad. Scale bars, 50 μm. Representative of three independently-generated transgenic lines. All images show anterior to the left; dorsal up.

	Replicate 1	Replicate 2	Replicate 2	Average CTCF
Figure 1B: *daf-2; Ex[rgef-1p::gfp::rab-7]*	14106.544	12112.461	13729.404	13316.136
Figure 1C: *daf-2; aak(0); Ex[rgef-1p::gfp::rab-7]*	631.596	771.840	565.800	656.412
Figure 1D: *daf-2; aak(0); tbc-7; Ex[rgef-1p::gfp::rab-7]*	15307.524	16187.969	13020.930	14838.808
Figure 1O: *daf-2; Ex[tph-1p::gfp::rab-7]*	12060.030	21123.940	20081.831	17755.267
Figure 1P: *daf-2; Ex[HSN-specific tph-1p::gfp::rab-7]*	13239.336	12458.916	11703.600	12467.284
Figure 1Q: *daf-2; Ex[ADF-specific srh-142p::gfp::rab-7]*	1726.686	829.274	980.934	1178.965
Figure 1R: *daf-2; Ex[NSM-specific tph-1p::gfp::rab-7]*	1815.933	1097.980	1174.242	1362.718
Figure 3A: *daf-2; aak(0); tbc-7; Ex[rgef-1p::mKate::alg-1]*	7077.636	10469.443	9128.259	8891.779
Figure 3B: *daf-2; aak(0); tbc-7; Ex[rgef-1p::mKate::alg-1] rab-7 RNAi*	1999.242	1399.380	1476.445	1625.022
Figure 3C: *daf-2; aak(0); tbc-7; Ex[rgef-1p::mKate::alg-1] L4440*	13931.631	12658.217	16657.900	14415.916
Figure S1A: *daf-2; Ex[rgef-1p::gfp::rab-7]*	575.691	1052.880	897.894	842.155
Figure S1B: *daf-2; aak(0); Ex[rgef-1p::gfp::rab-7]*	850.374	1257.036	1045.862	1051.091
Figure S1C: *daf-2; aak(0); tbc-7; Ex[rgef-1p::gfp::rab-7]*	894.325	578.208	648.327	706.953
Figure S1D: *daf-2; Ex[rgef-1p::gfp::rab-7]*	8894.028	8899.744	9781.672	9191.815
Figure S1E: *daf-2; aak(0); Ex[rgef-1p::gfp::rab-7]*	799.480	852.297	1367.100	1006.292

Figure S1F: *daf-2; aak(0); tbc-7; Ex[rgef-1p::gfp::rab-7]*	9267.750	11157.102	12220.095	10881.649
Figure S2A: *daf-7; Ex[rgef-1p::gfp::rab-7]*	15004.080	14820.000	16594.981	15473.020
Figure S2B: *N2; Ex[rgef-1p::gfp::rab-7]*	9155.295	11281.633	10344.418	10260.449
Figure S2C: *N2; Ex[rgef-1p::gfp::rab-7]*	6966.081	7710.469	7250.551	7309.034
Figure S3F: *daf-2; aak(0); tbc-7; Ex[rgef-1p::gfp::rab-7]; ral-1(RNAi)*	2693.347	1080.802	1758.336	1844.162
Figure S3G: *daf-2; aak(0); tbc-7; Ex[rgef-1p::gfp::rab-7] L4440*	19389.286	17283.074	20903.600	19191.987
Figure S3I: *daf-2; aak(0); tbc-7; Ex[rgef-1p::gfp::rab-7; rgef-1p::tat-5]*	7151.904	12466.124	12703.608	10773.879
Figure S4A: *daf-2; Ex[rgef-1p::gfp::rab-7]; gfp (RNAi)*	15789.627	16023.968	13618.098	15143.898
Figure S4B: *daf-2; Ex[rgef-1p::gfp::rab-7] L4440*	24287.725	20016.773	21038.997	21781.165
Figure S4C: *daf-2; Ex[rgef-1p::gfp::rab-7]; gfp (RNAi)*	5539.380	4261.509	3971.844	4590.911
Figure S4D: *daf-2; Ex[rgef-1p::gfp::rab-7] L4440*	17763.320	13639.507	17355.905	16252.911
Figure S4E GFP: *daf-2; Ex[rgef-1p::mKate::T2A::gfp::rab-7]*	17987.050	23855.196	19626.488	20489.578
Figure S4E mKate: *daf-2; Ex[rgef-1p::mKate::T2A::gfp::rab-7]*	3546.004	4741.130	6174.630	4820.588
Figure S4F: *daf-2; Is[rgef-1p::gfp::rab-7];*	8437.580	10444.698	12323.608	10401.962

Is[mex-5p::mCherry::his-11]				
Figure S4G: *daf-2; aak(0); Is[rgef-1p::gfp::rab-7]; Is[mex-5p::mCherry::his-11]*	354.393	592.050	1733.050	893.164
Figure S4H: *daf-2; aak(0); tbc-7; Is[rgef-1p::gfp::rab-7]; Is[mex-5p::mCherry::his-11]*	7031.114	9193.758	10676.787	8967.220
Figure S4I: *daf-2; Is[rgef-1p::gfp::rab-7]; Is[mex-5p::mCherry::his-11]*	4491.645	6879.399	10584.336	7318.460
Figure S4J: *daf-2; aak(0); Is[rgef-1p::gfp::rab-7]; Is[mex-5p::mCherry::his-11]*	1006.572	714.025	1501.920	1074.172
Figure S4K: *daf-2; aak(0); tbc-7; Is[rgef-1p::gfp::rab-7]; Is[mex-5p::mCherry::his-11]*	9836.865	7571.320	9772.020	9060.068
Figure S5A: *daf-2; Ex[myo-3p::gfp::rab-7]*	2657.635	2559.774	3106.224	2774.544
Figure S5B: *daf-2; Ex[nhx-2p::gfp::rab-7]*	1520.820	3092.250	2405.760	2339.610
Figure S5C: *daf-2; Ex[pgp-12p::gfp::rab-7]*	521.541	1087.427	1175.034	928.001
Figure S7A: *daf-2; Ex[rgef-1p::mKate::alg-1]*	12309.920	17797.481	11927.332	14011.578
Figure S7B: *daf-2; aak(0); Ex[rgef-1p::mKate::alg-1]*	821.100	858.990	977.784	885.958
Figure S7C: *daf-2; Ex[rgef-1p::alg-2::mKate]*	3718.554	5680.128	5277.480	4892.054
Figure S7D: *daf-2; aak(0); Ex[rgef-1p::alg-2::mKate]*	513.672	617.140	909.013	679.942
Figure S7E: *daf-2; aak(0); tbc-7 Ex[rgef-1p::alg-2::mKate]*	4729.760	4520.323	3243.295	4164.459
Figure S7F: *daf-2; Ex[rgef-1p::mKate]*	379.260	892.944	800.130	690.778

Figure S7G GFP: *daf-2; Ex[rgef-1p::gfp::rab-7; rgef-1p::mKate::alg-1]*	4068.098	3015.000	2582.566	3221.888
Figure S7G mKate: *daf-2; Ex[rgef-1p::gfp::rab-7; rgef-1p::mKate::alg-1]*	3840.515	3939.585	6352.840	4710.980
Figure S7H: *daf-2; Is[rgef-1p::mKate::alg-1]; Is[pie-1p::gfp::his-15]*	5895.345	8291.924	3398.367	5861.879
Figure S7I: *daf-2; aak(0); Is[rgef-1p::mKate::alg-1]; Is[pie-1p::gfp::his-15]*	941.528	1075.200	298.240	771.656
Figure S7J: *daf-2; aak(0); tbc-7; Is[rgef-1p::mKate::alg-1]; Is[pie-1p::gfp::his-15]*	6090.165	9611.016	5538.962	7080.048
Figure S7K: *daf-2; Is[rgef-1p::mKate::alg-1]; Is[pie-1p::gfp::his-15]*	12747.11	10174.4	9587.736	10836.413
Figure S7L: *daf-2; aak(0); Is[rgef-1p::mKate::alg-1]; Is[pie-1p::gfp::his-15]*	856.904	551.169	801.572	736.548
Figure S7M: *daf-2; aak(0); tbc-7; Is[rgef-1p::mKate::alg-1]; Is[pie-1p::gfp::his-15]*	16597.28	9301.356	14761.44	13553.359

Table S1: Quantification of relative fluorescence intensity of whole animal imaging, Related to Figure 1, 3, S1, S2, S3, S4, S5, S7.

Gene Target	Post-dauer fertility of *daf-2; aak(0)* mutants	Statistical Testing
L4440	0%	N/A
D2023.1	30%	*
zyg-11	26%	*
egg-6	26%	*
trpp-8	20%	*
catp-5	20%	*
mtm-6	20%	*
dmsr-4	18%	*
T07F12.2	18%	*
miga-1	18%	*
vang-1	16%	ns
F45D3.3	16%	ns
ptr-6	14%	ns
M01B12.4	12%	ns
hst-1	10%	ns
ptp-3	10%	ns
B0261.1	0	ns
F31C3.3	0	ns
pct-1	0	ns
ptr-18	0	ns
F41C3.2	0	ns
F45D3.4	0	ns
dph-3	0	ns
gly-20	0	ns
K08E4.3	0	ns
ddl-1	0	ns
klp-7	0	ns
oops-1	0	ns
ttc-17	0	ns
F11E6.3	0	ns
cpna-3	0	ns
lin-26	0	ns
hst-6	0	ns
ncx-6	0	ns
cnep-1	0	ns
skn-1	0	ns
srgp-1	0	ns
imph-1	0	ns
tin-44	0	ns
dcn-1	0	ns

B0393.5	0	ns
C04E6.11	0	ns
swsn-7	0	ns
R144.3	0	ns
C53D6.4	0	ns
F02E9.7	0	ns
tbck-1	0	ns

Table S2: Post-dauer fertility of *daf-2; aak(0)* mutants fed with dsRNA against *mir-51* gene targets, Related to Figure 6

STAR Methods Text

CONTACT FOR REAGENT AND RESOURCE SHARING

Further information and requests for resources and reagents should be directed to and will be fulfilled by the lead contact, Dr. Richard Roy (richard.roy@mcgill.ca).

EXPERIMENTAL MODEL AND SUBJECT DETAILS

C. elegans strains and maintenance

C. elegans were grown with standard procedures and maintained at 15°C on Nematode Growth Media (NGM) plates seeded with *E. coli* (OP50)[66]. The strains used in this study can be found in Table S3.

METHODS DETAILS

Transgenes and transgenic animals

To make the DNA plasmid containing *rgef-1p::HA::gfp::rab-7::rab-7 3'UTR*, the coding sequence and the 3'UTR of *rab-7* were amplified from genomic DNA using PCR and primers 1 and 2 and digested using HindIII and PstI and inserted into the pSK vector digested with HindIII and PstI. *rgef-1p* was amplified from plasmid pMR2093 containing *rgef-1p::aak-2::gfp* using PCR and primers 3 and 4. *gfp* was amplified from plasmid pPD95.77 from the Fire Lab kit containing *gfp* using PCR and primers 5 and 6. *rgef-1p*

and *gfp* were inserted into a vector containing the sequence *rab-7* amplified using PCR and primers 7 and 8 to create *rgef-1p::gfp::rab-7::rab-7 3'UTR* using Gibson assembly (NEB E2611). The sequence of *rgef-1p::HA::gfp::rab-7::rab-7 3'UTR* was inserted into pCFJ356 MosSCI vector targeting the *cxTi10816, IV* region (Addgene)[67]. A full list of primer sequences can be found in Table S4.

To generate a DNA plasmid containing *rgef-1p::mKate::T2A::HA::gfp::rab-7::rab-7 3'UTR*, the T2A sequence was inserted downstream of the coding sequence of mKate in a plasmid containing *rgef-1p::mKate::3xFlag::unc-54 3'UTR* using PCR and primers 42 and 43. The PCR product was subjected to T4 PNK (NEB M0201S) and T4 DNA ligase (NEB M0202S) to make *rgef-1p::mKate::T2A::unc-54 3'UTR*. The *mKate::T2A* sequence was amplified using PCR and primers 44 and 45 and inserted into a vector containing the *rgef-1p* and *HA::gfp::rab-7::rab-7 3'UTR* created by using PCR and primers 46 and 47 using Gibson assembly (NEB E2611).

To generate a DNA plasmid containing *tsp-7p::tsp-7::gfp::tsp-7 3'UTR*, the tsp-7p was amplified using PCR and primers 48 and 49, the tsp-7 coding sequence was amplified using PCR and primers 50 and 51, the gfp sequence was amplified using PCR and primers 52 and 53, and the tsp-7 3'UTR sequence was amplified using PCR and primers 54 and 55. The PCR products were inserted into an empty vector pPD95.77 from the Fire Lab kit amplified using PCR and primers 56 and 57 using Gibson assembly (NEB E2611) to generate *tsp-7p::tsp-7::gfp::tsp-7 3'UTR.*

To make the DNA plasmid containing *myo-3p::gfp::rab-7::rab-7 3'UTR*, *nhx-2p::gfp::rab-7::rab-7 3'UTR*, and *pgp-12p::gfp::rab-7::rab-7 3'UTR*, a 2.8 kb, 1.9 kb, and 3.3 kb DNA sequence upstream of each respective gene was amplified using PCR and

cloned into the vector containing the sequence *gfp::rab-7::rab-7 3'UTR* amplified from plasmid *rgef-1p::gfp::rab-7::rab-7 3'UTR* using PCR and primers 9 and were used to generate tissue-specific *gfp::rab-7::rab-7 3'UTR* by using Gibson assembly (NEB E2611).

For tissue-specific RNAi mutants, we used *rde-1(mkc36)* mutants where wild-type expression of *rde-1* was rescued using tissue-specific promoters in the appropriate genetic backgrounds required for that specific experiment[68]. Germline-specific and neuron-specific RNAi were validated in their original publications[4,68,69]. Muscle-specific RNAi was generated for this study. The strains MR2283 and MR2337 were validated by feeding of dsRNA against *unc-112* (muscle), *egg-5* (germ line), or *unc-13* (neurons) and the phenotypes were scored. Each dsRNA treatment exhibits a unique phenotype, such as paralysis (*unc-112* RNAi), embryonic lethal (*egg-5* RNAi), or paralysis (*unc-13* RNAi). Muscle-specific RNAi only exhibited paralysis when fed dsRNA against unc-112.

To generate a DNA plasmid containing *pie-1p::his-15::gfp::3xmir-51::tbb-2 3'UTR*, the *tbb-2 3'UTR* sequence was amplified from genomic DNA using PCR and primers 11 and 12 and the vector containing the sequence of *pie-1p::his-15::gfp* amplified from plasmid containing *pie-1p::his-15::gfp::egg-6 3'UTR* using PCR and primers 13 and 14 were used to generate *pie-1p::his-15::gfp::tbb-2 3'UTR* by using Gibson assembly (NEB E2611). The sequence of *pie-1p::his-15::gfp::tbb-2 3'UTR* was inserted into pCFJ151 MosSCI vector targeting the *ttTi5605, II* region (Addgene) to create a GFP germline marker[67]. To add the wild-type or mutant *3xmir-51* seed sequences, *pie-1p::his-15::gfp::tbb-2 3'UTR* was amplified using PCR with primers containing overhangs for the *3xmir-51* sequences using primers 15 and 16 for wild-type, and primers 17 and 18 for mutant. The PCR product was subjected to T4 PNK (NEB M0201S) and T4 DNA ligase

(NEB M0202S) to make *pie-1p::his-15::gfp::3xmir-51::tbb-2 3'UTR* with either wild-type or mutant *3xmir-51* sites. The plasmids were cloned into the pCFJ151 MosSCI vector targeting the *ttTi5605, II* targeting region (Addgene)[67]. The sequence of the scrambled seed sequence is as follows: 5'-TTTCGATTCATTTTaAgGcGaTTcctaTTTCGATTCATTTTaAgGcGaTTttctTTTCGATTCATTTTaAgGcGaTT-3'. The seed sequences are underlined, and the sites of mutagenesis are in lowercase.

To generate a DNA plasmid containing *rgef-1p::mir-51::unc-54 3'UTR*, the pre-microRNA sequence of *mir-51* was amplified from genomic DNA using PCR and primers 19 and 20 and the vector containing the sequence of *rgef-1p* and *unc-54 3'UTR* amplified from plasmid *rgef-1p::aak-2::unc-54 3'UTR* using PCR and primers 21 and 22 were used to generate *rgef-1p::mir-51::unc-54 3'UTR* by using Gibson assembly (NEB E2611).

To generate a DNA plasmid containing *rgef-1p::mir-51::unc-54 3'UTR* with scrambled EXOmotifs in the mature *mir-51* sequence, the *pre-mir-51* sequence was first inserted into a 3kb empty vector from pMR377 digested with XcmI. Then the three EXOmotifs on *pre-mir-51* were scrambled via site-directed mutagenesis using three sets of primers; set 1 primers 23 and 24, set 2 primers 25 and 26, and set 3 primers 27 and 28. The resulting PCR product was treated with T4 PNK (NEB M0201S) and T4 DNA ligase (NEB M0202S), then verified through sequencing. Plasmids containing neuronally expressed wild-type or scrambled *mir-51* were injected at 1 ng μl^{-1}. The sequence of the scrambled *mir-51* is as follows: 5'-GTCCGAAAAGTCCGTCTACCCGTAGCTCCTATCgttcTTACTGGTCAAAAAGTGAAgtc

cGAAGCAGGTACAGGTGCACGGCGAGTAGGGTgtccAAGCT-3' with the sites of mutagenesis in lowercase.

To generate a DNA plasmid containing *rgef-1p::mKate::3xFLAG::alg-1*, the coding sequence of *alg-1* was amplified from genomic DNA using PCR and primers 29 and 30 and the coding sequence of *mKate::3xFLAG* was amplified from a plasmid containing *mKate::3xFLAG* using PCR and primers 31 and 32 and the vector containing *rgef-1p* and *unc-54 3'UTR* was amplified from plasmid *rgef-1p::aak-2::unc-54 3'UTR* using PCR and primers 33 and 34 were used to generate *rgef-1p::mKate::3xFLAG::alg-1* by using Gibson assembly (NEB E2611). To generate a DNA plasmid containing *rgef-1p::mKate::3xFLAG::alg-2*, the same protocol was used but the coding sequence of *alg-1* was replaced with *alg-2* that was amplified from genomic DNA using PCR and primers 35 and 36. The sequence of *rgef-1p::mKate::3xFLAG::alg-1* was inserted into pCFJ356 MosSCI vector targeting the *cxTi10816, IV* region (Addgene)[67].

To generate a DNA plasmid containing *sur-5p::NeoR::unc-54 3'UTR*, the coding sequence of the neomycin resistance gene was amplified from plasmid containing the NeoR gene using PCR and primers 40 and 41 and a vector containing the sequence of *sur-5p* and *unc-54 3'UTR* was amplified from plasmid *sur-5p::aak-2::unc-54 3'UTR* using primers 21 and 22 to generate *sur-5p::NeoR::unc-54 3'UTR* using Gibson assembly (NEB E2611).

To generate a kinase dead variant of SID-3, aaa (lysine) was mutated into gca (alanine) in the MR1963 *daf-2; aak(0); tbc-7(rr166)* strain using CRISPR-Cas9 with sgRNA sequence primer 37 and a repair template/ultramer DNA oligonucleotide (Integrated DNA Technologies) containing the desired K139A mutation[43]. The sequence

of the repair template: 5'-CGTGGACACAGAGCAATGGGACGCATGTGAATGTCGCTGTggcAATcCTgCGCGAtATcTCcCCtAATATTATGGATGATTTGAGAgtgagttctacttgtatg-3'

Transgenic animals were generated by injecting transgenes (15 ng μl^{-1} each) mixed with a co-injection marker pRF-4 (120 ng μl^{-1}) (Addgene) expressing a dominant negative variant of the *rol-6* gene and an empty vector pSK (up to 200 ng μl^{-1} of DNA) (Addgene) using standard methods[70]. To create transgenic animals with germline *his-15::gfp* expression, EG6699[67] (*ttTi5605 II; unc-119(ed3) III; oxEx1578*) animals were injected with a target transgene (50 ng μl^{-1}) with plasmid pJL43.1 (50 ng μl^{-1}) (Addgene) that expresses Mos1 transposase under a germline promoter and plasmid pMR910 (20 ng μl^{-1}) that expresses GFP under a pharyngeal promoter using standard methods[70]. To create transgenic animals with neuronal HA::GFP::RAB-7 or mKate::3xFLAG::ALG-1 expression, EG6703 (unc-119(ed3) III; cxTi10816 IV; oxEX1582) animals were injected with a target transgene (50 ng μl^{-1}) with plasmid pCFJ601 (50 ng μl^{-1}) (Addgene) that expresses Mos1 transposase under a ubiquitous promoter and plasmid pMR910 (20 ng μl^{-1}) that expresses GFP under a pharyngeal promoter using standard methods[70].

Synchronization

A population of genetically identical animals were synchronized using alkaline hypochlorite. The resulting embryos were allowed to hatch in the absence of food in M9 buffer before they were plated on NGM plates seeded with OP50 (alternatively, on HT115 for RNAi experiments). The plates were incubated in 25°C for 96 hours to induce dauer

formation and to allow the animals to spend at least 48 hours in the dauer stage. Afterwards, the plates were switched back to 15°C to allow for recovery and resumption of normal development.

Quantification of AMPK germline defects

A population of genetically identical animals were synchronized and plated on either NGM plates seeded with OP50 or HT115 expressing dsRNA according to the conditions specified in the figures then incubated at the restrictive temperature of 25°C to induce dauer formation for a total of 96 hours. The dauer larvae were then separate onto individual plates and switched into the permissive temperature of 15°C to trigger dauer exit. The post-dauer fertility was assessed after 7 days and animals were deemed fertile if they gave rise to viable progeny.

For quantification of the number of germ cells in the dauer larvae. Dauer larvae were washed off a plate after spending a total of 96 hours in the restrictive temperature of 25°C and soaked in Carnoy's solution (60% ethanol, 30% acetic acid, 10% chloroform) overnight on a shaker. Afterwards, the Carnoy's solution was removed, and the worm pellet was washed twice with 1x PBS with 0.1% Tween-20 (PBST). The larvae were then stained with 0.1 mg mL^{-1} DAPI (Roche 10236276001) for 30 minutes while shaking. Next, the DAPI solution was removed, and the worm pellet was washed four times with PBST. Germ cells per dauer gonad was determined based on their position and their nuclear morphology and quantified manually. The conditions and genotypes of the animals were not blinded.

Confocal microscopy

All confocal images were taken and analysed as previously described[3,71]. Briefly, images were acquired in a stack of 56 z-planes in increments of 0.2 μm. The DAPI signal was acquired with a wide-field X-Cite 120 florescence illumination system (Excelitas Technologies), while the GFP and mKate signals were acquired with a Quorum WaveFX spinning disc confocal system (Quorum Technologies), both integrated with the Leica DMI6000B microscope with 63x oil-immersion objective. Maximum intensity projection was generated using NIH ImageJ. Each stack was spliced together with overlap to create images of whole animals. Worms were artificially straightened using NIH ImageJ. Scale bars were generated using NIH ImageJ. The conditions and genotypes of the animals were not blinded.

Negative-stain and immunogold labelling TEM

Carbon-coated copper grids (Agar Scientific) were glow-discharged for 20 seconds at 20 mA before sample preparation using EasiGlow Glow Discharge Cleaning System (PELCO). 5 μl of isolated exosomes was applied to the grid and allowed to settle for 5 minutes. The grids were blocked with 5 μl of PBS containing 0.5% BSA for 10 min at room temperature. The grids were incubated with mouse anti-HA.11 epitope tag antibody (BioLegend, 901501, 1:1000, RRID: AB_2565006) for 30 min at RT, then washed with PBS 3 times for a total of 10 min. The grids were incubated with 6 nm Colloidal Gold AffiniPure Goat Anti-Mouse IgG (H+L) (Jackson ImmunoResearch, 115-195-146, 1:20,

AB_2338728) for 30 min at RT, then washed with PBS 3 times for a total of 10 min. Grids were stained with 5 μl of 2% uranyl acetate (Electron Microscopy Sciences) for 45 seconds. The excess solution was blotted off the grid using filter paper after each step. Staining was finished at least 1 hour before imaging. The grids were imaged using a Talos^{TM} F200X G2 (S)TEM (Thermo Scientific).

The number of RAB-7-containing vesicles through immunogold TEM analysis was determined by staining for HA::GFP::RAB-7 using an anti-HA antibody. Five percentages were generated by dividing the number of RAB-7+ vesicles by the total number of vesicles. Each percentage represents one biological replicate. For each biological replicate, 50-100 vesicles were manually quantified. These percentages were plotted to generate Figure 1J.

RNA interference

For RNAi experiments, a population of genetically identical animals were synchronized and allowed to hatch in M9 buffer. L1 larvae are then plated on NGM plates supplemented with 1 mM IPTG (BioShop IPT002) and 50 μg mL^{-1} ampicillin (Fisher BioReagents BP176025) seeded with HT115 either containing an empty vector L4440 or expressing dsRNA against a gene of interest. RNAi constructs were obtained from the Ahringer RNAi library[72]. To generate a *tsp-7* clone for RNAi by feeding, a PCR product targeting a coding sequence of *tsp-7* was generated using primers 38 and 39 and inserted into the pPD129.36 vector digested by XcmI. The PCR product and L4440 vector was ligated overnight using T4 DNA ligase (NEB M0202S) to generate a plasmid that contains a fragment of the coding sequence of *tsp-7* between two T7 polymerase promoters. This

resultant plasmid was transformed into HT115 *E. coli*. All RNAi clones were sequence verified. The conditions and genotypes of the animals and bacteria were not blinded.

Soaking of *daf-2; aak(0)* dauer larvae with dsRNA

Gravid *daf-2* animals were synchronized and incubated at the restrictive temperature of 25°C to induce dauer formation. Animals were harvested after 48 hours at 25°C and subjected to TRIzol™ Reagent (Invitrogen 15596026) for RNA isolation. The isolated RNA was incubated at 65°C for 10 min and allowed to reanneal at room temperature for another 10 min. The reannealed RNA was either used directly for dsRNA soaking or subjected to RNase A (Thermo Scientific EN0531) treatment according to manufacturer's instruction for Figure 2D. For Figure 2B, the mRNA was separated from the isolated RNA using the Poly(A) mRNA Magnetic Isolation Module (NEB E7490S) and Magnetic Separation Rack (NEB S1507S) according to manufacturer's protocol. For Figure 2C, the RNA mixture was separate using the Monarch RNA Cleanup Kit (NEB T2040S) according to manufacturer's protocol. For Figure 2F, RNA was purified using TRIzol™ Reagent (Invitrogen 15596026) from 150 μL of RAB-7-containing exosomes isolated through immunoprecipitation using an anti-HA antibody (described below). Then, gravid *daf-2; aak(0)* animals were synchronized and the resulting embryos were soaked with RNA mixture from *daf-2* dauer larvae, RNase inhibitor (Applied Biosystems, N8080119), and a drop of worm HB101 superfood, and placed in the restriction temperature of 25°C to induce dauer formation. The animals were kept in 25°C for 96 hours before being switched into the permissive temperature of 15°C to trigger dauer

recovery. The post-dauer fertility was scored 7 days afterwards. The conditions and genotypes of the animals were not blinded.

Western blot

For Figure 7E, isolated exosomes were subjected to 1% Triton X-100 (Sigma-Aldrich X100), 50 μg mL^{-1} Proteinase K (Promega V3021), both, or neither then incubated at 60°C for 1 hr. For Figure 7D, the isolated exosomes were not subjected to any treatment before Western blot analysis. The isolated exosomes were mixed with 5 μl of loading buffer (5% β-mercaptoethanol, 0.02% bromophenol blue, 30% glycerol, 10% sodium dodecyl sulfate, 250 mM pH 6.8 Tris-Cl) and heated at 100°C for 5 minutes. Protein concentration was determined using a NanoDrop™ 2000c Spectrophotometer (Thermo Scientific ND-2000).

For whole protein lysates from *C. elegans*, either 500 dauer larvae or 200 post-dauer adult animals were mixed with loading buffer and subjected to multiple rounds of freeze-boiling. Protein lysates were frozen in liquid nitrogen and boiled on a 100°C heat block for 4.5 minutes for at least 4 cycles prior to SDS-PAGE. To verify the reactivity of the anti-CD63/TSP-7 (ABclonal, A5271, 1:500, RRID: AB_2766092), anti-Tsg101/TSG-101 (ABclonal, A2216, 1:500, RRID: AB_2764231), and anti-Alix/ALX-1 (ABclonal, A2215, 1:500, RRID: AB_2764230) antibodies in *C. elegans*, L4 *daf-2* animals were fed with either L4440 empty vector or with dsRNA corresponding to *tsp-7*, *tsg-101*, or *alx-1*. The following F1 generation was collected and used for Western blotting.

The exosome sample was separated using SDS-PAGE and transferred to a nitrocellulose membrane (Bio-Rad, 1620115) before subjected to immunoblotting. Western blot analysis was performed using anti-HA.11 epitope tag antibody (BioLegend, 901501, 1:1000, RRID: AB_2565006), anti-FLAG (Sigma-Aldrich, F7425, 1:1000, RRID: AB_439687), anti-CD63/TSP-7 (ABclonal, A5271, 1:500, RRID: AB_2766092), anti-Tsg101/TSG-101 (ABclonal, A2216, 1:500, RRID: AB_2764231), anti-Alix/ALX-1 (ABclonal, A2215, 1:500, RRID: AB_2764230), anti-α-tubulin (MilliporeSigma, T6199, 1:1000, RRID: AB_477583), or anti-GFP (produced by Roy Lab, 1:1000). Membranes were incubated with horseradish-peroxidase-conjugated anti-rabbit (Bio-Rad, 1721019, 1:2000, RRID: AB_11125143) or anti-mouse (SouthernBiotech, 1036-05, 1:2000, RRID: AB_2794348) secondary antibodies and visualized using a MicroChemi (DNR Bio Imaging Systems) and GelCapture software (Version 7.0.18).

Exosome isolation

daf-2 animals expressing HA::GFP::RAB-7 and mKate::3xFLAG::ALG-1 in the neurons under the *rgef-1p* promoter, as well as the neomycin-resistant gene in the soma under the *sur-5p* promoter were grown on NGM plates containing 0.40 mg mL^{-1} G-418/neomycin (ThermoFisher 11811023). These plates were seeded with HB101 *E. coli*. The G-418/neomycin selects for animals expressing the HA::GFP::RAB-7 and mKate::3xFLAG::ALG-1 transgenes[73]. Gravid animals were synchronized, placed on NGM plates with 0.40 mg mL^{-1} G-418/neomycin seeded with HB101, and put in the restrictive temperature of 25°C to induce dauer formation and incubated for 96 hours. Dauer larvae were harvested by washing the plates with M9 buffer. For each exosome

purification, 2 mL of densely-packed dauer larvae were lysed using a Dounce tissue grinder set (Kimble 885300-0007) in PBS with Halt™ Protease Inhibitor Cocktail (100X) (Thermo Scientific 78429) until no intact worms remained. No detergent was used during the purification process. The protein lysate was pre-cleared through centrifugation for 15 min at 13,500 rpm at 4°C. Exosomes were purified using the exoEasy maxi kit (Qiagen 76064) according to manufacturer's protocol. 440 μL of elution buffer XE (Qiagen) were used to elute the exosomes. The exosomes were stored in the elution buffer XE (Qiagen). RAB-7-containing exosomes were isolated using immunoprecipitation against HA-tagged RAB-7 using an anti-HA antibody (BioLegend, 901501, 1:1000, RRID: AB_2565006). The integrity was the isolated exosomes was verified using negative stain TEM and Western blotting against RAB-7. This sequential purification protocol ensured that the isolated exosomes were intact and of neuronal origin. EVs were first purified and then isolated for all analyses, except for the immunogold TEM analysis to determine the morphology, diameter, and % of RAB-7+ vesicles. Exosomes were isolated fresh for each experiment and were never subjected to freeze-thawing.

The number of RAB-7-containing vesicles were quantified through immunogold TEM analysis. The purified pan-isolated vesicles were stained with an anti-HA antibody (BioLegend, 901501, 1:1000, RRID: AB_2565006). For each biological replicate, the number of RAB-7-positive vesicles were divided by the total number of vesicles to generate a percentage. The percentages were plotted. For each biological replicate, 50-100 vesicles were randomly selected and manually quantified.

Immunoprecipitation

Immunoprecipitation against HA-tagged exosomes was performed using Abcam Immunoprecipitation protocol on pan-exosomes isolated using the exoEasy kit (Qiagen). Protein G beads (Thermo Scientific) were used according to manufacturer's instructions. Briefly, 10 mg of protein G agarose beads were crosslinked to 5 µL of mouse anti-HA antibody (BioLegend, 901501, 1:1000, RRID: AB_2565006) using an effective concentration of 6.5 mg mL^{-1} DMP. No antibody control beads did not contain any antibodies but was still subjected to the crosslinking process. The antibody-bead mixture was mixed with 400 µL of isolated exosomes overnight at 4°C and then subjected to three washes with PBS. For Western analysis, 150 µL of beads were boiled with loading buffer (described above) for 10 mins and loaded into the SDS-PAGE. For RNA analysis, 150 µL of beads were instead subjected to TRIzol™ Reagent (Invitrogen 15596026) for RNA purification. 40 µL of exosomes from the exosome isolation was loaded into the SDS-PAGE as an input control. For soaking of *daf-2; aak(0)* mutants with isolated RAB-7-containing exosomes, the exosomes were gently eluted from the anti-HA::protein G beads using 50 µL of 0.1 M glycine gradient, pH 2.0 on rotation at room temperature for 10 minutes. The eluate was neutralized using 50 µL of Tris, pH 9.0. This elution step was repeated three times. A rabbit anti-GFP primary antibody was used to detect HA::GFP::RAB-7 and a rabbit anti-CD63/TSP-7 antibody (Abclonal, A5271, 1:500, RRID: AB_2766092) was used to detect CD63/TSP-7.

Nanoparticle tracking analysis

Vesicle concentration was determined with dynamic light scattering technology using a ZetaView® PMX-120 (Particle Metrix) and ZetaView (version 8.05.16) software at

the Centre for Applied Nanomedicine at the Research Institute of the McGill University Health Centre. Particles were counted over 11 planes. The final concentration was determined as an average of three measurements. Samples were diluted to a range of 10^6 to 10^9 vesicles per milliliter for the NTA system with filtered PBS.

Then, gravid *daf-2; aak(0)* animals were synchronized and the resulting embryos were soaked with RAB-7-containing exosomes from *daf-2* dauer larvae, RNase inhibitor (Applied Biosystems, N8080119), and a drop of worm HB101 superfood, and placed in the restriction temperature of 25°C to induce dauer formation. The animals were kept in 25°C for 96 hours before being switched into the permissive temperature of 15°C to trigger dauer recovery. The post-dauer fertility was scored 7 days afterwards.

RT-qPCR

For mRNA transcripts, gravid animals were synchronized and incubated at the restrictive temperature of 25°C to induce dauer formation. Animals were harvested after 48 hours at 25°C and subjected to TRIzol™ Reagent (Invitrogen 15596026) for RNA isolation. For each genotype or condition, 200 μL of densely-packed dauer larvae were used for RNA isolation. For isogenic populations, dauer larvae were washed off NGM plates using M9 buffer. For animals expressing transgenes, transgenic animals were manually selected and placed in M9 buffer. Then, the M9 buffer supernatant was removed through centrifugation before the addition of the TRIzol™ Reagent (Invitrogen 15596026). The concentration of the RNA was determined with a NanoDrop™ 2000c Spectrophotometer (Thermo Scientific ND-2000). The quality of the RNA was determined

with a NanoDrop™ 2000c Spectrophotometer (Thermo Scientific ND-2000) and agarose gel electrophoresis. 1000 ng of purified RNA was used to synthesize cDNA using a High-Capacity RNA-to-cDNA™ Kit (AppliedBiosystems, 4387406). The gene expression levels were determined by RT-qPCR using a 2x SyberGreen qPCR Master-mix (ZmTech Scientifique, Q2100N) and a Bio-Rad CFX384 Real-Time 96-well PCR qPCR Detection System (Bio-Rad). 10 ng of cDNA was used for each qPCR reaction. The gene expression data was analyzed using CFX Maestro Software (Bio-Rad). Relative gene expression was calculated by normalizing to the expression of an alpha-tubulin gene, *tba-1*, which as the loading control. Each relative gene expression value is an independent biological replicate, with each replicate corresponding to the average of a triplicate qPCR reaction. The primer sequences for RT-qPCR can be found in Table S5.

For microRNA detection in whole animals, gravid animals were synchronized and incubated at the restrictive temperature of 25°C to induce dauer formation. Animals were harvested after 48 hours at 25°C and subjected to TRIzol™ Reagent (Invitrogen 15596026) for RNA isolation. For whole animal analysis, 200 μL of densely-packed dauer larvae were used for RNA isolation. For isogenic populations, dauer larvae were washed off NGM plates using M9 buffer. For animals expressing transgenes, transgenic animals were manually selected and placed in M9 buffer. Then, the M9 buffer supernatant was removed through centrifugation before the addition of the TRIzol™ Reagent (Invitrogen 15596026). For microRNA detection in purified exosomes, exosomes were harvested and immunoprecipitated as described above. 150 uL of the antibody-bead conjugate bound to the exosomes were subjected to TRIzol™ Reagent (Invitrogen 15596026) for RNA isolation. The concentration of the RNA was determined with a NanoDrop™ 2000c

Spectrophotometer (Thermo Scientific ND-2000). microRNAs were reverse transcribed using the TaqMan™ MicroRNA Reverse Transcription Kit (Applied Biosystems, 3266596), 10 ng of total purified or exosomal RNA, and 5X RT primer (Applied Biosystems) for either wild-type or EXOmotif scrambled *mir-51*. The levels of *mir-51* were quantified from the cDNA using TaqMan™ MicroRNA Assays (Applied Biosystems 4427975) using 20X probes specific for wild-type (Applied Biosystems 000211) or scrambled EXOmotif *mir-51* (Applied Biosystems 4440418). The levels of *mir-51* in whole animal and exosome were normalized to *mir-235*, a microRNA that has been previously shown to be incorporated into exosomes[74]. The gene expression data was analyzed using CFX Maestro Software (Bio-Rad). The relative gene expression was calculated by dividing the Cq value of *mir-51* (wild-type or scrambled) by the Cq value of *mir-235* for each sample and condition. Each relative gene expression value is an independent biological replicate, with each replicate corresponding to the average of a triplicate qPCR reaction. The mean and SEM of every relative gene expression value were plotted.

QUANTIFICATION AND STATISTICAL ANALYSIS

Bar graphs and fluorescence intensity graphs were generated through GraphPad Prism 7. Fluorescence intensity was measured using NIH ImageJ. Statistical tests were performed using GraphPad Prism 7 and XLSTAT plugin for Microsoft Excel. The types of statistical tests used in each experiment, n numbers, P values, and other related measures are indicated in each figure and the associated legend. In all figures, ****P < 0.0001, ***P < 0.001, **P < 0.01, *P < 0.05; ns, not significant. Replications were done by

using different worms performed on different days. Replications for all imaging experiments were performed on different worms on different days. Representative images were generated from more than 10 worms in at least three independently generated lines. RNAi experiments were performed on independently cultured animals and bacterial cultures. Western blots were performed on independently isolated exosomes purifications or animals at least twice. For all *C. elegans* strain used in this study, a population of worms was grown together under identical conditions, and the worms were randomly distributed into different conditions. Worms from a population were randomly chosen for RNAi analyses, post-dauer fertility, Western blot analysis, and imaging experiments.

References and Notes:

1. Riddle, D.L., Swanson, M.M., and Albert, P.S. (1981). Interacting genes in nematode dauer larva formation. Nature *290*, 668-671. 10.1038/290668a0.

2. Narbonne, P., and Roy, R. (2006). Inhibition of germline proliferation during C. elegans dauer development requires PTEN, LKB1 and AMPK signalling. Development *133*, 611-619. 10.1242/dev.02232.

3. Kadekar, P., and Roy, R. (2019). AMPK regulates germline stem cell quiescence and integrity through an endogenous small RNA pathway. PLoS Biol *17*, e3000309. 10.1371/journal.pbio.3000309.

4. Wong, C., Kadekar, P., Jurczak, E., and Roy, R. (2023). Germline stem cell integrity and quiescence are controlled by an AMPK-dependent neuronal trafficking pathway. PLOS Genetics *19*, e1010716. 10.1371/journal.pgen.1010716.

5. Colombo, M., Raposo, G., and Théry, C. (2014). Biogenesis, secretion, and intercellular interactions of exosomes and other extracellular vesicles. Annu Rev Cell Dev Biol *30*, 255-289. 10.1146/annurev-cellbio-101512-122326.

6. Rink, J., Ghigo, E., Kalaidzidis, Y., and Zerial, M. (2005). Rab conversion as a mechanism of progression from early to late endosomes. Cell *122*, 735-749. 10.1016/j.cell.2005.06.043.

7. Vanlandingham, P.A., and Ceresa, B.P. (2009). Rab7 regulates late endocytic trafficking downstream of multivesicular body biogenesis and cargo sequestration. J Biol Chem *284*, 12110-12124. 10.1074/jbc.M809277200.

8. Kalluri, R., and LeBleu, V.S. (2020). The biology, function, and biomedical applications of exosomes. Science *367*. 10.1126/science.aau6977.

9. Packer, J.S., Zhu, Q., Huynh, C., Sivaramakrishnan, P., Preston, E., Dueck, H., Stefanik, D., Tan, K., Trapnell, C., Kim, J., et al. (2019). A lineage-resolved molecular atlas of C. elegans embryogenesis at single-cell resolution. Science *365*, eaax1971. doi:10.1126/science.aax1971.

10. Poteryaev, D., Fares, H., Bowerman, B., and Spang, A. (2007). Caenorhabditis elegans SAND-1 is essential for RAB-7 function in endosomal traffic. Embo j *26*, 301-312. 10.1038/sj.emboj.7601498.

11. Ostrowski, M., Carmo, N.B., Krumeich, S., Fanget, I., Raposo, G., Savina, A., Moita, C.F., Schauer, K., Hume, A.N., Freitas, R.P., et al. (2010). Rab27a and Rab27b control different steps of the exosome secretion pathway. Nat Cell Biol *12*, 19-30; sup pp 11-13. 10.1038/ncb2000.

12. Fielenbach, N., and Antebi, A. (2008). C. elegans dauer formation and the molecular basis of plasticity. Genes Dev *22*, 2149-2165. 10.1101/gad.1701508.

13. Biglou, S.G., Bendena, W.G., and Chin-Sang, I. (2021). An overview of the insulin signaling pathway in model organisms Drosophila melanogaster and

Caenorhabditis elegans. Peptides *145*, 170640. https://doi.org/10.1016/j.peptides.2021.170640.

14. Ren, P., Lim, C.S., Johnsen, R., Albert, P.S., Pilgrim, D., and Riddle, D.L. (1996). Control of C. elegans larval development by neuronal expression of a TGF-beta homolog. Science *274*, 1389-1391. 10.1126/science.274.5291.1389.

15. Käser-Pébernard, S., Müller, F., and Wicky, C. (2014). LET-418/Mi2 and SPR-5/LSD1 cooperatively prevent somatic reprogramming of C. elegans germline stem cells. Stem Cell Reports *2*, 547-559. 10.1016/j.stemcr.2014.02.007.

16. Ahier, A., and Jarriault, S. (2014). Simultaneous Expression of Multiple Proteins Under a Single Promoter in Caenorhabditis elegans via a Versatile 2A-Based Toolkit. Genetics *196*, 605-613. 10.1534/genetics.113.160846.

17. Speese, S., Petrie, M., Schuske, K., Ailion, M., Ann, K., Iwasaki, K., Jorgensen, E.M., and Martin, T.F. (2007). UNC-31 (CAPS) is required for dense-core vesicle but not synaptic vesicle exocytosis in Caenorhabditis elegans. J Neurosci *27*, 6150-6162. 10.1523/jneurosci.1466-07.2007.

18. Richmond, J.E., Davis, W.S., and Jorgensen, E.M. (1999). UNC-13 is required for synaptic vesicle fusion in C. elegans. Nat Neurosci *2*, 959-964. 10.1038/14755.

19. Palmisano, N.J., and Meléndez, A. (2016). Detection of Autophagy in Caenorhabditis elegans by Western Blotting Analysis of LGG-1. Cold Spring Harb Protoc *2016*, pdb.prot086512. 10.1101/pdb.prot086512.

20. Raposo, G., and Stoorvogel, W. (2013). Extracellular vesicles: exosomes, microvesicles, and friends. J Cell Biol *200*, 373-383. 10.1083/jcb.201211138.

21. Khushman, M., Bhardwaj, A., Patel, G.K., Laurini, J.A., Roveda, K., Tan, M.C., Patton, M.C., Singh, S., Taylor, W., and Singh, A.P. (2017). Exosomal Markers (CD63 and CD9) Expression Pattern Using Immunohistochemistry in Resected Malignant and Nonmalignant Pancreatic Specimens. Pancreas *46*, 782-788. 10.1097/mpa.0000000000000847.

22. Logozzi, M., De Milito, A., Lugini, L., Borghi, M., Calabrò, L., Spada, M., Perdicchio, M., Marino, M.L., Federici, C., Iessi, E., et al. (2009). High Levels of Exosomes Expressing CD63 and Caveolin-1 in Plasma of Melanoma Patients. PLOS ONE *4*, e5219. 10.1371/journal.pone.0005219.

23. Logozzi, M., Mizzoni, D., Di Raimo, R., and Fais, S. (2020). Exosomes: A Source for New and Old Biomarkers in Cancer. Cancers (Basel) *12*. 10.3390/cancers12092566.

24. Théry, C., Zitvogel, L., and Amigorena, S. (2002). Exosomes: composition, biogenesis and function. Nature Reviews Immunology *2*, 569-579. 10.1038/nri855.

25. Razzauti, A., and Laurent, P. (2021). Ectocytosis prevents accumulation of ciliary cargo in C. elegans sensory neurons. eLife *10*, e67670. 10.7554/eLife.67670.

26. Von Stetina, S.E., Watson, J.D., Fox, R.M., Olszewski, K.L., Spencer, W.C., Roy, P.J., and Miller, D.M. (2007). Cell-specific microarray profiling experiments reveal

a comprehensive picture of gene expression in the C. elegans nervous system. Genome Biology *8*, R135. 10.1186/gb-2007-8-7-r135.

27. Kratsios, P., Stolfi, A., Levine, M., and Hobert, O. (2012). Coordinated regulation of cholinergic motor neuron traits through a conserved terminal selector gene. Nature Neuroscience *15*, 205-214. 10.1038/nn.2989.

28. Hyenne, V., Apaydin, A., Rodriguez, D., Spiegelhalter, C., Hoff-Yoessle, S., Diem, M., Tak, S., Lefebvre, O., Schwab, Y., Goetz, J.G., and Labouesse, M. (2015). RAL-1 controls multivesicular body biogenesis and exosome secretion. J Cell Biol *211*, 27-37. 10.1083/jcb.201504136.

29. Wehman, A.M., Poggioli, C., Schweinsberg, P., Grant, B.D., and Nance, J. (2011). The P4-ATPase TAT-5 inhibits the budding of extracellular vesicles in C. elegans embryos. Curr Biol *21*, 1951-1959. 10.1016/j.cub.2011.10.040.

30. Gao, J., Zhao, L., Luo, Q., Liu, S., Lin, Z., Wang, P., Fu, X., Chen, J., Zhang, H., Lin, L., and Shi, A. (2020). An EHBP-1-SID-3-DYN-1 axis promotes membranous tubule fission during endocytic recycling. PLoS Genet *16*, e1008763. 10.1371/journal.pgen.1008763.

31. Lee, Y.S., Pressman, S., Andress, A.P., Kim, K., White, J.L., Cassidy, J.J., Li, X., Lubell, K., Lim, D.H., Cho, I.S., et al. (2009). Silencing by small RNAs is linked to endosomal trafficking. Nat Cell Biol *11*, 1150-1156. 10.1038/ncb1930.

32. Saleh, M.C., van Rij, R.P., Hekele, A., Gillis, A., Foley, E., O'Farrell, P.H., and Andino, R. (2006). The endocytic pathway mediates cell entry of dsRNA to induce RNAi silencing. Nat Cell Biol *8*, 793-802. 10.1038/ncb1439.

33. Valadi, H., Ekström, K., Bossios, A., Sjöstrand, M., Lee, J.J., and Lötvall, J.O. (2007). Exosome-mediated transfer of mRNAs and microRNAs is a novel mechanism of genetic exchange between cells. Nat Cell Biol *9*, 654-659. 10.1038/ncb1596.

34. Bishop, J.M., and Koch, G. (1967). Purification and characterization of poliovirus-induced infectious double-stranded ribonucleic acid. J Biol Chem *242*, 1736-1743.

35. Edy, V.G., Szekely, M., Loviny, T., and Dreyer, C. (1976). Action of nucleases on double-stranded RNA. Eur J Biochem *61*, 563-572. 10.1111/j.1432-1033.1976.tb10051.x.

36. Ma, J., Wang, Y.T., Chen, L.H., Yang, B.Y., Jiang, Y.Z., Wang, L.X., Chen, Z.Q., Ma, G.R., Fang, L.Q., and Wang, Z.B. (2023). Dauer larva-derived extracellular vesicles extend the life of Caenorhabditis elegans. Biogerontology *24*, 581-592. 10.1007/s10522-023-10030-5.

37. Hutvágner, G., McLachlan, J., Pasquinelli, A.E., Bálint, É., Tuschl, T., and Zamore, P.D. (2001). A Cellular Function for the RNA-Interference Enzyme Dicer in the Maturation of the let-7 Small Temporal RNA. Science *293*, 834-838. doi:10.1126/science.1062961.

38. Jurczak, E.M., Christopher, W., Shaolin, L., Fabian, B., Ahilya, N.S., Thomas, F.D., Eric, A.M., and Richard, R. (2023). AMPK regulates small RNA pathway prevalence to mediate soma-to-germ line communication and establish germline stem cell quiescence. bioRxiv, 2023.2011.2015.567172. 10.1101/2023.11.15.567172.

39. Villarroya-Beltri, C., Gutiérrez-Vázquez, C., Sánchez-Cabo, F., Pérez-Hernández, D., Vázquez, J., Martin-Cofreces, N., Martinez-Herrera, D.J., Pascual-Montano, A., Mittelbrunn, M., and Sánchez-Madrid, F. (2013). Sumoylated hnRNPA2B1 controls the sorting of miRNAs into exosomes through binding to specific motifs. Nature Communications *4*, 2980. 10.1038/ncomms3980.

40. Hall, S.E., Beverly, M., Russ, C., Nusbaum, C., and Sengupta, P. (2010). A cellular memory of developmental history generates phenotypic diversity in C. elegans. Curr Biol *20*, 149-155. 10.1016/j.cub.2009.11.035.

41. Hinas, A., Wright, A.J., and Hunter, C.P. (2012). SID-5 is an endosome-associated protein required for efficient systemic RNAi in C. elegans. Curr Biol *22*, 1938-1943. 10.1016/j.cub.2012.08.020.

42. Zhang, Y., Grant, B., and Hirsh, D. (2001). RME-8, a conserved J-domain protein, is required for endocytosis in Caenorhabditis elegans. Molecular biology of the cell *12*, 2011-2021. 10.1091/mbc.12.7.2011.

43. Jose, A.M., Kim, Y.A., Leal-Ekman, S., and Hunter, C.P. (2012). Conserved tyrosine kinase promotes the import of silencing RNA into Caenorhabditis elegans

cells. Proceedings of the National Academy of Sciences of the United States of America *109*, 14520-14525. 10.1073/pnas.1201153109.

44. Shen, H., Ferguson, S.M., Dephoure, N., Park, R., Yang, Y., Volpicelli-Daley, L., Gygi, S., Schlessinger, J., and De Camilli, P. (2011). Constitutive activated Cdc42-associated kinase (Ack) phosphorylation at arrested endocytic clathrin-coated pits of cells that lack dynamin. Molecular biology of the cell *22*, 493-502. 10.1091/mbc.E10-07-0637.

45. Han, W., Sundaram, P., Kenjale, H., Grantham, J., and Timmons, L. (2008). The Caenorhabditis elegans rsd-2 and rsd-6 genes are required for chromosome functions during exposure to unfavorable environments. Genetics *178*, 1875-1893. 10.1534/genetics.107.085472.

46. Imae, R., Dejima, K., Kage-Nakadai, E., Arai, H., and Mitani, S. (2016). Endomembrane-associated RSD-3 is important for RNAi induced by extracellular silencing RNA in both somatic and germ cells of Caenorhabditis elegans. Scientific Reports *6*, 28198. 10.1038/srep28198.

47. Liu, L., Qi, H., Wang, J., and Lin, H. (2011). PAPI, a novel TUDOR-domain protein, complexes with AGO3, ME31B and TRAL in the nuage to silence transposition. Development *138*, 1863-1873. 10.1242/dev.059287.

48. Patil, V.S., and Kai, T. (2010). Repression of retroelements in Drosophila germline via piRNA pathway by the Tudor domain protein Tejas. Curr Biol *20*, 724-730. 10.1016/j.cub.2010.02.046.

49. He, B., Cai, Q., Qiao, L., Huang, C.-Y., Wang, S., Miao, W., Ha, T., Wang, Y., and Jin, H. (2021). RNA-binding proteins contribute to small RNA loading in plant extracellular vesicles. Nature Plants *7*, 342-352. 10.1038/s41477-021-00863-8.

50. Devanapally, S., Ravikumar, S., and Jose, A.M. (2015). Double-stranded RNA made in C. elegans neurons can enter the germline and cause transgenerational gene silencing. Proceedings of the National Academy of Sciences *112*, 2133-2138. doi:10.1073/pnas.1423333112.

51. Posner, R., Toker, I.A., Antonova, O., Star, E., Anava, S., Azmon, E., Hendricks, M., Bracha, S., Gingold, H., and Rechavi, O. (2019). Neuronal Small RNAs Control Behavior Transgenerationally. Cell *177*, 1814-1826.e1815. 10.1016/j.cell.2019.04.029.

52. Boulias, K., and Horvitz, H.R. (2012). The C. elegans MicroRNA mir-71 Acts in Neurons to Promote Germline-Mediated Longevity through Regulation of DAF-16/FOXO. Cell Metabolism *15*, 439-450. 10.1016/j.cmet.2012.02.014.

53. Dallière, N., Holden-Dye, L., Dillon, J., O'Connor, V., and Walker, R.J. (2017). Caenorhabditis elegans feeding behaviors. In Oxford Research Encyclopedia of Neuroscience.

54. Cunningham, K.A., Hua, Z., Srinivasan, S., Liu, J., Lee, B.H., Edwards, R.H., and Ashrafi, K. (2012). AMP-activated kinase links serotonergic signaling to glutamate

release for regulation of feeding behavior in C. elegans. Cell Metab *16*, 113-121. 10.1016/j.cmet.2012.05.014.

55. Nikonorova, I.A., Wang, J., Cope, A.L., Tilton, P.E., Power, K.M., Walsh, J.D., Akella, J.S., Krauchunas, A.R., Shah, P., and Barr, M.M. (2022). Isolation, profiling, and tracking of extracellular vesicle cargo in Caenorhabditis elegans. Curr Biol. 10.1016/j.cub.2022.03.005.

56. Mathivanan, S., Ji, H., and Simpson, R.J. (2010). Exosomes: extracellular organelles important in intercellular communication. Journal of proteomics *73*, 1907-1920.

57. Zhou, W., Fong, M.Y., Min, Y., Somlo, G., Liu, L., Palomares, M.R., Yu, Y., Chow, A., O'Connor, S.T., Chin, A.R., et al. (2014). Cancer-secreted miR-105 destroys vascular endothelial barriers to promote metastasis. Cancer Cell *25*, 501-515. 10.1016/j.ccr.2014.03.007.

58. van Balkom, B.W., de Jong, O.G., Smits, M., Brummelman, J., den Ouden, K., de Bree, P.M., van Eijndhoven, M.A., Pegtel, D.M., Stoorvogel, W., Würdinger, T., and Verhaar, M.C. (2013). Endothelial cells require miR-214 to secrete exosomes that suppress senescence and induce angiogenesis in human and mouse endothelial cells. Blood *121*, 3997-4006, s3991-3915. 10.1182/blood-2013-02-478925.

59. Umezu, T., Ohyashiki, K., Kuroda, M., and Ohyashiki, J.H. (2013). Leukemia cell to endothelial cell communication via exosomal miRNAs. Oncogene *32*, 2747-2755.

60. Hoshino, A., Costa-Silva, B., Shen, T.L., Rodrigues, G., Hashimoto, A., Tesic Mark, M., Molina, H., Kohsaka, S., Di Giannatale, A., Ceder, S., et al. (2015). Tumour exosome integrins determine organotropic metastasis. Nature *527*, 329-335. 10.1038/nature15756.

61. Skog, J., Würdinger, T., van Rijn, S., Meijer, D.H., Gainche, L., Sena-Esteves, M., Curry, W.T., Jr., Carter, B.S., Krichevsky, A.M., and Breakefield, X.O. (2008). Glioblastoma microvesicles transport RNA and proteins that promote tumour growth and provide diagnostic biomarkers. Nat Cell Biol *10*, 1470-1476. 10.1038/ncb1800.

62. Wang, W., Zheng, Y., Wang, M., Yan, M., Jiang, J., and Li, Z. (2019). Exosomes derived miR-126 attenuates oxidative stress and apoptosis from ischemia and reperfusion injury by targeting ERRFI1. Gene *690*, 75-80. 10.1016/j.gene.2018.12.044.

63. Zheng, D., Huo, M., Li, B., Wang, W., Piao, H., Wang, Y., Zhu, Z., Li, D., Wang, T., and Liu, K. (2021). The role of exosomes and exosomal microRNA in cardiovascular disease. Frontiers in cell and developmental biology *8*, 616161.

64. Luo, H., Li, X., Li, T., Zhao, L., He, J., Zha, L., Qi, Q., and Yu, Z. (2019). microRNA-423-3p exosomes derived from cardiac fibroblasts mediates the cardioprotective

effects of ischaemic post-conditioning. Cardiovasc Res *115*, 1189-1204. 10.1093/cvr/cvy231.

65. Darwin, C. (1871). Pangenesis. Nature *3*, 502-503. 10.1038/003502a0.

66. Brenner, S. (1974). The genetics of Caenorhabditis elegans. Genetics *77*, 71-94. 10.1093/genetics/77.1.71.

67. Frøkjaer-Jensen, C., Davis, M.W., Hopkins, C.E., Newman, B.J., Thummel, J.M., Olesen, S.P., Grunnet, M., and Jorgensen, E.M. (2008). Single-copy insertion of transgenes in Caenorhabditis elegans. Nat Genet *40*, 1375-1383. 10.1038/ng.248.

68. Zou, L., Wu, D., Zang, X., Wang, Z., Wu, Z., and Chen, D. (2019). Construction of a germline-specific RNAi tool in C. elegans. Sci Rep *9*, 2354. 10.1038/s41598-019-38950-8.

69. Calixto, A., Chelur, D., Topalidou, I., Chen, X., and Chalfie, M. (2010). Enhanced neuronal RNAi in C. elegans using SID-1. Nat Methods *7*, 554-559. 10.1038/nmeth.1463.

70. Mello, C.C., Kramer, J.M., Stinchcomb, D., and Ambros, V. (1991). Efficient gene transfer in C.elegans: extrachromosomal maintenance and integration of transforming sequences. Embo j *10*, 3959-3970. 10.1002/j.1460-2075.1991.tb04966.x.

71. Kostić, I., Li, S., and Roy, R. (2003). Cki-1 links cell division and cell fate acquisition in the C. elegans somatic gonad. Developmental Biology *263*, 242-252. https://doi.org/10.1016/j.ydbio.2003.07.001.

72. Fraser, A.G., Kamath, R.S., Zipperlen, P., Martinez-Campos, M., Sohrmann, M., and Ahringer, J. (2000). Functional genomic analysis of C. elegans chromosome I by systematic RNA interference. Nature *408*, 325-330. 10.1038/35042517.

73. Giordano-Santini, R., Milstein, S., Svrzikapa, N., Tu, D., Johnsen, R., Baillie, D., Vidal, M., and Dupuy, D. (2010). An antibiotic selection marker for nematode transgenesis. Nature Methods *7*, 721-723. 10.1038/nmeth.1494.

74. Duguet, T.B., Soichot, J., Kuzyakiv, R., Malmström, L., and Tritten, L. (2020). Extracellular Vesicle-Contained microRNA of C. elegans as a Tool to Decipher the Molecular Basis of Nematode Parasitism. Front Cell Infect Microbiol *10*, 217. 10.3389/fcimb.2020.00217.

Bridging statement between chapters 3 and 4

In chapter 3, we described the effects of RAB-7 activity. At the onset of the dauer stage, AMPK phosphorylates TBC-7 to induce its autoinhibition, allowing RAB-7 to remain active in the neurons. RAB-7 plays a critical role in the maturation of early endosomes into late endosomes. At the stage of the late endosome, the endosome can undergo membrane invaginations in order to create intralumenal vesicles. The entire entity is then known as a multivesicular body. The multivesicular body has two fates; it can fuse with a lysosome to degrade the contents of the intralumenal vesicles or it can fuse with the plasma membrane, secreting the intralumenal vesicles into the extracellular space, to which they are now referred to as extracellular vesicles or exosomes.

Animals with active RAB-7 secrete extracellular vesicles from serotonergic neurons that are taken up by the germ line. AMPK mutants with overactive TBC-7 activity do not produce extracellular vesicles. We showed that these vesicles are independent from classical neurotransmission, but instead rely on the endosomal system. Through transmission electron microscopy, we showed that these vesicles are within the diameter range of extracellular vesicles derived from the endosomal trafficking pathway. Western analysis indicates the presence of RAB-7 and known exosome markers such as CD63/TSP-7, Tsg101/TSG-101, and Alix/ALX-1 suggesting that these vesicles are indeed exosomes.

We further demonstrated that these exosomes transport a miRNA/miRISC cargo. Inhibition of miRNA biogenesis specifically in the neurons reverts the suppression of AMPK germline defects. We also show that short sequence motifs termed EXOmotifs found on the mature miRNA sequence is required for the proper incorporation of these

miRNAs into the exosomes. The scrambling of any of these EXOmotifs disrupts the ability of the miRNA to silence any mRNAs that contain a corresponding seed sequence. This finding was confirmed with qPCR probes designed specifically for miRNAs on RNA samples isolated from purified exosomes.

In the following chapter, we wanted to elucidate which mRNA targets are regulated by these exosomal miRNAs in the germ line during the dauer stage. Because AMPK mutants display abnormal levels of histone marks and an allele of *tbc-7* can suppress this defect, we wanted to examine if these exosomal miRNAs could be suppressing the expression of histone writers in the germ line. Through our mRNA sequencing database, we found that the expression of almost all examine histone writers were abnormally upregulated in AMPK mutants. Thus, we conducted an RNAi screen against histone writers identified in two datasets. Because we were unable to identify any suppressors of germline defects, we hypothesized that AMPK activation must trigger the activity of many miRNAs that travel to the germ line to suppress histone writers in one concerted effort. The expression of neuronal miRNAs in AMPK mutants corrects not only the expression of the histone writers but also the levels of epigenetic marks, suggesting that neuronal exosomes transports many miRNAs to downregulate histone writers. Lastly, we show that these histone writers and histone marks halt the germline cell cycle expression at the onset of the dauer stage.

Chapter 4: Neuronal miRNAs regulate the expression of histone writers to maintain quiescence and germ cell integrity

Christopher Wong[1], Maxime Verreault[1], Elena Jurczak[1],

Sabih Rashid[1], Richard Roy[1*]

[1]Department of Biology, McGill University; Montreal, H3A 1B1, Canada.

[*]Corresponding author. Email: richard.roy@mcgill.ca

Unpublished results

Abstract:

The cellular response to environmental stimuli is a complex interplay of genetic and epigenetic factors, and histone marks emerge as key players in orchestrating this adaptive landscape. Histone modifying enzymes, often referred to as "histone writers," dynamically add or remove chemical marks on histone proteins, influencing chromatin structure, and gene expression. While the effects of post-translational modification on histone tails by histone writers are relatively well studied, how the histone writers themselves are regulated is not. In this study, we use *Caenorhabditis elegans* to study the regulation of germline histone writers by neuronal miRNAs during periods of energetic stress.

We show that neuronal miRNAs downregulate a large subset of known histone writers to maintain germ cell integrity during the dauer stage. We tagged SET-17, a H3K4 methyltransferase with GFP to show that the expression of histone writers is affected by the absence of miRNAs and AMPK signalling. By repressing the expression of the histone writers, the neuronal miRNAs establish a dauer-appropriate chromatin landscape and prevent aberrant RNA polymerase II transcription, thereby arresting the germline cell cycle at the G2 cell cycle stage. Finally, we demonstrate that forcing the germ cells to progress in the cell cycle renders *daf-2* animals post-dauer sterile, presumably due to a loss of germline quiescence. Our findings demonstrate that exosomal miRNAs regulate the expression of histone writers to affect the germline chromatin landscape and gene expression, ultimately to halt the cell cycle.

Introduction

For a species to survive and flourish, it must be able to adapt. Organisms have evolved various strategies to overcome environmental stressors. At the molecular level, epigenetic modifiers such as histone erasers, readers, writers, and recruiters are constantly remodeling the chromatin to adjust gene expression in response to change (Devaskar and Raychaudhuri, 2007; Zoghbi and Beaudet, 2016). This dynamic fluctuation of chromatin states has been well documented in various developmental, physiological, and disease contexts and their misregulation is often reflected at the phenotypic level. However, a comprehensive understanding of how the histone writers themselves are regulated is, so far, comparatively understudied.

During periods of environmental stress, the nematode *C. elegans* can execute a stress-resistant developmental diapause-like state known as the “dauer” stage (Fielenbach and Antebi, 2008; Kimura et al., 1997). During this stage, the master metabolic regulator, AMP-activated protein kinase (AMPK) is required to maintain germline quiescence and reproductive competence throughout the diapause (Kadekar and Roy, 2019; Narbonne and Roy, 2006; Wong et al., 2023b). In replete conditions, mutants lacking both catalytic subunits of AMPK (*aak(0)*) are superficially wild-type (Kadekar and Roy, 2019). However, AMPK mutants that transit through the dauer stage are completely sterile, suggesting that these mutants cannot maintain the integrity of the germ cells during this period of energetic stress. Further examining why these germ cells lose their reproductive capacity, we found that the levels of both activating and repressive histone marks are upregulated in the absence of AMPK signalling. In addition to the increased deposition of these chromatin marks, the distribution of these histone marks

across the germ lines of dauer larvae and post-dauer animals is abnormal. These data suggest that the abnormal histone marks may establish a maladaptive gene expression program in the germ cells, which could be the cause, or contribute to, the observed post-dauer sterility in AMPK mutants.

We previously showed that compromising a RabGAP protein, *tbc-7*, can suppress the AMPK germline defects, including the abnormal levels and distribution of the histone marks (Wong et al., 2023b). TBC-7 directly regulates RAB-7 activity, converting it from its active GTP-bound form into its inactive GDP-bound form. By removing TBC-7 function, RAB-7 is active and can help in the maturation of early endosomes into late endosomes, where it can undergo membrane invaginations in order to create intralumenal vesicles/exosomes (Colombo et al., 2014; Kalluri and LeBleu, 2020; Rink et al., 2005). As the animal enters the dauer stage, the neurons load miRISC into exosomes that are produced from RAB-7 activity (Wong et al., 2023a). These exosomes act as carriers for the miRISC that ultimately impinge on the germ line to affect gene expression. However, it is unknown if or how the miRISC affects the abundance of histone marks, whether directly or indirectly.

In this study, we show that neuronal miRNAs repress the expression of a diverse class of histone writers in the germ line in a concerted manner to regulate the levels of histone marks and subsequent gene expression. We found that many set genes were upregulated in the absence of AMPK signalling. We focused on a germline H3K4 methyltransferase *set-17* that, when compromised, could partially suppress the AMPK germline defects during the dauer stage. We created a sensor that reports germline histone writer activity to show that the expression of *set-17* is regulated by the activity of

AMPK and neuronal miRNAs. By fine tuning the levels of H3K4me3 to precisely control global gene expression, we show that neuronal miRNAs can directly impact the expression of histone writers and ultimately the germline cell cycle during the dauer stage. Through RNAi experiments, we also identify key histone readers that are important for the maintenance of germ cell integrity. This analysis of histone writers and readers act as a platform to identify the exact genes responsible for maintaining quiescence and germ cell integrity that are cell nonautonomously regulated by AMPK through the activity of neuronal miRNAs.

Results:

Chromatin marks are upregulated in the absence of AMPK signalling

AMPK mutants have an increased abundance and abnormal distribution of histone marks in the germ line (Kadekar and Roy, 2019). To determine if this maladaptive increase of histone marks is due to the misregulation of histone writers, we conducted expression analysis of the histone writers using our mRNA-sequencing dataset (Rashid, personal communication). We decided to focus on the gene expression of histone writers that have a characterized mutant phenotype (Wormbook) and that were identified from WERAM, a database of writers, erasers and readers of histone acetylation and methylation in eukaryotes (Xu et al., 2017). We then generated a heat map to visually represent the data (Fig. 1). Out of the 152 genes analyzed, we found that all but 21 genes were upregulated in the absence of AMPK signalling compared to *daf-2* control animals.

This finding suggests that the upregulation of histone writers could be responsible for the abnormal increase in the abundance of histone marks in AMPK mutants.

Histone writers have many different enzymatic functions. For example, the trithorax-group proteins (TrxG) are a complex of heterogeneous proteins that are responsible for the maintenance of gene expression, and it does so through histone modifications, chromatin remodeling, and DNA-binding protein recruitment (Kingston and Tamkun, 2014). On the other hand, the polycomb-group proteins (PcG) play an antagonistic role by promoting the silencing of genes through the trimethylation of H3K27me2/3 and the monoubiquitination of lysine 119 on histone H2A (Di Croce and Helin, 2013). Therefore, to determine which groups of histone writers are required to maintain quiescence and germ cell integrity throughout the dauer stage, we conducted a RNAi screen of all histone writers: first, in *daf-2; aak(0)* mutants to identify writers that, when compromised, could suppress the AMPK germline defects; second, in *daf-2; aak(0); tbc-7* mutants to identify writers that are required to suppress these defects.

To determine which histone writers, when compromised, could suppress the AMPK germline defects, we conducted RNAi against histone writers that have a characterized mutant phenotype and were identified by WERAM in *daf-2; aak(0)* mutants. The RNAi analysis did not reveal any single suppressor of AMPK germline defects (Fig. 2A). We hypothesize that because many histone writers are downregulated in the absence of AMPK signalling, decreasing the expression of one histone writer is insufficient to suppress the deposition of a variety of histone marks. In addition, AMPK mutants do not exhibit robust RNAi phenotypes (Jurczak et al., 2023). Therefore, rather than conducting RNAi on *daf-2; aak(0)* mutants, we decided to conduct RNAi on *daf-2;*

aak(0) mutants that also carry a deletion of one of the genes that displayed a modest suppression of the germline defects, namely *set-17*. When we repeated the RNAi experiments on *set-17; daf-2; aak(0)* mutants, we observed a greater suppression of the AMPK germline defects when compared to just *daf-2; aak(0)* mutants alone (Fig. 2B). These data suggest that AMPK must regulate these histone writers in a concerted manner to maintain germ cell integrity during periods of energetic stress.

Next, to determine which gene products could be required to maintain quiescence and germ cell integrity during the dauer stage, we conducted RNAi against these histone writers in *daf-2; aak(0); tbc-7* mutants. From this RNAi analysis, we identified many genes that were required to maintain the reproductive capacity after the dauer stage (Table 1).

To better understand the physiological changes that result from the activity of these histone writers, we conducted a bioinformatic analysis on the genes that were able to revert the suppression of AMPK germline defects. Of the 40 genes interrogated, most were downregulated in response to AMPK signalling during the dauer stage, despite having a wide range of functions (Fig. 3A-C). By analyzing the 3'UTRs of these genes using TargetScanWorm (version 6.2), we also found that about a quarter also contain high stringency 8mer seed sequences for conserved miRNAs (Fig. 3D). In addition, all these genes have been shown to work in the germ line (Fig. 3E).

Neuronal miRNAs regulate the expression of histone writers

From our previous work, we know that AMPK mutants have elevated levels of histone marks associated with both activating and repressive transcriptional activity (Kadekar and Roy, 2019). We have shown that a hypomorphic allele of *tbc-7*, *(rr166)* suppresses this histone defect by allowing RAB-7 to remain in its active GTP-bound form to produce exosomes that bring miRNAs to the germ line during the dauer stage (Wong et al., 2023b). These miRNAs could be suppressing the expression of histone writers thereby preventing the deposition of maladaptive histone marks in the germ line. Current data suggests that AMPK phosphorylates DCR-1 and RBPL-1 at the onset of the dauer stage to lock this complex in a miRNA-producing conformation, producing many different families of miRNAs (Jurczak et al, 2023). By extension, by providing animals with extra copies of a singular miRNA, it re-prioritizes DCR-1 activity toward the miRNA biosynthesis pathway, likely through an altered interaction with RBPL-1, thus restoring the production of miRNAs to near wild-type dauer larvae levels.

To assess whether neuronal miRNAs could regulate the expression of histone writers, we conducted qPCR on *daf-2; aak(0)* mutants expressing extra copies of neuronal *mir-51* and compared it to *daf-2*, *daf-2; aak(0),* and *daf-2; aak(0); tbc-7* mutants. Our analyses showed that the levels of the histone writers were largely restored to *daf-2* control levels in *tbc-7*-suppressed animals and AMPK mutants expressing extra copies of *mir-51* (Fig. 4A).

To further assess whether neuronal miRNAs could be responsible for regulating the levels of histone marks in the germ line, we conducted Western analysis against histone marks associated with activate and repressive transcription. Our findings show

that the neuronal expression of *mir-51* can suppress the abnormal increase in histone marks seen in AMPK mutants (Fig. 4B-C). These data suggest that AMPK could be acting through miRNAs that are transported from the neurons to the germ line through the activity of RAB-7-dependent exosomes to somehow downregulate the levels of histone marks in the germ line.

Histone marks play an important role in regulating gene expression by altering level of chromatin accessibility around regions that harbour target genes. We previously showed that *daf-2; aak(0)* mutants have abnormal germline gene expression as compared to *daf-2* control animals (Kadekar and Roy, 2019), and suppressing *tbc-7* activity corrects this defect (Wong et al., 2023b). Since the expression of neuronal miRNAs can correct the expression of histone writers and the abundance of histone marks, we wanted to examine if the abnormal germline gene expression is also corrected. To examine if the expression levels of a set of germline-specific genes that has been previously shown to be misregulated in the absence of AMPK signalling can be corrected by the expression of neuronal *mir-51*, we conducted qPCR on *tbc-7*-suppressed animals and AMPK mutants expressing extra copies of *mir-51* in the neurons. Our analysis indicates that the germline gene expression is corrected by the expression of neuronal miRNAs (Fig. 4D). Statistical testing indicates that the expression of these germline genes is not significantly different between AMPK mutants expressing neuronal *mir-51* and *daf-2* control animals. Altogether, the data suggests that miRNAs packaged into exosomes in the neurons can repress the expression of many histone writers in a concerted way in the germ line, therefore preventing the establishment of a maladaptive chromatin landscape and subsequent gene expression.

Since many histone writers are downregulated in the absence of AMPK signalling and many histone writers are required for the *tbc-7*-mediated suppression of AMPK defects, it is possible that these writers could be regulated in one concerted wave rather than each individual chromatin factor possessing a unique regulatory mechanism. To examine this hypothesis, we expressed four histone writers, *gfl-1*, *rba-2*, *set-2*, and *C17E4.6*, that possess either endogenous miRNA binding sites within their native 3'UTR or, alternatively, that harbour a universal *tbb-2* 3'UTR, in the germ line of *daf-2; aak(0); tbc-7* mutants and examined the post-dauer fertility. If these histone writers are regulated in a concerted manner by miRNAs, then the expression of these writers with a universal 3'UTR should render the *tbc-7*-suppressed animals post-dauer sterile, while the writers that still retain their native 3'UTRs should remain sensitive to the corresponding cellular miRNA levels. Driving the expression of these writers in the germ line using the universal 3'UTR renders the animals post-dauer sterile, while the fertility was unaffected with writers using the native 3'UTR (Fig. 4E). This data suggests that the histone writers regulate the germ cell integrity during the dauer stage and that their function is dependent on an intact 3' UTR that possesses canonical miRNA binding sequences.

At the onset of the dauer stage, AMPK likely phosphorylates the miRNA biogenesis machinery in order to lock DCR-1/RBPL-1 into a miRNA competent conformation (Jurczak et al, 2023). Consistent with this finding, adding additional copies of one miRNA increases the biogenesis of other miRNAs in the neurons, as adding extra copies of pre-miRNA presumably stimulates the association of DCR-1 and RBPL-1. To show that this association is happening during the dauer stage and that the expression of histone writers and germline-specific genes are regulated in a concerted manner by miRNAs, we

expressed *mir-240* in the soma of *daf-2; aak(0)* mutants. We selected *mir-240* as it does not belong in a family, nor does it have any published interactions with other miRNAs. Thus, the phenotypes observed through adding additional copies of this miRNA can be attributed to the re-prioritization of the DCR-1 complex. Consistent with this hypothesis, *daf-2; aak(0)* expressing extra copies of *mir-240* in the soma can suppress the post-dauer sterility (approximately 26%) (Jurczak et al, 2023). Next, we examined if the somatic expression of *mir-240* can correct the expression of the histone writers as well as the germline gene expression. AMPK mutants expressing *mir-240* in the soma can largely correct the expression of the histone writers and the gene expression in the germ line (Fig. 4F-G), despite none of the histone writers possessing *mir-240* seed sequences. These data suggest that the activation of AMPK sets off an amplification system that releases a wave of miRNAs, which in turn post-transcriptionally regulate chromatin factors and gene expression in the germ line to adjust to novel cellular stressors.

To show that neuronal miRNAs can directly target the 3'UTR of histone writers, we created a germline miRNA activity sensor for a H3K4 methyltransferase *set-17*. This histone writer *set-17* was chosen because it can partially suppress the AMPK germline defects during the dauer stage when compromised, indicating that its expression in the germ line must be affected by AMPK signalling. Additionally, we found that the expression of members of the *set* family of histone modifiers to be lower in *daf-2* animals compared to AMPK mutants (Fig. 5A). To create this sensor a transgenic strain was designed to carry a copy of SET-17 that was translationally fused to GFP while retaining the native the *set-17* 3'UTR and promoter (Fig. 5B) (Engert et al., 2018). This transgene was then

crossed into the *daf-2*, *daf-2; aak(0)*, and *daf-2; aak(0); tbc-7* expressing a germline mCherry::HIS-11 marker and expression was quantified in the resulting dauer larvae.

We first assessed the expression of the *set-17* sensor in the germ line of *daf-2* and *daf-2; aak(0)* mutants in replete conditions and found that the sensor is stably expressed (Fig. 5C-E). The same transgene/allele was used to ensure consistency in the expression levels. However, when we allowed the animals to enter the dauer stage, we found that the expression of *set-17* was greatly reduced in *daf-2* mutants, but remained stably expressed in *daf-2; aak(0)* mutants (Fig. 5F-H). Altogether, these data suggest that AMPK can affect the expression, and therefore, presumably, the activity of histone writers in the germ line, which can affect the chromatin landscape and ultimately post-dauer fertility.

The levels of transcription are affected in mutants lacking AMPK signalling

Transcriptional activity is governed by the histone code, where different post-translational modifications on the C-terminal domain of histone proteins can affect the expression of its target gene (Jenuwein and Allis, 2001). Our data so far suggest that the regulation of histones is critical to maintaining germ cell integrity, perhaps by regulating the accessibility of RNA polymerase II. The activity of RNA polymerase II is regulated by two critical phosphorylation events on the C-terminal domain (CTD) of the largest subunit of the polymerase (Hsin and Manley, 2012). The CTD consists of multiple heptad repeats: Tyr1–Ser2–Pro3–Thr4–Ser5–Pro6–Ser7. The number of repeats differs somewhat between species, but the presence of a minimal domain is nevertheless essential. During transcription initiation, CDK7 the protein kinase subunit of TFIIH, a critical general transcription factor, phosphorylates Ser5 of the CTD of RNA polymerase II during

initiation (Glover-Cutter et al., 2009). Therefore, the phosphorylation pattern of Ser5 peaks around the transcription start site. As RNA polymerase II elongates, Ser2 is increasingly phosphorylated by CDK9/p-TEFb, while Ser5 phosphorylation is gradually removed by phosphatases (Marshall et al., 1996). Therefore, to examine if transcriptional activity of RNA polymerase II is affected by the aberrant deposition of chromatin marks in mutants lacking AMPK signalling, we first conducted western analysis on whole dauer larvae using antibodies against phosphorylated Ser5 of the CTD of RNA polymerase II.

Because we have shown that neuronally-expressed miRNAs can directly affect the germline chromatin landscape, we wanted to assess if neuronally-expressed *mir-51* can also affect transcriptional activity. Mutants lacking AMPK signalling had increased levels of Ser5 phosphorylation compared to *daf-2* control animals and AMPK mutants expressing neuronal *mir-51* (Fig. 6A-B). These data suggest that AMPK mutants have increased levels of transcription initiation.

Next, we wanted to examine if the level of transcriptional elongation is affected by the lack of AMPK signalling. To do this, we repeated our western analysis using antibodies against phosphorylated Ser2 of CTD of RNA polymerase II. Our data show that the levels of transcriptional elongation between *daf-2* control animals and AMPK mutants were not significantly different (Fig. 6A-B). Interestingly, the levels of transcription elongation were relatively lower in AMPK mutants expressing neuronal *mir-51* compared to *daf-2* animals and AMPK mutants. Altogether, our data suggests that the levels of transcriptional activity and the number of transcripts produced could be equal, however AMPK mutants may have more transcription initiation events that presumably stall at around the start site and do not being elongation.

Histone marks may affect the germline cell cycle

When wild-type animals enter the dauer stage, all the germ cells arrest at the G2 cell cycle stage and neither spermatogenesis nor oogenesis should occur (Wong et al., 2023b). The germline cell cycle is misregulated in mutants that lack AMPK signalling, resulting in a dramatic germline hyperplasia. In wild-type animals, spermatogenesis starts in the L4 stage in the hermaphrodite germline (Ellis and Stanfield, 2014), but in AMPK mutants, sperm can be detected in the dauer larvae. Genetic analyses of crosses between wild-type males with AMPK hermaphrodites and AMPK males with wild-type hermaphrodites indicate that the sperm produced are defective (Kadekar and Roy, 2019). Thus, it is possible that the loss of the sperm integrity could be attributed to a misregulation of the cell cycle of each individual germ cell.

To examine if the misregulation of the cell cycle is the cause of the AMPK-dependent germline defects, we first examined the expression of known markers of the cell cycle through our mRNA sequencing dataset (Rashid, personal communication). We found that the expression of markers for G1 cell cycle were highly upregulated in *daf-2* animals compared to AMPK mutants (Table 2). This finding was expected as wild-type animals undergo cell cycle arrest during the dauer stage. On the contrary, AMPK mutants had highly upregulated levels of all cell cycle markers, while the meiotic marker HIM-3 was the most relatively upregulated. This finding is consistent with the observation of spermatogenesis in AMPK dauer larvae, suggesting that the germ cells of AMPK mutants are not undergoing cell cycle arrest but rather progressing through the meiotic cell cycle. Interestingly, these findings are reversed in post-dauer animals. *daf-2* animals have very strong expression of all cell cycle markers except for G1 stage-specific genes. Notably,

him-3, the meiotic marker is very highly expressed, indicating that *daf-2* post-dauer animals are producing gametes, which is consistent with our findings that wild-type animals can transit through the dauer stage with no reproductive consequences. This finding suggests that AMPK mutants cannot adjust their cell cycle according to the needs of the dauer stage and is uncoupled from the energy status of the animal.

To further explore if the misregulation of the cell cycle is the cause of the loss of germ cell integrity in AMPK mutants, we disrupted the proliferation of the germline stem cells using the auxin-inducible degradation system and assessed for AMPK germline defects (Zhang et al., 2015). We crossed a strain harbouring a CRISPR/Cas9 endogenously tagged LAG-1::degron with a MosCI inserted TIR1 receptor driven by the *gld-1p* promoter into the *daf-2* background (Chen et al., 2020). When these animals were treated with auxin, the TIR1 receptor becomes activated causing the degradation of all degron-tagged proteins. The loss of LAG-1 forces all the germline stem cells to enter meiosis (Chen et al., 2020). When these mutants were treated with auxin during their entry into and recovery from the dauer stage, the animals become post-dauer sterile (Fig. 7A). Because the complete loss of *lag-1* is lethal, we repeated the experiment but removed the animals from auxin only during their recovery from the dauer stage. These animals remained post-dauer sterile, suggesting that tampering with the timing of the germline cell cycle as the animals enter the dauer stage affects the integrity of the germ cells even when the germline cell cycle is undisturbed during the recovery period (Fig. 7A). Interestingly, the germline hyperplasia observed in AMPK mutants was not seen in dauer larvae treated with auxin, suggesting that the germline hyperplasia and the integrity of each individual germ cell could be governed by different mechanisms (Fig. 7B).

The overall gene expression in AMPK mutant dauer larvae and post-dauer adults is highly misregulated, and is associated with abnormalities in the chromatin landscape both in the soma and in the germ cells of these animals (Kadekar and Roy, 2019). We therefore wanted to determine if the aberrant chromatin marks are misregulated as a result of disrupting the germline cell cycle. We conducted Western analysis against animals treated with or without auxin using antibodies against transcriptionally activating and repressive histone marks. Interestingly, there were no significant differences of the relative abundances of both types of marks (Fig. 7C-D). These data suggest that disrupting the germline cell cycle does not affect the germline chromatin landscape. However, since *daf-2* animals with disrupted germline cell cycle are post-dauer sterile, we cannot rule out that these animals have disrupted germline gene expression that could be the cause of the post-dauer sterility. Thus, we propose a mechanism where the miRNAs regulate the histone writers during the dauer stage. These histone writers then modify the germline chromatin landscape and subsequent gene expression accordingly to halt the cell cycle at the G2 stage. The misregulation of this regulatory mechanism results in the loss of germ cell integrity.

Discussion:

Histone writers, also known as histone modifying enzymes, play a pivotal role in regulating gene expression and orchestrating various cellular processes (Devaskar and Raychaudhuri, 2007; Jenuwein and Allis, 2001; Zoghbi and Beaudet, 2016). These enzymes are responsible for adding and removing specific chemical marks, such as

acetyl groups, methyl groups, or phosphate groups, on the disordered N-terminal tails of histone proteins within chromatin. This process culminates in a specific "histone code" and serves as a dynamic and intricate mechanism for controlling chromatin structure and, consequently, gene expression by influencing the accessibility of regions of the DNA to the transcriptional machinery (Zoghbi and Beaudet, 2016). By modifying histones through the addition of these chemical groups, these enzymes, or "histone writers", either facilitate or impede the binding of regulatory proteins, thereby impacting the initiation of gene transcription (Di Croce and Helin, 2013; Marshall et al., 1996). This regulatory role is fundamental in developmental processes, cellular differentiation, and in adjusting gene expression in response to environmental cues. Furthermore, dysregulation of histone writers has been implicated in various diseases, including cancer, highlighting the critical nature of these enzymes in maintaining cellular homeostasis and proper genomic function (Zoghbi and Beaudet, 2016). In essence, histone writers are integral players in the epigenetic landscape, shaping the dynamic interplay between genes and their expression in response to internal and external signals.

While the effects of histone modifications have been relatively well studied in various contexts, how histone writers are regulated have been largely unexplored. Here, we describe a mechanism in which exosomal-derived miRNAs directly regulate the expression of a subset of histone writers during the dauer stage of *C. elegans*. By inhibiting the expression of these histone writers, these miRNAs prevent the inappropriate deposition of chromatin marks in the germ cells of developmentally arrested animals. RNAi screens of histone modifying genes identified in two datasets in AMPK mutants revealed two histone writers that played critical roles in regulating germ cell integrity.

The H3K4 methyltransferase SET-17 is a critical player in maintaining germ cell integrity during the dauer stage. The compromise of *set-17* through RNAi suppresses the AMPK germline defects. Therefore, the timely, and region-specific methylation of H3K4 on genes targeted by *set-17* or SET domain-containing proteins is critical. It can ultimately influence gene expression, either directly or indirectly, in individual germ cells, consequently modifying reproductive competence (Engert et al., 2018). Moreover, SET-17 has been shown to drive the transcription of spermatocyte-specific genes and functions primarily in the germ line, suggesting the possibility that SET-17 may be at least one of the players in preventing entry into meiosis and halting the germline cell cycle during the dauer stage.

Previously, our analysis showed that the distribution of the chromatin marks across the germ line was misregulated in AMPK mutants (Kadekar and Roy, 2019). For example, H3K4me3 in *daf-2* and *tbc-7*-suppressed mutants is evenly distributed across the germ line. However, in the absence of AMPK signalling, there is little H3K4me3 detected in the distal end but an accumulation of these marks in the proximal end of the germ line (Wong et al., 2023b). We do not know if there is a correlation between the expression of the histone writers, *set-17* responsible for H3K4me3 deposition, and the abnormal pattern of H3K4me3 in AMPK mutants. It is possible that there are factors outside of the germ line in addition to regulation by miRNAs that are responsible for the proper distribution of the histone writers across the germ line. Furthermore, the abnormal distribution of histone marks could contribute to the loss of germ cell integrity. Perhaps the activity of the *rsd* (RNAi spreading defective) genes are responsible for the distribution of the miRNA

silencing throughout the germ line in order to modify the chromatin landscape accordingly (Wong et al., 2023a).

Our analysis indicates that the levels of transcription initiation are elevated in AMPK mutants, while the levels of transcription elongation are not significantly different compared to *daf-2* and AMPK mutants expressing neuronal *mir-51*. Overall, these data suggest that AMPK mutants exhibit more transcription initiation events. Although the overall level of gene expression is suppressed during the dauer stage in wild-type animals, there is still transcription of some gene families related to stress, such as HSP proteins and genes involved in ubiquitination (Dalley and Golomb, 1992). We can speculate that AMPK mutants may be transcribing genes that are maladaptive for the dauer stage, resulting in the progression of the cell cycle and eventually causing the germ cells to undergo meiosis to produce gametes, in addition to transcribing stress related genes.

Our work highlights the downstream effects of exosomal miRNAs in the germ line (Wong et al., 2023a). Through the activity of RAB-7, neuronally produced miRNAs are delivered to the germ line in order to affect changes in gene expression. We propose that these miRNAs inhibit the expression of germline histone writers, although we cannot rule out that these miRNAs may be also targeting other mRNAs. Because most miRNAs are upregulated at the onset of the dauer stage (Jurczak et al, 2023), we speculate that many miRNAs are delivered to the germ line through the activity of exosomes. These miRNAs then in turn downregulate the expression of a cohort of germline histone writers to establish a chromatin landscape and gene expression program suitable for arresting the germline cell cycle in order to preserve germ cell integrity (Fig. 7E).

Materials and Methods:

CONTACT FOR REAGENT AND RESOURCE SHARING

Further information and requests for resources and reagents should be directed to and will be fulfilled by the lead contact, Dr. Richard Roy (richard.roy@mcgill.ca).

EXPERIMENTAL MODEL AND SUBJECT DETAILS

C. elegans strains and maintenance

C. elegans were grown with standard procedures and maintained at 15°C on Nematode Growth Media (NGM) plates seeded with *E. coli* (OP50) (Brenner, 1974). The strains used in this study can be found in Table S1.

METHODS DETAILS

Transgenes and transgenic animals

A full list of oligonucleotides used in this study can be found in Table S2. To create *pie-1p* driving the expression of *glf-1*, *rba-2*, *set-2*, and *C17E4.6*, primers 1-8 were used to amplify the cDNA sequence. Primers 9-13 were used to amplify the universal 3'UTR *tbb-2*. A vector was created using primers 14 and 15. Fragments were ligated using Gibson assembly (NEB E2611).

Synchronization

A population of genetically identical animals were synchronized using alkaline hypochlorite. The resulting embryos were allowed to hatch in the absence of food in M9 buffer on a rotating stand at 15°C before they were plated on NGM plates seeded with OP50 (alternatively, on HT115 for RNAi experiments). The plates were incubated in 25°C for 96 hours to induce dauer formation and to allow the animals to spend at least 48 hours in the dauer stage. Afterwards, the plates were switched back to 15°C to allow for recovery and resumption of normal development.

Quantification of AMPK germline defects

A population of genetically identical animals were synchronized and plated on either NGM plates seeded with OP50 or HT115 expressing dsRNA according to the conditions specified in the figures then incubated at the restrictive temperature of 25°C to induce dauer formation for a total of 96 hours. The dauer larvae were then separate onto individual plates and switched into the permissive temperature of 15°C to trigger dauer exit. The post-dauer fertility was assessed after 7 days and animals were deemed fertile if they gave rise to viable progeny.

RNA interference

For RNAi experiments, a population of genetically identical animals were synchronized and allowed to hatch in M9 buffer. L1 larvae are then plated on NGM plates supplemented with 1 mM IPTG (BioShop IPT002) and 50 μg mL^{-1} ampicillin (Fisher

BioReagents BP176025) seeded with HT115 either containing an empty vector L4440 or expressing dsRNA against a gene of interest. RNAi constructs were obtained from the Ahringer RNAi library (Fraser et al., 2000). All RNAi clones were sequence verified. The conditions and genotypes of the animals and bacteria were not blinded.

Western blot

For whole protein lysates from *C. elegans*, either 500 dauer larvae or 200 post-dauer adult animals were mixed with loading buffer (5% β-mercaptoethanol, 0.02% bromophenol blue, 30% glycerol, 10% sodium dodecyl sulfate, 250 mM pH 6.8 Tris-Cl) and subjected to multiple rounds of freeze-boiling. Protein lysates were frozen in liquid nitrogen and boiled on a 100°C heat block for 4.5 minutes for at least 4 cycles prior to SDS-PAGE. The protein sample was separated using SDS-PAGE and transferred to a nitrocellulose membrane (Bio-Rad, 1620115) before subjected to immunoblotting.

Western blot analysis was performed using anti-histone H3 (tri methyl K4) antibody (abcam, ab8580, 1:1000, RRID: AB_306649), anti-histone H3 (tri methyl K9) antibody (abcam, ab8898, 1:1000, RRID: AB_306848), anti-RNA polymerase II CTD repeat YSPTSPS (phospho S5) (abcam, ab5131, 1:1000, RRID: AB_449369), recombinant anti-RNA polymerase II CTD repeat YSPTSPS (phospho S2) (abcam, ab193468, 1:1000, RRID: N/A), or anti-tubulin (Sigma-Aldrich, T6199, 1:1000, AB_477583). Membranes were incubated with horseradish-peroxidase-conjugated anti-rabbit (Bio-Rad, 1721019, 1:2000, RRID: AB_11125143) or anti-mouse (SouthernBiotech, 1036-05, 1:2000, RRID: AB_2794348) secondary antibodies and visualized using a MicroChemi (DNR Bio Imaging Systems) and GelCapture software (Version 7.0.18).

qPCR

For mRNA transcripts, gravid animals were synchronized and incubated at the restrictive temperature of 25°C to induce dauer formation. Animals were harvested after 48 hours at 25°C and subjected to TRIzol™ Reagent (Invitrogen 15596026) for RNA isolation. The concentration of the RNA was determined with a NanoDrop™ 2000c Spectrophotometer (Thermo Scientific ND-2000). The quality of the RNA was determined with a NanoDrop™ 2000c Spectrophotometer (Thermo Scientific ND-2000) and agarose gel electrophoresis. 1000 ng of purified RNA was used to synthesize cDNA using a High-Capacity RNA-to-cDNA™ Kit (AppliedBiosystems, 4387406). The gene expression levels were determined by qPCR using a 2x SyberGreen qPCR Master-mix (ZmTech Scientifique, Q2100N) and a Bio-Rad CFX384 Real-Time 96-well PCR qPCR Detection System (Bio-Rad). 10 ng of cDNA was used for each qPCR reaction. The gene expression data was analyzed using CFX Maestro Software (Bio-Rad). Relative gene expression was calculated by normalizing to the expression of an alpha-tubulin gene, *tba-1*, which as the loading control. Each relative gene expression value is an independent biological replicate, with each replicate corresponding to the average of a triplicate qPCR reaction. The primer sequences for qPCR can be found in Table S3.

Auxin-inducible degradation (AID) system

Animals were synchronized as described above. To create petri dishes for AID, NGM was prepared as described above but allowed to cool to approximately 30-45°C before auxin is added to the media to a final concentration of 1 mM. A stock solution of auxin was prepared by dissolving it in 70% ethanol. Auxin-containing NGM petri dishes

were then seeded with a thick layer of OP50, allowed to dry at room temperature, and always protected from light. Auxin-containing plates were used within 2 days of drying. NGM plates without auxin were used as a negative control.

QUANTIFICATION AND STATISTICAL ANALYSIS

Bar graphs and fluorescence intensity graphs were generated through GraphPad Prism 7. Pie charts and heat maps were generated through Microsoft Excel. Fluorescence intensity and relative protein abundance were measured using NIH ImageJ. Statistical tests were performed using GraphPad Prism 7 and XLSTAT plugin for Microsoft Excel. The types of statistical tests used in each experiment, n numbers, P values, and other related measures are indicated in each figure and the associated legend. In all figures, ****$P < 0.0001$, ***$P < 0.001$, **$P < 0.01$, *$P < 0.05$; ns, not significant. Replications were done by using different worms performed on different days. Replications for all imaging experiments were performed on different worms on different days. Representative images were generated from more than 10 worms in at least three independently generated lines. RNAi experiments were performed on independently cultured animals and bacterial cultures. Western blots were performed on independently isolated exosomes purifications or animals at least twice. For all *C. elegans* strain used in this study, a population of worms was grown together under identical conditions, and the worms were randomly distributed into different conditions. Worms from a population were randomly chosen for RNAi analyses, post-dauer fertility, Western blot analysis, and imaging experiments.

Acknowledgements: The Canadian Institutes of Health Research (Project Grant, CIHR PJT-180267) supported this work. We acknowledge the *Caenorhabditis elegans* Genetics Center (CGC) for providing *C. elegans* strains. We thank Shaolin Li and Ryan Dawson for technical assistance.

Competing interests: The authors declare no competing interests.

Funding: The Canadian Institutes of Health Research Project Grant CIHR PJT-180267 (RR)

Author contributions: CW, MV, and EJ conceptualized the study, designed the methodology, and conducted the investigation. CW and MV analyzed the data. RR acquired the funding and supervised the study. CW wrote the original draft.

Data and materials availability: All data are available in the main text.

Figures and Tables

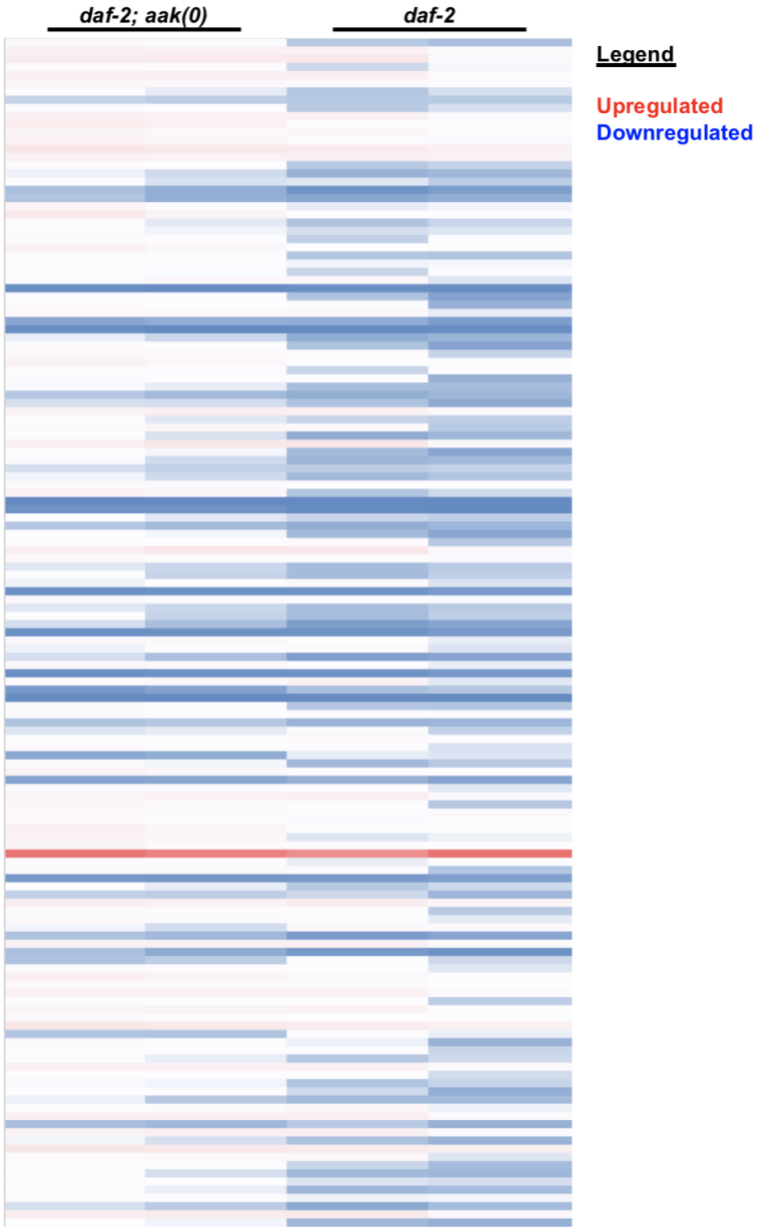

Fig. 4.1. The expression levels of histone writers are downregulated in *daf-2* animals.

Heat map that represents the normalized expression levels of histone writers in *daf-2* and *daf-2; aak(0)* mutants during the dauer stage. Genes that are upregulated or

downregulated are in red or blue colour, respectively. Genes were extracted from Wormbook and WERAM.

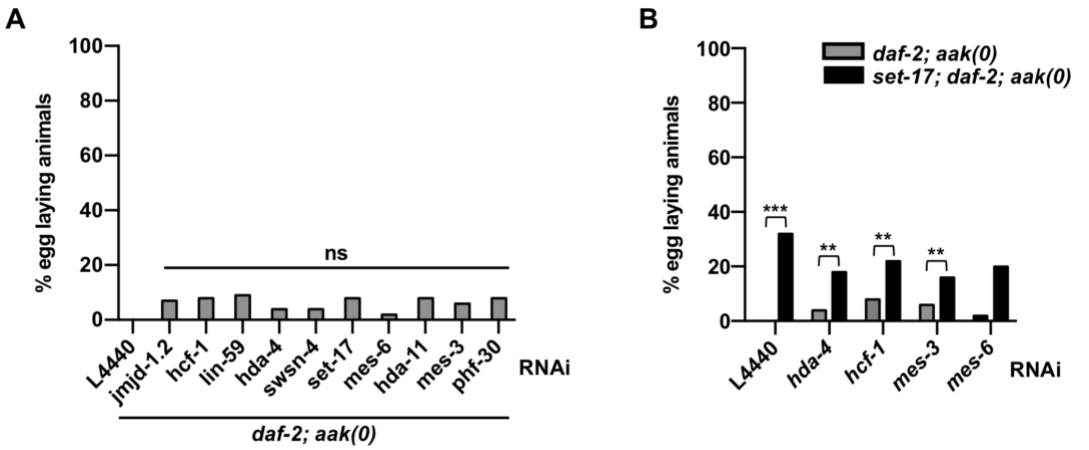

Fig. 4.2. Histone writers act in a concerted manner to ensure quiescence and germ cell integrity.

(**A**) Post-dauer fertility of *daf-2; aak(0)* mutants fed with bacteria expressing dsRNA against various histone writers.

(B) Post-dauer fertility of *daf-2; aak(0)* and *set-17; daf-2; aak(0)* mutants fed with bacteria expressing dsRNA against various histone writers.

***P < 0.001, **P < 0.01, ns, not significant using Marascuilo procedure for post-dauer fertility. n = 50.

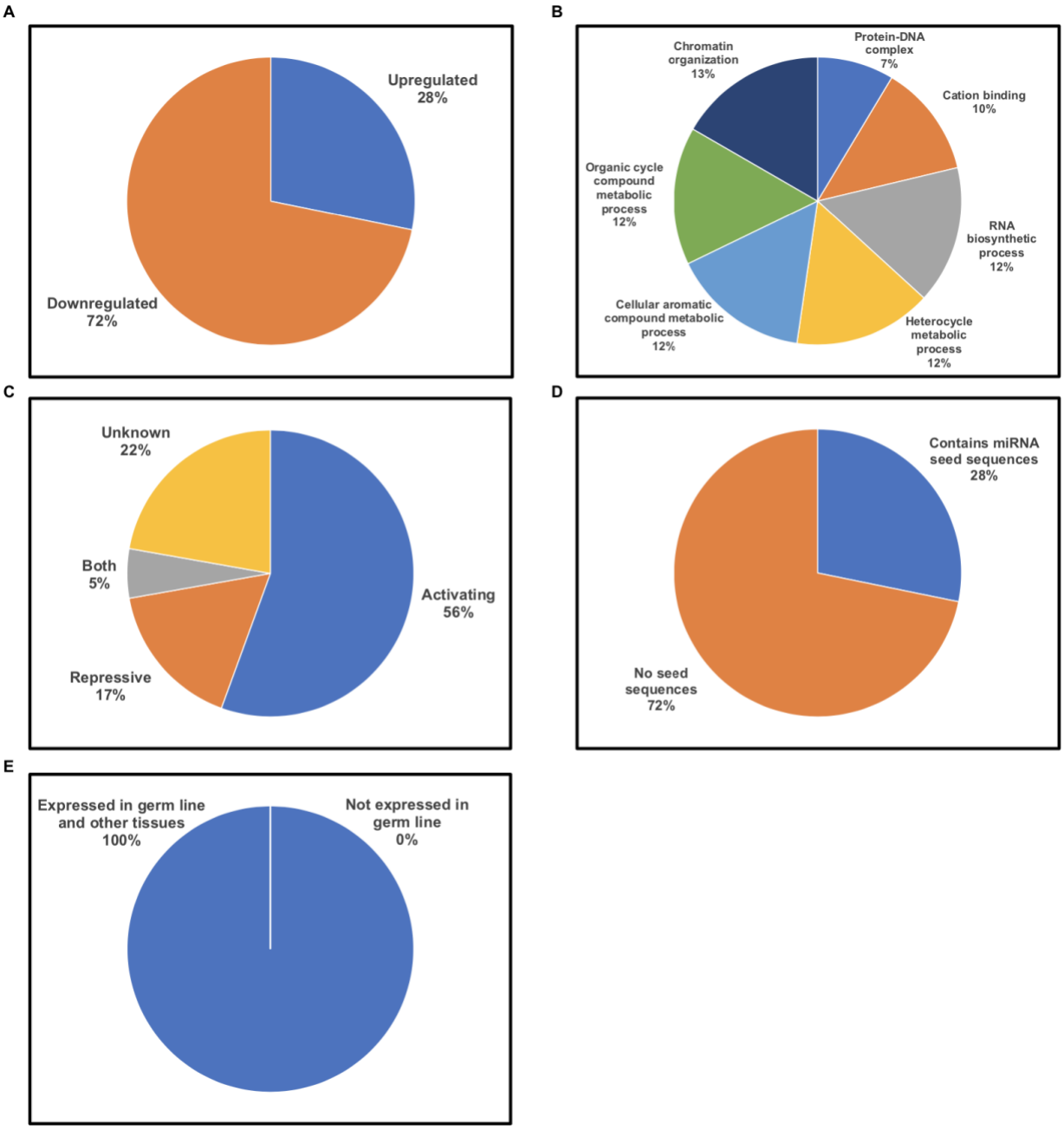

Fig. 4.3. Histone writers that revert the suppression of AMPK defects have a wide range of functions.

(**A-C**) Pie charts of the (A) expression analysis of mRNA extracted from *daf-2* animals, (B) GO term enrichment analysis, (C) predicted function, (D) presence of any high-

stringency miRNA binding sites on the 3'UTR, and (E) tissue-specific expression of the genes that revert the suppression of AMPK germline defects by *tbc-7*. Bioinformatics analysis was conducted using Wormbase (B, C, E) and TargetScanWorm6.2 (D) databases.

Gene (RNAi)	*daf-2* (%)	*daf-2; aak(0); tbc-7* (%)
L4440	100	84
jmjd-1.2	60	0
prmt-5	60	0
swsn-9	68	4
chd-3	64	8
lsy-12	60	16
D1065.3	72	16
psr-1	100	16
jmjc-1	68	20
utx-1	72	20
athp-1	64	24
pbrm-1	68	24
lin-61	76	24
taf-3	83	24
rbr-2	60	28
set-12	80	28
set-4	82	28
hda-6	60	32
sir-2.2	64	32
sea-2	68	32
set-11	75	32
met-1	76	32
sir-2.3	72	40
chd-1	80	40
dpff-1	100	40
jhdm-1	72	48
baz-2	72	48
hat-1	76	48
hda-10	80	48
athp-2	80	52
gfl-1	52	34
ssl-1	88	49
met-2	92	49
isw-1	88	53
htz-1	96	58
ubc-9	92	64
zfp-1	80	64
M03C11.3	92	71
mys-1	88	78
sop-2	88	78
mep-1	92	84

Table 4.1: Post-dauer fertility of *daf-2* and *daf-2; aak(0); tbc-7* mutants fed with dsRNA targeting histone writers.

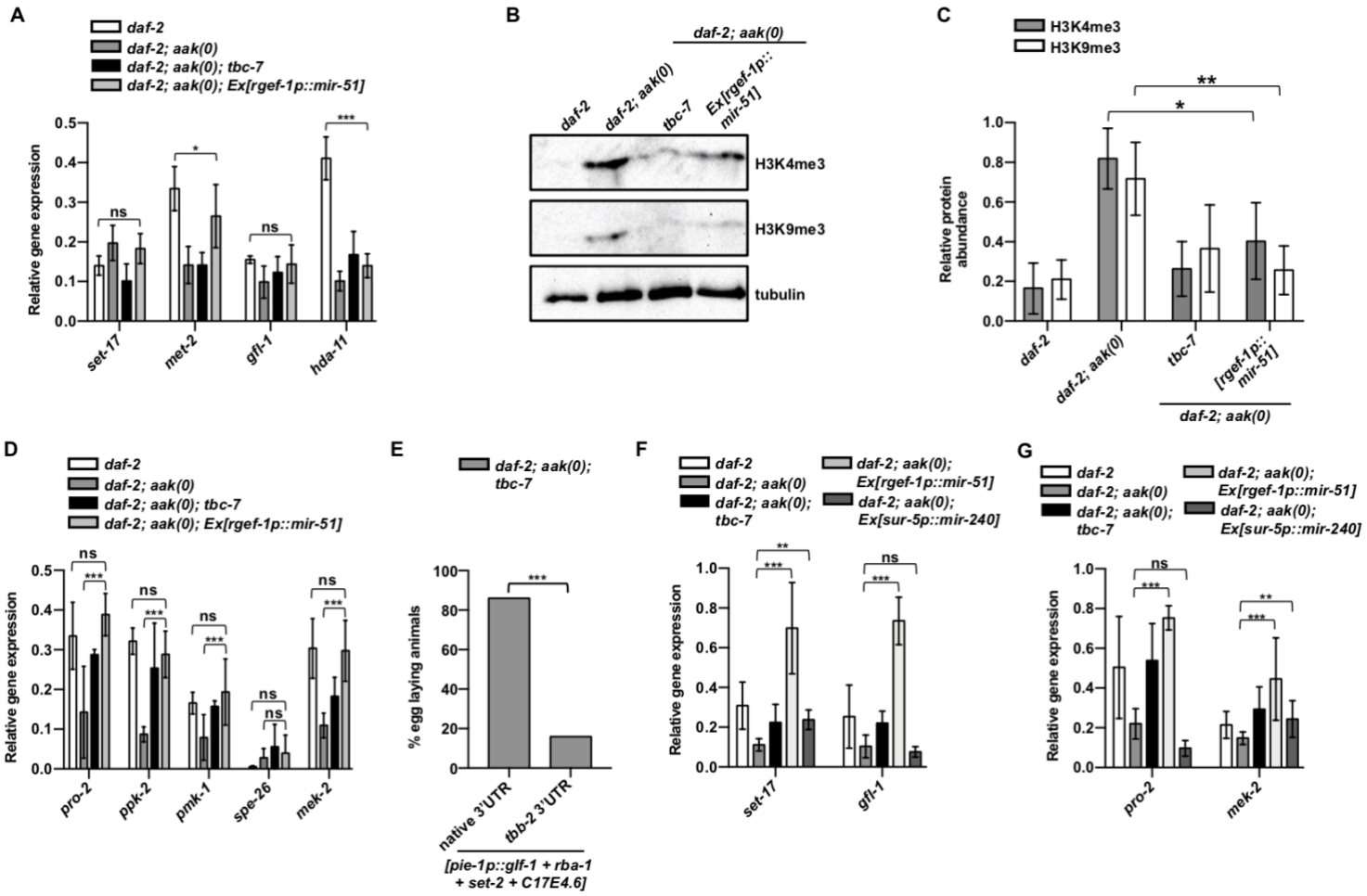

Fig. 4.4. Neuronally-expressed miRNAs regulate the expression of histone writers in the germ line to establish a dauer-specific chromatin landscape and gene expression.

(**A**) qPCR was conducted on *daf-2; aak(0); Ex[rgef-1p::mir-51]* mutants to quantify the levels of histone writers during the dauer stage.

(**B**) Western analysis of whole dauer larvae using antibodies against histone marks associated with active (H3K4me3) and repressive (H3K9me3) transcription in *daf-2*, *daf-2; aak(0)*, *daf-2; aak(0); tbc-7*, and *daf-2; aak(0)* mutants expressing neuronal *mir-51*.

(**C**) Quantification of the Western analysis against histone marks normalized to tubulin loading control using ImageJ software. Representative of three independent experiments. Quantification was generated by ImageJ. **P < 0.001, *P < 0.01 using Student's t-test.

(**D**) qPCR was conducted on *daf-2; aak(0); Ex[rgef-1::mir-51]* mutants to quantify the levels of germline genes that were previously shown to be differentially expressed in the dauer stage.

(E) Post-dauer fertility of *daf-2; aak(0); tbc-7* expressing extra copies of *rba-2*, *C17E4.6*, *gfl-1*, and *set-2* in the germ line using a *pie-1p* promoter with either a universal *tbb-2* 3'UTR or each respective gene's native 3'UTR.

(**F-G**) qPCR was conducted on *daf-2; aak(0); Ex[rgef-1p::mir-240]* mutants to quantify the levels of (F) histone writers and (G) germline-specific genes during the dauer stage. The expression between genotypes were normalized to *tba-1* tubulin loading control.

***P < 0.001, **P < 0.01, ns, not significant using two-way ANOVA. Post-dauer fertility is mean ± SEM. qPCR data are representative of three independent experiments. Relative gene expression is normalized to *tba-1* loading control. Relative protein expression is normalized to tubulin.

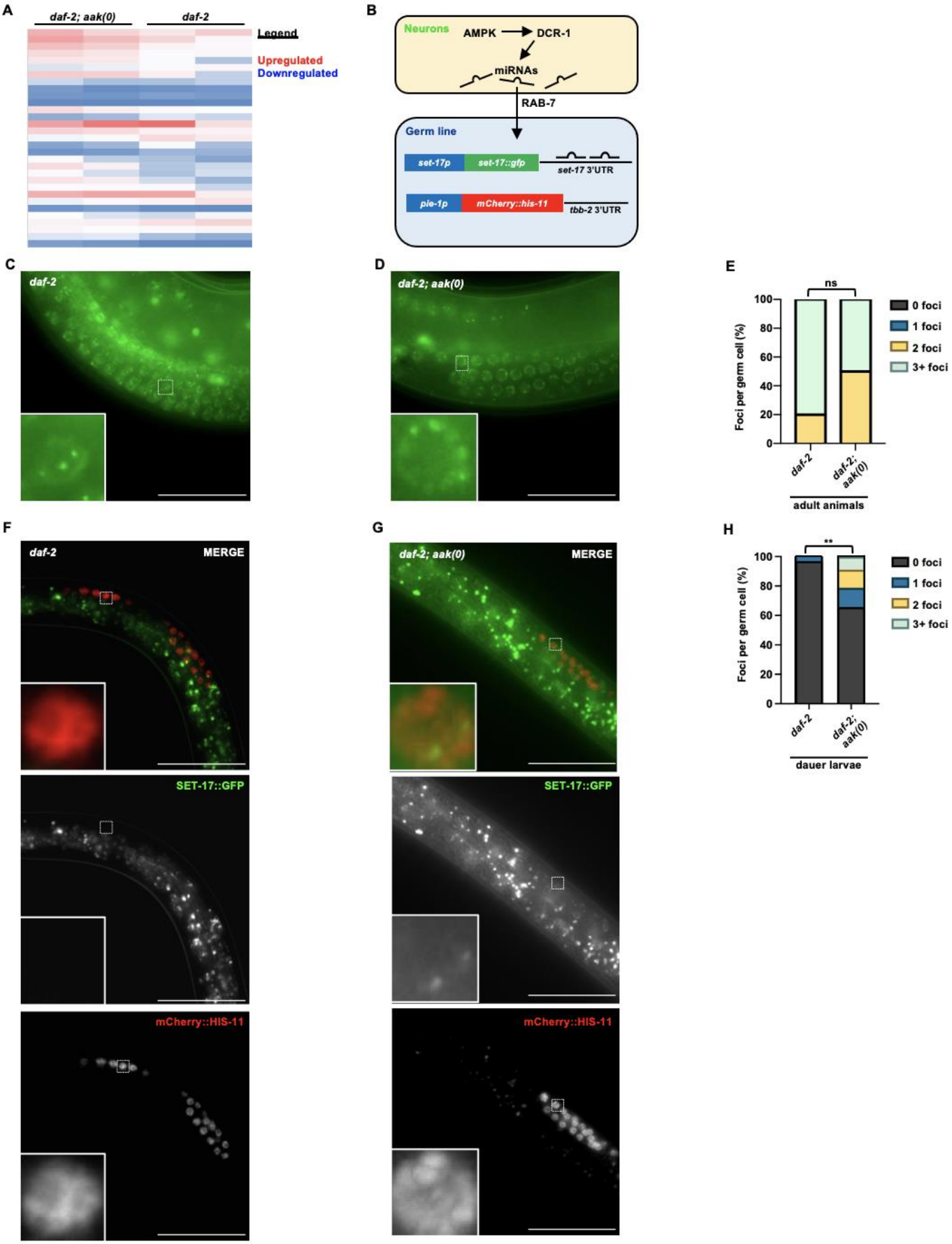
A
daf-2; aak(0)
daf-2
Legend
Upregulated
Downregulated
B
Neurons
AMPK
DCR-1
miRNAs
RAB-7
Germ line
set-17p
set-17::gfp
set-17 3'UTR
pie-1p
mCherry::his-11
tbb-2 3'UTR
C
daf-2
D
daf-2; aak(0)
E
ns
Foci per germ cell (%)
0 foci
1 foci
2 foci
3+ foci
daf-2
daf-2; aak(0)
adult animals
F
daf-2
MERGE
SET-17::GFP
mCherry::HIS-11
G
daf-2; aak(0)
MERGE
SET-17::GFP
mCherry::HIS-11
H
**
Foci per germ cell (%)
0 foci
1 foci
2 foci
3+ foci
daf-2
daf-2; aak(0)
dauer larvae

Fig. 4.5. AMPK regulates germline gene expression during the dauer stage.

(A) Heat map that represents the normalized expression levels of SET domain-containing genes in *daf-2* and *daf-2; aak(0)* mutants during the dauer stage. Genes that are upregulated or downregulated are in red or blue colour, respectively.

(**B**) Graphic description of the germline sensor for histone methyltransferase *set-17*.

(**C-D**) Confocal images of the miRNA sensor for SET-17::GFP in (C) *daf-2* and (D) *daf-2; aak(0)* adult animals.

(**E**) Quantification of the number of SET-17 foci per germ cell in adult stage animals for panels C and D.

(**F-G**) Confocal images of the miRNA sensor for SET-17::GFP in (F) *daf-2* and (G) *daf-2; aak(0)* dauer larvae expressing a germline mCherry::HIS-11 marker.

(**H**) Quantification of the number of SET-17 foci per germ cell in dauer larvae for panels F and G.

Quantification data is representative of three independent experiments; n = 15 animals per condition. **P < 0.01, ns, not significant using two-way ANOVA. Solid white frame indicates position of the higher magnification insets (below). Dotted white lines outline the

gonad. Scale bars, 50 μm. Representative of three independently-generated transgenic lines.

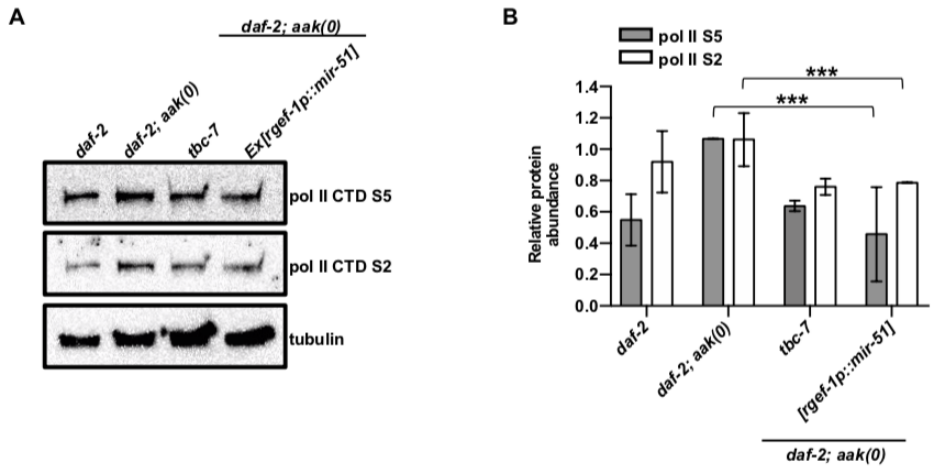

Fig. 4.6. The activity of RNA pol II is affected in AMPK mutants.

(**A**) Western analysis of whole dauer larvae using antibodies against phosphorylated serine 5 and serine 2 of the C-terminal domain of RNA polymerase II in *daf-2*, *daf-2; aak(0)*, *daf-2; aak(0); tbc-7*, and *daf-2; aak(0)* mutants expressing neuronal *mir-51*. Tubulin was used as a loading control.

(**B**) Quantification of the Western analysis against phosphorylated serine residues of the CTD of RNA polymerase II normalized to tubulin loading control using ImageJ software.

Representative of two independent experiments. Quantification was generated by ImageJ. ***P < 0.0001 using Student's t-test.

Cell cycle stage	Gene	Fold Change (Log_2) (dauer)	Fold Change (Log_2) (post-dauer)
G1	*cdk-4*	1.22265192	-0.63239
	cyd-1	1.0322584	0.044672
S	*cdk-2*	-1.9649896	1.824573
	cye-1	-2.0383166	2107.552681
G2	*cdk-2*	-1.9649896	1.824573
	cya-1	-1.790944	1.850527
	cya-2	-2.3421098	0.009119
Mitosis	*cdk-1*	-2.3412024	2.310474
	cyb-1	-2.5330647	3.04981
	cyb-2.1	-2.923514	4.954248
	cyb-2.2	-2.6388067	4.715299
	cyb-3	-2.1811889	3.544366
Meiosis	*him-3*	-3.4057900	1.795598

Table 4.2: Expression analysis of cell cycle markers in *daf-2* animals compared to *daf-2; aak(0)* mutants through mRNA sequencing.

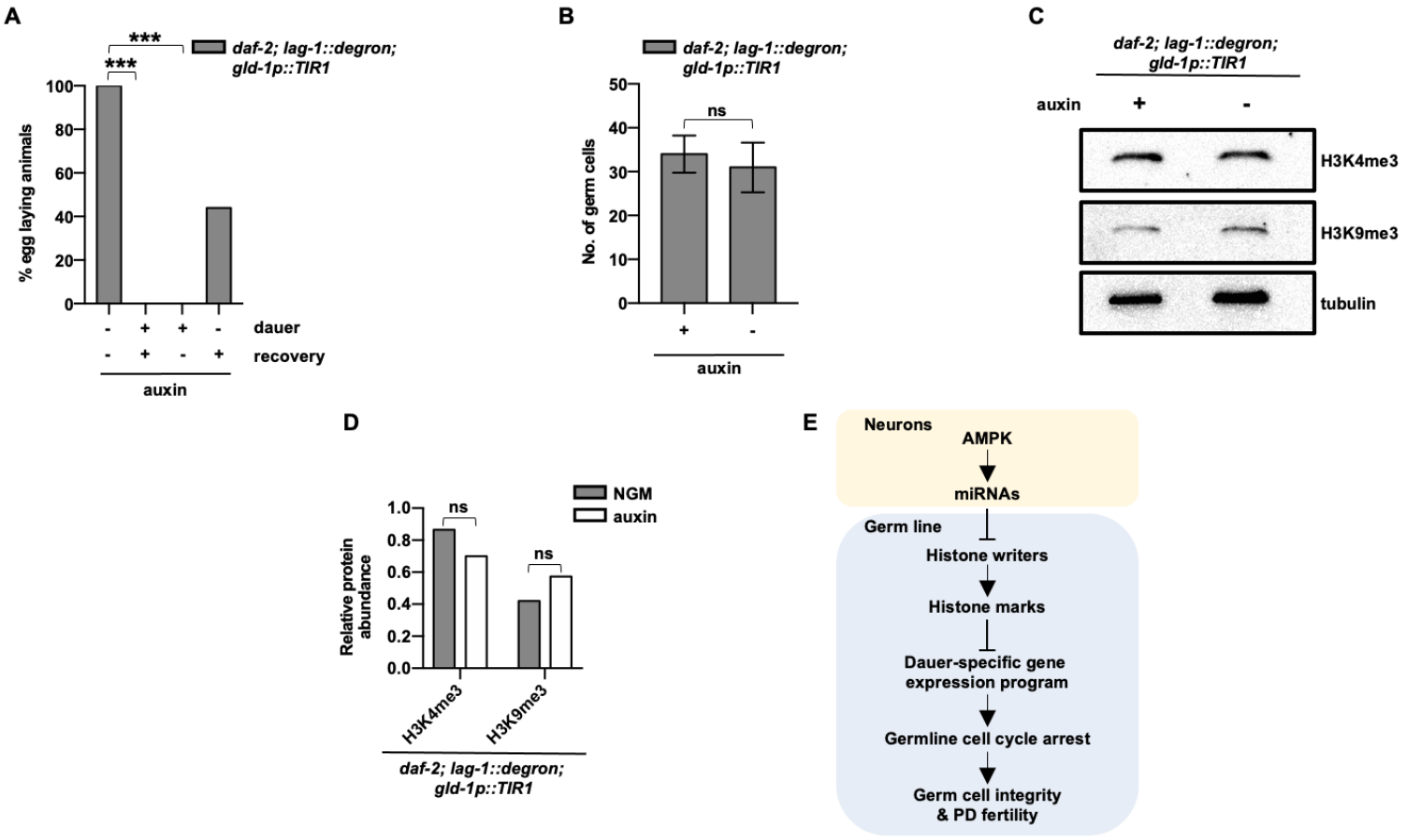

Fig. 4.7. Disrupting the cell cycle does not affect the histone marks.

(**A**) Post-dauer fertility of *daf-2* mutants expressing an endogenously-tagged LAG-1::degron and a single-copy insertion of the TIR1 receptor in the germ line treated with (+) or without (-) auxin during dauer or recovery. ***P < 0.001 using Marascuilo procedure. n = 50.

(**B**) A quantification of the number of germ cells in the dauer larvae of *daf-2* mutants with (+) and without (-) the LAG-1 ligand during the dauer stage. ns, not significant using two-way ANOVA. n = 25.

(**C**) Western analysis using antibodies against histone marks associated with active (H3K4me3) and repressive (H3K9me3) transcription in *daf-2* mutants with (+) and without (-) the LAG-1 ligand during the dauer stage. Tubulin was used as a loading control.

(**D**) Quantification of the Western analysis against histone marks normalized to tubulin loading control using ImageJ software. Representative of one experiment. Quantification was generated by ImageJ. ns, not significant using Student's t-test.

(**E**) Proposed model of the regulation of histone writers by miRNAs to protect germ cell integrity and post-dauer fertility during the dauer stage.

References

Brenner, S. (1974). The genetics of *Caenorhabditis elegans*. Genetics *77*, 71-94.

Chen, J., Mohammad, A., Pazdernik, N., Huang, H., Bowman, B., Tycksen, E., and Schedl, T. (2020). GLP-1 Notch-LAG-1 CSL control of the germline stem cell fate is mediated by transcriptional targets *lst-1* and *sygl-1*. PLoS Genet *16*, e1008650.

Colombo, M., Raposo, G., and Théry, C. (2014). Biogenesis, secretion, and intercellular interactions of exosomes and other extracellular vesicles. Annu Rev Cell Dev Biol *30*, 255-289.

Dalley, B.K., and Golomb, M. (1992). Gene expression in the *Caenorhabditis elegans* dauer larva: developmental regulation of Hsp90 and other genes. Dev Biol *151*, 80-90.

Devaskar, S.U., and Raychaudhuri, S. (2007). Epigenetics – A Science of Heritable Biological Adaptation. Pediatric Research *61*, 1-4.

Di Croce, L., and Helin, K. (2013). Transcriptional regulation by Polycomb group proteins. Nature Structural & Molecular Biology *20*, 1147-1155.

Elena Jurczak, C.W., Richard Roy (2023). AMPK determines small RNA pathway prevalence though Dicer reallocation to enhance miRNA synthesis and mediate soma-to-germ line communication. In 23rd International C elegans Conference (Glasgow, Scottland).

Ellis, R.E., and Stanfield, G.M. (2014). The regulation of spermatogenesis and sperm function in nematodes. Semin Cell Dev Biol *29*, 17-30.

Engert, C.G., Droste, R., van Oudenaarden, A., and Horvitz, H.R. (2018). A *Caenorhabditis elegans* protein with a PRDM9-like SET domain localizes to chromatin-

associated foci and promotes spermatocyte gene expression, sperm production and fertility. PLOS Genetics *14*, e1007295.

Fielenbach, N., and Antebi, A. (2008). *C. elegans* dauer formation and the molecular basis of plasticity. Genes Dev *22*, 2149-2165.

Fraser, A.G., Kamath, R.S., Zipperlen, P., Martinez-Campos, M., Sohrmann, M., and Ahringer, J. (2000). Functional genomic analysis of *C. elegans* chromosome I by systematic RNA interference. Nature *408*, 325-330.

Glover-Cutter, K., Larochelle, S., Erickson, B., Zhang, C., Shokat, K., Fisher, R.P., and Bentley, D.L. (2009). TFIIH-associated Cdk7 kinase functions in phosphorylation of C-terminal domain Ser7 residues, promoter-proximal pausing, and termination by RNA polymerase II. Mol Cell Biol *29*, 5455-5464.

Hsin, J.P., and Manley, J.L. (2012). The RNA polymerase II CTD coordinates transcription and RNA processing. Genes Dev *26*, 2119-2137.

Jenuwein, T., and Allis, C.D. (2001). Translating the histone code. Science *293*, 1074-1080.

Jurczak, E.M., Wong, C., Li, S., Braukmann, F., Sawh, A.N., Duchaine, T.F., Miska, E.A., and Roy, R. (2023). AMPK regulates small RNA pathway prevalence to mediate soma-to-germ line communication and establish germline stem cell quiescence. bioRxiv, 2023.2011.2015.567172.

Kadekar, P., and Roy, R. (2019). AMPK regulates germline stem cell quiescence and integrity through an endogenous small RNA pathway. PLoS Biol *17*, e3000309.

Kalluri, R., and LeBleu, V.S. (2020). The biology, function, and biomedical applications of exosomes. Science *367*.

Kimura, K.D., Tissenbaum, H.A., Liu, Y., and Ruvkun, G. (1997). *daf-2*, an insulin receptor-like gene that regulates longevity and diapause in *Caenorhabditis elegans*. Science *277*, 942-946.

Kingston, R.E., and Tamkun, J.W. (2014). Transcriptional regulation by trithorax-group proteins. Cold Spring Harb Perspect Biol *6*, a019349.

Marshall, N.F., Peng, J., Xie, Z., and Price, D.H. (1996). Control of RNA polymerase II elongation potential by a novel carboxyl-terminal domain kinase. J Biol Chem *271*, 27176-27183.

Narbonne, P., and Roy, R. (2006). Inhibition of germline proliferation during *C. elegans* dauer development requires PTEN, LKB1 and AMPK signalling. Development *133*, 611-619.

Rink, J., Ghigo, E., Kalaidzidis, Y., and Zerial, M. (2005). Rab conversion as a mechanism of progression from early to late endosomes. Cell *122*, 735-749.

Wong, C., Jurczak, E.M., and Roy, R. (2023a). Neuronal exosomes transport a miRNA/RISC cargo to preserve germline stem cell integrity during energy stress. bioRxiv, 2023.2011.2015.567290.

Wong, C., Kadekar, P., Jurczak, E., and Roy, R. (2023b). Germline stem cell integrity and quiescence are controlled by an AMPK-dependent neuronal trafficking pathway. PLOS Genetics *19*, e1010716.

Xu, Y., Zhang, S., Lin, S., Guo, Y., Deng, W., Zhang, Y., and Xue, Y. (2017). WERAM: a database of writers, erasers and readers of histone acetylation and methylation in eukaryotes. Nucleic Acids Res *45*, D264-d270.

Zhang, L., Ward, J.D., Cheng, Z., and Dernburg, A.F. (2015). The auxin-inducible degradation (AID) system enables versatile conditional protein depletion in *C. elegans*. Development *142*, 4374-4384.

Zoghbi, H.Y., and Beaudet, A.L. (2016). Epigenetics and Human Disease. Cold Spring Harb Perspect Biol *8*, a019497.

Chapter 5: General discussion

Animals continuously navigate their ever-changing environments, requiring their tissues to sense and to respond to external cues (Cardoso-Moreira et al., 2019). This communication necessitates the transmission of signals from sensing tissues to both proximal and distal counterparts. Consequently, cells have evolved a repertoire of communication mechanisms, including surface proteins/receptors and neurotransmitter-containing synaptic vesicles for local signalling, as well as hormones and small RNAs for long-range signalling to distant tissues (Nair et al., 2019).

This work highlights a novel form of cellular communication mediated by small RNAs, distinct from traditional neuroendocrinological processes. These small RNAs, including miRNAs, are packaged into extracellular vesicles like exosomes and secreted by donor cells. Upon release, these vesicles travel through the organism and are taken up by the recipient cells, where the small RNAs can modulate gene expression. Unlike hormonal signaling, which relies on the bloodstream, passive diffusion, or active transport to distribute the chemical signals, small RNA-based communication is a direct intercellular transfer of genetic information. Together with traditional hormone or peptide signalling, these intricate communication networks enable coordinated responses across various cellular and physiological contexts.

In *C. elegans*, the neurons are responsible for signalling to other tissues in response to environmental stimuli. For example, during replete conditions, animals will develop through four larval stages to become reproductive adults (Kenyon, 1988). However, if the animal encounters unfavourable growth environments, such as crowding, high temperatures, or starvation, at the end of the L1 stage, it can choose to enter an

alternative life stage known as the dauer stage (Dalley and Golomb, 1992; Fielenbach and Antebi, 2008; Riddle et al., 1981). In its natural settings, *C. elegans* are most often found in the dauer stage due to its enhanced ability to resist environmental challenges. The dauer stage is marked by morphological, metabolic, and behavioural changes. The animal will ration its fat stores and halt reproduction for when growth conditions improve. Most importantly, the germline stem cells will undergo mitotic arrest at the G2 cell cycle stage, presumably to protect the genomic integrity of these cells and to conserve energy during this diapause (Fukuyama et al., 2006; Narbonne and Roy, 2006; Wong et al., 2023b). When growing conditions improve, the animal can exit the dauer stage and continue development with almost no reproductive consequences, and in some cases, with increased reproductive capacity (Hall et al., 2010).

Previous genetic analyses indicate that the LBK1/AMPK signalling axis is important for establishing germline quiescence during the dauer stage (Kadekar et al., 2018; Narbonne et al., 2010; Narbonne and Roy, 2006, 2009). The loss of either LKB1/*par-4* or AMPK/*aak(0)* results in germline hyperplasia during the dauer stage. Many of these mutants will die during this stage, but those that recover will exhibit a highly penetrant post-dauer sterility (Kadekar and Roy, 2019). This finding suggests that although the number of germ cells increase, these cells do not have any reproductive potential and cannot give rise to viable progeny. These defects correlate with an increase in activating and repressive histone marks. Immunofluorescence experiments indicates that the distribution of these histone marks throughout the germ lines of AMPK mutants is misregulated. This abnormal chromatin landscape is the most likely cause of the

aberrant germline gene expression that results in the germline hyperplasia in the dauer stage and the sterility in the post-dauer adult.

Through a forward genetic screen, we identified 8 suppressors of the AMPK germline defect that corresponded to 5 complementation groups (Wong et al., 2023c). Two of the identified alleles, *rr166* and *rr289*, corresponded to *tbc-7*, a RabGAP protein. The detection of multiple alleles affecting the same gene strongly indicates the thoroughness of our genetic screen, affirming its saturation. While deletions of *tbc-7* are sterile, we were able to isolate two unique point mutations that gave rise to hypomorphic *tbc-7* mutants, underscoring the power of genetic screens.

These *tbc-7* alleles were able to suppress the germline hyperplasia and post-dauer sterility typical of AMPK mutants (Wong et al., 2023c). Consistently, the compromise of *tbc-7* activity restores the abundance and distribution of germline histone marks to near wild-type levels. RT-qPCR analyses also indicate that the germline gene expression is corrected in *tbc-7* compromised mutants (Wong et al., 2023a). Intriguingly, these *tbc-7*-suppressed mutants cannot suppress the reduced dauer survival typical of AMPK mutants (Wong et al., 2023c). Wild-type animals can survive in the dauer stage for months, while AMPK mutants die after seven days (Narbonne and Roy, 2009). This loss of dauer survival is partly due to overactive ATGL-1 activity and the premature depletion of lipid stores. Overall, this data suggests that TBC-7 does not regulate triglyceride hydrolysis, but rather it likely regulates the germ line through a separate mechanism during the dauer stage.

By conducting RNAi against every predicted and known Rab protein in the *C. elegans* genome, we identified RAB-7 as one of the potential downstream Rab targets of

TBC-7 (Wong et al., 2023c). While we meticulously examined all Rabs and ensured reproducibility, the trafficking and cell biology fields require more robust, biochemical-based assays (Barr and Lambright, 2010). For example, a yeast two-hybrid or a GFP protein reconstitution assay could be conducted between TBC-7 and every Rab protein to potentially identify additional Rab targets. However, these results would need to be verified *in vivo* in dauer larvae, perhaps through a proximity ligation assay, to claim that any interactions with TBC-7 are physiologically relevant.

Consistent with the neuronal role of AMPK in maintaining quiescence, TBC-7 and its putative target Rab protein, RAB-7, also work in the neurons during the dauer stage (Wong et al., 2023a; Wong et al., 2023c). Genetic analysis indicates that the GAP activity of TBC-7 is regulated by two independent mechanisms; first, AMPK directly phosphorylates TBC-7 to presumably induce the autoinhibition of the RabGAP domain and second, two miRNAs, *mir-1* and *mir-44*, repress the translation of TBC-7 (Wong et al., 2023c). These two mechanisms work in conjunction to ensure that RAB-7 remains active in the neurons at the onset of the dauer stage.

In addition to identifying two alleles of *tbc-7* in our genetic suppressor screen for AMPK germline defects, we also identified 6 additional unique suppressors (Wong et al., 2023c). 5 of the remaining 6 suppressors were predicted to be primarily expressed in the neurons, which is consistent with the role of AMPK and TBC-7 functioning in the neurons. One of the six suppressors is *pmk-2*. PMK-2 is the p38 MAPK ortholog in *C. elegans* that is involved in regulating innate immunity and is activated by the TIR-1/NSY-1/SEK-1 complex (*C. elegans* ortholog of ASK1/SARM/MKK3/6) (Pagano et al., 2015). Similarly, in mammalian systems, the p38 signalling pathway is activated by environmental

stressors, such as osmotic, redox, or radiation (Zarubin and Han, 2005). Activation of this pathway inhibits proliferation and activates cellular differentiation such as transcription factor activity and chromatin remodeling, as well as cell migration.

In *C. elegans*, *pmk-1*, *pmk-2*, and *pmk-3*, are expressed from a single operon along with an upstream gene *islo-1* (Pagano et al., 2015). In wild-type animals, PMK-1 is ubiquitously expressed, while PMK-2 is expressed primarily in the neurons. The expression of the *pmk* genes is regulated by the *mir-58* family in *C. elegans*, wherein *mir-58*, *mir-80*, *mir-81*, and *mir-82* work redundantly to destabilize the *pmk-2* mRNA in non-neuronal cells, thus restricting the expression of *pmk-2* to neuronal cells (Pagano et al., 2015). Interestingly, our genetic analysis shows that *pmk-2* functions in the germ line to cell autonomously regulate germline quiescence during the dauer stage, while the compromise of *pmk-2* in somatic tissues does not suppress the post-dauer sterility. In AMPK mutants, miRNAs, including the *mir-58* family are not expressed in sufficient levels, thus resulting in germline defects (Jurczak et al., 2023). Therefore, in the absence of these miRNAs, *pmk-2* could be aberrantly expressed in non-neuronal tissues including the germ line, resulting in the abnormal regulation of the germline cell cycle. Further exploration into the mechanisms of *pmk-2*, as well as the other remaining 5 suppressors, could elucidate how AMPK establishes germline quiescence during the dauer stage.

The next question that we wanted to address was how RAB-7, a conserved Rab GTPase in the neurons was able to regulate the germ line during the dauer stage. This mechanism is hinted by one of the functions of RAB-7. In endosome maturation, early endosomes and late endosomes are marked with RAB-5 and RAB-7, respectively (Kinchen and Ravichandran, 2010; Poteryaev et al., 2010; Wang et al., 2002). The late

endosome can undergo membrane invaginations to create intralumenal vesicles. This entity, now known as a multivesicular body, can fuse with the plasma membrane to secrete the intralumenal vesicles along with its cargo into the extracellular space. Consistent with the function of RAB-7, when we drove neuronal RAB-7 translationally fused with GFP in dauer larvae, we were able to observe GFP in the germ cells of animals with abrogated TBC-7 function (Wong et al., 2023a).

We purified these GFP::RAB-7-containing vesicles to further characterize them. Through negative-stain transmission electron microscopy combined with immunogold-labelling, we found that RAB-7 localized to the vesicle membrane (Wong et al., 2023a). These vesicles were also within the diameter range of 30-150 nm, which is consistent with exosomes derived from the endosomal route. Western analysis against known exosomal markers, such as CD63/TSP-7, Tsg101/TSG-101, and Alix/ALX-1 indicated that these vesicles could indeed be exosomes (Kalluri and LeBleu, 2020; Wong et al., 2023b). Although there are no widely accepted negative markers for each class of extracellular vesicle, markers for other types of extracellular vesicles (eg. mitochondrial components and cytochrome C for large oncosomes and large EVs, or annexin A1 and ARF6 for microvesicles) could further support the claim that these vesicles are exosomes (Lötvall et al., 2014; Théry et al., 2018). Nanoparticle tracking analysis also indicated the presence of GFP::RAB-7 of neuronal origin and confirmed the diameter range (Wong et al., 2023a).

One active area of research is understanding how these GFP::RAB-7 entities are targeted to the germ line. Strikingly, when GFP::RAB-7 expression was driven in all neurons, these vesicles were only observed in the germ line and in no other tissues

(Poteryaev et al., 2010). This observation suggests that there must be a specific set of surface receptors on the exosomal and germline membranes that allow only the germ line to take up these vesicles. In the *C. elegans* genome, there are 29 SNARE genes with 10 t-SNARE syntaxin homologs, 3 t-SNARES SNAP-25 family, and 16 other SNARES including v-SNARES (Sato et al., 2014). To explore if SNARE proteins play a role in targeting these exosomes for fusion with the germline membrane, a RNAi screen of all SNARE proteins could be conducted in *tbc-7*-suppressed mutants. Compromising the required SNARE protein should reverse the suppression of AMPK germline defects. Any identified genes can be subjected to tissue-specific RNAi experiments to determine whether it is required in the neurons as a v-SNARE or in the germ line as a t-SNARE. Alternatively, it is possible that these RAB-7-derived exosomes do not rely on the activity of SNARE proteins to tether and fuse with the germline membrane. Thus, other avenues such as tandem mass spectrometry of the isolated RAB-7-containing exosomes should be explored to identify the navigator and/or the factors required for cell-type specific docking of these exosomes.

Furthermore, we found that TBC-7/RAB-7 works in serotonergic neurons to secrete these exosomes during the dauer stage (Wong et al., 2023a). There are three major pairs of neurons, NSM, ADF, and HSN, that belong in the serotonergic class in addition to other individual neurons (Chase and Koelle, 2007). The NSM and ADF neurons reside in the head of the animal near the pharynx and the terminal bulb. On the contrary, HSN resides near the mid body of the animal and enervates the vulva muscles and vulval in the adult animal (Adler et al., 2006; Olsson-Carter and Slack, 2010). The HSN neuron does not elongate and form an axon until the late L4 larval stage, thus the

HSN neuron is in close proximity to the germ line during the dauer stage. Therefore, proximity between the neuron and the germ line could also be a reason as to why these RAB-7-derived exosomes only end up in the germ line.

This hypothesis can be tested in two different ways. HSN is a hermaphrodite-specific neuron, so the germ lines of males carrying the neuronal GFP::RAB-7 transgene could be examined for presence of GFP (White et al., 1986). If these males have GFP during the dauer stage, then the hypothesis of the compatibility between surface receptors or SNARE proteins on the two membranes would be strengthened, as males do not have HSN neurons. Conversely, if these males do not have germline GFP expression, it could be possible that HSN neurons are responsible for secreting the RAB-7-containing exosomes. Furthermore, if proximity is the key for targeting these exosomes to the germ line, then only the HSN neurons should be capable of providing the germ line with exosomes, while other serotonergic neurons like NSM and ADF that reside in the head of the animal should not be able to. With the recent advancement of reporter gene technology and single-cell sequencing and mapping, there are now ADF- and HSN-specific promoters (Fagan et al., 2018; Lloret-Fernández et al., 2018). Therefore, the question of proximity between the neurons and the germ line could be addressed by driving GFP::RAB-7 using these ADF- or HSN-specific promoters and examining the germ lines of dauer larvae for the presence of GFP. However, we cannot eliminate the possibility that multiple mechanisms are working in tandem, where the HSN neurons could be secreting exosomes that contain v-SNARES that target t-SNARES that are only found on the germline membrane.

In a separate study, we observed that AMPK mutants are insensitive towards exogenous dsRNA, regardless of how these dsRNA are introduced (Jurczak et al., 2023). We found that by introducing extra copies of DCR-1 in AMPK mutants, we could restore the sensitivity of these animals towards dsRNA, suggesting that a lack of dsRNA processing machinery could be the basis of the RNAi deficient phenotype. We also found that the introduction of extra copies of DCR-1 in somatic cells suppressed the dsRNA insensitivity and, surprisingly, the AMPK germline defects, suggesting a correlation between the RNAi defective phenotype and the germ cell integrity. Consistent with this hypothesis, small RNA sequencing analysis of AMPK mutants compared to *daf-2* control animals indicates that all classes of small RNAs are upregulated while only miRNAs are downregulated, suggesting that there is an imbalance of RNA processing in AMPK mutants. Moreover, when we introduced extra copies of these downregulated miRNAs in these mutants, we were able to suppress the AMPK germline defects.

Interestingly, when we conducted RNAi against the mRNA targets of these miRNAs, we were unable to identify any additional genes that suppressed the AMPK germline defects to the same degree as the *tbc-7* alleles, *rr166* and *rr289 (Wong et al., 2023a)*. Additionally, introducing extra copies of individual miRNAs that are downregulated in the absence of AMPK suppresses the defects (Jurczak et al., 2023; Wong et al., 2023a) These findings suggest that the downregulation of the mRNA targets of any single miRNA is not the primary factor that maintains germ cell integrity. Rather, the introduction of an exogenous miRNA locks DCR-1 and its binding partner RBPL-1 in a miRNA production competent formation establishing germline quiescence and germ cell integrity during the dauer stage (Jurczak et al., 2023). Overall, these findings imply that

AMPK mutants are transcribing sufficient levels of pri-miRNAs and that at least one cause of the AMPK germline defects is a lack of machinery needed for the processing of pre-miRNA into mature miRNA.

The small RNA sequencing data also prompted an investigation into what small RNAs, if any, are packaged into these RAB-7-derived exosomes. By screening all the small RNA biogenesis components using RNAi in *tbc-7*-suppressed mutants, we found that only the miRNA biogenesis pathway in the neurons is required to maintain germ cell integrity (Wong et al., 2023a). This data was complemented by the detection of *mir-51* using qPCR in purified exosomes using specialized TaqMan primers.

One question that still remains is how do the DCR-1/RBPL-1 and TBC-7/RAB-7 pathways fit together? We found that correcting either one of these pathways in AMPK mutants is sufficient to suppress the AMPK germline defects (Jurczak et al., 2023; Wong et al., 2023a). However, it is not clear if suppressing TBC-7 activity also corrects the production of miRNAs, as the incorporation of the miRISC into exosomes is required to maintain germ cell integrity. On the contrary, how are the mature miRNAs produced by DCR-1 and RBPL-1 delivered to the germ line in the absence of RAB-7 activity? These questions remain to be answered. It is possible that these two pathways are independently regulated or perhaps there is an additional link or feedback cycle that has yet to be uncovered. One immediate experiment would be to assess the levels of pre-miRNAs and mature miRNAs in *tbc-7*-suppressed mutants. If the levels of mature miRNAs are similar to the levels found in wild-type control *daf-2* animals, then perhaps there is a RAB-7 effector that stimulates the association of DCR-1 and RBPL-1.

We used *mir-51* as a proxy for miRNAs in this work, as we assumed that many families of miRNAs were produced when any exogenous miRNA is introduced. We found that short motifs on the mature sequence of *mir-51* are required for its loading into exosomes (Wong et al., 2023a). By scrambling these EXOmotifs, we disrupt the incorporation of *mir-51* into exosomes and also inhibit its ability to suppress the AMPK germline defects. These experiments highlighted the role and significance of EXOmotifs in *C. elegans*. However, the physiological relevance of CELLmotifs, short cis-regulator sequences that signal the loading machinery to exclude a particular miRNA from exosomes, has yet to be described in *C. elegans* (Garcia-Martin et al., 2022). To explore this avenue, the EXOmotifs found on *mir-51* could be converted into CELLmotifs through CRISPR/Cas9 genome editing. Then, the presence of *mir-51* could be assessed in purified exosomes through TaqMan RT-qPCR. If *C. elegans* possessed the cellular machinery that can distinguish between EXOmotifs and CELLmotifs, then replacing the EXOmotifs with CELLmotifs should lead to the exclusion of *mir-51* from the exosomes. Instead, through qPCR analysis, we should observe high levels of *mir-51* in RNA purified from whole dauer larvae and a significant reduction in RNA purified from the exosomes. Alternatively, all miRNAs could be retained by default in *C. elegans* and only miRNAs containing EXOmotifs are directed into vesicles.

We also showed that SID-3, SID-5, and RME-8 were required to either produce these exosomes in the neurons (RME-8 and SID-5) or take up these exosomes in the germ line (SID-3) (Wong et al., 2023a). Through tissue-specific RNAi experiments, we were able to pinpoint whether these genes were required in the neurons or in the germ line. Other works have highlighted the importance of the kinase domain of SID-3 as an

importer of dsRNA (Jose et al., 2012; Shen et al., 2011). By mutating the catalytic lysine into an adenine, we found that the kinase domain of SID-3 is required to import a neuronally produced miRNA into the germ line (Wong et al., 2023a). However, additional research must be conducted to meticulously determine the exact function of each gene product in this TBC-7/RAB-7 signalling pathway. While there is literature to suggest that SID-3 phosphorylates dynamin and other cytoskeletal components to stimulate endocytosis, more detailed imaging experiments are required to determine if the kinase activity is essential for the importing of exosomes by reshaping the germline plasma membrane during the dauer stage (Gao et al., 2020; Shen et al., 2011). While this hypothesis is probable, we cannot rule out that other phosphorylation targets of SID-3 could be involved in the importing of exosomes or that SID-3 could be directly regulating the cell cycle, downstream of exosomal miRISC activity.

In AMPK mutants, we found that the abundance and distribution of the histone marks in the germ line are misregulated, suggesting that the activity of the histone writers is maladaptive for the dauer larvae (Kadekar and Roy, 2019; Wong et al., 2023a). mRNA sequencing reveals that the expression of many histone writers are upregulated in AMPK mutants, which is consistent with the increase of histone marks. Therefore, we conducted RNAi against histone writers that have been previously characterized and were identified through WERAM, an online database for all histone writers in the *C. elegans* genome. To our surprise, we could not identify one histone writer that when compromised could suppress the AMPK germline defects. These data suggest that the expression of many histone writers must be suppressed in a concerted manner at the onset of the dauer stage to prevent the establishment of a reproductive program in the germ line. Therefore, we

examined the expression of a subset of histone writers after driving *mir-51* expression in the neurons of AMPK mutants and found that the levels of histone writers and histone marks in the germ line were corrected.

To show that the expression of one miRNA increases the expression of most miRNAs in AMPK mutants, we drove *mir-240*, a miRNA that does not have any known interactions with other miRNA families in *C. elegans*, and assessed the expression of the histone writers and germline-specific genes. We found that the expression of *mir-240* corrected the expression of histone writers and germline-specific genes. Overall, our data suggests that the miRNAs produced in the neurons are transported to the germ line through exosomes produced by RAB-7 activity. At the germ line, these miRISC are released to suppress the expression of these histone writers to maintain germline quiescence and germ cell integrity during the dauer stage.

While histone writers were identified as a potential mRNA target for the exosomal miRISC, these exosomal miRNAs may be post-transcriptionally regulating other genes. Recent studies have also shown interactions between miRNAs and lncRNAs to regulate gene expression (López-Urrutia et al., 2019; Ratti et al., 2020). Thus, miRNAs may interact with other RNA populations to establish a gene expression program that is appropriate for the dauer stage.

By using genetic tools like the auxin-inducible degradation system, we assessed the effects of altering the germline cell cycle during the dauer stage on germ cell integrity (Zhang et al., 2015). By reducing LAG-1 expression, we forced all the germline stem cells to undergo meiosis at the onset of the dauer stage (Chen et al., 2020). Consistent with our phenotype in AMPK mutants, disrupting the quiescence during the dauer stage

renders the otherwise wild-type animals post-dauer sterile (Kadekar and Roy, 2019; Narbonne and Roy, 2006). Using this tool, we wanted to determine if the histone marks were responsible for the cell cycle arrest, or alternatively, if the cell cycle arrest dictates the establishment of the chromatin landscape. Interestingly, forcing the germ cells to undergo meiosis does not phenocopy the germline hyperplasia and increased abundance of histone marks observed in AMPK mutants. Western analysis of activating and repressive histone marks in animals with reduced LAG-1 expression resembles *daf-2* control animals rather than AMPK mutants. These data suggest that the changes in histone marks and germline gene expression could regulate the germline cell cycle. However, further experiments such as examining the germline gene expression of animals with reduced LAG-1 expression are needed to place the regulation of the germline cell cycle downstream of the activity of histone writers.

The nervous system constitutes the perfect organ system for AMPK activation. During unfavourable growth conditions, AMPK becomes activated in the serotonergic neurons to signal the germ line to enter a quiescent state and adopt a stress-resistant gene expression program (Wong et al., 2023a). Thus, our findings that AMPK works primarily in the neurons to maintain quiescence and germ cell integrity during the dauer stage are consistent with the evolutionary role of neurons as a bridge between external stimuli and physiological responses.

Strikingly, the mechanism that we described in this work where AMPK indirectly activates RAB-7 activity to produce miRISC-containing exosomes is similar to the packaging of chemical signals in synaptic vesicles to elicit a physiological response in the downstream interneuron or motor neuron (Citri and Malenka, 2008). In synaptic neurons,

neurotransmitters are stored in vesicles that localize to the axon terminal. Upon receiving the appropriate signals, these vesicles are released into the synaptic cleft and taken up by the postsynaptic receptors to enervate the downstream neuron. Similarly, when the dauer cues are received by the neurons, AMPK becomes activated in the serotonergic neurons to stimulate the packaging and release of neuronal exosomes that contain miRISC (Wong et al., 2023a). Rather than exciting a downstream neuron, these miRISC-containing exosomes target the germline stem cells where the miRISC are poised to act upon delivery (Ratti et al., 2020). This novel mechanism is consistent with the role of the amphid sensory neurons, ADF, ASI, and ASG in dauer formation (Fielenbach and Antebi, 2008).

Final Statement

In this study, I have identified an AMPK-dependent signalling pathway between the neurons and the germ line, which is mediated by miRNAs encapsulated in exosomes. I showed that these exosomes are derived from the endosomal pathway and are loaded with active miRISC complexes (Wong et al., 2023a). Upon entry into the dauer stage, these exosomes are secreted from the neurons and impinge upon the germ line to affect gene expression. I showed that neuronal miRNAs repress the expression of germline histone modifying enzymes in a concerted manner. By establishing a chromatin landscape that is suitable for the metabolic requirements of the dauer stage, these neuronal exosomal miRNAs ensure that the animal can maintain their germ cell quiescence to preserve its reproductive capacity (Wong et al., 2023a).

The discovery and characterization of exosomes and extracellular vesicles in *C. elegans* particularly their RNA cargo provides an interesting avenue for the development of more efficient and targeted RNA-based therapies. In the wake of the COVID-19 pandemic, mRNA-based vaccines were developed in record time and relied on the packaging of the RNA contents in lipid-based nanoparticles (Baden Lindsey et al., 2021; Polack Fernando et al., 2020). While these vaccines were sufficient to trigger an immune response, it is estimated that only a small percentage of these particles are taken up by the immune cells (Castruita et al., 2023; Sahay et al., 2013). The efficiency of these particles are dependent on a variety of factors including their lipid composition and diameter (Gilleron et al., 2013; Hou et al., 2021). Here we show that exosomes produced by the neurons of *C. elegans* are readily taken up by the germ line, resulting in the strong expression of fluorescently-labelled exosomal components in the recipient cells (Wong et al., 2023c). These data suggest that key proteins, which could enhance the uptake efficiency of lipid nanoparticles, may reside in the lipid and/or protein composition of these RAB-7-dependent neuronal exosomes. By fine-tuning the lipid bilayer composition, the efficiency of RNA-based therapies could be dramatically improved. Identifying these enhancing factors would decrease the quantity of particles required per dose, make the therapy more cost-effective, reduce patient toxicity risk, and potentially increase the availability of doses worldwide to treat a wide spectrum of diseases.

References

Adler, C.E., Fetter, R.D., and Bargmann, C.I. (2006). UNC-6/Netrin induces neuronal asymmetry and defines the site of axon formation. Nat Neurosci *9*, 511-518.

Baden Lindsey, R., El Sahly Hana, M., Essink, B., Kotloff, K., Frey, S., Novak, R., Diemert, D., Spector Stephen, A., Rouphael, N., Creech, C.B.*, et al.* (2021). Efficacy and Safety of the mRNA-1273 SARS-CoV-2 Vaccine. New England Journal of Medicine *384*, 403-416.

Barr, F., and Lambright, D.G. (2010). Rab GEFs and GAPs. Curr Opin Cell Biol *22*, 461-470.

Cardoso-Moreira, M., Halbert, J., Valloton, D., Velten, B., Chen, C., Shao, Y., Liechti, A., Ascenção, K., Rummel, C., Ovchinnikova, S.*, et al.* (2019). Gene expression across mammalian organ development. Nature *571*, 505-509.

Castruita, J.A.S., Schneider, U.V., Mollerup, S., Leineweber, T.D., Weis, N., Bukh, J., Pedersen, M.S., and Westh, H. (2023). SARS-CoV-2 spike mRNA vaccine sequences circulate in blood up to 28 days after COVID-19 vaccination. Apmis *131*, 128-132.

Chase, D.L., and Koelle, M.R. (2007). Biogenic amine neurotransmitters in *C. elegans*. WormBook, 1-15.

Chen, J., Mohammad, A., Pazdernik, N., Huang, H., Bowman, B., Tycksen, E., and Schedl, T. (2020). GLP-1 Notch-LAG-1 CSL control of the germline stem cell fate is mediated by transcriptional targets *lst-1* and *sygl-1*. PLoS Genet *16*, e1008650.

Citri, A., and Malenka, R.C. (2008). Synaptic Plasticity: Multiple Forms, Functions, and Mechanisms. Neuropsychopharmacology *33*, 18-41.

Fagan, K.A., Luo, J., Lagoy, R.C., Schroeder, F.C., Albrecht, D.R., and Portman, D.S. (2018). A Single-Neuron Chemosensory Switch Determines the Valence of a Sexually Dimorphic Sensory Behavior. Curr Biol *28*, 902-914.e905.

Fielenbach, N., and Antebi, A. (2008). *C. elegans* dauer formation and the molecular basis of plasticity. Genes Dev *22*, 2149-2165.

Fukuyama, M., Rougvie, A.E., and Rothman, J.H. (2006). *C. elegans* DAF-18/PTEN Mediates Nutrient-Dependent Arrest of Cell Cycle and Growth in the Germline. Current Biology *16*, 773-779.

Gao, J., Zhao, L., Luo, Q., Liu, S., Lin, Z., Wang, P., Fu, X., Chen, J., Zhang, H., Lin, L.*, et al.* (2020). An EHBP-1-SID-3-DYN-1 axis promotes membranous tubule fission during endocytic recycling. PLoS Genet *16*, e1008763.

Garcia-Martin, R., Wang, G., Brandão, B.B., Zanotto, T.M., Shah, S., Kumar Patel, S., Schilling, B., and Kahn, C.R. (2022). MicroRNA sequence codes for small extracellular vesicle release and cellular retention. Nature *601*, 446-451.

Gilleron, J., Querbes, W., Zeigerer, A., Borodovsky, A., Marsico, G., Schubert, U., Manygoats, K., Seifert, S., Andree, C., Stöter, M.*, et al.* (2013). Image-based analysis of lipid nanoparticle–mediated siRNA delivery, intracellular trafficking and endosomal escape. Nature Biotechnology *31*, 638-646.

Hall, S.E., Beverly, M., Russ, C., Nusbaum, C., and Sengupta, P. (2010). A cellular memory of developmental history generates phenotypic diversity in *C. elegans*. Curr Biol *20*, 149-155.

Hou, X., Zaks, T., Langer, R., and Dong, Y. (2021). Lipid nanoparticles for mRNA delivery. Nature Reviews Materials *6*, 1078-1094.

Jose, A.M., Kim, Y.A., Leal-Ekman, S., and Hunter, C.P. (2012). Conserved tyrosine kinase promotes the import of silencing RNA into *Caenorhabditis elegans* cells. Proceedings of the National Academy of Sciences of the United States of America *109*, 14520-14525.

Jurczak, E.M., Wong, C., Li, S., Braukmann, F., Sawh, A.N., Duchaine, T.F., Miska, E.A., and Roy, R. (2023). AMPK regulates small RNA pathway prevalence to mediate soma-to-germ line communication and establish germline stem cell quiescence. bioRxiv, 2023.2011.2015.567172.

Kadekar, P., Chaouni, R., Clark, E., Kazanets, A., and Roy, R. (2018). Genome-wide surveys reveal polarity and cytoskeletal regulators mediate LKB1-associated germline stem cell quiescence. BMC Genomics *19*, 462.

Kadekar, P., and Roy, R. (2019). AMPK regulates germline stem cell quiescence and integrity through an endogenous small RNA pathway. PLoS Biol *17*, e3000309.

Kalluri, R., and LeBleu, V.S. (2020). The biology, function, and biomedical applications of exosomes. Science *367*.

Kenyon, C. (1988). The nematode *Caenorhabditis elegans*. Science *240*, 1448-1453.

Kinchen, J.M., and Ravichandran, K.S. (2010). Identification of two evolutionarily conserved genes regulating processing of engulfed apoptotic cells. Nature *464*, 778-782.

Lloret-Fernández, C., Maicas, M., Mora-Martínez, C., Artacho, A., Jimeno-Martín, Á., Chirivella, L., Weinberg, P., and Flames, N. (2018). A transcription factor collective defines the HSN serotonergic neuron regulatory landscape. Elife *7*.

López-Urrutia, E., Bustamante Montes, L.P., Ladrón de Guevara Cervantes, D., Pérez-Plasencia, C., and Campos-Parra, A.D. (2019). Crosstalk Between Long Non-coding RNAs, Micro-RNAs and mRNAs: Deciphering Molecular Mechanisms of Master Regulators in Cancer. Front Oncol *9*, 669.

Lötvall, J., Hill, A.F., Hochberg, F., Buzás, E.I., Di Vizio, D., Gardiner, C., Gho, Y.S., Kurochkin, I.V., Mathivanan, S., Quesenberry, P.*, et al.* (2014). Minimal experimental requirements for definition of extracellular vesicles and their functions: a position statement from the International Society for Extracellular Vesicles. J Extracell Vesicles *3*, 26913.

Nair, A., Chauhan, P., Saha, B., and Kubatzky, K.F. (2019). Conceptual Evolution of Cell Signaling. Int J Mol Sci *20*.

Narbonne, P., Hyenne, V., Li, S., Labbé, J.-C., and Roy, R. (2010). Differential requirements for STRAD in LKB1-dependent functions in *C. elegans*. Development *137*, 661-670.

Narbonne, P., and Roy, R. (2006). Inhibition of germline proliferation during *C. elegans* dauer development requires PTEN, LKB1 and AMPK signalling. Development *133*, 611-619.

Narbonne, P., and Roy, R. (2009). *Caenorhabditis elegans* dauers need LKB1/AMPK to ration lipid reserves and ensure long-term survival. Nature *457*, 210-214.

Olsson-Carter, K., and Slack, F.J. (2010). A developmental timing switch promotes axon outgrowth independent of known guidance receptors. PLoS Genet *6*.

Pagano, D.J., Kingston, E.R., and Kim, D.H. (2015). Tissue Expression Pattern of PMK-2 p38 MAPK Is Established by the miR-58 Family in *C. elegans*. PLOS Genetics *11*, e1004997.

Polack Fernando, P., Thomas Stephen, J., Kitchin, N., Absalon, J., Gurtman, A., Lockhart, S., Perez John, L., Pérez Marc, G., Moreira Edson, D., Zerbini, C.*, et al.* (2020). Safety and Efficacy of the BNT162b2 mRNA Covid-19 Vaccine. New England Journal of Medicine *383*, 2603-2615.

Poteryaev, D., Datta, S., Ackema, K., Zerial, M., and Spang, A. (2010). Identification of the switch in early-to-late endosome transition. Cell *141*, 497-508.

Ratti, M., Lampis, A., Ghidini, M., Salati, M., Mirchev, M.B., Valeri, N., and Hahne, J.C. (2020). MicroRNAs (miRNAs) and Long Non-Coding RNAs (lncRNAs) as New Tools for Cancer Therapy: First Steps from Bench to Bedside. Target Oncol *15*, 261-278.

Sahay, G., Querbes, W., Alabi, C., Eltoukhy, A., Sarkar, S., Zurenko, C., Karagiannis, E., Love, K., Chen, D., Zoncu, R.*, et al.* (2013). Efficiency of siRNA delivery by lipid nanoparticles is limited by endocytic recycling. Nature Biotechnology *31*, 653-658.

Sato, K., Norris, A., Sato, M., and Grant, B.D. (2014). *C. elegans* as a model for membrane traffic. WormBook, 1-47.

Shen, H., Ferguson, S.M., Dephoure, N., Park, R., Yang, Y., Volpicelli-Daley, L., Gygi, S., Schlessinger, J., and De Camilli, P. (2011). Constitutive activated Cdc42-associated kinase (Ack) phosphorylation at arrested endocytic clathrin-coated pits of cells that lack dynamin. Molecular biology of the cell *22*, 493-502.

Théry, C., Witwer, K.W., Aikawa, E., Alcaraz, M.J., Anderson, J.D., Andriantsitohaina, R., Antoniou, A., Arab, T., Archer, F., Atkin-Smith, G.K.*, et al.* (2018). Minimal information for studies of extracellular vesicles 2018 (MISEV2018): a position statement of the International Society for Extracellular Vesicles and update of the MISEV2014 guidelines. J Extracell Vesicles *7*, 1535750.

Wang, C.-W., Stromhaug, P.E., Shima, J., and Klionsky, D.J. (2002). The Ccz1-Mon1 protein complex is required for the late step of multiple vacuole delivery pathways. Journal of biological chemistry *277*, 47917-47927.

White, J.G., Southgate, E., Thomson, J.N., and Brenner, S. (1986). The structure of the nervous system of the nematode *Caenorhabditis elegans*. Philos Trans R Soc Lond B Biol Sci *314*, 1-340.

Wong, C., Jurczak, E.M., and Roy, R. (2023a). Neuronal exosomes transport a miRNA/RISC cargo to preserve germline stem cell integrity during energy stress. bioRxiv, 2023.2011.2015.567290.

Wong, C., Kadekar, P., Jurczak, E., and Roy, R. (2023b). Germline stem cell integrity and quiescence are controlled by an AMPK-dependent neuronal trafficking pathway. PLoS Genet *19*, e1010716.

Wong, C., Kadekar, P., Jurczak, E., and Roy, R. (2023c). Germline stem cell integrity and quiescence are controlled by an AMPK-dependent neuronal trafficking pathway. PLOS Genetics *19*, e1010716.

Zarubin, T., and Han, J. (2005). Activation and signaling of the p38 MAP kinase pathway. Cell Research *15*, 11-18.

Zhang, L., Ward, J.D., Cheng, Z., and Dernburg, A.F. (2015). The auxin-inducible degradation (AID) system enables versatile conditional protein depletion in *C. elegans*. Development *142*, 4374-4384.